Optimal pose selection for the identification of geometric and elastostatic parameters of machining robots

Yier Wu

l'université nantes angers le mans
PÔLE DE RECHERCHE ET D'ENSEIGNEMENT SUPÉRIEUR

MINES Nantes

Thèse de Doctorat

Yier WU

Mémoire présenté en vue de l'obtention du
grade de Docteur de l'École Nationale Supérieure des Mines de Nantes
sous le label de L'Université Nantes Angers Le Mans

École doctorale : *SPIGA*

Discipline : *Génie Mécanique, Productique, Transport*
Spécialité : *Robotique*
Unité de recherche : *Institut de Recherche en Communications et Cybernétique de Nantes*

Soutenue le *15 Janvier 2014*
Thèse N° : *2014EMNA0123*

Optimal Pose Selection for the Identification of Geometric and Elastostatic Parameters of Machining Robots

JURY

Rapporteurs :	**Gabriel ABBA**	Professeur, Ecole Nationale d'Ingénieurs de Metz
	Laurent SABOURIN	Maître de Conférences, IFMA Institut Français de Mécanique Avancée
Examinateurs :	**Anatol PASHKEVICH**	Professeur, Ecole des Mines de Nantes
	Benoît FURET	Professeur, Université de Nantes
	Stéphane CARO	Chargé de recherche, CNRS, IRCCyN
	David DANEY	Chargé de recherche, INRIA Bordeaux
	Claire LARTIGUE	Professeur, IUT de Cachan, Université Paris-Sud
	Christelle BOUTOLLEAU	Ingénieur, Europe Technologies
Invité :	**Alexandr KLIMCHIK**	Ingénieur de recherche, Ecole des Mines de Nantes
Directeur de Thèse :	**Anatol PASHKEVICH**	Professeur, Ecole des Mines de Nantes
Co-directeur de Thèse :	**Benoît FURET**	Professeur, Université de Nantes
Co-encadrant de Thèse :	**Stéphane CARO**	Chargé de recherche, CNRS, IRCCyN

ACKNOWLEDGEMENTS

Before beginning this manuscript, I would like to express my gratefulness to people who have guided and helped me in my research and who have provided all possible assistance throughout the time of working on the thesis.

First and foremost I am sincerely thankful to my supervisor, Professor Anatol Pashkevich, for his continuous aid in my research. It is difficult to assess his contribution in my researches, he always directed my research in a right way, gave invaluable advices, and spent a lot of time to improve the quality of my thesis and research significance. He taught me to write high-quality scientific papers and carry out independent research.

Special thanks also goes to my another supervisor, Stéphane Caro, who was the tutor of my Master thesis, and who proposed and encouraged me to continue the research work by making this Ph.D. thesis. It is an honor for me to thank another supervisor, Professor Benoît Furet, who has provided me the opportunity to exploit experimentally my theoretical work on a real industrial robot. They offered me valuable scientific suggestions, acquainted me with researchers from all over the world, and helped me with everyday life in France as well.

I am grateful for all conversations and discussions with my colleague, Alexandr Klimchik, who always gave reasonable answers and high-quality advices when I met difficulties during these three years. He always finds problems and important questions in my research, which needed further investigations, and offers interesting ideas, that aided to enrich my scientific background and enhance my research work.

I would like to thank the colleagues from IUT Nantes, Claire Dumas, Fabien Truchet, Guillaume Gallot, Joachim Marais, who provided great helps for the experimental study with robot. Thanks to all colleagues from Ecole des Mines de Nantes (people from DAP and all persons with whom I had the opportunity to cross) and IRCCyN (people from Equip Robotique) who provided any aid or assist during last three years. In addition, I want to thank Isabelle Laine, Anita Niebroj-Kaelbel for their administrative support.

The last and most important thanks go to my family, especially my parents, who always supported me in all my pursuits. Thank them for all their love and encouragement.

RÉSUME ET MOTS CLÉS

Résumé: La thèse porte sur la sélection de poses optimales pour la calibration géométrique et élasto-statique de robots industriels utilisés pour l'usinage de pièces des grandes dimensions. Une attention particulière est accordée à l'amélioration de la précision de positionnement du robot après compensation des erreurs géométriques et élasto-statiques. Pour répondre aux exigences industrielles des opérations d'usinage, une nouvelle approche pour la définition d'essais pour la calibration de robots sériels et quasi-sériels est proposée. Cette approche est basée sur un nouveau critère de performance, orienté applications industrielles, qui évalue la qualité du plan d'essais pour la calibration via la précision de positionnement du manipulateur après compensation d'erreurs, et tient compte des spécificités de la tâche manufacturière à réaliser au moyen de configurations tests. Contrairement aux travaux précédents, l'approche développée requiert seulement une mesure des positions de points et non d'orientation de corps rigides à l'aide d'un système de mesure externe tel qu'un laser tracker. Cette méthode permet ainsi d'éviter les problèmes de non-homogénéité dans les équations d'identification. Par ailleurs, afin de prendre en compte l'impact du compensateur de gravité, qui induit une chaîne cinématique fermée, le modèle de raideur est étendu en y incluant certains paramètres élasto-statiques dont les valeurs dépendent de la configuration du robot. Une méthodologie pour la calibration des modèles de compensateurs de gravité est ainsi proposée. Les avantages des techniques développées pour la calibration de robots industriels dédiés à des opérations d'usinage sont validés et mis en évidence expérimentalement, à travers la calibration géométrique et élasto-statique du robot industriel KUKA KR-270.

Mots-clés: calibration géométrique et élasto-statique, définition d'essais de calibration, mesure de poses partielles, robots sériels et quasi-sériels, compensateur de gravité, robotique d'usinage

ABSTRACT AND KEYWORDS

Abstract: The thesis deals with the optimal pose selection for geometric and elastostatic calibration for industrial robots employed in machining of large parts. Particular attention is paid to the improvement of robot positioning accuracy after compensation of the geometric and elastostatic errors. To meet the industrial requirements of machining operations, a new approach for calibration experiments design for serial and quasi-serial industrial robots is proposed. This approach is based on a new industry-oriented performance measure that evaluates the quality of calibration experiment plan via the manipulator positioning accuracy after error compensation, and takes into account the particularities of prescribed manufacturing task by introducing manipulator test-poses. Contrary to previous works, the developed approach employs an enhanced partial pose measurement method, which uses only direct position measurements from an external device and allows us to avoid the non-homogeneity of relevant identification equations. In order to consider the impact of gravity compensator that creates closed-loop chains, the conventional stiffness model is extended by including in it some configuration dependent elastostatic parameters, which are assumed to be constant for strictly serial robots. Corresponding methodology for calibration of the gravity compensator models is also proposed. The advantages of the developed calibration techniques are validated via experimental study, which deals with geometric and elastostatic calibration of a KUKA KR-270 industrial robot.

Keywords: geometric and elastostatic calibration, design of calibration experiments, partial pose measurements, serial/quasi-serial industrial robots, gravity compensator, robotic-based machining

RESUME EN FRANÇAIS

SELECTION DE POSES OPTIMALES POUR L'IDENTIFICATION DES PARAMETRES GEOMETRQUES ET ELASTO-STATIQUES DE ROBOTS D'USINAGE

INTRODUCTION GENERALE

Motivation. Actuellement, les industries des secteurs automobile, navale et aéronautique tentent de remplacer progressivement les machines CNC par des robots industriels pour effectuer de nombreuses tâches de fabrication. En général, les robots industriels sont considérés comme très concurrentiels en raison de leur flexibilité d'utilisation, leurs grands espaces de travail et leur rentabilité. En même temps, la robotique d'usinage introduit quelques difficultés complémentaires. En effet, dans le cas, par exemple, où le robot est soumis à une charge externe substantielle durant l'usinage, les compliances des liaisons deviennent non négligeables. Ainsi, afin d'obtenir une grande précision de traitement, une révision des modèles mathématiques et des stratégies de commande des axes est nécessaire. Cette pratique est l'objectif principal de cette thèse.

Pour les procédés de fabrication pris en compte dans ce travail, le robot manipulateur travaille sous des sollicitations importantes due au procédé d'usinage. Ce chargement est souvent assez grand pour provoquer des déformations qui se concentrent dans les composants élastiques du robot utilisé. Les erreurs de déformations dépendent à la fois du chargement externe et des propriétés élasto-statiques des robots. Ces déformations affectent fortement par conséquence la qualité du produit usiné. D'autre part, pour les applications industrielles où les forces externes appliquées à l'effecteur du manipulateur sont relativement faibles, les sources principales d'imprécision du robot sont les erreurs géométriques. Ces erreurs sont liées aux différences entre les valeurs nominales et réelles des paramètres caractéristiques de la géométrie des bras et des articulations. Dans ce cas, pour obtenir la précision de positionnement voulue pour la robotique d'usinage, les modèles mathématiques correspondants doivent être soigneusement calibrés avant d'être utilisées dans les algorithmes de commande. Pour ces deux raisons, le renforcement de modélisations géométriques et élasto-statiques, ainsi que l'amélioration de la précision dans l'identification des paramètres du modèle, deviennent les moyens de compenser les problèmes importants de déviation de l'outil durant l'usinage.

Dans la littérature, le problème de la calibration du modèle de manipulateur a été au centre des travaux de la communauté de la recherche en robotique depuis plusieurs décennies. Beaucoup de travaux ont été menés sur la calibration géométrique, qui a été étudiée sous différents aspects (les méthodes de modélisation et de mesure, les algorithmes d'identification, etc.) Actuellement, une attention particulière est accordée à la calibration élasto-statique, mais la majorité des travaux se concentrent sur le développement de modèles de raideur simplifiés et l'utilisation des techniques d'identification classiques. L'équipe Robotique de l' IRCCyN a eu des contributions essentielles dans le domaine de la calibration du robot, y compris un certain nombre de travaux théoriques/pratiques et des logiciels pour la modélisation géométrique de robots "SYMORO+" et la calibration "GECARO" (Khalil and Creusot, 1997; Khalil and Lemoine, 1999), méthodologies pour l'identification de la

raideur articulaire (Gautier et al., 2011) (Caro, Dumas, Garnier et Furet, 2013), la modélisation de la raideur des manipulateurs sur-contraints (Pashkevich et al., 2009) et aussi certains travaux liés à l'identification des paramètres dynamiques (Gautier and Briot, 2013; Pashkevich et al., 2009). Cette thèse s'appuie sur ces travaux antérieurs et a pour but d'améliorer la précision des modèles de manipulateur existants.

En dépit de nombreuses contributions consacrées à la calibration du robot, les problèmes de l'amélioration de la précision de l'identification et de la réduction de l'impact du bruit de mesure n'ont pas trouvé suffisamment d'écho dans la littérature., Il n'y a qu'un nombre limité de travaux sur le sujet (Sun and Hollerbach, 2008). Une façon d'améliorer la précision de l'identification sans augmenter le nombre d'essais de calibration est l'optimisation préliminaire des configurations de mesures. Cette approche a été considérée dans plusieurs travaux, dont les auteurs ont adapté l'idée de plan optimal d'essais de calibration de robot pour la sélection des configurations optimales de mesures (Khalil et al., 1991) (Borm and Meng, 1991) (Daney, 2002). Pour définir le plan optimal, de nombreux indices de performance ont été proposés dans la littérature. Cependant, la majorité de ces indices ont leurs limites qui affectent la précision de la calibration. En outre, ils ne correspondent pas entièrement aux exigences industrielles et sont souvent abstraits. Pour cette raison, il est nécessaire de développer une nouvelle mesure de la performance pour la sélection de configurations de mesure, qui est directement liée aux exigences industrielles des processus d'usinage et qui vise à améliorer la précision de positionnement du robot après calibration.

Objectifs de la thèse et problèmes de recherche. La thèse se concentre sur le renforcement des techniques de calibration des paramètres géométriques et élasto-statiques de robots afin d'améliorer leur précision et l'efficacité de la compensation d'erreurs. Cette méthode développée pour la robotique d'usinage de pièces des grandes dimensions obtient les performances recherchées au moyen de la définition d'essais optimaux pour la calibration du robot en réduisant l'impact de l'erreur de mesure. Pour atteindre cet objectif, les problèmes suivants sont formulés et résolus dans le cadre dans le cadre de cette thèse de doctorat :

Problème 1:

> Développement d'un nouvel indice de performance, orienté applications industrielles, pour la définition d'essais pour la calibration et des algorithmes d'optimisation qui garantissent la précision requise pour les applications industrielles considérées dans cette thèse.

Problème 2:

> Développement de modèles géométrique et élasto-statique avancés de robots industriels utilisés pour l'usinage de pièces de grandes dimensions. Ces modèles doivent également permettre d'appréhender l'effet des compensateurs de gravité.

Problème 3:

> La validation expérimentale de la technique développée et son application pour l'identification des paramètres des modèles géométrique et élasto-statique de robots utilisés pour l'usinage de pièces de grandes dimensions dans l'industrie aéronautique.

Organisation de la thèse. Pour résoudre les problèmes de recherche définis ci-dessus, la thèse est organisée de la manière suivante :

Le Chapitre 1 est consacré à l'état de l'art sur les particularités de la robotique d'usinage et décrit les techniques existantes pour la calibration géométrique et élasto-statique de robots. Une attention particulière est accordée aux applications de robots pour l'usinage de pièces de grandes dimensions, la détermination des exigences industrielles, l'analyse des travaux existants sur la calibration de robots et la détermination des configurations de mesures. L'objectif principal de ce chapitre est ainsi de mettre en évidence les limitations des techniques existantes et la nécessité de renforcer ces techniques, qui permettent de définir les objectifs et les problèmes de recherche de la thèse.

Le Chapitre 2 porte sur la définition d'essais optimaux pour la calibration des paramètres géométriques du manipulateur. Une attention particulière est accordée à l'amélioration des techniques de mesure et d'optimisation utilisées pour la calibration géométrique des robots sériels. Ce chapitre présente un modèle géométrique complète irréductible pour des robots d'architecture sérielle, qui prend en compte les différentes sources d'erreur (longueurs de corps, offsets entre les liaisons, etc.) Il propose également un indice de performance orienté applications industrielles pour la sélection des configurations optimales de mesure et améliore la technique de mesure via l'utilisation de mesures des coordonnées cartésiennes des points à l'aide d'un système de mesure externe. Cette nouvelle approche vise à trouver les configurations de la calibration qui garantissent la meilleure précision de positionnement du robot après compensation d'écarts géométriques. Dans ce chapitre, plusieurs exemples de simulation illustrent les avantages de la technique développée pour la sélection des poses et l'amélioration de la précision.

Le Chapitre 3 est consacré à la définition d'essais pour la calibration des paramètres élasto-statiques du manipulateur. Une attention particulière est accordée à l'amélioration des méthodes de modélisation, de mesure et d'identification utilisées pour la calibration élasto-statique de robots industriels d'architecture sérielle, en tenant compte de la particularité de la chaîne cinématique fermée induite par le compensateur de gravité. Il présente la méthode de mesure renforcée pour le cas de la calibration élasto-statique et applique la technique des moindres carrés pondérés pour l'identification des paramètres correspondants. Dans ce chapitre, la mesure de performance proposée est prolongée dans le cas de la sélection de configurations optimales de mesure pour des essais de la calibration élasto-statiques. Contrairement aux travaux précédents, le modèle de la raideur du manipulateur développé est capable de prendre en compte l'impact des compensateurs de gravité.

Le Chapitre 4 traite de la validation expérimentale de la technique développée pour la sélection de poses optimales employées dans la procédure de la calibration, où une attention particulière est accordée à l'amélioration de la précision de positionnement du robot industriel KUKA KR-270 installé sur la plate-forme robotique de production de l'IRCCyN à l'IUT de Nantes et qui est équipé d'un compensateur de gravité. Il présente l'environnement des cellules de travail où les essais de calibration doivent être effectués. Aussi bien pour la calibration géométrique que pour la calibration élasto-statique, les essais expérimentaux et les procédures de mesure, les configurations optimales de mesure et des résultats d'identification ainsi que l'analyse de la précision sont fournis. Contrairement à d'autres travaux, la précision du manipulateur est évaluée non seulement pour les configurations de mesure, mais aussi pour un plus large éventail de configurations (différentes de celles utilisées pour la calibration).

Enfin, *la Conclusion* résume les contributions principales de la thèse et définit les perspectives pour les travaux futurs.

CHAPITRE 1

MODELISATION DE MANIPULATEURS POUR LA ROBOTIQUE D'USINAGE ET IDENTIFICATION DES PARAMETRES DU MODELE

Pour l'usinage de pièces de grandes dimensions, l'utilisation de robots industriels d'architecture sérielle est très attrayante. En effet, ils ont un grand espace de travail et une plus grande souplesse d'utilisation comparés aux machines CNC. Cependant, à cause de certaines particularités de la cinématique du robot, les erreurs de positionnement de l'effecteur sont accumulées de bras en bras et affectent la précision d'usinage. Pour obtenir une précision désirée du procédé d'usinage, la commande du robot doit utiliser un modèle du manipulateur précis qui soit capable de compenser les erreurs géométriques et les déformations élastiques sous sollicitations provoquées par les forces d'usinage et de gravité appliquées aux composants du manipulateur.

• LA ROBOTIQUE D'USINAGE DE PIECES DE GRANDES DIMENSIONS

Avant d'examiner les spécificités de la robotique d'usinage, nous analysons en général les exigences industrielles de précision d'usinage. La présente les procédés de fabrication les plus courants et les tolérances typiques associées à chacun d'eux. Pour le processus de fraisage étudié dans cette thèse, qui est souligné ici, les tolérances désirées sont de l'ordre de 0,05-0,25 mm. Il est ainsi important d'évaluer leur faisabilité dans la commande de robots conventionnels sans compensation d'erreur.

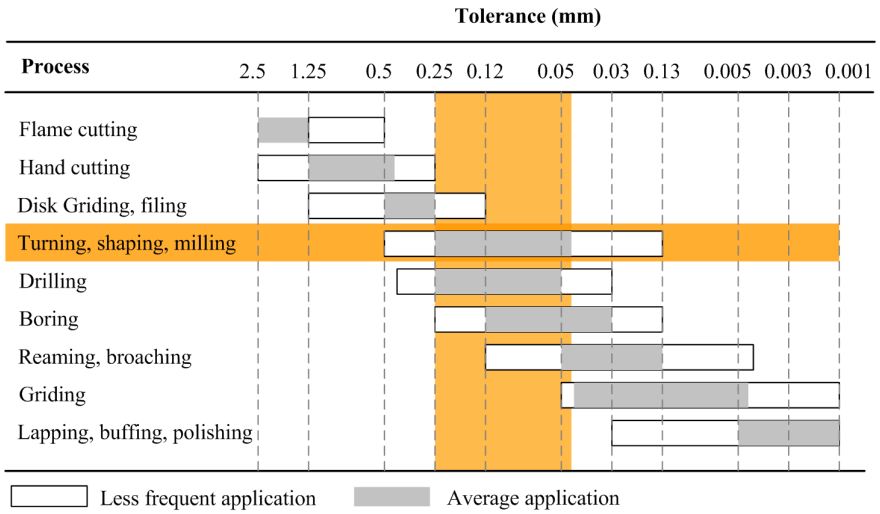

Figure 1. Tolérances typiques de différents procédés d'usinage

Pour les robots industriels, en particulier ceux utilisés pour l'usinage de matériaux à hautes performances (l'Inconel 718 ou le Monel® 400 alliages de nickel-cuivre utilisé dans l'industrie aérospatiale), le chargement essentiel est habituellement du à l'interaction de l'outil d'usinage et la pièce. Pour le fraisage d'une telle matière avec la profondeur de coupe de 0,2 mm, largeur de coupe de 8 mm et la vitesse de coupe de 2000 m/min, une force de 7 kN est requise (Klimchik, 2011). Une telle force est suffisante pour provoquer des déformations importantes des corps et des liaisons du robot industriels. Par exemple, pour le robot industriel KUKA KR240 (Dumas, 2011), une telle force peut provoquer des déviation de positionnement de l'ordre de 5 mm, ce qui est 20 fois plus important que

les tolérances de fabrication souhaitées. Ainsi, pour obtenir la précision désirée pour une bonne qualité d'usinage, ces déviations doivent être compensées par une stratégie appropriée de commande.

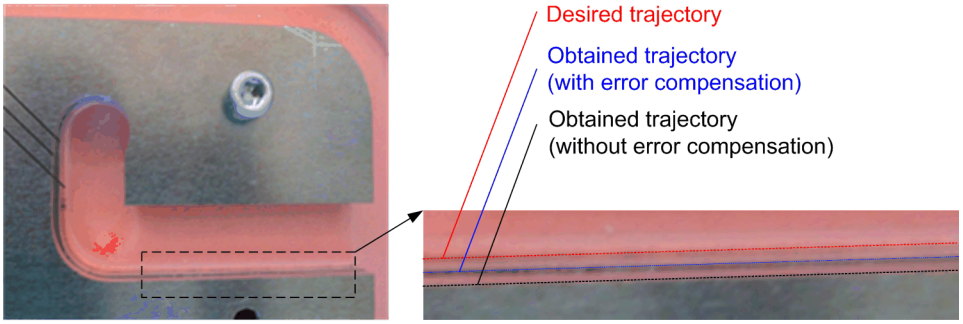

(a) Machining piece (b) Zoom of the obtained machining trajectories

Figure 2. Les différences entre la trajectoire désirée et celles obtenues avec et sans compensation d'erreurs (Dumas, 2011)

Afin de montrer l'importance des paramètres de manipulateur sur la qualité de fabrication, nous présentons un essai d'usinage effectué à la plate-forme IRCCyN à l'IUT de Nantes. Le processus technologique comprend une opération de fraisage sur une pièce en utilisant un robot industriel KUKA KR-270. La pièce en alliage d'aluminium avec une épaisseur de 5 mm a été usinée avec un outil de coupe de diamètre égal à 21 mm et comprenant quatre dents. La vitesse de rotation de l'outil est égale à 6670 tr/mn et la vitesse d'avance est égale à 3,6 m/min. Les résultats expérimentaux liés à ce processus sont présentés dans la Figure 2, qui montrent les différences entre la trajectoire désirée et celles obtenues (en utilisant différentes stratégies de commande). Les erreurs d'usinage sans compensation d'erreur peuvent atteindre 0,7 mm, ce qui n'est pas acceptable pour les opérations d'usinage réalisées dans l'industrie aéronautique.

- **MODELES GEOMETRIQUES DE MANIPULATEURS ET IDENTIFICATION DE LEURS PARAMETRES**

Les modèles géométriques d'un manipulateur peuvent comprendre de nombres de paramètres différents. Généralement, il n'est pas possible d'identifier l'ensemble de ces paramètres à partir des mesures de la position de l'effecteur. En pratique, certains paramètres ne peuvent pas être identifiés séparément, ils sont présentés dans le modèle géométrique comme des sommes ou des combinaisons linéaires. Par conséquent, pour être adapté à l'identification, le modèle géométrique du manipulateur doit être approprié (au moyen de la réduction des paramètres redondants).

Ce problème a été abordé dans (Everett et al., 1987), où trois propriétés pour le modèle géométrique approprié pour l'identification ont été définis: la complétude, l'irréductibilité et la continuité. Une contribution dans ce domaine a été faite par (Zhuang et al., 1989), qui a porté sur la détermination du nombre minimum de paramètres géométriques de la complétude du modèle. Une autre solution possible basée sur la technique SVD a été proposée dans (Pashkevich, 2001), où les paramètres géométriques du manipulateur sont divisés en trois groupes, les paramètres identifiables, non identifiables et semi-identifiables. De même, une approche alternative a été proposée dans (Khalil and Dombre, 2004) basée sur la décomposition QR.

En pratique, les paramètres géométriques du robot diffèrent des valeurs nominales déclarées dans les spécifications techniques et varient d'un robot à l'autre. Donc, pour être utilisé dans la

commande du robot, le modèle géométrique doit être correctement calibré pour un manipulateur donné. En général, la procédure de calibration est divisée en quatre étapes successives: la modélisation, les mesures, l'identification et l'implémentation.

La première étape porte sur le développement d'un modèle mathématique approprié du robot. Lors de la deuxième étape, les mesures sont effectuées. La troisième étape porte sur l'identification des paramètres inconnus en utilisant certains algorithmes numériques. Enfin, la dernière étape met en œuvre les paramètres identifiés dans le modèle utilisé dans la commande du robot ou la technique de compensation. Plus en détail, deux stratégies de compensation sont décrites dans la Figure 3, où le modèle de manipulateur réel est considéré comme "non-nominal", contrairement au modèle "nominal" qui est donné dans documentation technique du robot.

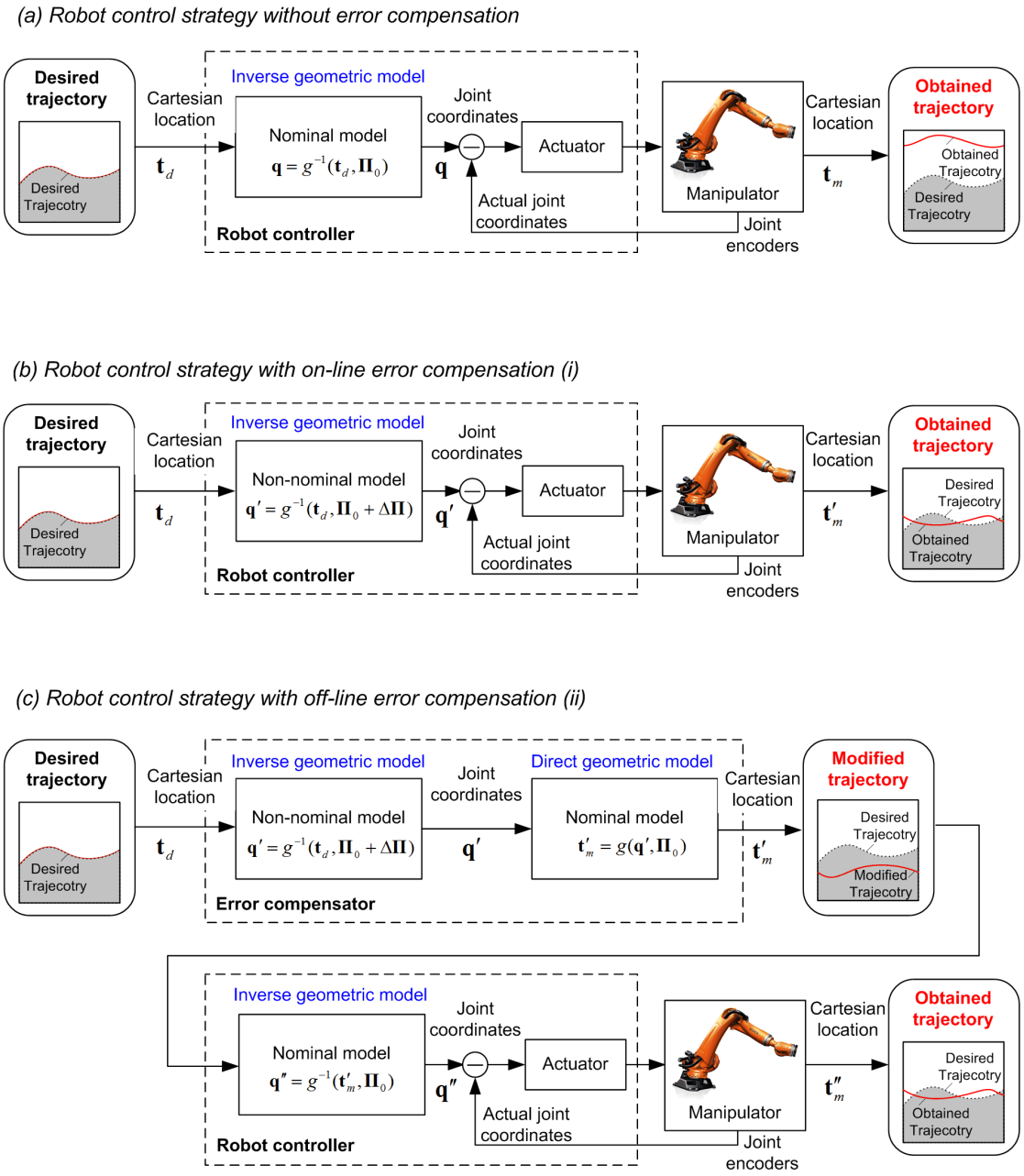

Figure 3. Stratégies de commande du robot avec différentes techniques de compensation des erreurs

Tableau 1 Résumé de la revue sur la calibration géométrique

	Open-loop methods			Closed-loop methods	
	Location measure	Position measure	Distance measure	Position constraint	Plane constraint
Publications	(Besnard and Khalil, 1999) (Zhuang et al., 1998)	(Bai et al., 2003)	(Goswami et al., 1993) (Driels and Swayze, 1994)	(Meggiolaro et al., 2000)	(Ikits and Hollerbach, 1997)
Measurement device	Theodolite/ inclinometers	LTS	Ball-bar system/ Wire potentiometer	—	—
Applications	Stewart platform	PUMA 560	PUMA 560	Schilling Titan II	PUMA 560
Number of parameters	35/42*	27	36/24*	—	23
Number of configurations	80/12	40	800/48	800	120
Achieved accuracy	0.4mm/0.5mm	0.1mm	0.08mm/0.5mm	5.7mm	0.25mm

*The number of identified parameters varies with different parameterization methods

Le Tableau 1 résume les travaux existants sur la calibration géométrique de robots. La meilleure précision a été atteinte en utilisant des mesures de position (0,1 mm en utilisant le laser tracker). L'efficacité des méthodes restantes est essentiellement inférieure. Pour cette raison, la mesure de coordonnées de l'effecteur semble prometteuse pour des applications industrielles. D'autre part, plusieurs problèmes se posent également ici. Par exemple, la mesure devrait fournir les coordonnées de position et d'orientation, mais celles-ci sont généralement calculées en utilisant les coordonnées de position de plusieurs points de référence. Intuitivement, cela peut causer une perte de la précision de l'identification. Par ailleurs, les résidus 6D ne sont pas homogènes pour être utilisés directement dans la méthode des moindres carrés, de sorte qu'ils devraient être normalisés dans les équations d'identification. Par conséquent, il est nécessaire d'améliorer les techniques de mesure en vue de surmonter ces difficultés.

- **MODELES ELASTOSTATIQUES DE MANIPULATEURS ET IDENTIFICATION DE LEURS PARAMETRES**

Les paramètres élastiques de manipulateurs peuvent être obtenus seulement à partir des essais de calibration. Similairement à la calibration géométrique, le cas élasto-statique comprend quatre étapes. Actuellement, la plupart des travaux connexes porte sur le développement de modèles de raideur simplifiés et appliquent les techniques d'identification classiques. En particulier, le Tableau 2 résume les particularités principales et souligne les difficultés de la calibration élasto-statique.

Contrairement au cas géométrique, la calibration élasto-statique est basée sur le modèle géométrique étendu et le modèle de raideur, et nécessite des capteurs de force supplémentaires. La difficulté principale est liée à l'application de la force dans des directions différentes, dont l'amplitude est limitée par les contraintes admissibles dans les composants du manipulateur. Celui-ci affecte sensiblement la précision de l'identification, qui dépend de l'amplitude de la force.

Tableau 2 Particularités et difficultés de la calibration élasto-statique

Calibration steps	Particularities	Difficulties
Step 1: Modeling	● Extended geometric model ● Lumped stiffness model ● Take into account robot configurations and applied forces	● Huge number of parameters ● Influence of gravity compensator
Step 2: Measurement	● Measurements with two different loadings ● Both position and force sensors are required	● Application of force in different directions ● Limited force magnitude
Step 3: Identification	● Large number of parameters must be identified	● Identifiability of stiffness parameter ● Non-homogeneity of the least-square objective ● Problem of the weights assigning
Step 4: Compensation	● Compensation relies on both geometric and elastostatic models ● Application of off-line compensation strategy only ● Deflections depend on robot configurations and applied forces	● Evaluation of the machining forces ● Influence of the dynamic factors: oscillation and chattering effects

Le Tableau 3 synthétise l'état de l'art de la calibration élasto-statique de robots. Tous les auteurs ont utilisé des méthodes qui s'appuient sur la mesure de position/orientation de l'effecteur. Puisque ces travaux traitent de différents robots dont les propriétés élasto-statiques diffèrent essentiellement, les niveaux des forces appliquées varient de 5 à 250 kg. La différence principale dans ces essais de calibration est liée au nombre de configurations de mesure qui diffère d'un cas à l'autre et varie de seulement 6 configurations allant jusqu'à 1000. Bien que les auteurs aient utilisé différents montages expérimentaux, ils ont pu atteindre à peu près la même précision de l'ordre de 0,3-0,7 mm.

Tableau 3 Summary of the review on elastostatic calibration

Publications	Application: manipulator	Applied forces	Measurement devices	N° of poses	Achieved accuracy
(Alici and Shirinzadeh, 2005)	Motoman SK 120	0-50kg	Laser sensing system Wrist force/torque sensor	20	0.43 mm
(Meggiolaro et al., 2005)	Patient positioning system	0-136kg	Leica 3D laser tracker	125	0.49 mm
(Marie and Maurine, 2008)	KUKA IR663	30-100kg	Three dial indicators	—	0.3 mm
(Lightcap et al., 2008)	Mitsubishi PA10-6CE	0-9.2kg	MicroVal PFX454 touch trigger probe CMM	10	0.71 mm
(Wang et al., 2009)	ABB IRB4400	0-30.6kg	ATI Omega force sensor, Portable coordinate measurement arm	6	0.4 mm
(Dumas et al., 2012)	KUKA KR240	0-250kg	Faro laser tracker Spring balance	23	0.6 mm
(Nubiola and Bonev, 2012)	ABB IRB 1600-6/1.45	1.85-4.8kg	Faro laser tracking system	1000	0.7 mm

- **DETERMINATION DES ESSAIS OPTIMAUX POUR LA CALIBRATION DES MODELES DE ROBOTS**

Afin de réduire les erreurs d'identification, il est très attrayant d'appliquer à la calibration du robot les idées de la théorie de la conception d'essais. Pourtant, dans la robotique, le problème de la conception d'essais optimaaux de calibration n'a pas reçu suffisamment d'attention. Dans des travaux précédents, il a été appliqué au problème de la calibration géométrique utilisant uniquement des mesures de performance abstraites (développées à l'origine pour les modèles de régression linéaire) qui ne sont pas directement liés à la précision du robot dans les processus d'usinage. En outre, un nombre limité de travaux a abordé la question de la calibration élasto-statique, où les configurations de mesures ont été obtenues en utilisant des approches intuitives. La limite des techniques existantes pour la calibration géométrique et élasto-statique a été démontrée par une étude de cas pour un manipulateur à deux corps et deux liaisons. La précision de l'identification correspondant à tous les critères examinés est présentée dans la Figure 4. Cette figure montre qu'il n'y a pas de solution optimale unique.

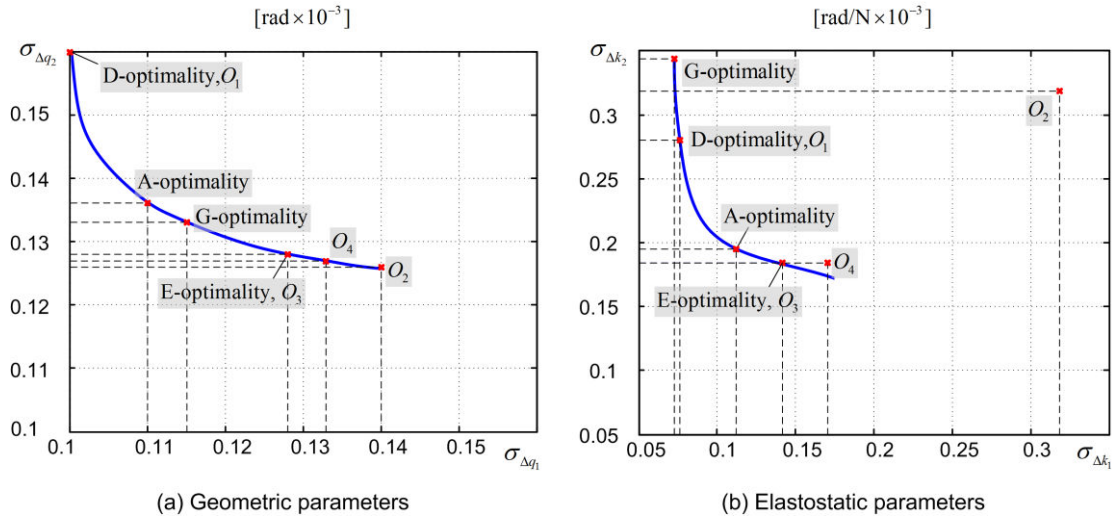

(a) Geometric parameters (b) Elastostatic parameters

Figure 4. Influence des indices de performance utilisés pour la détermination des configurations de mesure sur la qualité d'identification des paramètres

Par conséquent, il est nécessaire de réviser et d'améliorer les approches existantes pour la planification d'essais de la calibration pour l'identification des paramètres géométriques et élasto-statiques des robots industriels. En tenant compte des spécificités des applications industrielles visées, il est nécessaire de développer un nouvel indice de performance pour la détermination des configurations de mesure et qui assure une très bonne précision de positionnement du robot sous la charge.

CHAPITRE 2

CONCEPTION D'ESSAIS DE LA CALIBRATION DES PARAMETRES GEOMETRIQUES DE MANIPULATEURS

Dans ce travail, l'objectif principal est d'atteindre la précision désirée de positionnement du robot en utilisant un nombre minimum d'essais. Ici, il est proposé d'introduire une étape supplémentaire, la conception d'essais, qui est effectuée avant que les mesures soient faites et vise à obtenir des configurations de mesure qui assurent de bons résultats de la calibration (précision du

robot après compensation d'erreurs). Il nous permet d'améliorer l'efficacité de la compensation d'erreurs et d'estimer la précision du robot, qui est très important pour les applications industrielles. La procédure modifiée comprend cinq étapes, qui sont schématiquement présentés dans la Figure 5 Dans cette figure, les procédures mises en évidence sont liées aux contributions principales de ce chapitre et sont présentées ci-dessous.

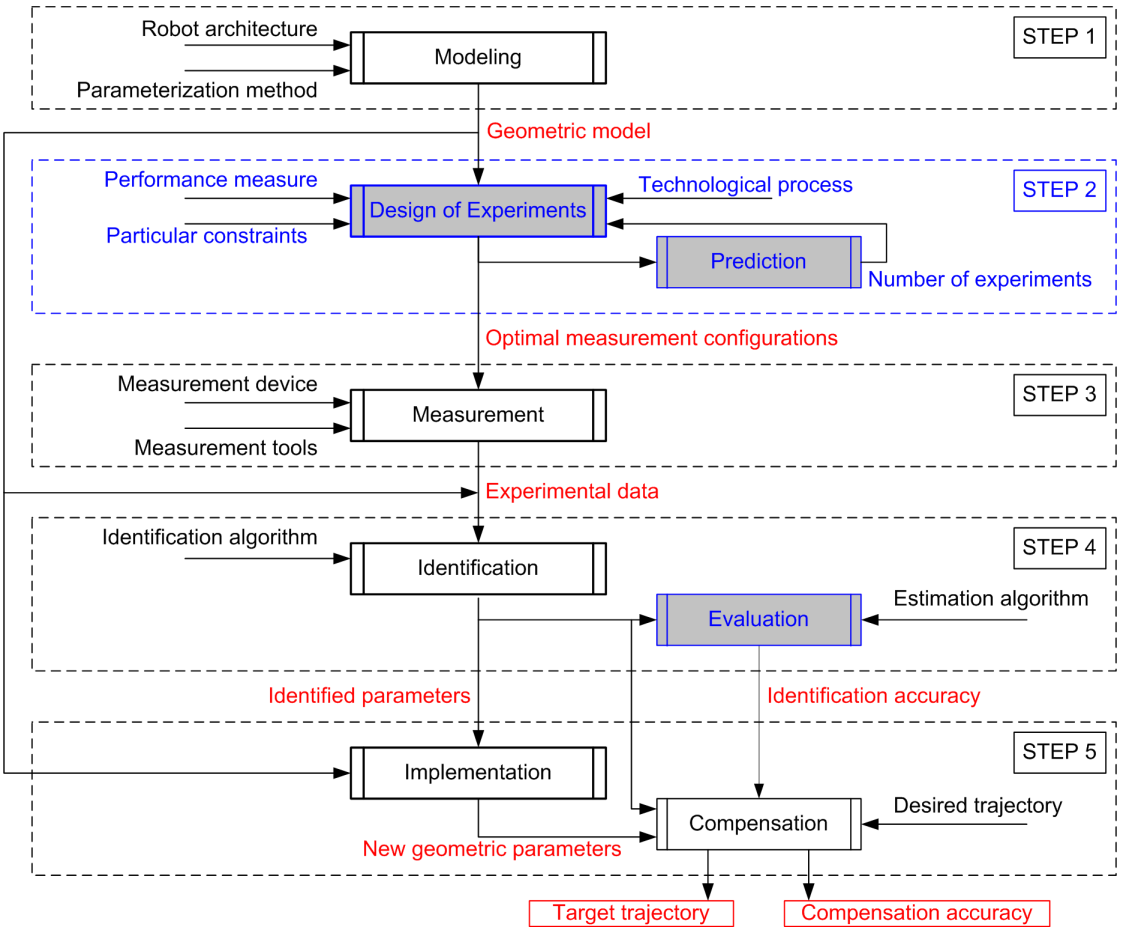

Figure 5. Le schéma de la procédure de calibration du robot.

- **METHODE RENFORCEE DE MESURE DES POSES PARTIELLES**

La principale difficulté avec la méthode de mesure des poses est que les composantes d'orientation du manipulateur ne peuvent pas être mesurées directement, et sont calculées en utilisant un nombre excessif de mesures de position. Cela provoque une non-homogénéité des équations pertinentes d'identification qui nécessitent une normalisation ultérieure. Pour éviter ce problème, la méthode proposée de mesure des poses partielles utilise des mesures directes pour plusieurs points de référence qui sont disponibles à partir de l'appareil externe. Le problème d'optimisation correspondant est écrit comme suit

$$\sum_{i=1}^{m}\sum_{j=1}^{n}\left\|\Delta\mathbf{p}_i^j-\mathbf{J}_{\pi i}^{j(p)}\Delta\boldsymbol{\pi}\right\|^2\rightarrow\min_{\Delta\boldsymbol{\pi}} \tag{1}$$

Ici, la matrice $\mathbf{J}_{\pi i}^{j(p)}$ avec l'exposant " (p) " désigne les lignes de positionnement du Jacobien d'identification $\mathbf{J}_{\pi i}^{j}$, l'indice " i " définit le numéro de la configuration, et l'indice " j " dénote le numéro du point de référence.

Afin d'illustrer les avantages de l'approche proposée, nous présentons un exemple numérique qui traite de l'identification des paramètres pour un manipulateur spatial comprenant 3 liaisons. A des fins de comparaison, les deux méthodes de mesure classiques et proposées sont évaluées. Les résultats de simulation sont résumés dans le Tableau 4, qui présente les écarts-types pour les estimations des paramètres: les erreurs des longueurs des corps Δl_i et les offsets articulaires. L'approche proposée permet l'amélioration de la précision dans l'estimation de la déviation de longueur des corps de 125-283%, tandis que l'amélioration de la précision des estimations offsets articulaires est légèrement inférieure, jusqu'à 233%. Cela confirme les avantages de l'approche proposée, qui conduit toujours à de meilleurs résultats.

Tableau 4 Comparaison de différentes méthodes de mesure et leur influence sur la précision de l'identification (nombre d'itérations : 1000, nombre de configurations : 3; $\sigma = 0.01\text{mm}$)

Parameters	Assigned geometric errors	Standard deviations of parameter estimates		Improvement
		Conventional approach	Proposed approach	
l_1	3 mm	0.069mm	0.018mm	283%
l_2	5 mm	0.019mm	0.006mm	217%
l_3	5 mm	0.009mm	0.004mm	125%
q_1	1 deg	0.187mdeg	0.185mdeg	1%
q_2	0.5 deg	3.742mdeg	1.123mdeg	233%
q_3	2 deg	1.432mdeg	0.866mdeg	65%

La méthode de mesure améliorée qui fonctionne avec plusieurs points de référence donne des avantages sur la précision de l'identification. Dans le cadre de cette méthode, l'algorithme d'identification dédié est divisé en deux étapes. La première étape porte sur l'estimation de $\mathbf{p}_{base}$, $\mathbf{R}_{base}$, $\mathbf{p}_{tool}^{j}$, qui sont liés à les transformations de base et d'outil. Ces vecteurs désirés peuvent être exprimés comme suit

$$\left[\mathbf{p}_{base};\boldsymbol{\varphi}_{base};\mathbf{u}_{tool}^{1};...\mathbf{u}_{tool}^{n}\right]=\left(\sum_{i=1}^{m}\mathbf{A}_i^{j\,T}\mathbf{A}_i^{j}\right)^{-1}\left(\sum_{i=1}^{m}\mathbf{A}_i^{j\,T}\Delta\mathbf{p}_i\right) \tag{2}$$

où

$$\mathbf{A}_i^j=\begin{bmatrix}\mathbf{I} & \left[\sim\mathbf{p}_{robot}^{i}\right]^T & \mathbf{R}_{robot}^{i} & \mathbf{0} & ... & \mathbf{0}\\ \mathbf{I} & \left[\sim\mathbf{p}_{robot}^{i}\right]^T & \mathbf{0} & \mathbf{R}_{robot}^{i} & ... & \mathbf{0}\\ ... & ... & ... & ... & ... & ...\\ \mathbf{I} & \left[\sim\mathbf{p}_{robot}^{i}\right]^T & \mathbf{0} & \mathbf{0} & ... & \mathbf{R}_{robot}^{i}\end{bmatrix} \tag{3}$$

Les variables définissant l'emplacement des points de référence sont exprimées par $\mathbf{p}_{tool}^{j}=\mathbf{R}_{base}^{T}\cdot\mathbf{u}_{tool}^{j}$, ce qui nous permet de trouver les matrices de transformation homogènes $\mathbf{T}_{base}$ et $\mathbf{T}_{tool}^{j}$. A la deuxième étape, les paramètres géométriques du manipulateur $\boldsymbol{\pi}$ sont estimés. En appliquant la technique des moindres carrés pour le système linéarisé des équations d'identification, c'est à dire, $\Delta\mathbf{p}_i^j=\mathbf{J}_{\pi i}^{j(p)}\cdot\Delta\boldsymbol{\pi}$, les vecteurs désirés d'estimations d'erreurs géométriques peuvent être obtenus comme suit :

$$\Delta\boldsymbol{\pi} = \left(\sum_{i=1}^{m} \sum_{j=1}^{n} \mathbf{J}_{\pi i}^{j(p)T} \mathbf{J}_{\pi i}^{j(p)} \right)^{-1} \left(\sum_{i=1}^{m} \sum_{j=1}^{n} \mathbf{J}_{\pi i}^{j(p)T} \Delta\mathbf{p}_i^j \right) \tag{4}$$

Il faut cependant noter que pour atteindre la précision souhaitée, les étapes 1 et 2 doivent être répétées de manière itérative. L'algorithme présenté ci-dessus est capable de fournir une bonne estimation des paramètres désirés, dans le cas où les données expérimentales sont parfaites. Néanmoins, en pratique, les erreurs de mesure sont généralement non négligeables. Pour évaluer l'impact des erreurs de mesure sur la précision de l'identification des paramètres, la matrice de covariance est utilisée et est exprimée ci-après :

$$\mathrm{cov}(\Delta\hat{\boldsymbol{\pi}}) = \sigma^2 \left(\sum_{i=1}^{m} \sum_{j=1}^{n} \mathbf{J}_{\pi i}^{j(p)T} \mathbf{J}_{\pi i}^{j(p)} \right)^{-1} \tag{5}$$

Pour atteindre la meilleure précision, les éléments de la matrice de covariance (5) doivent être aussi faibles que possible. Ceci peut être réalisé par un choix approprié des configurations de mesure.

- **L'APPROCHE DE POSE TEST POUR LA CONCEPTION D'ESSAIS DE CALIBRATION**

Dans la littérature, le problème de la sélection de poses de mesure a été étudié dans un certain nombre de travaux, mais les approches existantes se concentrent sur la précision de l'estimation des paramètres, tandis que l'application industrielle à examiner nous motive à nous concentrer sur la précision du positionnement du robot après calibration. Pour développer une nouvelle mesure de performance pour la conception d'essais de calibration, il est nécessaire de prendre en compte le fait qu'en pratique, la précision désirée est nécessaire à atteindre pour un espace de travail plutôt limité. Pour cette raison, il est proposé de limiter les configurations possibles à une seule configuration, appelée *configuration test du manipulateur* (Figure 6).

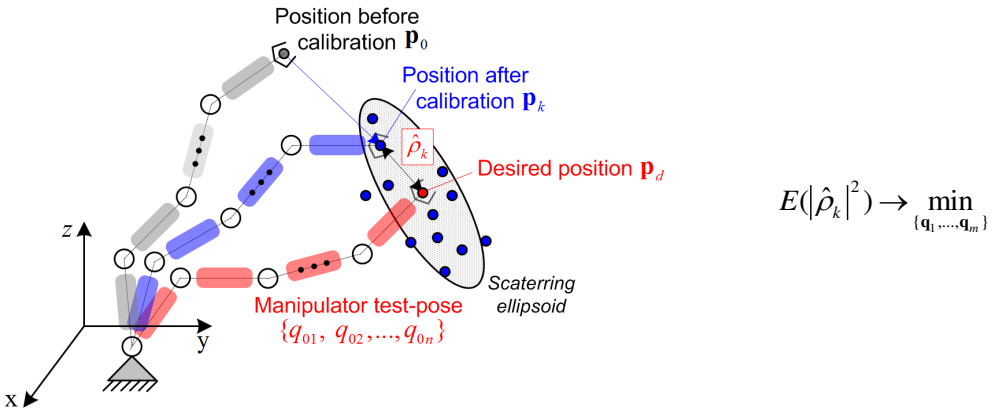

Figure 6. Dispersion des erreurs de positionnement du manipulateur après la calibration et la mesure de performance pour la sélection des configurations de mesure

Grâce à cette idée, le problème de l'intérêt de trouver un plan d'essais optimal, en fournissant les configurations de mesure, ce qui nous permet d'atteindre la plus grande *efficacité de la compensation d'erreur de positionnement* (ρ_0) pour une *configuration test du manipulateur* $\mathbf{q}_0$ définie dans le processus technologique. Ici, une nouvelle mesure de performance orientée vers l'industrie est proposée, qui est la distance moyenne quadratique entre la position cible et la position de l'effecteur après calibration. Cet indice de performance est défini par l'équation suivante :

$$\rho_0^2 = \sigma^2 \cdot \text{trace}\left(\mathbf{J}_{\pi 0}^{(p)} \left(\sum_{i=1}^{m} \sum_{j=1}^{n} \mathbf{J}_{\pi i}^{j(p)T} \mathbf{J}_{\pi i}^{j(p)} \right)^{-1} \mathbf{J}_{\pi 0}^{(p)T} \right) \quad (6)$$

et peut être considéré comme la trace pondéré de la matrice de covariance $\text{cov}(\hat{\boldsymbol{\pi}})$, où les coefficients de pondération sont calculés en utilisant la configuration test. Pour un cas plus général, le processus d'usinage peut exiger des changements dans la posture du manipulateur et la précision désirée devrait être atteinte pour l'ensemble de la trajectoire. Ainsi, l'approche développée est généralisée en introduisant les poses multiples, le problème d'optimisation correspondant à la sélection de poses vise ainsi à minimiser les erreurs de positionnement maximales de l'effecteur après compensation pour l'ensemble de la trajectoire.

Nous illustrerons les avantages de l'approche proposée par un exemple de la calibration géométrique d'un manipulateur comprenant deux corps et des liaisons. On suppose que les longueurs nominales des corps diffèrent, et ces déviations doivent être identifiées au moyen de la calibration. A des de comparaison, les plans d'essais ont été obtenus en utilisant trois stratégies différentes:

(i) les configurations de mesure sont générées de façon aléatoire;

(ii) les configurations de mesure sont obtenues en utilisant l'approche classique basée sur le principe de D-optimalité;

(iii) les configurations de mesure sont obtenues en utilisant l'approche proposée.

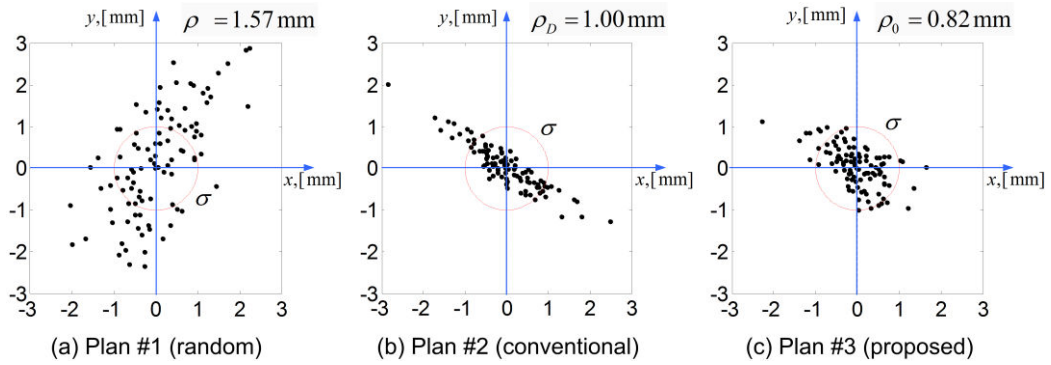

Figure 7. Dispersion des erreurs de positionnement du manipulateur après calibration pour différents plans d'essais: cas de réglage de deux paramètres $\{\Delta l_1, \Delta l_2\}$

Les résultats correspondants présentés dans la Figure 2.11 montrent que l'approche proposée permet d'augmenter la précision de positionnement de l'effecteur en moyenne de 18% en comparaison au plan D-optimal et de 48% en comparaison au plan généré aléatoirement. Par conséquent, les résultats présentés confirment que l'approche proposée permet l'amélioration de l'efficacité de la calibration et permet d'atteindre la meilleure précision de positionnement de manipulateur pour les configurations test définies par la tâche de fabrication.

- **AMELIORATION DE L'EFFICACITE DE LA SELECTION DE POSES OPTIMALES DE MESURE**

Pour améliorer l'efficacité de la sélection de poses de mesure, deux techniques ont été proposées: (i) l'application des calculs parallèles et hybrides, (ii) la production de solutions quasi-optimales à l'aide de plans de la calibration de les dimensions inférieurs.

Afin d'obtenir l'optimum global pour le problème considéré, il est requis de nombreuses répétitions de l'optimisation avec des points de départ différents. Des calculs parallèles nous ont permis d'accélérer le processus de détermination des configurations de mesures et de profiter de l'architecture multi-core des ordinateurs modernes. Les calculs ont été faits sur une station de travail avec 12 coeurs, qui nous permet de diminuer le temps de calcul par un facteur de 10-12. En utilisant une approche hybride qui combine l'algorithme génétique et recherche de gradient, qui est très efficace en termes de temps de calcul et nous permet d'éviter la convergence vers les minima locaux.

Au lieu d'augmenter le nombre d'essais et de résoudre le problème d'optimisation correspondant, il a été proposé d'utiliser une solution *quasi-optimale pour la sélection de poses de mesur*es. D'après notre expérience, la diversité des configurations de mesure ne contribue pas essentiellement à l'amélioration de la précision si le nombre total d'essais est assez grand. Ainsi, il a été proposé de répéter les essais de calibration en utilisant plusieurs fois les mêmes configurations de mesure, ce qui nous permet de simplifier le processus d'optimisation (avec dimension inférieure) et d'accélérer les mesures. L'efficacité de cette technique est illustrée dans la Figure 8.

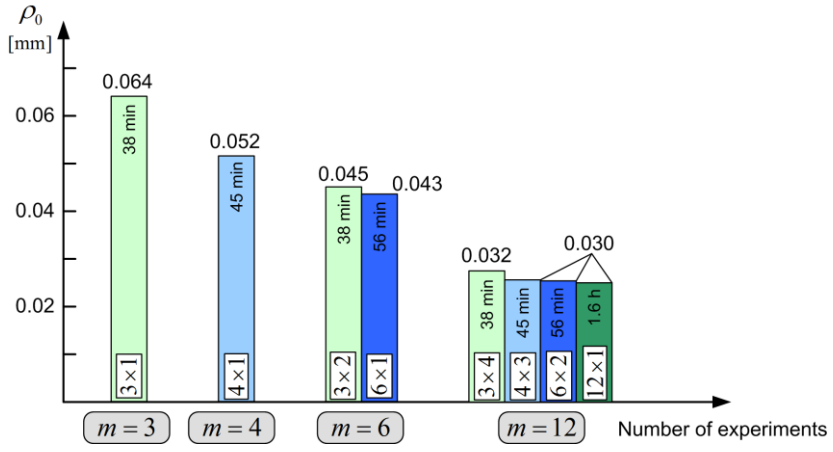

Figure 8. Comparaison des solutions quasi-optimales et optimales pour la sélection de configurations de mesure pour la calibration du robot

Le chapitre a été consacré à l'amélioration des techniques de mesure et d'optimisation employées pour la calibration géométrique des robots sériels. Les principales contributions sont dans le domaine de la conception d'essais de calibration, c'est à dire, la sélection optimale de configurations de mesure. Contrairement à d'autres travaux, l'approche développée est basée sur une nouvelle mesure de performance, orientée vers l'industrie, qui évalue la précision de positionnement du robot après compensation d'erreurs géométriques. Il convient de mentionner que les techniques développées peuvent être généralisés pour le cas de la calibration élasto-statique. Néanmoins, certaines modifications sont requises pour tenir compte des différences entre les modèles correspondants de manipulateurs et les systèmes d'expérimentation.

CHAPITRE 3

PLANS D'EXPERIENCES POUR L'IDENTIFICATION DES PARAMETRES ELASTOSTATIQUES DE ROBOTS

Le but de ce chapitre est *le renforcement des techniques de la calibration élasto-statiques au moyen de la conception d'essais*. Il est évident que certains résultats présentés dans le chapitre 2

peuvent être adaptés pour le cas élasto-statique. Ainsi, une attention particulière a été accordée à l'amélioration de la méthode de mesure des poses partielles pour le cas élasto-statique; extension de l'approche développée et mesure de performance correspondant pour la conception d'essais de calibration, ainsi que le développement d'une méthodologie pour la modélisation et la calibration des robots industriels équipés de compensateurs de gravité.

- **MODELISATION DE LA RAIDEUR ET IDENTIFICATION DES PARAMETRES ELASTO-STATIQUES**

Pour estimer les matrices désirées décrivant l'élasticité des éléments du manipulateur sur la base de la méthode VJM, le modèle élasto-statique correspondante s'écrit

$$\Delta\mathbf{t} = \mathbf{A}_k(\mathbf{q},\mathbf{w})\cdot\mathbf{k} \tag{7}$$

où $\mathbf{A}_k(.)$ est la matrice d'observation qui définit la correspondance entre le vecteur de compliance inconnue $\mathbf{k} = (k_{\theta,1}, k_{\theta,2}, ...k_{\theta,n\theta})^T$ et les déviations de l'effecteur $\Delta\mathbf{t}$ sous la charge $\mathbf{w}$ pour la configuration $\mathbf{q}$. Il peut être prouvé que la matrice $\mathbf{A}_k$ peut être exprimée par les colonnes de la Jacobienne cinématique $\mathbf{J}_\theta$ et la torsion externe $\mathbf{w}$ de la manière suivante

$$\mathbf{A}_k = \left[\mathbf{J}_{\theta,1}\mathbf{J}_{\theta,1}{}^T\mathbf{w},\ \ldots,\mathbf{J}_{\theta,i}\mathbf{J}_{\theta,i}{}^T\mathbf{w},\ldots,\mathbf{J}_{\theta,n\theta}\mathbf{J}_{\theta,n\theta}{}^T\mathbf{w}\right] \tag{8}$$

où $\mathbf{J}_{\theta,i}$ est le vecteur colonne i-ième de la matrice Jacobienne agrégée.

Comme pour la calibration géométrique, les équations de l'identification de paramètres élasto-statiques comprennent à la fois la position et l'orientation des composants des résidus. Pour éviter le problème de la non-homogénéité, nous appliquons l'idée de la méthode proposée de mesure de poses partielles pour le cas de la calibration élasto-statique. Le problème d'optimisation correspondant s'écrit comme suit

$$\sum_{i=1}^{m}\sum_{j=1}^{n}\left\|\Delta\mathbf{p}_i^j - \mathbf{A}_k^{j(p)}(\mathbf{q}_i,\mathbf{w}_i)\cdot\mathbf{k}\right\|^2 \to \min_{\mathbf{k}} \tag{9}$$

En comparaison avec le cas géométrique, il existe certaines particularités de la calibration élasto-statique concernant les montages expérimentaux. Le montage et la procédure de mesure sont présentés dans la Figure 9.

En utilisant les expressions présentées ci-dessus, les paramètres élasto-statiques peuvent être identifiés par un algorithme en trois étapes. A la première étape, les transformations de base et d'outil du manipulateur sont identifiées. Il fournit les données d'entrée pour la seconde étape, où les paramètres géométriques du manipulateur sont estimés. A la dernière étape, les paramètres de compliances $\mathbf{k}$ sont obtenus sur la base de configurations de mesure présélectionnés (qui diffèrent de celles de la calibration géométrique) et de charge externe correspondant. L'application de la technique des moindres carrés pour le système d'équations d'identification, la solution fournit les estimations du vecteur de paramètres désiré

$$\mathbf{k} = \left(\sum_{i=1}^{m}\sum_{i=1}^{n}\mathbf{A}_{ki}^{j(p)T}\mathbf{A}_{ki}^{j(p)}\right)^{-1}\cdot\left(\sum_{i=1}^{m}\sum_{j=1}^{n}\mathbf{A}_{ki}^{j(p)T}\Delta\mathbf{p}_i^j\right) \tag{10}$$

Tenant en compte que les erreurs de mesure ne sont pas i.i.d. et dépendent fortement de la direction et l'emplacement de la cible dans l'espace de travail du manipulateur, la technique des moindres carrés pondérée peut être appliquée pour l'identification. Dans ce cas, la matrice de covariance des paramètres est

$$\mathrm{cov}(\hat{\mathbf{k}}) = \left(\sum_{i=1}^{m} \sum_{i=1}^{n} \mathbf{A}_{ki}^{j(p)T} \left(\boldsymbol{\Sigma}_i^{j2} \right)^{-1} \mathbf{A}_{ki}^{j(p)} \right)^{-1} \tag{11}$$

où la matrice $\boldsymbol{\Sigma}_i^{j2} = E\left(\boldsymbol{\varepsilon}_i^j \boldsymbol{\varepsilon}_i^{jT}\right)$ désigne la covariance des erreurs de mesure et la meilleure sélection des coefficients de pondération correspond à l'équation $\mathbf{W}_i^{j2} \cdot \boldsymbol{\Sigma}_i^{j2} = \mathbf{I}$. Ainsi, ces coefficients peuvent être calculés de la manière suivante :

$$w_i^j = \frac{\sigma_0}{\sigma_0 + \lambda \cdot \hat{\sigma}_i^j} \tag{12}$$

où λ nous permet de régler l'impact de l'estimation de la variance $\hat{\sigma}_i^j$, et σ_0 est un facteur de normalisation (attribué en utilisant la précision de la système de mesure)

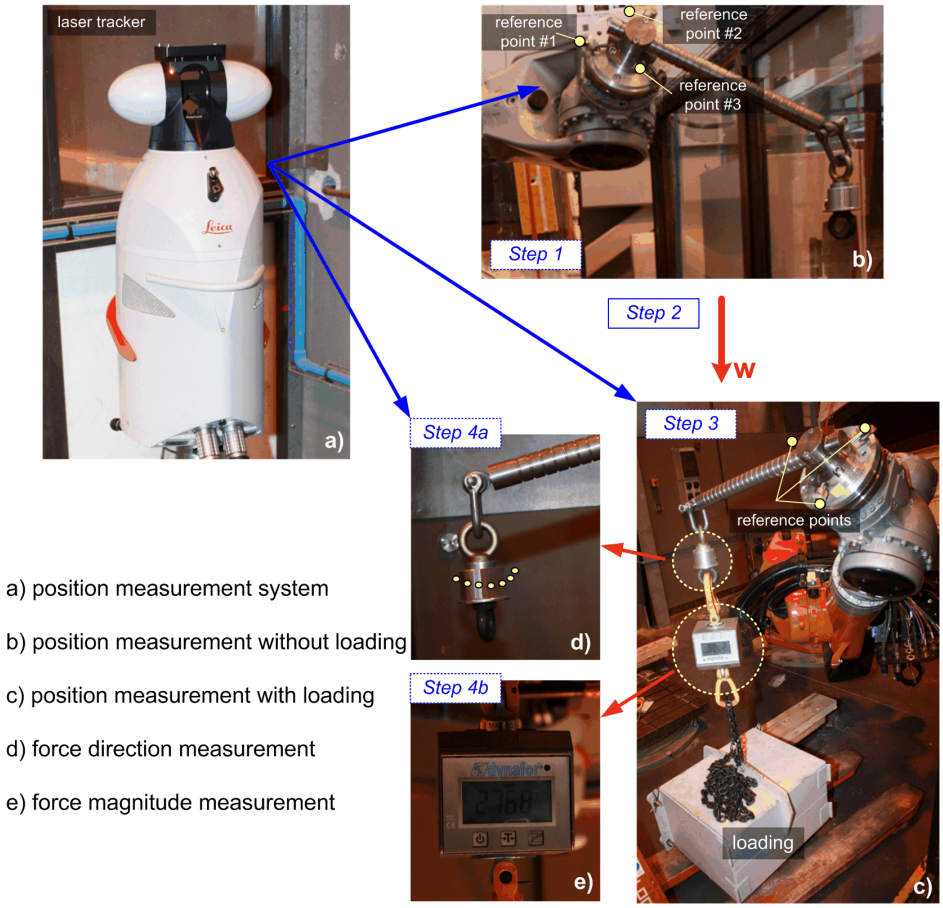

Figure 9. Procédure de mesures pour la calibration élasto-statique

- **EXTENSION DE L'APPROCHE DE POSE TEST POUR L'IDENTIFICATION DES PARAMETRES ELASTO-STATIQUES**

Les avantages de l'approche de pose test en termes d'efficacité de la calibration ont été démontrés dans le cas géométrique. Ainsi, il est raisonnable d'adapter cette approche et la mesure de performance à la calibration élasto-statique. Le problème d'optimisation pour la sélection des configurations de mesures est formulé de la manière suivante

$$\mathrm{trace}\left(\mathbf{A}_{k0}^{(p)} \left(\sum_{i=1}^{m} \sum_{j=1}^{n} \mathbf{A}_{ki}^{j(p)T} \mathbf{A}_{ki}^{j(p)} \right)^{-1} \mathbf{A}_{k0}^{(p)T} \right) \rightarrow \min_{\{\mathbf{q}_i, \mathbf{w}_i,\ i=1,m\}} \tag{13}$$

Lorsqu'il y a plusieurs configurations tests, la conception d'essais de calibration peut être réduite au problème de min-max suivant :

$$\max_{s}\left\{\text{trace}\left(\mathbf{A}_{k0s}^{(p)}\left(\sum_{i=1}^{m}\sum_{j=1}^{n}\mathbf{A}_{ki}^{j(p)T}\mathbf{A}_{ki}^{j(p)}\right)^{-1}\mathbf{A}_{k0s}^{(p)T}\right)\right\}\rightarrow\min_{\{q_i,w_i,\ i=\overline{1,m}\}}$$

Tel que (14)

$$\mathbf{C}_i(\mathbf{q}_i,\mathbf{w}_i)\le 0,\quad i=\overline{1,r}$$

où les matrices $\mathbf{C}_i(\mathbf{q}_i,\mathbf{w}_i)$ décrivent les contraintes.

Nous illustrerons les avantages de l'approche proposée par un exemple de calibration élasto-statique d'un manipulateur à deux corps. Les résultats de la simulation pour cette étude de cas ont été obtenus pour les paramètres suivants: les longueurs des corps sont $l_1=1\,\text{m}$, $l_2=0.8\,\text{m}$, la magnitude de la force $F=1\,\text{N}$, la paramètre de bruit de mesure $\sigma=0.1\,\text{mm}$. Plusieurs plans d'essais de calibration ont été comparés (basés sur différentes mesures de performance), en tenant compte à la fois la précision de l'identification des paramètres $k_{\theta 1},k_{\theta 2}$ et la précision de positionnement du manipulateur après calibration ρ_0. Les résultats présentés (Tableau 5) confirment que l'approche proposée est attrayante pour l'industrie et offre la meilleure précision de positionnement de l'effecteur. Dans le chapitre 4, cette approche sera appliquée à la calibration d'un robot industriel à six degrés de liberté de la famille KUKA.

Tableau 5 Comparaison de la précision de manipulateurs après calibration pour différents principes de la sélection de poses de mesure (manipulateur à 2 degrés de liberté, $\sigma=0.1\,\text{mm}$)

Experiment design principle	Identification accuracy [rad/N$\times 10^{-3}$]		Manipulator accuracy ρ_0 [mm]	Improvement factor $\chi=\rho_0^{test}/\rho_0$
	σ_{k_1}	σ_{k_2}		
Using test-pose as measurement pose	0.0888	0.2818	2.1265	1.0
A-optimality	0.1123	0.1948	0.9544	2.2
D-, O_1-optimality	0.0765	0.2804	0.4425	4.8
E-, O_3-optimality	0.1416	0.1840	1.5167	1.4
O_4-optimality	0.1707	0.1840	2.2061	0.9
Measurement pose selection via minimization of ρ_0	0.0719	0.3175	0.3915	5.4

- **LA CALIBRATION ELASTO-STATIQUE POUR LES ROBOTS AVEC COMPENSATEURS DE GRAVITE**

Les robots industriels sont généralement équipés de différents types de compensateurs de gravité, ce qui complique considérablement la modélisation de la raideur de ces manipulateurs. On présente un modèle de raideur basé sur la méthode VJM pour un manipulateur sériel avec un compensateur fixé à la seconde articulation. L'attention principale est accordée à l'identification des paramètres du modèle et de la planification d'essais de calibration.

La structure mécanique du compensateur de gravité est présenté dans la Figure 10a. Le compensateur comporte un ressort passif fixé au premier et au second corps, ce qui induit une chaîne cinématique fermée qui génère le couple appliqué à la deuxième liaison du manipulateur. Il peut être prouvé que la raideur équivalente de la deuxième liaison (incluant à la fois le manipulateur et la raideur du compensateur) est exprimée ainsi :

$$K_{\theta_2} = K^0_{\theta_2} + K_c \, a L \, \eta_{q_2} \tag{15}$$

où le coefficient η_{q_2} est exprimé comme suit

$$\eta_{q_2} = \frac{s_0}{s}\left(\frac{aL}{s^2}\sin^2(\alpha - q_2) + \cos(\alpha - q_2)\right) - \cos(\alpha - q_2) \tag{16}$$

et dépend fortement de la variable articulaire q_2 et le pré-chargement initial du ressort du compensateur décrit par paramètre s_0.

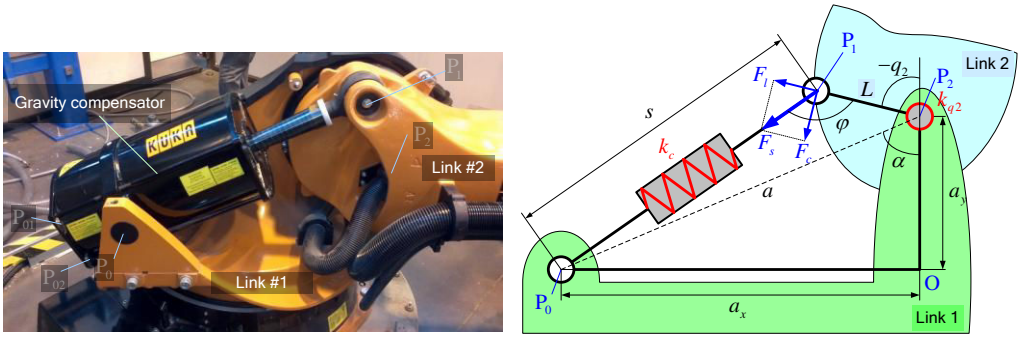

(a) gravity compensator of KUKA KR-270 robot (b) model of gravity compensator

Figure 10. Compensateur de gravité et son modèle

La structure géométrique du compensateur de gravité est représentée par la Figure 10b. Ses principaux paramètres sont L, a_x, a_y. Le problème d'identification correspondant peut être résolu en deux étapes. La première étape est consacrée à la détermination de l'emplacement relatif des points P_1 et P_2. Ici, pour différentes valeurs des variables articulaires q_{2i}, à l'aide d'un laser tracker nous avons obtenu les positions $\{\mathbf{p}_1^i\}$ qui décrivent des points d'arc. Après avoir fait correspondre ces points avec un cercle, on peut obtenir la valeur désirée de L (le rayon du cercle). La deuxième étape concerne l'identification de la position relative des points P_0 et P_2. L'information pertinente est extraite à partir des données $\{\mathbf{p}_{01}^i\}$ et $\{\mathbf{p}_{02}^i\}$ qui sont fournies par le laser tracker, en ciblant les marqueurs P_{01} et P_{02}. Ici, les points sont appariés aux deux arcs de cercles de même centre. Les valeurs désirées a_x, a_y sont calculées comme une projection du vecteur de différence $\mathbf{a} = \mathbf{p}_2 - \mathbf{p}_0$.

Pour le problème d'identification, les variables de conception sont les angles $\{\mathbf{q}_{2i}\}$ et les emplacements des marqueurs. Les fonctions objectives à minimiser sont calculées via la matrice de covariance qui décrit les erreurs d'identification des paramètres géométriques L et a à estimer. Pour le point P_2, les conditions optimales sont $\sum_{i=1}^{m}\cos q_{2i} = 0$ et $\sum_{i=1}^{m}\sin q_{2i} = 0$. Pour le point P_0, les conditions optimales sont $\sum_{j=1}^{k}\cos\beta_j = 0$ et $\sum_{j=1}^{k}\sin\beta_j = 0$.

Pour tenir en compte de l'influence du compensateur, tout en conservant notre approche développée pour les robots sériels sans compensateur, il est proposé d'inclure dans la seconde articulation un ressort virtuel équivalent avec une raideur non-linéaire en fonction de la variable articulaire q_2. Grâce à cette idée, il est commode de considérer plusieurs paramètres indépendants correspondant à chaque valeur de q_2. Notons les paramètres désirés $k_1, (k_{21}, k_{22}...), k_3, ..., k_6$ comme le vecteur $\mathbf{k}$, ce qui nous permet de présenter la relation de force- déviation sous la forme

$$\Delta \mathbf{p}_i = \mathbf{B}_i^{(p)} \mathbf{k} \tag{17}$$

où les matrices $\mathbf{B}_i^{(p)}$ sont composées d'éléments de la matrice d'observation $\mathbf{A}_{ki}$ qui est habituellement utilisée dans l'analyse de la raideur des manipulateurs sériels. En utilisant ces notations, les paramètres élasto-statiques désirés peuvent être obtenus par :

$$\mathbf{k} = \left(\sum_{i=1}^{m} \mathbf{B}_i^{(p)T} \mathbf{B}_i^{(p)} \right)^{-1} \cdot \left(\sum_{i=1}^{m} \mathbf{B}_i^{(p)T} \Delta \mathbf{p}_i \right) \tag{18}$$

Ensuite, l'expression désirée peut être écrite comme suit :

$$\left[K_{\theta_2}^0 \quad K_c \quad s_0 \cdot K_c \right]^T = \left(\sum_{i=1}^{m_q} \mathbf{C}_i^T \mathbf{C}_i \right)^{-1} \left(\sum_{i=1}^{m_q} \mathbf{C}_i^T K_{\theta_{2i}} \right) \tag{19}$$

où m_q est le nombre d'angles q_2 différents,

$$\mathbf{C}_i = \left[1 \quad -aL \cdot \cos\gamma_i \quad aL/s \cdot \left(aL/s^2 \cdot \sin^2\gamma_i + \cos\gamma_i \right) \right] \tag{20}$$

ici $\gamma_i = \alpha - q_{2i}$. Ainsi, la modification proposée de la technique de calibration développée nous permet de trouver les paramètres du manipulateur et du compensateur simultanément.

Ce chapitre est consacré au renforcement des méthodes de modélisation, de mesure et d'identification utilisées pour la calibration élasto-statique de robots sériels et quasi-sériels. Les contributions sont dans le domaine de la conception d'essais de calibration, qui vise à améliorer la précision de positionnement du manipulateur utilisant un nombre limité de mesures. La limitation des résultats obtenus est liée aux questions de complétude du modèle. Néanmoins, pour le robot étudié, le modèle considéré nous a permis de compenser plus de 90% des erreurs de compliance.

CHAPITRE 4

VALIDATIONS EXPERIMENTALES DES TECHNIQUES DE SELECTION DE POSES OPTIMALES DE CALIBRATION DU ROBOT

Suite aux chapitres précédents, l'efficacité de la calibration géométrique et élasto-statique peut être améliorée par la sélection appropriée des poses de mesure utilisées dans les essais de la calibration. Dans ce travail, un certain nombre de techniques numériques ont été proposées qui nous permettent de réduire l'impact des erreurs de mesure et de compenser les erreurs de positionnement du robot de manière optimale. Pour montrer les avantages de ces techniques, ce chapitre présente les résultats expérimentaux de la caliration géométrique et élasto-statique de notre robot KUKA KR-270.

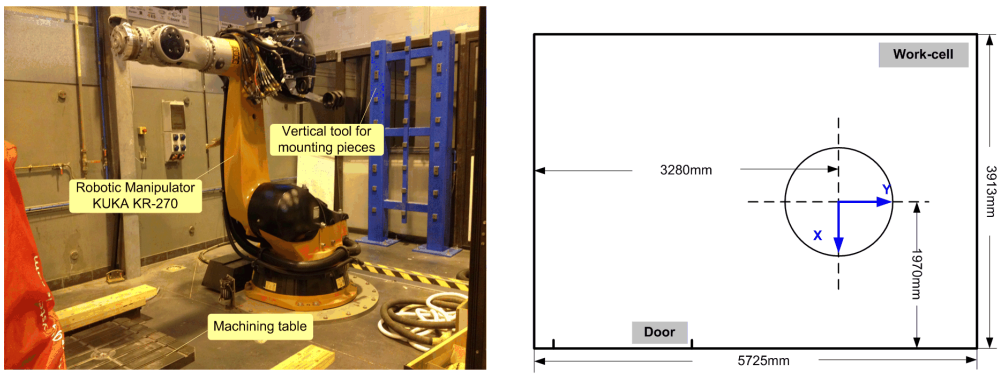

(a) General view (b) Main dimensions

Figure 11. L'environnement de cellule expérimentale: (a) vue générale; (b) la dimension principale

La cellule de fabrication, où le robot a été installé est présenté à la Figure 11, il est situé à IUT de Nantes, Carquefou. Selon le procédé d'usinage considérée, la pose test du manipulateur a été défini par $\mathbf{q}_0 = (76.7°, -56.9°, 89.3°, 45.1°, 76°, 57.2°)$ et le chargement est $\mathbf{w}_0 = (0,\ 280\text{N},\ -180\text{N},\ 0,\ 0,\ 0)$. En utilisant cette cellule robotisée, un certain nombre d'essais a été effectuée afin de calibrer les modèles du robot employées dans les algorithmes de compensation d'erreurs.

- **RESULTATS EXPERIMENTAUX POUR LA CALIBRATION GEOMETRIQUE**

En utilisant les données correspondent aux configurations optimales de mesure, la procédure d'identification en deux étapes a été appliquée. A la première étape, les transformations de base et d'outil ont été calculées, les résultats y compris deux emplacements de bases et trois positions de l'outil. A la deuxième étape, ces transformations ont été utilisées pour l'identification des paramètres géométriques du manipulateur avec une précision de 0,15 mm pour les paramètres linéaires et de 0,01 degrés pour ceux angulaires.

A des fins de comparaison, l'amélioration de la précision de manipulateur grâce à la calibration a été étudiée à base d'analyse de résidu avant et après calibration. Ici, deux types de résidus ont été examinés, ceux à base de coordonnées et de la distance. Les résultats correspondants sont présentés dans le Tableau 6. En particulier, les résidus maximum ont été réduits par un facteur de 4 et 3,5, tandis que les valeurs RMS de ces deux critères ont été réduites, respectivement, par un facteur de 5,3 et 5,5.

Tableau 6 Évaluation de l'amélioration de la précision de manipulateur basée sur l'analyse de résidus

Criterion		Before calibration	After calibration	Improvement factor
Coordinate-based residuals, [mm]	max	1.25	0.32	4.0
	RMS	0.54	0.10	5.3
Distance-based residuals, [mm]	max	1.31	0.39	3.5
	RMS	0.94	0.17	5.5

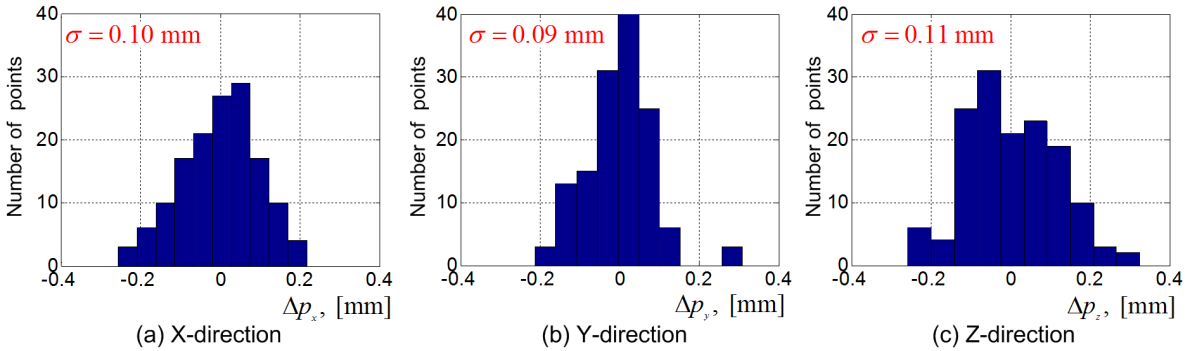

Figure 12. Histogrammes de distribution du résidu dans les directions X, Y et Z après la calibration géométrique

Afin d'évaluer les résultats de calibration, nous analyserons les résidus calculés à partir des équations d'identification pour chaque coordonnée séparément ; les histogrammes correspondants sont présentés dans la Figure 12. Les résidus ont tendance à suivre les distributions normale avec une moyenne zéro et presque le même paramètre σ. C'est ce qui justifie l'utilisation de la technique des moindres carrés ordinaires pour l'identification des paramètres et nous permet de conclure que le σ dans nos essais est égal à 0,1 mm. Les limites statistiques n'ont pas été atteintes en raison des

limitations du modèle, néanmoins, la calibration géométrique permet une amélioration essentielle de la précision du robot.

- **RESULTATS EXPERIMENTAUX POUR LA CALIBRATION ELASTO-STATIQUE**

En utilisant les données correspondent aux configurations optimales de mesure pour la calibration élasto-statique, l'identification a été effectuée par deux techniques : les moindres carrés ordinaire (MCO) et les moindres carrés pondérés (MCP). Les valeurs correspondantes des paramètres élasto-statiques sont présentées dans le Tableau 7. Les résultats montrent que les intervalles de confiance pour les MCO et MCP ont intersections pour tous les paramètres d'intérêt. En outre, les intervalles de confiance pour WLS sont toujours à l'intérieur de ceux pour les MCO et sont considérablement plus petits.

Tableau 7 Résultats d'identification pour les techniques de MCO et MCP

Parameter [rad × μm/N]	Ordinary least square		Weighted least square		Mutual location of Confidence Intervals	Improvement factor
k_1	0.623	±0.022				
k_{21}	0.297	±0.010	0.287	±0.0003		40.5
k_{22}	0.287	±0.012	0.277	±0.0004		33.2
k_{23}	0.315	±0.018	0.302	±0.0005		33.9
k_{24}	0.302	±0.032	0.293	±0.0010		33.1
k_{25}	0.251	±0.020	0.246	±0.0007		30.1
k_3	0.396	±0.031	0.416	±0.0011		28.8
k_4	3.017	±0.248	2.786	±0.0071		35.1
k_5	3.294	±0.506	3.483	±0.0120		42.0
k_6	2.248	±0.725	2.074	±0.0267		27.2

A base de valeurs obtenues pour $\{k_{21},...,k_{25}\}$, il a été identifié un paramètre équivalent k_2, qui est utilisé dans la modélisation de raideur du manipulateur avec le compensateur de gravité. Les paramètres géométriques et élasto-statiques identifiés sont présentés dans Tableau 8.

Tableau 8 Résultats d'identification des paramètres géométriques et élasto-statiques du compensateur

Geometric parameters	L, [mm]	a_x, [mm]	a_y, [mm]
Value	184.72	685.93	123.30
CI	± 0.06	± 0.70	± 0.69
Elastostatic parameters	k_c, [rad × μm/N]	s_0, [mm]	k_2^0, [rad × μm/N]
Value	0.144	458	0.302
CI	±0.031	±27	±0.004

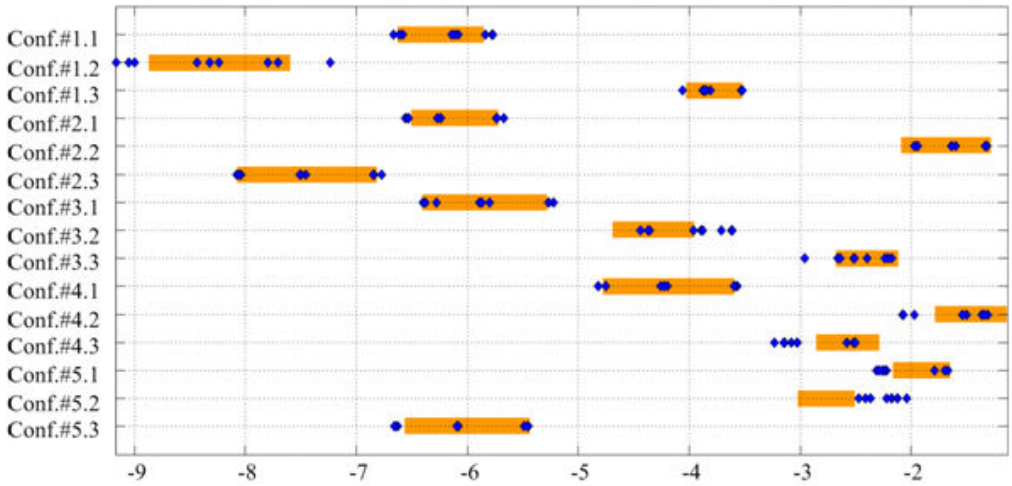

Figure 1. La distribution de déviation dans la direction de la force de gravité

En utilisant les configurations optimales de mesure, les paramètres élasto-statiques du manipulateur ont été identifiés avec la précision relative d'environ 0,7% (en moyenne). Ces résultats nous ont permis de compenser environ 95% des erreurs de compliance dans le sens de la force de gravité (voir Figure 1). La précision de positionnement sous une charge de 2.7KN est égale à 0,21 mm, ce qui est 11,1 fois meilleure que celle des robots non compensés (pour une direction arbitraire).

- **VALIDATION DE LA TECHNIQUE DE SELECTION DE POSES DEVELOPPEE**

Pour montrer les avantages de technique développée de sélection de poses optimales, la précision du manipulateur après calibration a été comparée par deux plans d'essais distincts. La première a été obtenue en utilisant la technique de calibration développée dans ce travail. Le deuxième plan utilisé configurations de mesure qui ont été sélectionnés semi-intuitivement, selon certains indices de performance cinématique.

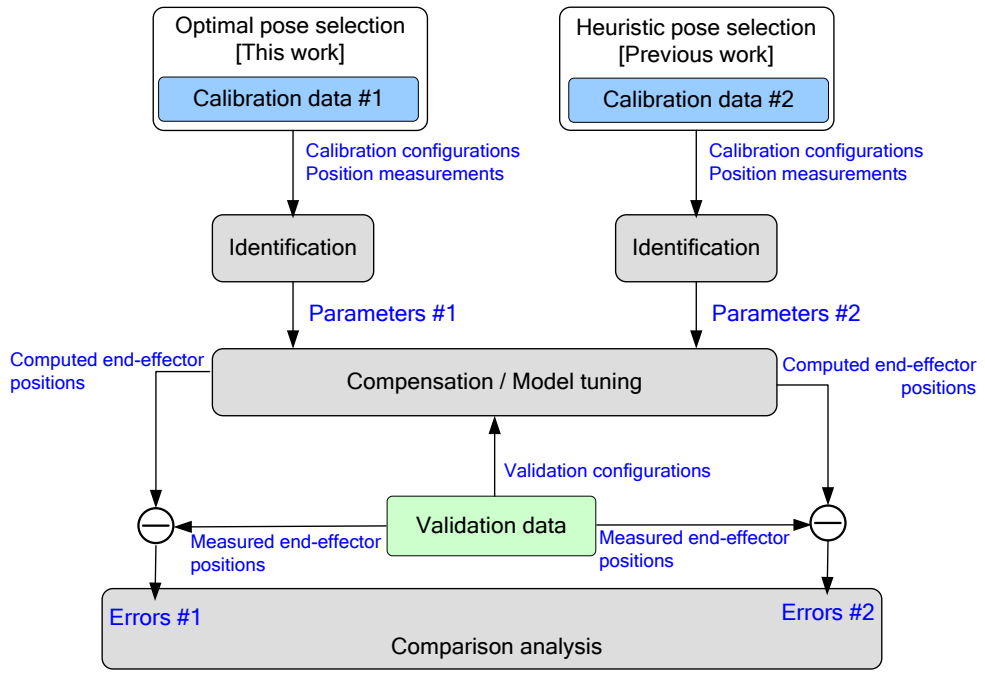

Figure 13. Schéma de validation de la technique de sélection de poses optimales développée

En utilisant ces deux données de calibration, l'identification a donné deux ensembles de paramètres différents (Tableau 9). Ensuite, les paramètres obtenus sont utilisés pour calculer les positions de l'effecteur pour les configurations de validation (différentes de celles de mesure). En comparant ces résultats avec les mesures de positionnement correspondants, il est possible d'évaluer la "qualité de calibration" et les plans d'essais. Plus en détail, le schéma de validation de la technique de sélection de poses optimales est représenté dans la Figure 13.

Tableau 9 Les paramètres élasto-statiques obtenus par des méthodes connues et développées

[µrad/Nm]	k_1	k_2	k_3	k_4	k_5	k_6
Parameters, [This work]	0.623	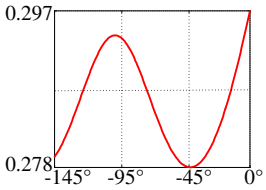	0.416	2.786	3.483	2.074
Parameters, [Previous work]	3.798	0.248	0.276	1.975	2.286	3.457

Tableau 10 L'amélioration de la précision du manipulateur après compensation d'erreur élasto-statique

Criterion		Coordinate-based residual, [mm]				
		Before compensation	After compensation		Improvement factor	
			[Previous work]*	[This work]**	[Previous work]*	[This work]**
X	max	0.79	0.51	0.46	1.5	1.7
	RMS	0.51	0.23	0.21	2.1	2.4
Y	max	1.35	0.68	0.63	1.9	2.2
	RMS	0.81	0.44	0.44	1.8	1.8
Z	max	8.06	1.63	0.43	4.9	18.7
	RMS	5.82	1.17	0.21	5.0	28.0
		Distance-based residual, [mm]				
	max	8.28	1.77	0.78	4.6	10.4
	RMS	5.90	1.27	0.53	4.6	11.1

*Using full-pose measurement method, semi-intuitively selected measurement configurations, corresponding model does not take into account the gravity compensator impact.

**Using enhanced partial pose measurement method, optimal pose selection technique and manipulator stiffness model that takes into account the gravity compensator impact.

Suite à la méthodologie de validation proposée, la précision du robot a également été évaluée en utilisant la stratégie de compensation d'erreur qui implémente les paramètres identifiés dans les travaux précédents. En comparant leurs résultats (Table 4.33), l'efficacité de la compensation a été augmentée par un facteur de 2,4 en utilisant presque le même nombre de configurations. Par conséquent, la technique de calibration développée nous permet d'augmenter sensiblement la précision de positionnement du manipulateur sous charge externe en utilisant nombre raisonnable de configurations de mesure.

CONCLUSIONS ET PERSPECTIVES

CONTRIBUTIONS DE LA THESE

Cette thèse est consacrée au renforcement des techniques de calibration de modèles géométriques et élasto-statiques pour des robots industriels utilisés pour l'usinage de pièces de grandes dimensions. Une attention particulière est accordée à l'amélioration de la précision de positionnement du robot au moyen de la compensation des erreurs géométriques et élasto-statiques. Les principales contributions sont dans le domaine de la définition d'essais pour la calibration (la sélection de poses optimales de mesure), ce qui permet de réduire l'impact du bruit de mesure et d'atteindre une précision désirée à l'aide d'un petit nombre d'essais de la calibration. Plus en détail, les principales contributions théoriques sont résumées comme suit:

(i) Une *nouvelle approche pour la définition d'essais pour la calibration* de robots sériels et quasi-sériels. Cette approche utilise une nouvelle mesure de performance orientée vers l'industrie, qui évalue la qualité du plan de calibration via la précision de positionnement du manipulateur après compensation d'erreurs géométrique et élasto-statique, et prend en compte les exigences industrielles de la tâche de fabrication prescrit (en utilisant une ou plusieurs configurations tests). Il est démontré que la mesure de performance proposée peut être présentée comme la trace pondérée de la matrice de covariance, où les coefficients de pondération sont définis par la configuration test correspondante. Cette approche nous permet de trouver les configurations optimales de mesure pour des essais de calibration et d'améliorer essentiellement la précision de positionnement du robot pour une configuration test.

(ii) *Renforcement de la méthode de mesure de poses partielles*, qui utilise directement des mesures de positions de plusieurs points de référence de l'effecteur à l'aide d'un système de mesure externe. Il permet d'éviter des calculs supplémentaires des composants d'orientation de l'effecteur, qui causent la non-homogénéité dans les équations d'identification et ne nécessitent pas de normalisation (qui se pose dans le cas où les coordonnées de la position et l'orientation sont utilisées). Il a été démontré que cette méthode permet d'augmenter la précision de l'identification des paramètres.

(iii) Approche de modélisation de la raideur pour les manipulateurs *quasi-sériel avec compensateurs de gravité* qui induit des chaînes cinématiques fermées. L'approche proposée est basée sur une extension du modèle conventionnelle de la raideur du manipulateur sériel en y incluant certains paramètres élasto-statiques dont les valeurs dépendent de la configuration du robot (qui sont généralement traitées comme constantes). La méthodologie correspondante pour la calibration des modèles de compensateur de gravité proposée, est capable d'identifier les paramètres géométriques et élasto-statiques. Contrairement à d'autres travaux, elle est basée sur la décomposition en valeurs singulières et utilise les informations de mesure obtenue à partir de capteurs de position et des codeurs.

Les résultats théoriques obtenus ont été validés par l'étude expérimentale qui traite de la calibration géométrique et élasto-statique de notre robot industriel KUKA KR -270 utilisé pour le fraisage de pièces de grandes dimensions dans l'industrie aéronautique. Les paramètres identifiés nous ont permis de décrire à la fois les propriétés géométriques et élasto-statiques du manipulateur avec compensateur de gravité. Les modèles obtenus ont été utilisés pour la compensation d'erreur de

positionnement au cours du processus de fraisage. Pour le mode déchargé, les résultats de calibration nous ont permis d'améliorer la précision de positionnement du manipulateur par un facteur de 5,5 par rapport au robot non-calibré. Pour le mode chargé, la précision de positionnement correspondant chargé sous la force de 2.7kN est 11,1 fois meilleure que celle des robots non compensée. Par rapport aux travaux antérieurs consacrés à un problème similaire, le robot sous la charge est de 2,4 fois plus précise en raison de la sélection correcte de la pose de mesure (avec le même nombre de configurations utilisées pour les essais de calibration).

LIMITES DE RÉSULTATS OBTENUS

En dépit des avantages essentiels, l'approche développée a certaines limites qui sont principalement liées aux hypothèses de modélisation des manipulateurs et à la technique de calibration utilisée dans ce travail. Elles sont résumées comme suit:

Limites des hypothèses de modélisation des manipulateurs:

(i) On a supposé que la compliance du manipulateur est principalement due à l'élasticité des articulations et le modèle de raideur ne comprend que des ressorts virtuels unidimensionnels. Néanmoins, dans le cas général, la raideur du corps doit également être prise en compte. Cela produit un modèle de raideur plus sophistiqué, où les compliances des couples corps/liaison sont décrits par des matrices 6×6 qui peuvent être difficilement identifiés en utilisant la procédure de la calibration considérée dans ce travail.

(ii) On a supposé que la force externe est appliquée à l'effecteur du robot seulement. Néanmoins, dans certains cas, l'influence des poids des corps doit également être prise en compte si elles induiront des déformations non négligeables dans les composants élastiques de manipulateur. Cela nécessite une révision du modèle élasto-statique utilisé dans ce travail.

(iii) On a supposé que d'autres sources d'erreurs de positionnement (différents de ceux géométriques et élasto-statiques) sont négligeables. Ils comprennent friction/ contrecoup dans les articulations, les effets thermiques, les facteurs environnementaux, etc. Dans certains cas, ils peuvent également affecter la précision de positionnement du manipulateur et doivent être pris en compte.

Limites de la technique de calibration:

(iv) L'approche développée pour la sélection de poses optimales de mesure est basée sur la notion de configuration(s) test, pour lesquels la précision du robot est évaluée (après compensation d'erreur). Cependant, il n'est pas évident que la même précision de manipulation peut être atteinte pour d'autres points de l'espace de travail.

(v) La technique de mesure utilisée à l'aide d'un laser tracker, fournissant les coordonnées Cartésiennes pour les points de référence pertinents. Ce type de système de mesure est généralement très cher et impose certaines limites pour l'essais de la calibration en raison de la problème de la visibilité. Comme une alternative, une autre technique de mesure peut être utilisée (la méthode en boucle fermé, par exemple) mais les expressions pertinentes devraientt être révisées, et l'origine des erreurs de mesure doit être redéfinie. En outre, dans le cadre de ce travail, on a supposé que les erreurs de

mesure proviennent du laser tracker seulement, tandis que d'autres sources telles que les erreurs codeurs et appareils de mesure d'efforts ont été négligés.

Pourtant, pour les applications considérées, les limites concernant les hypothèses du modèle ne sont pas critiques, car la précision désirée a été atteinte dans l'étude expérimentale. En outre, il est possible d'étendre/modifier l'approche développée dans le but d'adapter d'autres techniques de mesure. Cependant, certaines des limites mentionnées ci-dessus nous donnent des directions de recherche pour les travaux futurs.

PERSPECTIVES ET TRAVAUX FUTURS

Pour généraliser les résultats obtenus et élargir le domaine d'application, il est raisonnable de poursuivre les recherches dans plusieurs directions et de se concentrer sur les questions suivantes:

(i) Le renforcement de la technique développée pour la sélection de poses optimales pour le cas où les propriétés de la raideur du manipulateur sont décrits par des matrices qui décrivent l'élasticité des corps et des liaisons. Certains problèmes découlant comprennent la synthèse de complètude, irréductibibilité de modèle élasto-statique pour les robots manipulateurs et les questions d'identifiabilité des paramètres.

(ii) L'extension de la famille de compensateurs de gravité inclus dans le modèle de raideur du manipulateur. Les problèmes pertinents comprennent le développement de modèles mathématiques qui décrivent l'élasticité du compensateur (en tenant compte de l'influence du vérin pneumatique, par exemple), les méthodologies et les algorithmes d'identification des paramètres du modèle, et la détermination d'essais de calibration. Il est également intéressant d'étendre/généraliser la technique pour la calibration de robots quasi-sériels, qui comprennent des chaînes cinématiques fermées dans le cas général.

(iii) Le développement d'une technique permettant aux utilisateurs de générer automatiquement des configurations tests (utilisées dans l'approche proposée) à partir de la description basée sur la CAO du procédé d'usinage. Cette technique devrait être intégrée dans le logiciel de simulation fournissant la conception optimale d'essais et le placement optimal de la pièce par rapport au robot manipulateur.

CONTENTS

Acknowledgements ..... **- 3 -**
Résume et mots clés ..... **- 5 -**
Abstract and keywords ..... **- 6 -**
Résumé en français ..... **- 7 -**
List of tables ..... **- 35 -**
List of figures ..... **- 37 -**
General introduction **1**
Chapter 1 Manipulator modeling for robotic-based machining and identification of the model parameters **5**
1.1 Robotic-based machining of large dimensional parts 6
1.1.1 Modern trends in machining 6
1.1.2 Industrial requirements for machining accuracy 8
1.1.3 Robot application for machining operation 9
1.1.4 Robot errors and their compensation in machining application 12
1.2 Manipulator geometric model and identification of its parameters 14
1.2.1 Manipulator geometric modeling 14
1.2.2 Geometric model suitable for identification 17
1.2.3 Calibration of manipulator geometric model 21
1.3 Manipulator elastostatic model and identification of its parameters 25
1.3.1 Manipulator stiffness modeling and existing approaches 25
1.3.2 Calibration of manipulator elastostatic model 28
1.4 Optimal design of experiments in calibration of manipulator models 35
1.4.1 Design of experiments for linear regression models 36
1.4.2 Limitations of conventional techniques for robot calibration 40
1.4.3 Design of experiments for robot calibration 43
1.4.4 Measurement pose selection for geometric and elastostatic calibration 45
1.5 Summary: thesis goal and research problems 49
Chapter 2 Design of experiments for calibration of manipulator geometric parameters **50**
2.1 Introduction 51
2.2 Manipulator geometric modeling 54
2.2.1 Complete, irreducible geometric model for serial manipulator 54
2.2.2 Linearization of the manipulator geometric model 58
2.3 Measurement methods in robot calibration 61
2.3.1 Existing measurement methods 62
2.3.2 Enhancing of partial pose measurement method 66
2.4 identification of model parameters 70
2.4.1 Identification algorithm for the enhanced partial pose method 70
2.4.2 Influence of the measurement errors on the identification accuracy 73
2.5 Optimal selection of measurement configurations 74
2.5.1 New approach for calibration experiment design 74
2.5.2 Generalization for the case of multiple test configurations 77
2.5.3 Comparison analysis of proposed and conventional approaches 78
2.6 Efficiency improvement of measurement pose selection 82
2.6.1 Analysis of the conventional numerical optimization techniques 82
2.6.2 Hybrid approach to optimal configuration selection 84
2.6.3 Quasi-optimal solution for measurement configuration selection 86
2.7 Summary 88

Chapter 3 Design of experiments for calibration of manipulator elastostatic parameters 90
3.1 Introduction 91
3.2 Manipulator elastostatic modeling 93
3.2.1 Stiffness modeling background 93
3.2.2 Stiffness model suitable for calibration 96
3.3 Measurement methods for elastostatic calibration 99
3.3.1 Conventional measurement methods 99
3.3.2 Enhanced partial pose measurement method in elastostatic calibration 102
3.4 Identification of elastostatic parameters 106
3.4.1 Identification algorithm for the enhanced partial pose method 106
3.4.2 Influence of the measurement errors on the identification accuracy 109
3.4.3 Weighted least square technique for elastostatic calibration 110
3.5 Optimal selection of measurement configurations 112
3.5.1 Extension of the test-pose based approach for elastostatic calibration 112
3.5.2 Generalization for the case of multiple test configurations 115
3.5.3 Evaluation of the test-pose based approach for elastostatic calibration 116
3.5.4 Efficiency improvement of measurement pose selection 119
3.6 Elastostatic calibration for heavy industrial robots with gravity compensators 121
3.6.1 Mechanics of gravity compensator 122
3.6.2 Identification of gravity compensator geometric parameters 123
3.6.3 Identification of gravity compensator elastostatic parameters 128
3.7 Summary 132
Chapter 4 Experimental validations of developed optimal pose selection techniques for robot calibration 134
4.1 The experimental work-cell environment 135
4.2 Geometric calibration experiments for KUKA KR-270 industrial robot 137
4.2.1 Experimental setup and measurement procedure 137
4.2.2 Optimal measurement pose selection for geometric calibration 140
4.2.3 Identification of manipulator geometric parameters 144
4.2.4 Analysis of the identification results for geometric calibration 147
4.3 Elastostatic calibration experiments for KUKA KR-270 industrial robot 149
4.3.1 Experimental setup and measurement procedure 149
4.3.2 Identification of the gravity compensator geometry 153
4.3.3 Identification of manipulator elastostatic parameters using the gravity force 156
4.3.4 Identification of manipulator elastostatic parameter using work-cell constraints 161
4.3.5 Analysis of the identification results for elastostatic calibration 164
4.4 Validation of the developed pose selection technique 167
4.4.1 Validation methodology 167
4.4.2 Validation of the developed technique for geometric calibration 170
4.4.3 Validation of the developed technique for elastostatic calibration 171
4.5 Summary 174
Conclusions and perspectives 175
Contributions of the thesis 175
Limitations of obtained results 176
Perspectives and future work 177
Publications of thesis contributions 177
References 179

LIST OF TABLES

Table 1.1 Summary of existing parameterization methods in manipulator geometric modeling 17

Table 1.2 Particularities and difficulties of the elastostatic calibration 31

Table 1.3 Summary of the review on elastostatic calibration 35

Table 1.4 Optimal plans of experiments for one- and two-variable models 38

Table 1.5 Different plans of calibration experiments and corresponding covariance matrices (case of a two-link manipulator $\lambda_i = 1/l_i,\ i = 1,2$) 43

Table 1.6 Comparison of measurement poses for geometric calibration 46

Table 1.7 Comparison of measurement poses results for elastostatic calibration 47

Table 1.8 Summary of the existing approaches to calibration experiment design 48

Table 2.1 Nominal geometric parameters of KUKA KR270 industrial robot 56

Table 2.2 Elementary homogeneous transformation matrices and their derivatives 59

Table 2.3 Matrix derivatives for geometric model of robot KUKA KR270 61

Table 2.4 Summary of different measurement methods 65

Table 2.5 Comparison of different measurement methods and their influence on the identification accuracy (number of iterations : 1000; number of configurations : 3; $\sigma = 0.01$mm) 69

Table 2.6 Accuracy comparison of the proposed and conventional approaches 80

Table 2.7 Accuracy of conventional optimization techniques (case of 6-dof manipulator, initial points are random) 83

Table 2.8 Computational time of examined optimization techniques (case of 6-dof manipulator) 83

Table 2.9 Reduction of computational time using parallel computing 85

Table 2.10 Efficiency of the quasi-optimal solutions (evaluated via ρ_0) for calibration experiment design problem: case of a 6-dof manipulator, repetitions of measurements 87

Table 3.1 Force application methods and measurement equipments used in existing works 101

Table 3.2 Comparison of manipulator accuracy after calibration for different principles for the measurement pose selection (2-dof planar manipulator, measurement noise $\sigma = 0.1$ mm) 119

Table 3.3 Comparison of quasi-optimal and optimal solutions for measurement pose selection for elastostatic calibration (case of 6-dof manipulator, total number of measurements $m = 12$) 120

Table 3.4 Efficiency improvement factors for applying different heuristic techniques (case of optimal pose selection with 12 measurements) 121

Table 4.1 Example of measurement data structure (for a single manipulator configuration) ... 140

Table 4.2 The joint limits of robot KUKA KR-270 141

Table 4.3 The work-cell space boundaries with respect to the robot base frame 141

Table 4.4 Optimal measurement configurations for geometric calibration 142

Table 4.5 Comparison of calibration plans with different diversity of measurement configurations 143

Table 4.6 Laser tracker placements for different reference points and measurement configurations 144
Table 4.7 Identification results for manipulator base transformations (for geometric calibration) 145
Table 4.8 Identification results for manipulator tool transformations (for geometric calibration) 145
Table 4.9 Identification results for manipulator geometric parameters 146
Table 4.10 Evaluation of the manipulator accuracy improvement based on residual analysis.... 147
Table 4.11 Positioning errors after geometric calibration for each measurement configuration. 149
Table 4.12 Example of the measurement data structure (for a single manipulator configuration) 153
Table 4.13 Measurement data for the marker point coordinates for different values of q_2 155
Table 4.14 Identification results for the compensator geometric parameters 156
Table 4.15 The work-cell space boundaries for elastostatic calibration 157
Table 4.16 Optimal measurement configurations for elastostatic calibration 158
Table 4.17 Dispersions of the deflection measurements for different configurations and directions 159
Table 4.18 Identification results for manipulator base and tool transformations 159
Table 4.19 Identification results for ordinary and weighted least square techniques 160
Table 4.20 Comparison of the ordinary and weighted least square techniques 160
Table 4.21 Identification results for the compensator elastostatic parameters 161
Table 4.22 Evaluation of the manipulator accuracy improvement based on residual analysis.... 161
Table 4.23 Measurement configurations for calibration of elastostatic parameter k_1 162
Table 4.24 Specifications of the ATI Theta IP68 force/torque sensor..... 163
Table 4.25 Identification result of elastostatic parameter k_1 164
Table 4.26 Positioning errors after elastostatic calibration for each measurement configuration 167
Table 4.27 Evaluation of the elastostatic parameters identification accuracy impact on the end-effector positioning accuracy..... 167
Table 4.28 Manipulator configurations for validation of the calibration results 168
Table 4.29 Manipulator elastostatic parameters obtained using known and developed approaches 169
Table 4.30 Positioning errors after geometric compensation for each validation configuration (subset #2, without loading) 171
Table 4.31 The manipulator accuracy improvement after geometric error compensation 171
Table 4.32 Positioning errors after elastostatic calibration for each validation configuration (subset #2, under loading)..... 173
Table 4.33 The manipulator accuracy improvement after elastostatic error compensation 173

LIST OF FIGURES

Figure 1.1 Influencing factors in the machining process (Garant, 2010) 6

Figure 1.2 Modern machining technologies and their comparison for the same material removal volume (Garant, 2010) 7

Figure 1.3 Typical tolerances of different machining processes (DML) 8

Figure 1.4 Statistical overview of the use of industrial robots (Guizzo, 2008) 9

Figure 1.5 End of line robotic palletizer (ICC.com) 9

Figure 1.6 The new PowerMill robot interface for multi-axis machining operations (Delcam, 2013) 10

Figure 1.7 The Great Wall motors robotic assembly line (Murray, 2012) 10

Figure 1.8 Automatic robot welding of complex ship sections (Kranendonk.com) 10

Figure 1.9 Robot performs non-destructive inspection on a Boeing 787 (Waurzyniak, 2013) 11

Figure 1.10 Machining experiment (Dumas, 2011) 11

Figure 1.11 Differences between the desired trajectory and the obtained ones with and without error compensation (Dumas, 2011) 12

Figure 1.12 Classification of robot errors in machining applications 13

Figure 1.13 The schematic representation of manipulator geometric model. 14

Figure 1.14 Existing parameterization methods for consecutive revolute joints 17

Figure 1.15 Robot control strategies with different errors compensation techniques 23

Figure 1.16 The "mirror" strategy for error compensation 24

Figure 1.17 Serial industrial robot and its VJM-based stiffness model 26

Figure 1.18 Off-line compliance errors compensation strategy 30

Figure 1.19 Experimental setups of elastostatic calibration 33

Figure 1.20 The linear regression model 36

Figure 1.21 Two-link planar manipulator 40

Figure 1.22 The Pareto-optimal solutions (normalized with respect to $\lambda_1\lambda_2$, assuming $\lambda_1 = \lambda_2 = 1$) 42

Figure 1.23 Identification accuracy for different approaches to calibration experiments design 47

Figure 2.1 The schematic of robot calibration procedure 52

Figure 2.2 Manipulator segment with perpendicular and parallel axes 55

Figure 2.3 The industrial serial robot KUKA KR270 and its geometric model. 55

Figure 2.4 Classification of the existing measurement techniques for manipulator calibration 62

Figure 2.5 Open-loop measurement methods and related external devices. 63

Figure 2.6 Closed-loop measurement methods. 64

Figure 2.7 Typical manipulator mounting flange with several reference points 66

Figure 2.8 Input data for two identification approaches 68

Figure 2.9 Dispersion of the manipulator positioning errors after calibration and performance measure for selection of measurement configurations (for given single target point). 75

Figure 2.10 Performance measure for selection of measurement configurations that ensure high precision along the given trajectory 77

Figure 2.11 Dispersion of manipulator positioning errors after calibration for different plans of experiments: case of tuning two parameters $\{\Delta l_1, \Delta l_2\}$ 81

Figure 2.12 Dispersion of manipulator positioning errors after calibration for different plans of experiments: case of tuning four parameters $\{\Delta l_1, \Delta l_2, \Delta q_1, \Delta q_2\}$ 81

Figure 2.13 Efficiency of genetic algorithm for selection of three measurement poses for 6-dof manipulator (population size 50, generation number 20) 84

Figure 2.14 Efficiency of the hybrid approach for selection of three measurement poses for 6-dof manipulator (combination of parallel gradient search and parallel genetic algorithm) 85

Figure 2.15 Comparison of quasi-optimal and optimal solutions for selection of measurement configurations for robot calibration 87

Figure 3.1 Schematics of robot elastostatic calibration procedure 92

Figure 3.2 Serial manipulator and its VJM-based elastostatic model 94

Figure 3.3 Serial industrial robot KUKR KR270 and its VJM-based stiffness model 98

Figure 3.4 Measurement methods for elastostatic calibration 99

Figure 3.5 Mechanisms for the force/torque application using the gravity force 101

Figure 3.6 Measurement steps for elastostatic calibration (steps 1 to 4) 104

Figure 3.7 End-effector and force measurement device used for elastostatic calibration experiments 105

Figure 3.8 Three-step algorithm for manipulator elastostatic parameters identification 108

Figure 3.9 Dispersion of the manipulator positioning errors after calibration (for a given machining configuration and test loading) 112

Figure 3.10 A typical machining configuration and a measurement configuration 114

Figure 3.11 Definition of the performance measure for selection of measurement configurations that ensures high precision along the given trajectory 115

Figure 3.12 The test pose and corresponding optimal measurement configurations for 2-dof planar manipulator 117

Figure 3.13 Selection of optimal measurement configuration for a given test pose (case of 2-dof planar manipulator, identification of two parameters $k_{\theta 1}, k_{\theta 2}$ from a single measurement providing deflections $\Delta p_x, \Delta p_y$) 118

Figure 3.14 The Pareto-optimal solutions with respect to the criteria $\sigma_{k_1}, \sigma_{k_2}$ and ρ_0 118

Figure 3.15 Gravity compensator and its model 122

Figure 3.16 Variation of the gravity compensator impact on the equivalent stiffness of the second joint 123

Figure 3.17 Geometric parameters of the gravity compensator and location of the measurement points labeled with markers 124

Figure 3.18 End-effector used for elastostatic calibration experiments 129

Figure 4.1 The experimental work-cell environment: (a) general view; (b) main dimensions ... 135

Figure 4.2 The machining configuration (test-pose) and the workpiece location 136

Figure 4.3 Experimental setup for manipulator geometric calibration 138

Figure 4.4 Locations of the laser tracker in the work-cell (LT1 and LT2) 138
Figure 4.5 Manipulator base frame calibration using work-cell environment 139
Figure 4.6 Intersection of manipulator workspace and work-cell boundaries 141
Figure 4.7 Residual distribution after geometric calibration for different measurement configurations 147
Figure 4.8 Histograms of residual distribution along X-, Y-, and Z-directions after geometric calibration 148
Figure 4.9 Experimental setup for manipulator elastostatic calibration 150
Figure 4.10 Laser tracker placement used in elastostatic calibration 151
Figure 4.11 Manipulator base frame calibration using robot movements 152
Figure 4.12 Calibration of the laser tracker base frame location for identification of gravity compensator geometry 154
Figure 4.13 The marker point locations on the gravity compensator 156
Figure 4.14 The work-cell arrangement for elastostatic calibration 157
Figure 4.15 Compliance of equivalent non-linear spring in the second joint 161
Figure 4.16 Experimental setup for calibration of elastostatic parameter k_1 162
Figure 4.17 Residual distribution after elastostatic calibration for different measurement configurations 164
Figure 4.18 Histograms of residual distribution along X-, Y-, and Z-directions after elastostatic calibration 164
Figure 4.19 Distributions of the manipulator end-effector deflections along X, Y, and Z directions: ♦ - experimental data; - computations based on the identified parameters 166
Figure 4.20 Validation scheme for the calibration results 168
Figure 4.21 Validation scheme for the developed optimal pose selection technique 169
Figure 4.22 Geometric error distribution for validation configurations (from subset #2) 170
Figure 4.23 Histograms of error distribution along X, Y, and Z directions after geometric calibration (for validation configurations, data subset #2) 170
Figure 4.24 Elastostatic error distributions for validation configurations (from subset #2) 172
Figure 4.25 Histograms of error distribution along X-, Y-, and Z-directions after elastostatic calibration (for validation configurations, data subset #2) 172

GENERAL INTRODUCTION

Motivation. At present, the automotive, shipbuilding and aerospace industries progressively replace the conventional CNC machines by robotic manipulators to perform numerous manufacturing tasks. Generally, industrial robots are considered to be very competitive due to their manufacturing flexibility, large workspace, cost-effectiveness, etc. At the same time, the robotic-based machining introduces some difficulties. For instance, in the case when robot is under substantial external loading, the compliances in links and joints become non-negligible. So, in order to achieve high processing accuracy, essential revision of relevant mathematical models and control strategies are required, which are in the focus of this thesis.

For the manufacturing processes considered in this work, the robotic manipulator usually works under significant loading, which is generated during the machining process. This loading is often high enough to cause essential deformations in the elastic components of an industrial robot (particularly with a serial architecture). The corresponding *compliance errors* depend on both the external loading and robot elastostatic properties. They highly influence the quality of final machined product. On the other hand, for the industrial applications where the external forces applied to the manipulator end-effector are relatively small, the prime source of the manipulator inaccuracy is the *geometric errors*. These errors are associated with the differences between the nominal and actual values of the link/joint parameters. They can be also induced by the non-perfect assembling of different links and lead to shifting and/or rotation of the frames associated with different elements, which are normally assumed to be matched and aligned. In these cases, to achieve the desired positioning accuracy for robotic-based machining, corresponding mathematical models should be carefully calibrated before being employed in the control algorithms. For this reason, enhancement in manipulator geometric and stiffness modeling, as well as accuracy improvement in identification of the model parameters, become crucial issues.

In the literature, the problem of manipulator model calibration has been in the focus of the research community for several decades. Most of the efforts have been made for manipulator geometric calibration, which has been studied from different aspects (modeling and measurement methods, identification algorithms, etc) (Elatta et al., 2004; Hollerbach, 1989; Mooring et al., 1991). Currently, more and more attention is paid to the elastostatic calibration, but the majority of the related works focus on the development of simplified stiffness models and the use of conventional identification techniques (Alici and Shirinzadeh, 2005; Meggiolaro et al., 2005; Nubiola and Bonev, 2012). The robotic team of IRCCyN laboratory (where this thesis has been done) has had essential contributions in the area of robot calibration, including a number of theoretical/practical works and software packages for robot geometric modeling "SYMORO+" and calibration "GECARO" (Khalil and Creusot, 1997; Khalil and Lemoine, 1999), methodologies for joint stiffness identification (Gautier et al., 2011), stiffness modeling of overconstrained manipulators (Pashkevich et al., 2009a) and also some works related to the identification of the dynamic parameters (Gautier and Briot, 2013). This thesis uses this background and focuses on the manipulator model accuracy improvement.

In spite of numerous works devoted to robot calibration, the issues of the identification accuracy improvement and reduction of the measurement noise impact have not found enough attention in the literature; only limited number of works directly addressed these problems (Hollerbach et al., 2008; Sun and Hollerbach, 2008b). One way to improve the identification accuracy without increasing the number of calibration experiments is preliminary *optimization of the measurement configurations* (so-called design of experiments). This approach has been considered in several works (Borm and Meng,

1991; Daney, 2002; Khalil et al., 1991), where the authors adapted the idea of optimal plan of experiments (which was originally developed for linear regression models) to robot calibration for selection of the optimal measurement configurations. To define the optimal plan, numerous quantitative performance measures have been proposed. However, the majority of existing performance measures have their limitations that affect the calibration accuracy. Moreover, they do not entirely correspond to the industrial requirements and operate with abstract notions. For this reason, it looks rather promising to develop a new problem-oriented performance measure for measurement pose selection, which is related directly to the industrial requirements of relevant machining processes and aims at improving robot positioning accuracy after calibration.

Thesis goal and research problems. The thesis focuses on the enhancement of robot calibration techniques for geometric and elastostatic parameters in order to improve the accuracy and efficiency of error compensation for robotic-based machining of large dimensional parts by means of optimal design of calibration experiments (to reduce the measurement error impact). To achieve this goal, the following problems are addressed and have to be solved:

Problem 1:

> Development of a new problem-oriented performance measure for robot calibration experiment design and related optimization algorithms that ensure required accuracy for the industrial applications considered in this thesis.

Problem 2:

> Development of advanced geometric and elastostatic models for heavy industrial robots employed in machining of large dimensional parts, which allow taking into account the particularities of the manipulators with gravity compensators.

Problem 3:

> Experimental validation of the developed calibration technique and its application for the identification of geometric and elastostatic model parameters for robotic work-cell employed in machining of large dimensional parts for aerospace industry.

Thesis organization. To address the above defined research problems, the thesis is organized as follows:

Chapter 1 is devoted to the state of the art and literature review on the particularities of robotic-based machining and describes existing techniques for manipulator geometric and elastostatic calibration. Particular attention is paid to robot application for machining of large dimensional parts, determination of corresponding industrial requirements, the analysis of current works in robot calibration that employ the idea of experiment design. The main purpose of this chapter is to show the limitation of existing calibration techniques and the necessity of enhancing these techniques, which allow us to define the goal and the research problems of the thesis.

Chapter 2 focuses on the design of experiments for calibration of manipulator geometric parameters. Particular attention is paid to the enhancement of measurement and optimization techniques employed in geometric calibration of serial industrial robots. It presents a complete, irreducible geometric model for serial manipulator, which takes into account different sources of error (link lengths, joint offsets, etc). In contrast to other works, it proposes a new industry-oriented performance measure for optimal measurement configuration selection and improves the partial pose measurement technique via using only the direct measurement data from the external device. This new

approach aims at finding the calibration configurations that ensure the best robot positioning accuracy after geometric error compensation. In this chapter, several simulation examples illustrate the benefits of the developed pose selection technique and corresponding accuracy improvement.

Chapter 3 is devoted to the design of experiments for calibration of manipulator elastostatic parameters. Particular attention is paid to the enhancement of modeling, measurement and identification methods employed in the elastostatic calibration of heavy industrial robots of serial architecture, taking into account the particularity of the close-loop chain created by the gravity compensator. It presents the enhanced partial pose measurement method for the case of elastostatic calibration and applies the weighted least square technique for corresponding parameter identification. In this chapter, the proposed performance measure is extended for the case of optimal measurement configurations selection in elastostatic calibration experiments. In contrast to previous works, the developed manipulator stiffness model is able to take into account the impact of the gravity compensator.

Chapter 4 deals with experimental validation of the developed optimal pose selection technique employed in the calibration procedure, where particular attention is paid to the positioning accuracy improvement of KUKA KR-270 industrial robot (that includes a gravity compensator). It presents the work-cell environment where the calibration experiments are carried out. For both the manipulator geometric and elastostatic calibration, the experimental setups and measurement procedures, optimal measurement configurations and relevant identification results as well as the accuracy analysis are provided. In contrast to other works, the manipulator accuracy is evaluated not only for the measurement configurations, but also for a wider set of configurations (different from those used for calibration).

Finally, *Conclusion* summarizes the main contributions of the thesis and defines perspectives for future research work.

Main contributions of the thesis. Theoretical contributions of this thesis are in the area of design of experiments for geometric and elastostatic calibration of industrial robots. The most essential results are briefly summarized below:

(i) A *new approach for calibration experiments design* for serial and quasi-serial industrial robots. This approach employs a new industry-oriented performance measure, which evaluates the quality of calibration plan via the manipulator positioning accuracy after geometric and elastostatic error compensation. It is proved that this performance measure can be presented as the weighted trace of the relevant covariance matrix. It allows us to improve essentially the robot positioning accuracy for a desired manipulator test-pose.

(ii) *Enhanced partial pose measurement method*, which uses direct measurements from the external device only and allows to avoid additional computations of orientation components that can cause non-homogeneity in relevant identification equation. It is proved that such method increases the parameter identification accuracy.

(iii) Stiffness modeling approach for quasi-serial *manipulators with gravity compensators*, which is based on an extension of the conventional stiffness model of serial manipulator by including in it some configuration dependent parameters (that are usually treated as constants). The corresponding methodology for calibration of the

gravity compensator models is proposed, which is able to identify the geometric and elastostatic parameters.

The obtained theoretical results have been validated via experimental study that deals with geometric and elastostatic calibration of KUKA KR-270 industrial robot employed in milling of large dimensional parts for aerospace industry. The identified set of parameters allowed us to describe both geometric and elastostatic properties of the manipulator and corresponding gravity compensator. The obtained models were used for positioning error compensation during the milling process.

Dissemination of research results. The main results obtained in this thesis have been published in 16 works and have been presented in 10 international conferences. Amongst them, there are three papers in international journals (Applied Mechanics and Materials, Mechanics Engineering and Automation, and Pomiary Automatyka Robotyka), three book chapters (New Trends in Mechanism and Machine Science: Theory and Applications in Engineering, Springer's Lecture Notes in Artificial Intelligence, and Springer Computational Kinematics), proceedings of 10 international conferences (IEEE International Conference on Robotics and Automation, IEEE/ASME International Conference on Advanced Intelligent Mechatronics, IFToMM European Conference on Mechanism Science, IFToMM Workshop on Computational Kinematics, ASME Biennial Conference on Engineering Systems Design and Analysis, IFAC Conference on Manufacturing Modeling, Management and Control, International Conference on Intelligent Robotics and Applications, Joint Conferences on Mechanisms and Mechanical Transmissions (MTM) and Robotics, IEEE International Conference on Methods and Models in Automation and Robotics, International Conference Mecatronics).

The scientific contribution of this thesis have been developed and validated experimentally in the framework of research projects "Modeling and control of robots for machining operation of large composite parts and friction stir welding" (COROUSSO), founded by "l'Agence Nationale de la Recherche" (ANR) and FEDER ROBOTEX, France.

CHAPTER 1

MANIPULATOR MODELING FOR ROBOTIC-BASED MACHINING AND IDENTIFICATION OF THE MODEL PARAMETERS

1.1 Robotic-based machining of large dimensional parts 6
1.1.1 Modern trends in machining 6
1.1.2 Industrial requirements for machining accuracy 8
1.1.3 Robot application for machining operation 9
1.1.4 Robot errors and their compensation in machining application 12
1.2 Manipulator geometric model and identification of its parameters 14
1.2.1 Manipulator geometric modeling 14
1.2.2 Geometric model suitable for identification 17
1.2.3 Calibration of manipulator geometric model 21
1.3 Manipulator elastostatic model and identification of its parameters 25
1.3.1 Manipulator stiffness modeling and existing approaches 25
1.3.2 Calibration of manipulator elastostatic model 28
1.4 Optimal design of experiments in calibration of manipulator models 35
1.4.1 Design of experiments for linear regression models 36
1.4.2 Limitations of conventional techniques for robot calibration 40
1.4.3 Design of experiments for robot calibration 43
1.4.4 Measurement pose selection for geometric and elastostatic calibration 45
1.5 Summary: thesis goal and research problems 49

This chapter presents a state of the art and literature review on the particularities of robotic-based machining and describes existing techniques for manipulator geometric and elastostatic calibration. Particular attention is paid to robot application for machining of large dimensional parts, determination of corresponding industrial requirements, the analysis of current works in robot calibration that employ the idea of experiment design. The main purpose of this chapter is to show the limitation of existing calibration technique and the necessity of enhancing these techniques, which allow defining the goal and the research problems of the thesis

1.1 ROBOTIC-BASED MACHINING OF LARGE DIMENSIONAL PARTS

Machining, as one of the most important manufacturing process, is widely employed in various industrial applications. In particular, in the modern automotive, shipbuilding and aerospace industry, it is often required to process some large dimensional parts of high performance materials. For such applications, the industrial robot with large workspace looks very attractive and progressively replaces the conventional CNC machines. The obvious advantages of robotic-based machining are high efficiency, low manufacturing time and cost, good flexibility and ability to follow complex trajectories. However, this new area of robotic applications creates a number of theoretical problems that have not been previously considered to be essential. This section presents some of them and focuses on manipulator positioning error compensation in machining applications.

1.1.1 Modern trends in machining

Modern trends in machining aim at improving machining efficiency while reducing the manufacturing cost. However, these two contradictive objectives motivate researchers to find a compromise that ensures high manufacturing accuracy and lower cost. This compromise can be realized by defining suitable values of the influencing factors in the machining process (Figure 1.1). The most effective ways to achieve this goal are related to the *optimization of tool path* and *enhancement of cutting technology*.

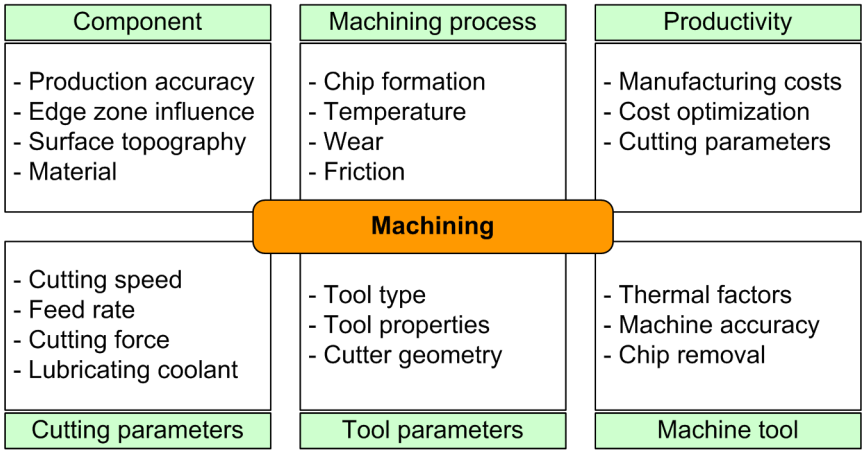

Figure 1.1 Influencing factors in the machining process (Garant, 2010)

The first approach aims at decreasing the non-cutting time (also called "airtime" (Castelino et al., 2003)) as well as minimizing the efforts in actuator drives by proper selection of the tool moving direction. As follows from the related works (Oysu and Bingul, 2009; Veeramani and Gau, 1998), the airtime can be quite significant when multiple tools are used or a number of small regions are machined. The second issue, optimization of the tool path in the manipulator workspace can be realized using kinematic criterion, which ensures smooth and fast end-effector motion along a parametric path (Nektarios and Aspragathos, 2010).

For the second approach, there have been developed several modern manufacturing techniques that are aimed towards different machining processes and different industrial applications. In relevant literature, three main trends are usually distinguished: the high speed machining (HSM), the high performance machining (HPM) and the multi task machining (MTM). The specificity of each technique may be represented by three influencing factors in the machining process: spindle speed,

machine dynamics and cutting force (Garant, 2010). They are compared in Figure 1.2 for the same volume of material removal. In more details, these techniques are described below.

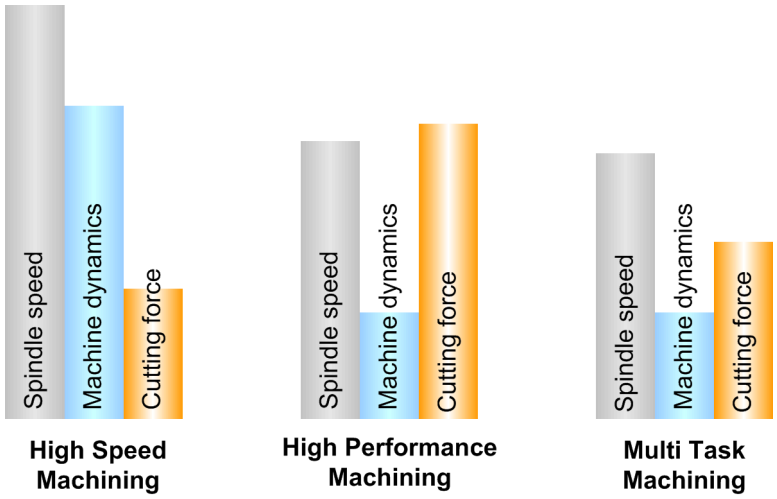

Figure 1.2 Modern machining technologies and their comparison for the same material removal volume (Garant, 2010)

High Speed Machining (HSM) means machining with *high spindle speed* (≥18000 rpm), *fast feed rate* (up to 10 m/min) and *small cutting depths* (0.25-2.5 mm, vary with machining process). It has been and will continue to be an eminent technique in the production of aerospace components, typically for the parts with very thing walls (Korn, 2005). The obvious advantage is the considerable reduction of operating time, which is achieved due to the high cutting speed. But this technique provides slightly compromising quality of the finished part, and can only be used in certain applications since the cutting depths are quite limited.

High Performance Machining (HPM) focuses on optimizing the cutting efficiency to maximize the material removal rate. In practice, it is achieved by using *deeper cutting depth* (in times compared to HSM, depending on the materials) and *high feed rate*, while keeping the spindle speed at the maximum allowable level (~15000 rpm). This technique removes the largest volume of materials as fast as possible, which yields essential reduction of the machining time. However, it increases significantly the cutting forces and requires high spindle power.

Multi Task Machining (MTM) is the most innovative and is also a rapidly growing trend in machining techniques, such as a turning/milling process, where the main power is applied to *turning*, while the *milling* is performed by auxiliary spindles with essentially less power. To take advantage of this technique, the cutting edge of the tool must be modified to achieve the maximum machining volume at lower forces. Comparing to HPM, here the same machining volume can be achieved using significantly low power consumption.

It is worth mentioning that, in the production of aerospace components, the best machining strategy is the combination of HSM and HPM (Korn, 2005), where the manufacturing technology changes with different processing tasks. Such combination yields both high quality of the product and essential reduction of the manufacturing time. However, the high performance machining requires an *increase of cutting force*, which is not very critical for the conventional CNC-machines with rather stiff mechanical structure. In contrast, for robotic-based machining, these forces may cause *essential deformations of the manipulator*, which consequently affect the machining accuracy.

In order to reduce relevant machining errors, there exist two main approaches. The first one aims at increasing the machine tool or robot stiffness as well as optimal part placement in the workspace (Caro et al., 2013). However, increasing the mechanism stiffness obviously leads to decreasing of the dynamic properties (due to higher mass and inertia of the manipulator links). The second approach is based on robot error compensation via proper off-line (or on-line) modification of control program describing desired tool trajectory or by using the force feedback in the online mode. To implement this approach, suitable geometric and stiffness models of the robotic manipulator are required, which is in the focus of this thesis.

1.1.2 Industrial requirements for machining accuracy

Before considering specificities of robotic-based machining, let us analyze in general the industrial requirements for machining accuracy. Figure 1.3 presents the most common manufacturing processes and the typical tolerances associated with each of them. In this figure, the dark segments of the bars represent the tolerances required in most of the cases. The remaining parts of the bar indicate the less frequent cases (with either higher/lower precision that are obtained under ideal/worst machining conditions). For the milling process studied in this thesis, which is highlighted here, the desired tolerances are in the range of 0.05-0.25 mm. Let us evaluate their feasibility in conventional robot control, without dedicated error compensation.

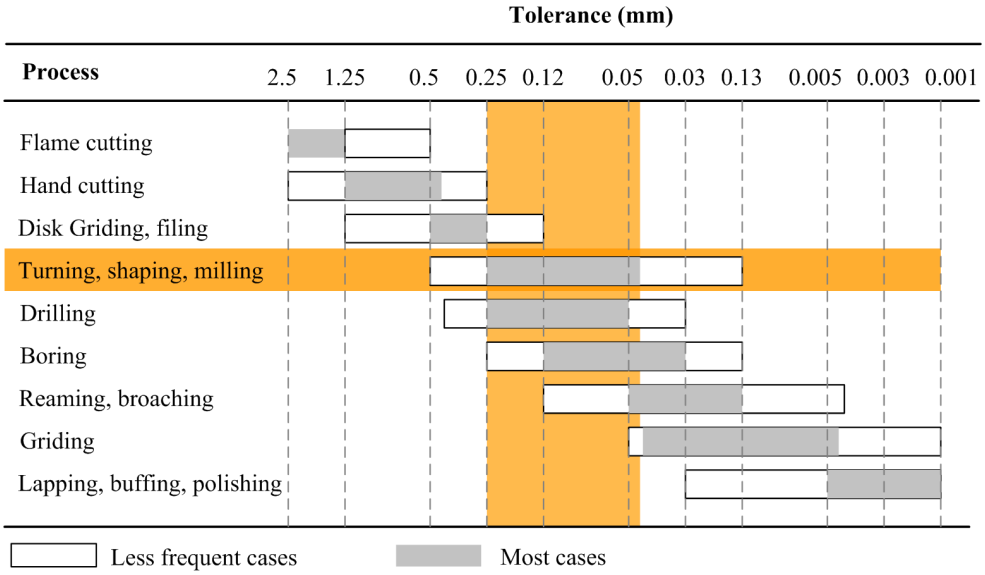

Figure 1.3 Typical tolerances of different machining processes (DML)

For industrial robots, especially ones employed in machining of high performance materials, essential loading is usually generated by the interaction of machining tool and workpiece during the processing. For example, the Monel®400 nickel-copper alloy is widely used in aerospace industry due to its favorable mechanical and chemical-corrosion properties. For milling of such material with the cutting depth of 0.2 mm, cutting width of 8 mm and feed rate of 10 m/min, a 7 kN force is required (Klimchik, 2011). It is evident that this force is high enough to cause significant deformations of the robotic manipulator components. For instance, for KUKA KR-240 industrial robot (Dumas, 2011), such force may cause positioning deflections up to 5 mm and angular ones up to 0.2 deg, depending on the cutting force direction and manipulator configuration. These deflections are about 20 times higher than the required process tolerances. So, to achieve the desired accuracy of robotic-based machining, these deflections must be compensated by proper control strategy.

It is worth mentioning that for the alternative solution, which employs conventional CNC machines, the above mentioned problem is not critical (because accuracy of 50μm is quite feasible here). However, for machining of large dimensional parts, the CNC machines can be hardly applied. In particular, large-scale CNC machines (gantry, for instance) can be extremely expensive. For these reasons, relevant industries have a rapidly growing need for using robotic manipulator to perform the machining tasks. So, in order to meet the industrial requirements, improvement of the robot accuracy in such applications becomes a crucial issue.

1.1.3 Robot application for machining operation

The robotic manipulators are used in numerous industrial applications, they progressively replace the traditional machine centers and human workers. The application of robots has enabled the manufacturing industry to perform certain operations automatically, at high speeds, more precise than a human operator that lead to productivity improvement (Groover, 2010). Figure 1.4 presents a statistical overview of the use of industrial robots both in industry and for some applications.

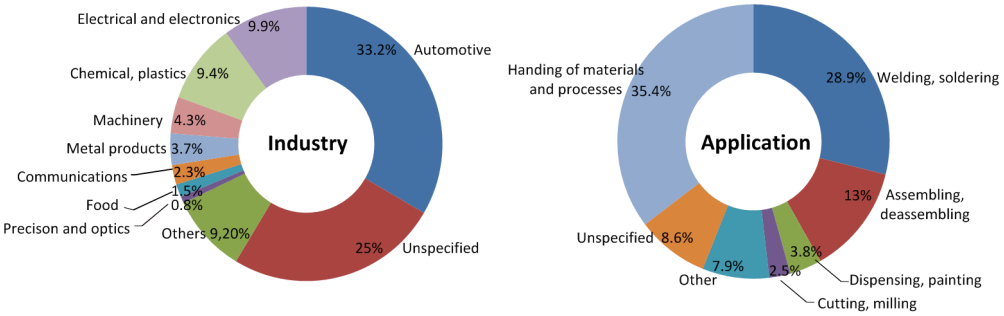

Figure 1.4 Statistical overview of the use of industrial robots (Guizzo, 2008)

As follows from the figure, the robots have taken over a large share in both light and heavy industries. Generally, they are considered to be very competitive in terms of their automation, flexibility, safety, cost-effectiveness and other advantages. In particular, the industrial application such as palletizing has successfully implemented the robotic manipulators into their production chains for over several decades. While heavy industry requires a growing number of robots in automotive, shipbuilding and aerospace manufacturing, which motivate researchers and robot manufacturers to improve the robot stiffness and accuracy in order to meet the requirements. These application areas and the most recent developments are briefly presented below.

Industrial palletizing (packing, pick-and-place, etc.) refers to load and unload products from/to a pallet. The robotic-based automated palletizing has been successfully employed in many industries such as food processing, shipping, etc. since the 1980s.

Figure 1.5 End of line robotic palletizer (ICC.com)

Figure 1.6 The new PowerMill robot interface for multi-axis machining operations (Delcam, 2013)

Robotic sculpting/milling and rapid prototyping help the designer to create a physical model from a conceptual design. Traditionally, this design-to-manufacturing process uses CNC machines and is quite time consuming, while robots are faster and can perform machining tasks with a large diversity of the lightweight materials (plastic, wood, foam, etc.) (Huang and Lin, 2003).

Figure 1.7 The Great Wall motors robotic assembly line (Murray, 2012)

Automotive manufacturing is the most important customer of industrial robots. Over 30% of all robots in use today are employed in automotive industry. Robots are able to produce consistent and high quality products. They are safe and cost-effective. For example, the robots are so fast, they can complete the welding of an entire Haval SUV in just 86 seconds. (Murray, 2012).

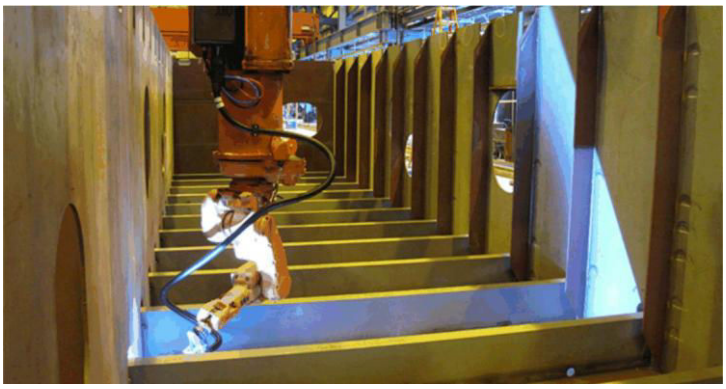

Figure 1.8 Automatic robot welding of complex ship sections (Kranendonk.com)

Shipbuilding industry often involves machining of pieces with very large scale, such as profile cutting, panel welding, double hull welding, etc. Recently, Hyundai Heavy industry, one of the world's biggest shipbuilder, has developed a mini welding robot for building ships. Such a robot weights only 15 kg with a magnet in its body, and is able to attached to the steel walls/ceilings. One operator can control three robots at the same time, so the productivity may increase essentially (HHI.co).

Aerospace industry. More than thousands of fastener locations required to be drilled to complete a plane. Industrial robots stand a great opportunity for relevant machining applications. Highly rigid robot has been developed specially towards aerospace application, with very good accuracy, about 0.1 mm, during the drilling process (Fanuc.co).

Figure 1.9 Robot performs non-destructive inspection on a Boeing 787 (Waurzyniak, 2013)

Despite the above mentioned advantages, robotic manipulators are less accurate than conventional CNC machines (that may reach an accuracy of 50µm), especially in heavy industry where the robots perform manufacturing tasks with essential forces. This inaccuracy is caused by the influence of the external forces and by the differences between the parameter true values and the nominal ones. The influence of these factors on the machining accuracy depends on corresponding industrial applications and robot configurations.

To show the significance of the manipulator parameters on the final manufacturing product, let us present a typical machining experiment performed at IRCCyN laboratory / IUT Nantes. The technological process includes a milling operation on a machining piece using KUKA KR-270 industrial robot. The machining piece (Figure 1.10a) of aluminum alloy with thickness 5 mm was trimmed with a cutting tool of diameter 21 mm and 4 cutting teeth. The rotational speed of the tool was 6670 rpm and the feed rate was 3.6 m/min. In the frame of this experiment, the robot performed milling along certain pre-defined trajectories (Figure 1.10c).

(a) Raw piece

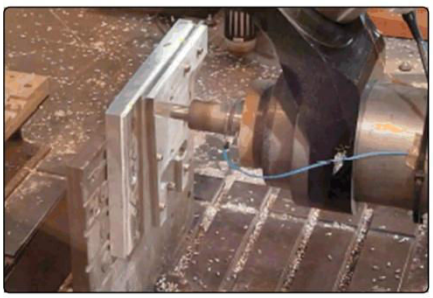

(b) machining tool

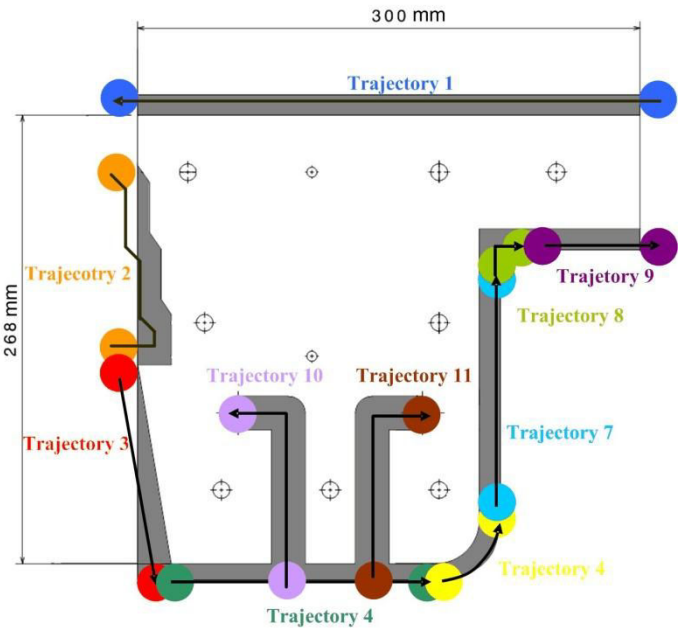

(c) Machining trajectoires

Figure 1.10 Machining experiment (Dumas, 2011)

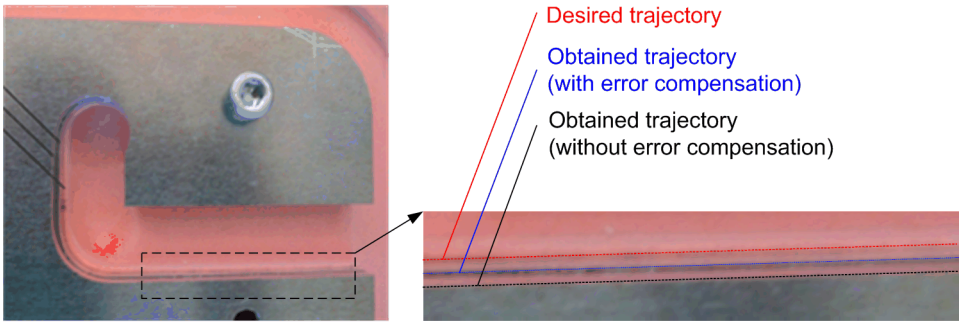

(a) Machining piece (b) Zoom of the obtained machining trajectories

Figure 1.11 Differences between the desired trajectory and the obtained ones with and without error compensation (Dumas, 2011)

Experimental results related to this machining process are presented in Figure 1.11, which show the differences between the desired trajectory and the obtained ones (using different control strategies). As follows from this figure, the machining errors without error compensation can reach 0.7 mm, which is not acceptable for aerospace industry. It should be mentioned that in this machining experiment, an error compensation technique has already been applied, the "mirror" approach, which allowed to compensate about 50% of the machining errors (in the case when the cutting speed is equal to 6670 rpm). In order to achieve higher machining accuracy, let us investigate the sources of robot errors in machining applications.

1.1.4 Robot errors and their compensation in machining application

In the literature, precision of the robotic manipulator is described by three criteria: resolution, repeatability and accuracy (Conrad et al., 2000). The resolution defines the minimum increment that robot may produce. The repeatability measures the ability of a robot to return repeatedly to a given position. The accuracy refers to the robot ability to move precisely to a desired Cartesian location. In the frame of this work, the main attention will be paid to the robot accuracy that can be essentially improved using the calibration techniques developed in the following chapters.

In accordance with (Khalil and Besnard, 2002; Paziani et al., 2009), the sources of manipulator positioning errors can be classified into two main groups: geometric errors and non-geometric ones. In more details, the classification of these errors is presented in Figure 1.12. It should be noted that these error sources may be independent or correlated. In practice, they are usually treated sequentially, assuming that they are statistically independent.

Usually, in the robot applications such as packing and palletizing, or machining with light materials (wood or plastic, for instance), external forces/torques applied to the end-effector are relatively small. In this case, the primary sources of robot inaccuracy are the geometric errors, which are responsible for about 90% of the total positioning error (Elatta et al., 2004; Rolland, 2003). Typical examples of geometric errors are the differences between nominal and true values of the link lengths, the differences between zero values of actuator coordinates in real robot and mathematical model employed in control unit (the joint offsets). It is worth mentioning that they can be also caused by non-perfect assembling of different manipulator components, which yield mismatching and misalignment in shifting and/or rotation of the associated frames. At present, there exists a number of well-known calibration techniques that allow to identify these geometric errors (Bennett et al., 1991; Daney et al., 2006; Khalil and Dombre, 2004; Roth et al., 1987) and to compensate them efficiently either by tuning

the controller input (i.e. the target point location) or by straightforward modification of the geometric model parameters that are accessible in the robot controller.

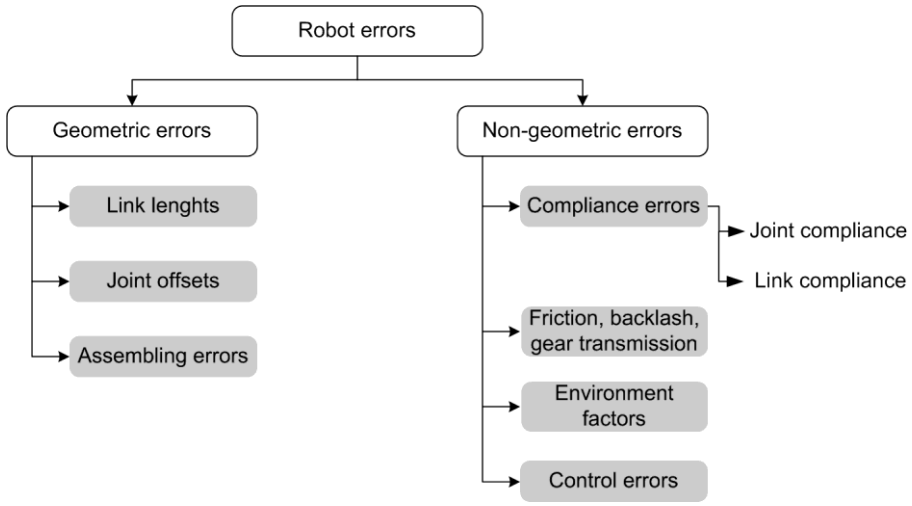

Figure 1.12 Classification of robot errors in machining applications

Considering the geometric errors, corresponding compensation techniques are already well developed. Generally, when the main sources of errors are concentrated in the link lengths and/or in the joint offsets, straightforward compensation strategy can be applied by adjusting the geometric parameters employed in the robot control unit. On the other hand, if any geometric errors are not presented in the nominal direct/inverse models, relevant modification of the controller input is required. In this case, it is possible to use a relevant non-linear function that describes the error distribution throughout the workspace. An example of such approach has been given in (Lu et al., 1997), where the neural network technique is applied. More detailed review of different strategies dedicated to geometric errors compensation will be presented in Section 1.2.

For the robots that are employed in machining of high performance materials (such as milling, drilling, turning, etc), the geometric errors are usually dominated by the non-geometric ones (Bogdan and Abba, 2009; Cui and Zhu, 2006; Gong et al., 2000). In this case, the cutting forces/torques are quite high and may cause essential deformations of the manipulator components (link/joint compliance errors). Besides, some environmental factors (thermal effects, atmospheric pressure, etc.) may also affect physical properties of the manipulator components and may cause some undesirable changes. Nevertheless, under usual circumstances, the compliance errors are the most significant ones and may be responsible for over 90% of the total positioning errors. Particularly, their influence is critical for heavy industrial robots and manipulators with low stiffness. The compliance errors depend on two key factors: (i) the manipulator stiffness and (ii) the applied external loading. In addition, in some cases, the influence of link gravity, the effect of gravity compensation mechanisms, and the preloading in joints introduced to eliminate backlashes should be also considered.

For the compliance errors, the compensation technique must rely on two components: (i) the manipulator stiffness matrix describing the elastostatic properties, (ii) the loading describing the forces/torques acting on the manipulator end-effector while performing certain manufacturing tasks. In this work, it is assumed that the loading can be estimated from corresponding technological process model. To obtain the Cartesian stiffness matrix, there exist various approaches (Akin, 2005; Angeles, 2007; Deblaise et al., 2006). More detailed review of different stiffness modeling methods and compliance error compensation techniques will be presented in the Section 1.3.

1.2 MANIPULATOR GEOMETRIC MODEL AND IDENTIFICATION OF ITS PARAMETERS

1.2.1 Manipulator geometric modeling

Serial robotic manipulator is an open-loop kinematic chain with several links connected in sequence by either revolute or prismatic joints driven by actuators. One end of the chain is usually fixed to a supporting base while the other end moves within the robot workspace. The latter is often equipped with a technological tool (an end-effector) that is used to manipulate objects or to perform particular tasks. To ensure the accurate location of the robot end-effector, the geometric model employed in the robot controller should precisely describe the relation between the joint space and the Cartesian space (Waldron and Schmiedeler, 2008). Such a relation is illustrated in Figure 1.13, in which the inputs of the direct geometric model are the joint angles (actuator coordinates) that define the robot configuration, and the output is the manipulator end-effector location (position and orientation). The inverse problem gives the joint angles from a given robot end-effector location. In this review of manipulator geometric modeling methods, it is assumed that the manipulator consists of rigid links, and the non-geometric effects such as the gear transmissions, joint backlashes and link deformations due to environmental changes are negligible.

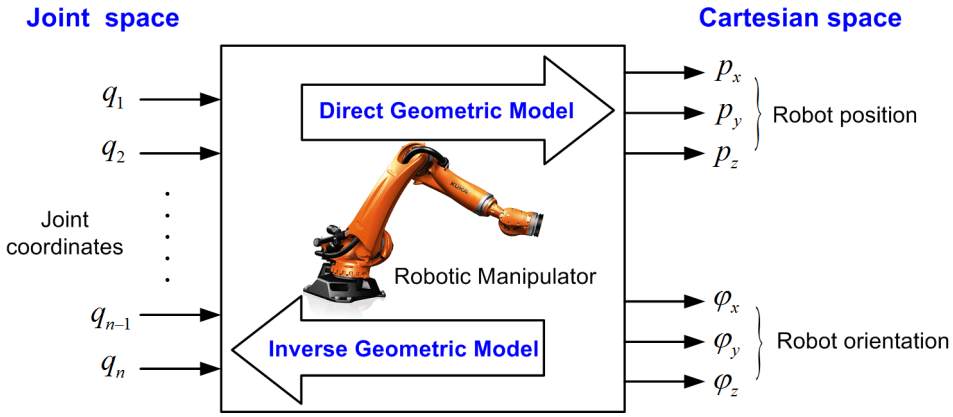

Figure 1.13 The schematic representation of manipulator geometric model.

The robot end-effector position that is defined by the vector of the Cartesian coordinates $\mathbf{p}=\{p_x, p_y, p_z\}$ is usually computed using different mathematical techniques that give similar results. In contrast, the end-effector orientation that usually described by the vector $\boldsymbol{\varphi}=\{\varphi_x, \varphi_y, \varphi_z\}$ highly depends on the parameterization. In the robotics literature, to express the orientation, various forms exist. The most commonly used are the following: orthogonal rotation matrix of size 3×3, Euler angles, Rodrigues parameters, lie algebra, quaternion (Aspragathos and Dimitros, 1998; Chou and Kamel, 1991; Funda et al., 1990; Gu, 1988; Kuipers, 1999). They have been developed for different applications or have been adapted to some special algorithms. For this reason, there exists different ways to describe the manipulator geometric model, which differ in the mathematical techniques and the parameterization methods.

One of the most popular approaches used by robotics community for describing the manipulator kinematics is the homogeneous transformation (Paul, 1981; Paul and Zhang, 1986). In this method, the robot end-effector location (i.e., position and orientation) is described by a 4×4 transformation matrix, which includes a 3×3 rotation matrix defining the robot orientation and a 3×1 translational vector that defines the robot position. It should be mentioned that the angle convention of the end-effector orientation used in the robot controller differs from one to another, so the extraction of the

orientation angles from the rotation matrix highly depends on it as well as the order of rotational axes. For example, the KUKA robot uses ABC angles (yaw-pitch-rooll convention), PUMA robot uses OAT angle coordinates; other Euler angles (ZYZ convention, for instance) are also used in other robots (Slabaugh, 1999). An alternative method is based on the screw theory, which expresses a rigid body transformation by a screw displacement (Funda and Paul, 1990; Huang et al., 2013). Its main advantage is that it avoids the use of local coordinates systems that induce singularities. To represent a screw motion, there are several ways which are based on Lie algebra, quaternion algebra, etc (Aspragathos and Dimitros, 1998; Gu, 1990; Sariyildiz and Temeltas, 2011).

Using any modeling method, similar results in the definition of the manipulator spatial location can be achieved. Therefore, since the homogeneous transformation may operate with the parameters that are employed in the robot controller, it will be used for further computations. This method found wide applications both in geometric modeling and robot calibration. In the frame of this technique, the manipulator geometric model is defined by a sequence of transformations from the reference frame to the robot end-effector frame. These transformations are computed using elementary homogeneous matrices $\left\{\mathbf{T}_x, \mathbf{T}_y, \mathbf{T}_z, \mathbf{R}_x, \mathbf{R}_y, \mathbf{R}_z\right\}$, where $\mathbf{T}$ and $\mathbf{R}$ represent a pure translation and rotation about the related axis (Maxwell, 1951). It should be noted that the order of the sequence is quite important here and is defined by the robot architecture and parameterization method. In general, the transformation matrix that describes the manipulator geometric model can be expressed as

$$\mathbf{T} = \mathbf{T}_{\text{Base}} \cdot \prod_{j=1}^{n} \left(\mathbf{T}_{\text{Link}}(\boldsymbol{\pi}_j) \cdot \mathbf{T}_{\text{Joint}}(q_j) \right) \cdot \mathbf{T}_{\text{Tool}} \tag{1.1}$$

where $\mathbf{T}_{\text{Base}}$ and $\mathbf{T}_{\text{Tool}}$ are the base and tool transformations, $\mathbf{T}_{\text{Link}}$ and $\mathbf{T}_{\text{Joint}}$ are the link and joint transformations; vector $\boldsymbol{\pi}_j$ collects the geometric parameters of each link and varies with the parameterization methods, where j is the link/joint number; $q_j, (j = 1,2,...,n)$ are the joint coordinates defining the robot configuration and n is the number of joints. Generally, each manipulator component can be defined by six sequential elementary transformations. In fact, some of them are redundant and can be eliminated from the model (for example, for a revolute joint, only one angular motion is required). In practice, $\mathbf{T}_{\text{Joint}}$ is defined by a single rotation/translation joint and can be expressed as

$$\mathbf{T}_{\text{Joint}} = \begin{cases} \mathbf{R}_i(q_j), & \text{for a revolute joint} \\ \mathbf{T}_i(q_j), & \text{for a prismatic joint} \end{cases} \tag{1.2}$$

where $i = x, y, z$ specifies the rotational/translational axis. In contrast, $\mathbf{T}_{\text{Link}}$ is usually described by a sequence of six transformation matrices.

In order to reduce the number of parameters, Denavit and Hartenberg proposed an approach to describe the transformation between adjacent links using only four parameters (Denavit and Hartenberg, 1955). Such benefits have been achieved using special locations of the reference frames, where z-axis coincides with the direction of the joint axis and x-axis is aligned with the common normal to the previous and current joint axes. Here, the model parameters define the shift and rotation between x- and z-axes and the relation between consecutive links is described by the following transformation matrix

$$\mathbf{T}_{\text{Link}} = \mathbf{R}_z(\theta_j)\mathbf{T}_z(r_j)\mathbf{T}_x(d_j)\mathbf{R}_x(\alpha_j) \tag{1.3}$$

where θ_j is defined by the angle between x_{j-1} and x_j about z_{j-1}, noted that $\theta_j = q_j + \Delta q_j$, where Δq_j is the joint offset that should be identified as a geometric parameter; r is the distance between x_{j-1} and x_j along z_{j-1}, α is the angle between z_{j-1} and about x_j, and d is the distance between

z_{j-1} and z_j along x_j, $\{\mathrm{x}_j, \mathrm{z}_j\}$ and $\{\mathrm{x}_{j-1}, \mathrm{z}_{j-1}\}$ are the reference frames of the current and previous joints.

This method has been widely used in many robotic applications and is very convenient for direct geometric modeling of serial manipulators. However in robot calibration, such parameterization may cause some difficulties if the axes of consecutive joints are parallel. It has been detected in (Mooring, 1983) that when these axes are slightly misaligned, they may produce large changes in the geometric parameters, which cannot be modeled by D-H parameterization. In this case, the calibration Jacobian is singular. For example, in the case study of (Stone, 1987), it has been pointed out that this singularity provides non-acceptable values of the identified parameters.

In order to overcome this limitation, several alternative parameterization methods have been proposed based on the modification or extension of the D-H approach. For example, to represent small misalignment between the consecutive parallel axes, Hayati introduced an extra notation $\mathbf{R}_y(\beta_j)$ (Hayati, 1983). In this case, the link transformation matrix is defined as

$$\mathbf{T}_{\text{Link}} = \mathbf{R}_z(\theta_j)\mathbf{T}_z(r_j)\mathbf{T}_x(d_j)\mathbf{R}_x(\alpha_j)\mathbf{R}_y(\beta_j) \tag{1.4}$$

Later on, this idea has been used in (Veitschegger and Wu, 1987) for the identification of PUMA 560 robot. In addition, this notation is specifically defined for the case of consecutive joints with parallel axes, otherwise it is non-identifiable.

Another approach has been proposed by Stone whose S-model added two extra parameters to the D-H model, in order to allow an arbitrary placement of link frames and avoid the problem of misalignment in consecutive parallel axes as well (Stone et al., 1986). In this model, the link transformation is expressed as

$$\mathbf{T}_{\text{Link}} = \mathbf{R}_z(\beta'_j)\mathbf{T}_z(d'_j)\mathbf{T}_x(a_j)\mathbf{R}_x(\alpha_j)\mathbf{R}_z(\gamma_j)\mathbf{T}_z(b_j) \tag{1.5}$$

where γ_j is the angle between axes $\mathrm{x}_j^{\mathrm{DH}}$ and $\mathrm{x}_j^{\mathrm{S}}$, and b_j is the distance between the origin of D-H link frame and S-model link frame. Using these parameters, it is also possible to obtain the D-H parameters as $\theta_j = \beta'_j + \gamma_{j-1}$ and $d_j = d'_j + b_{j-1}$. The benefits of such a method are confirmed by geometric calibration of PUMA 560, where small misalignment is identified between the second and third joint axes.

Whitney and Lozinski developed another 6-parameter model for the purpose of robot parameter identification (Whitney et al., 1985). In this method, the reference frame is located such that the y-axis is along the joint axis and the subsequent frame lies in the y-z plane. The link transformations contain six independent components, in which the rotation is parameterized by a general Roll-Pitch-Yaw rotational transformation, and has the following form

$$\mathbf{T}_{\text{Link}} = \mathbf{R}_y(\theta_j)\mathbf{T}_y(y_j)\mathbf{T}_z(z_j)\mathbf{R}_z(\phi_j)\mathbf{R}_y(\Omega_j)\mathbf{R}_x(\varphi_j) \tag{1.6}$$

where θ_j is the joint displacement including offset, y_j and z_j are the translational displacements along joint axis and the direction of the link; ϕ_i, Ω_j and φ_j are consecutive rotation angles about z-, y- and x-axes, respectively.

The above presented approaches are summarized in Table 1.1, where the parameters as well as the link transformation matrices are given. The differences between the presented methods are illustrated in Figure 1.14, where the link frames are assigned and corresponding parameters are defined.

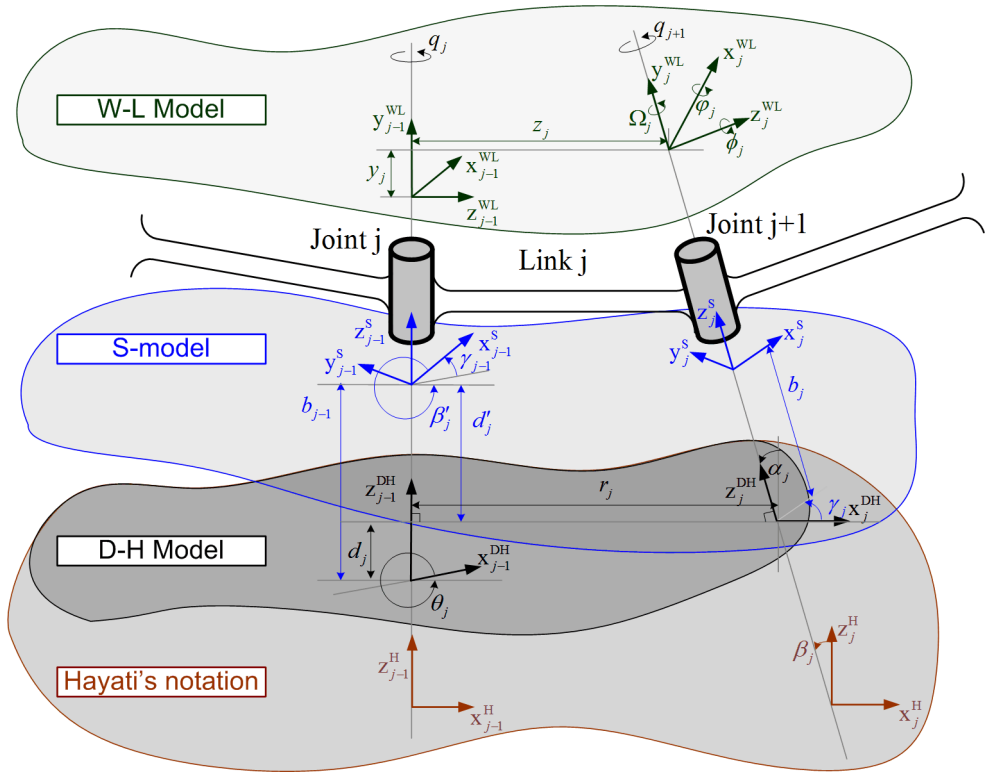

Figure 1.14 Existing parameterization methods for consecutive revolute joints

Table 1.1 Summary of existing parameterization methods in manipulator geometric modeling

Parameterization method	Link transformation $\mathbf{T}_{\text{Link}}$	Parameters $\boldsymbol{\pi}_j$
D-H model	$\mathbf{R}_z(\theta_j)\mathbf{T}_z(r_j)\mathbf{T}_x(d_j)\mathbf{R}_x(\alpha_j)$	$\{\theta_j, r_j, d_j, \alpha_j\}$
Hayati's model	$\mathbf{R}_z(\theta_j)\mathbf{T}_z(r_j)\mathbf{T}_x(d_j)\mathbf{R}_x(\alpha_j)\mathbf{R}_y(\beta_j)$	$\{\theta_j, r_j, d_j, \alpha_j, \beta_j\}$
S-model	$\mathbf{R}_z(\beta'_j)\mathbf{T}_z(d'_j)\mathbf{T}_x(r_j)\mathbf{R}_x(\alpha_j)\mathbf{R}_z(\gamma_j)\mathbf{T}_z(b_j)$	$\{\beta'_j, d'_j, r_j, \alpha_j, \gamma_j, b_j\}$
Whitney-Lozinski model	$\mathbf{R}_y(\theta_j)\mathbf{T}_y(y_j)\mathbf{T}_z(z_j)\mathbf{R}_z(\phi_j)\mathbf{R}_y(\Omega_j)\mathbf{R}_x(\varphi_j)$	$\{\theta_j, y_j, z_j, \phi_j, \Omega_j, \varphi_j\}$

Although the incompleteness of D-H parameterization can be overcome by introducing extra parameters, it may provoke undesirable redundancy and increase the computational complexity. So, it does not solve the problem of singularities of the calibration Jacobian. Besides, it can be proved that with each new parameter, which is not significant or redundant, the model precision decreases. Therefore, the key issue in the geometric modeling is to find the minimum set of parameters that can describe the manipulator end-effector position with required accuracy after calibration. This problem will be in the focus of the next subsection.

1.2.2 Geometric model suitable for identification

As follows from previous subsection, manipulator geometric models may include different number of parameters. In particular, for a conventional 6-dof industrial robot, the number of parameters varies from 24 for DH representation to 36 for Whitney-Losinski approach. In addition, it is necessary to increase these numbers by 12 to describe the robot base location and the tool geometry.

It is clear that for the inverse and direct kinematics, number of parameters is not critical and does not create any particular numerical difficulties. However, to identify all these parameters from the measurements of the end-effector location only, usually is not possible. In practice, some parameters cannot be identified separately, they are presented in the geometric model as sums or linear combinations. Any attempt to solve the identification problem for the whole set of these parameters leads to the fail of the numerical routines (that is caused by singularity of the relevant aggregated Jacobian). Hence, to be suitable for the identification, the manipulator geometric model must be proper prepared (by means of reduction of redundant parameters). On the other side, the number of parameters should be high enough, to describe all possible variation in the link/joint geometry of the manipulator. In other words, the number of parameters should be minimal, but sufficient.

The above mentioned problem has been firstly addressed in (Everett et al., 1987), where the authors defined three essential properties for geometric model suitable for identification: completeness, irreducibility and continuity. To be complete, the geometric model should contain a sufficient number of parameters to specify the motion of the robot end-effector for any geometry of the link and joint (which are assumed to be non-flexible). The irreducibility means that minimum number of independent parameters is included in the model. And finally, the continuity implies that small changes in the manipulator geometry are reflected by small changes in the parameters. For the geometric model that satisfies all the above mentioned requirements, the rank of the corresponding aggregated Jacobian $\mathbf{J}_{\Pi a}$ is equal to the number of the parameters to be identified, and the desired parameters $\Delta\boldsymbol{\pi}$ can be found using the following expression

$$\Delta\mathbf{t}_a = \mathbf{J}_{\pi a}\Delta\boldsymbol{\pi} \tag{1.7}$$

where $\Delta\mathbf{t}_a$ is the vector of aggregated deviations of the manipulator end-effector location caused by inaccuracy in the manipulator geometry. Further, the problem of the parameter identifiability has been investigated by several researchers, where some analytical tools and/or numerical routines for model reduction were proposed (Besnard and Khalil, 2001).

Another essential contribution in this area has been done by (Zhuang et al., 1989), who focused on the determination of the minimum number of geometric parameters for the model completeness. The authors used the screw theory and proved that, for the serial robot that consists of low-pair joints, this number is equal to

$$N_p = 4n_R + 2n_P + 6 \tag{1.8}$$

where n_R and n_P is the number of revolute and prismatic joints, respectively. It should be mentioned that the number 6 in Eq. (1.8) corresponds to the base transformation, which must be also taken into account in the geometric model (see Eq.(1.1)).

The above expression has been derived for the case when all components of the manipulator end-effector location (both position and orientation) can be measured. In the case when the orientation is not available (due to the limitation of measurement device), Eq.(1.8) should be replaced by

$$N_p = 4n_R + 2n_P + 3 \tag{1.9}$$

In practice, for majority of existing robotic manipulators, which are equipped with so called "in-line" wrist and the links 4 and 5 cannot be distinguished in the nominal design, the number of identifiable parameters should be further revised. For this particular case, (Pashkevich, 2001) proposed an alternative expression for relative measurements that is able to take into account the above effect

$$N_p = 4n_R + 2n_P - 2s \tag{1.10}$$

where s is the number if singular rotational joints (usually $s=1$ or $s=0$). It should be mentioned that number N_p can be still decreased depending on particular architecture of the manipulator (for example, the model of the last link cannot be separated from the tool model). Besides, the above expressions are able to provide the minimum (and sufficient) number of parameters, while it does not give an answer to the questions about which parameters should remain in the geometric model and how to generate the models suitable for calibration in the simplest and more efficient way.

One of the possible solution has been proposed in (Pashkevich, 2001), where on the first step the manipulator is described by obviously redundant (but sufficient) model that uses six parameters for each link, one parameter for each joint, six parameters for the base and six parameters for the tool. Further, on the second step, the model is reduced using specially developed reduction technique based on the SVD decomposition. In the frame of this technique, the manipulator geometric parameters are split into three groups, the identifiable, non-identifiable and semi-identifiable parameters, which have the following definitions:

The *identifiable* parameters have direct influence on the robot end-effector position accuracy and can be independently identified by robot calibration.

The *non-identifiable* parameters do not affect the manipulator end-effector position accuracy and should be eliminated from the geometric model. Typical example of such parameter is the tool orientation when the partial pose measurements (position only) are used for calibration.

The *Semi-identifiable* parameters are linear dependent, their influence on the robot accuracy cannot be identified separately. In robot calibration, they are usually combined together in such a way that any element can be treated identifiable while the remaining parameters can be treated as redundant/non-identifiable (fixed to be equal to zero, for instance). For example, parameters d_2 and d_3 in the robot PUMA 560 are included in the geometric model as a difference $d_2 - d_3$ and cannot be identified separately. For this reason, straightforward identification in such a case may lead to unreasonable values for both parameters. Relevant example is given in (Stone, 1987), where identification of d_2 and d_3 individually provided unacceptable result $d_2 = 49310.6\,\text{mm}$ and $d_3 = 49160.6\,\text{mm}$ (instead of something close to the nominal values 250.0 mm and 101.0 mm), while the corresponding difference remains correct $d_2 - d_3 = 149.0\,\text{mm}$.

In the scope of the above mentioned work (Pashkevich, 2001), the non-identifiable parameters are extracted by detecting zero columns in the aggregated Jacobian $\mathbf{J}_{\pi a}$ and they are eliminated from the model in the straightforward way. Further, to deal with the semi-identifiable parameters, the SVD-based technique can be applied to the reduced Jacobian $\mathbf{J}_{\pi r}$, and Eq.(1.7) can be rewritten as

$$\sigma_i V_i^T \Delta\boldsymbol{\pi} = U_i^T \Delta\mathbf{t}_a, \quad i = \overline{1,r} \tag{1.11}$$

where U_i is vector of size $MP \times 1$, V_i is a $N_P \times 1$ column vector and σ_i is the element of $\boldsymbol{\Sigma}$ that is a $MP \times N_P$ matrix of the singular values; r is the rank of matrix $\mathbf{J}_{\pi r}$; M is the dimension of measurement data, P is number of measured points and N_p is the number of parameters. Here, the matrices $\mathbf{U}, \boldsymbol{\Sigma}, \mathbf{V}$ are obtained using the following decomposition

$$\mathbf{J}_{\pi r} = \mathbf{U}\boldsymbol{\Sigma}\mathbf{V}^T \tag{1.12}$$

where $\mathbf{U} = [U_1, U_2, ..., U_r]$ and $\mathbf{V} = [V_1, V_2, ..., V_r]$. This leads to the general solution of the linear system (1.7) as

$$\Delta\boldsymbol{\pi} = \Delta\boldsymbol{\pi}_{part} + \sum_{i>r} \mu_i \mathbf{V}_i \tag{1.13}$$

where μ_i are arbitrary scalar values, $\Delta\boldsymbol{\pi}_{part}$ is a partial solution of the considered system. Analysis of Eq.(1.13) for the desired parameters shows that the relation between the eigenvectors V_i and the parameter identifiability can be described using the following rules:

If the ith row of the matrix $[V_{r+1},...,V_m]$ is equal to zero, the parameter $\Delta\boldsymbol{\pi}_i$ is identifiable.

If the ith column of the matrix $[V_1,...,V_r]$ is equal to zero, the parameter $\Delta\boldsymbol{\pi}_i$ is non identifiable.

If $\mathbf{L}_i^T\Delta\boldsymbol{\pi}=0,\ \ i=\overline{1,r}$, where $\mathbf{L}_{ij}=0$ for identifiable or non-identifiable parameters, and $\mathbf{L}_{ij}=\mathbf{V}_{ij}$ for others, the parameter $\Delta\boldsymbol{\pi}_i$ is semi-identifiable.

So, this technique allows us to classify all parameters of the redundant geometric model into three particular groups and to obtain the complete, irreducible and continuous model that is suitable for identification.

An alternative approach has been proposed in (Khalil and Dombre, 2004), which is based on the QR decomposition. In the frame of this method, the first step is the detection of the parameters that have no effect on the geometric model. Similar to the previous approach, these parameters correspond to the zero columns in matrix $\mathbf{J}_{\pi a}$, and are eliminated from the model parameters. On the second step, the number of identifiable parameters is defined by the rank of the reduced calibration Jacobian $\mathbf{J}_{\pi r}$. Further, the identifiable parameters are determined by those corresponding to the independent columns of $\mathbf{J}_{\pi r}$, by means of QR decomposition

$$\mathbf{J}_{\pi r}=\mathbf{Q}_{MP\times MP}\cdot\begin{bmatrix}\mathbf{R}_{Np\times Np}\\ \mathbf{0}_{(MP-Np)\times Np}\end{bmatrix} \tag{1.14}$$

where $\mathbf{Q}$ is an orthogonal matrix, $\mathbf{R}$ is a upper triangular matrix and $\mathbf{0}_{(MP-Np)\times Np}$ is the zero matrix; Then, the non-identifiable parameters are those whose related elements on the diagonal of the matrix $\mathbf{R}$ that are zero or "close to zero". It should be noted that here the identifiable parameters are not uniquely defined, while the QR decomposition method provides those parameters that correspond to the first r (rank of $\mathbf{J}_{\pi r}$) independent columns of the reduced calibration Jacobian. In order to ensure some parameters to be a priori presented in the model (which are included in the geometric model embedded in the robot controller), it is suggested to adjust the order of the columns of $\mathbf{J}_{\pi r}$ in accordance with the specific rules. This simplifies integration of the identified parameters in the control loop. The validity of this approach has been confirmed in (Khalil and Dombre, 2004), where the authors identified 24 (out of 30) parameters of Stäubli robot RX-90, and 6 semi-identifiable parameters.

It should be also mentioned that, it is possible to solve the model reduction problem straightforwardly, without using decomposition of the aggregated Jacobian. This approach has been proposed in (Meggiolaro and Dubowsky, 2000) and is based on evaluation the ranks of different subsets of $\mathbf{J}_{\pi r}$ (where the subsets are formed by eliminating one or several columns that are linked with the model parameters). If the rank for the subset remains the same as for the original Jacobian, the eliminated column corresponds to non-identifiable (or semi-identifiable) parameters and should be taken out from the geometric model. Otherwise, if the matrix rank decreases, the relevant parameters will be identifiable and should be conserved in the geometric model. This approach is quite simple and can be easily realized in practice, while the column elimination order is not unique, so the final set of parameters highly depends on the prescribed algorithm. The latter provides the user some flexibility in the determination of the identifiable parameters.

All the above presented methods provide equivalent solutions, while the SVD-based approach is more suitable for semi-analytical analysis. Therefore, it will be used further for generation of suitable geometric model for calibration of a particular manipulator.

1.2.3 Calibration of manipulator geometric model

In practice, the robot geometric parameters non-negligibly differ from the nominal values declared in technical specifications and vary from one robot to another. So, to be used in the robot controller, the geometric model should be properly tuned (calibrated) for a particular manipulator. In general, the calibration procedure is divided into four sequential steps: modeling, measurement, identification and implementation. Let us briefly present the key issues for each step.

Step 1: Modeling. This first step focuses on the development of proper geometric model of robotic manipulator. In the pioneer works (Veitschegger and Wu, 1987), researches have used the classical DH model for robot calibration. However, this model was soon discovered to be discontinuous in some cases and may lead to unacceptable identification results (Mooring, 1983). So, several alternative approaches have been proposed to overcome these difficulties by means of introducing extra parameters (Hayati, 1983). Since the inclusion of additional parameters causes redundancy, these methods raise the problem of parameter non-identifiability, which leads to the necessary investigation of model completeness, irreducibility and continuity. Detail analysis and review on these issues concerning geometric modeling has been presented in the previous Subsection.

Step 2: Measurement. This step involves data collecting of robot pose information. Generally, six parameters are required to specify the manipulator end-effector location (three translations and three rotations) (Driels, 1993; Driels and Swayze, 1994), but sometimes the end-effector position is measured only (three translations). Various calibration methods based on different measurement techniques were proposed, they are usually categorized as closed-loop and open-loop ones. The closed-loop calibration uses physical constraints on the manipulator end-link (point, line or plane constraints, for instance). It is claimed to be autonomous and does not require any external device (Ikits and Hollerbach, 1997; Meggiolaro and Dubowsky, 2000; Rauf and Ryu, 2001). However in this case, the manipulators must have some redundancy to perform self-motion, and the robot configuration should be carefully selected to satisfy particular constraints. Therefore, the open-loop methods have found wide applications, they measure the full or partial pose of the end-effector using external devices. In practice, the partial pose information is often used that provides from one to five dimensional measurements (Besnard and Khalil, 1999; Daney and Emiris, 2001; Rauf et al., 2006) instead of the full pose measures (6-dimensional location). In general, the lower dimensional measurement is more attractive due to the ease of data processing. For this reason, numerous external devices have been developed for relevant measurement methods, more details concerning those methods will be presented in Chapter 2.

Step 3: Identification. The problem of parameter identification of the robot manipulator can be treated as the best fitting of the experimental data (given input variables and measured output variables) by corresponding models. This problem has been addressed by a number of researchers who have used various modeling methods and identification algorithms, such as linear least square, Levenberg-Marquardt algorithm, Kalman filtering technique and maximum likelihood estimator etc. (Mooring et al., 1991; Renders et al., 1991). Among them, the least square technique is the most often applied one, which aims at minimizing the sum of squared residuals (Rao and Toutenburg, 1999).

$$\sum \left\| g(\mathbf{T}(\mathbf{q}_i, \boldsymbol{\pi})) - g_i \right\|^2 \to \min_{\boldsymbol{\pi}} \qquad i = \overline{1, m} \tag{1.15}$$

where $g(\cdot)$ is the function for extraction of location coordinates, and g_i is the related measurements. However, there is a source of errors here if the components of the function $g(\cdot)$ are not homogeneous (distances and angles, for instance, which can be measured in millimeter and radian, meter and degree, etc.). Usually, a straightforward solution is applied to overcome the non-homogeneity: assigning weights or normalization, but this weight assigning procedure is very non-formal and uncertain (while very essential for the final results).

To solve the problem (1.15), there exist various numerical optimization algorithms such as gradient search, heuristic search and the others (Fletcher, 2013), which aim at providing the minimum of the objective function. However, these numerical techniques are often difficult to apply here due to large number of parameters to be tuned, that often leads to low convergence and local minima. On the other hand, for the case of geometric calibration, the errors in the parameters are relatively small, so the linearization technique can be successfully applied. In this case, the solution of a linear least square problem can be found straightforwardly (i.e., via the pseudo-inverse of Moore–Penrose) (Moore 1920; Penrose, 1955). It should be mentioned that in some particular cases (when the geometric errors are relatively large), the solution can only be found iteratively (linearizing the function $g(\cdot)$ several times in the neighbourhood of current parameters).

Step 4: Compensation. This is the last step that implements the identification results in the control strategy. There are two main approaches here that include some adjustments either in on-line or off-line modes. They are respectively based on:

(i) modification of the control algorithm by adjusting the manipulator model embedded in the relevant software;

(ii) modification of the control program by adjusting the reference trajectory, which defines the controller input.

In more details, these two approaches are described in Figure 1.15, where the real (identified) manipulator model is referred to as the "non-nominal" one, in contrast to the "nominal" model that is based on the technical documentation. The corresponding inverse/direct geometric model depends on the actual parameters $\boldsymbol{\pi}_0 + \Delta\boldsymbol{\pi}$ and the nominal ones $\boldsymbol{\pi}_0$, respectively. The desired trajectory $\mathbf{t}_d$ is defined by a set of Cartesian locations of the manipulator end-effector (position and orientation), i.e. $\left\{p_{xi}, p_{yi}, p_{zi}, \varphi_{xi}, \varphi_{yi}, \varphi_{zi}\right\}$. The notations $\left\{\mathbf{t}_m, \mathbf{t}'_m, \mathbf{t}''_m\right\}$ and $\left\{\mathbf{q}, \mathbf{q}', \mathbf{q}''\right\}$ are obtained from manipulator trajectories and relevant joint coordinates used in different control strategies (Figure 1.15(a)-(c)), respectively.

The first approach requires essential intervention in the robot control software and modification of the inverse/direct kinematics in accordance with the identification results. But in the most of cases, it cannot be applied in practice because usually the control software is not opened for the final user and the set of the accessible manipulator parameters (in relevant tables) is very limited. As a rule, these parameters correspond to the nominal manipulator geometry, so it is impossible to include some essential deviations in the joint axis orientation (they may be not strictly parallel or orthogonal, etc.). For this reason, the second approach that is based on the modification of the reference trajectory is applied in engineering practice (Ozaki et al., 1991). These modifications can be performed in off-line mode and deal with correction of the set of end-effector locations (nodes) that define the target trajectory. Because of the universality of this method, it found wide applications and numerous modifications have been proposed. For instance, neural networks has been used in (Ishiguro et al., 1992) and (Huang et al., 2000). In practice, the most popular method is a so called "mirror technique" (Dumas, 2011; Chen et al., 2013), where the reference and non-compensated trajectory are

symmetrical with respect to the desired one (in terms of nodes). As shown in Figure 1.16, the machined trajectory is measured and described by a set of points $\{\mathbf{p}_i,\ i=1,2,...\}$. Using these points, the target trajectory can be generated by defining relevant set of points $\{\mathbf{p}_i^*,\ i=1,2,...\}$, which are symmetric of points $\mathbf{p}_i$ with respect to the desired trajectory. It is worth mentioning that such a technique cannot predict the errors, each time it is required to perform the machining operation in order to obtain the corrupted trajectory. It should be also noted that the selection of compensation technique highly depends on the application area and robot complexity.

(a) Robot control strategy without error compensation

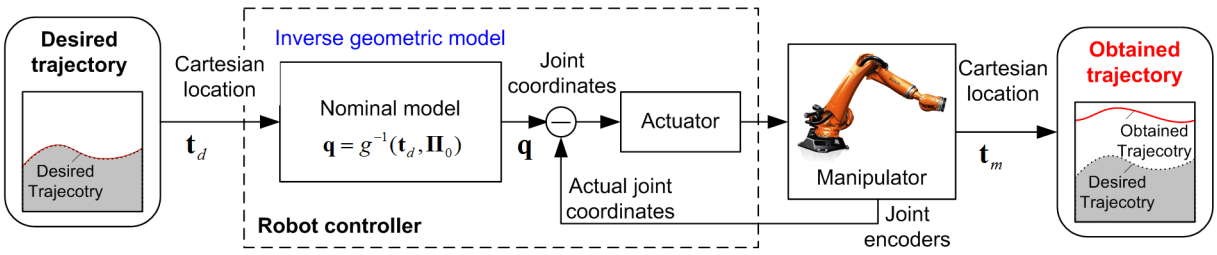

(b) Robot control strategy with on-line error compensation (i)

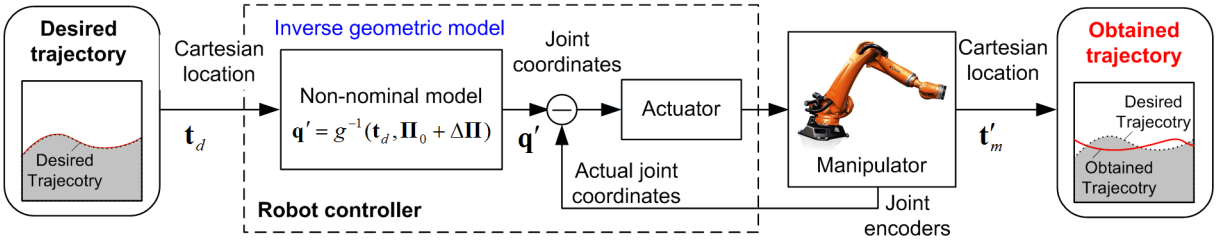

(c) Robot control strategy with off-line error compensation (ii)

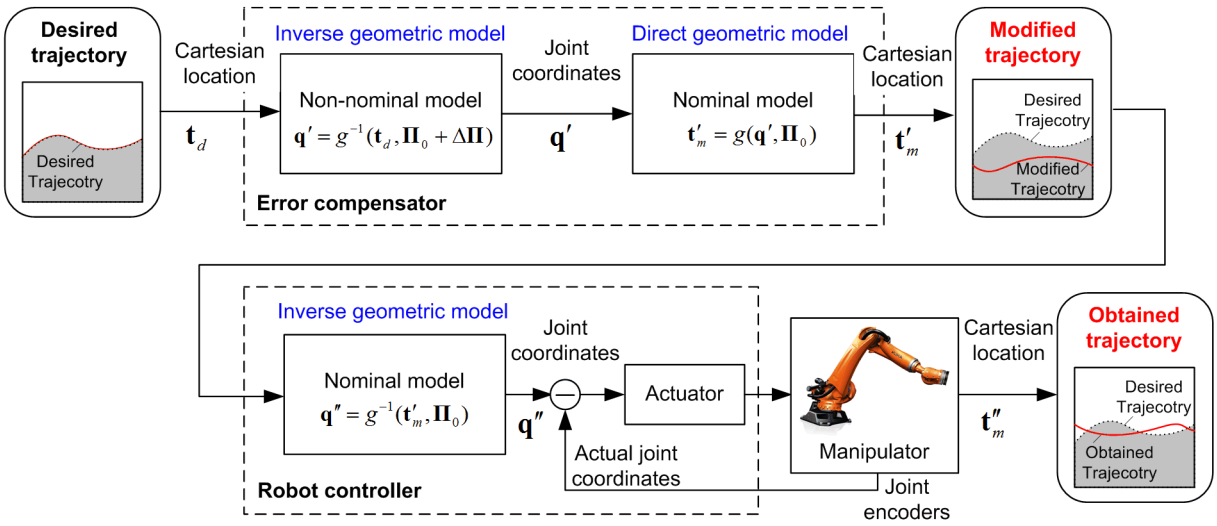

Figure 1.15 Robot control strategies with different errors compensation techniques

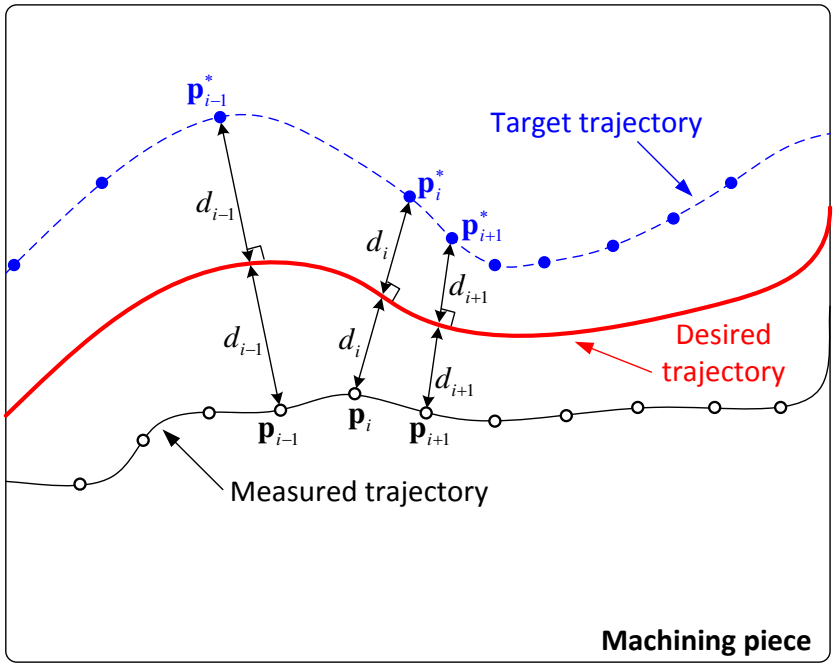

Figure 1.16 The "mirror" strategy for error compensation

The above described steps 1-4, which are typical for all calibration techniques, allow final user to improve the robot accuracy but the degree of this improvement depends on number of factors, such as validity of the modeling assumptions, precision of the measurement system, manipulator configurations used for measurements, objective function employed in the identification algorithm, as well as compensation strategy. As follows from our experience, the most essential here is optimal selection of the measurement configurations that can be also treated as the "calibration experiments design" (under assumptions that the measurement errors are random variables). In other words, the question is how to organize in the best way the step 2 (measurements) in order to obtain the best results on the step 3 (identification). However, formal definition of the best set of measurement poses is not trivial and highly depends on the assumptions concerning the measurement errors and on the definition of the robot accuracy (in terms of the end-effector location or values of the model parameter).

Some previous works devoted to the above mentioned problem (calibration experiments design) concentrated on evaluation of the covariance matrix, which describes the dispersion of the identified parameters caused by random distortion of the measurement data. In order to ensure high identification accuracy, the components of the covariance matrix should be as small as possible, which leads to the problem of finding the "minimum covariance matrix". In particular, several optimality criteria have been proposed (Franceschini and Macchietto, 2008), which deal with the trace, determinant, eigenvalues of the covariance matrix or its inverse (information matrix). Later, these concepts have been adapted to the selection of measurement poses, where several so-called observability indices based on SVD of the identification Jacobian were proposed (Nahvi and Hollerbach, 1996; Sun and Hollerbach, 2008b). However, there are still a number of open questions here, such as how to handle the accuracy of parameters of different units (millimeter and radian, for instance), how to estimate the impacts of different parameters on the end-effector position accuracy, etc. More details concerning these issues will be further discussed in Section 1.4.

1.3 MANIPULATOR ELASTOSTATIC MODEL AND IDENTIFICATION OF ITS PARAMETERS

In industrial application, the robotic based machining is usually accompanied by essential forces/torques caused by technological process. In this case, the compliance errors are not negligible and should be considered together with the geometric ones. For this reason, the manipulator stiffness modeling and the identification of its elastostatic parameters become important issues.

1.3.1 Manipulator stiffness modeling and existing approaches

The robot stiffness describes the manipulator resistance to the deformations caused by the external forces/ torques applied to the end-effector (Angeles, 2007). This manipulator elasticity is usually defined by the 6×6 stiffness matrix $\mathbf{K}_C$ that describes the linear mapping

$$\mathbf{w} = \mathbf{K}_C \cdot \Delta\mathbf{t} \tag{1.16}$$

between the end-effector displacement $\Delta\mathbf{t}$ and the external forces/torques (wrench) $\mathbf{w}$. The inverse of $\mathbf{K}_C$ is called the compliance matrix and is usually denoted as $\mathbf{k}$. In stiffness modeling of robotic manipulator, the matrix $\mathbf{K}$ is often referred to as the "Cartesian stiffness matrix", which is distinguished from the "Joint stiffness matrix" $\mathbf{K}_\theta$ that defines the relation

$$\boldsymbol{\tau} = \mathbf{K}_\theta \cdot \boldsymbol{\theta} \tag{1.17}$$

between the reaction forces/torques $\boldsymbol{\tau}$ to the corresponding joint deflections $\boldsymbol{\theta}$ (Ciblak and Lipkin, 1999). Both of the stiffness matrices $\mathbf{K}_C$ and $\mathbf{K}_\theta$ can be mapped to each other using the so-called *Conservative Congruency Transformation* if the external loading is small enough (Chen and Kao, 2000; Kao and Ngo, 1999). However, if the loading is essential, the relevant mapping is described by more complicated equation that includes the Jacobian, its derivatives and the loading vector (Chen and Kao, 2002; Yi and Freeman, 1993). In more details, these issues are addressed below.

It should be mentioned that the above equations (1.16) and (1.17) are common in robotics and correspond to the *linear* stiffness properties of the manipulator (they may be also treated as the generalization of the classical Hooke's law). However, there are several works that deal with the *non-linear* stiffness models of robotic manipulators that should be used for the case of high loadings, which may provoke some specific manipulator behavior, such as buckling (sudden change of manipulator configuration and its elastostatic properties) (Pashkevich et al., 2009b). In robotics, both for linear and non-linear cases, there exist three main approaches in the manipulator stiffness modeling: (i) the Finite Elements Analysis (FEA), (ii) the Matrix Structural Analysis (MSA) and (iii) the Virtual Joint Method (VJM). Their main features, advantages and limitations can be summarized as follows.

(i) **Finite Elements Analysis (FEA).** The basic idea of this method is to decompose the physical model of a mechanism into a number of small (but finite) elements and to introduce compliant relations between adjacent nodes described by corresponding stiffness matrices. These finite elements have a standard shape (pyramids, cubes, etc) for which the stiffness matrix can be computed analytically. Using this discretization, the static equilibrium equations for each node are derived, and they are aggregated in a global matrix expression defining relations between the applied forces/torques and node deflections. Then, the obtained matrix of rather large size is inverted and is used to obtain the desired stiffness matrix by simple extraction of proper elements. In the modern CAD software, the above process is fully automated and is integrated with 3D modeling of mechanical structures and mechanisms. An advantage of the FEA modeling is its high accuracy that is limited by the discretization step only. It is very attractive for robotic application, since the manipulator links/joints are modeled with its true dimension and shape (Akin, 2005; Bouzgarrou et al., 2004; Corradini et al.,

2003). However, while increasing the number of finite elements, the problem of limited computer memory and the difficulty of high-dimension matrix inversion become critical. Besides, this matrix inversion may generate numerous accumulative round-off errors, which obviously reduce the accuracy. This also causes rather high computational efforts for the repeated re-meshing and re-computing. For this reason, the FEA modeling method is usually applied only at the final design stage in this application area (Long et al., 2003; Rizk et al., 2006).

(ii) **Matrix Structural Analysis (MSA).** This method employs the main ideas of FEA but operates with rather large compliant elements such as beams, arcs, cables, etc. (Martin, 1966). This obviously leads to the reduction of computational efforts and in some particular cases, allows us to obtain analytical stiffness matrix. Similar to the FEA modeling, the MSA method provides forces/torques and displacements for each node, but here it corresponds to the connection point of two adjacent elements. This method has found application for the case of parallel robots, where manipulators include number of passive joints and closed-loop topology. In (Deblaise et al., 2006), this method has been used to compute the stiffness of a Delta robot whose links were approximated by regular beams. However, this approach is hardly applicable for the manipulator behavior in the loaded mode, which is very essential in machining applications.

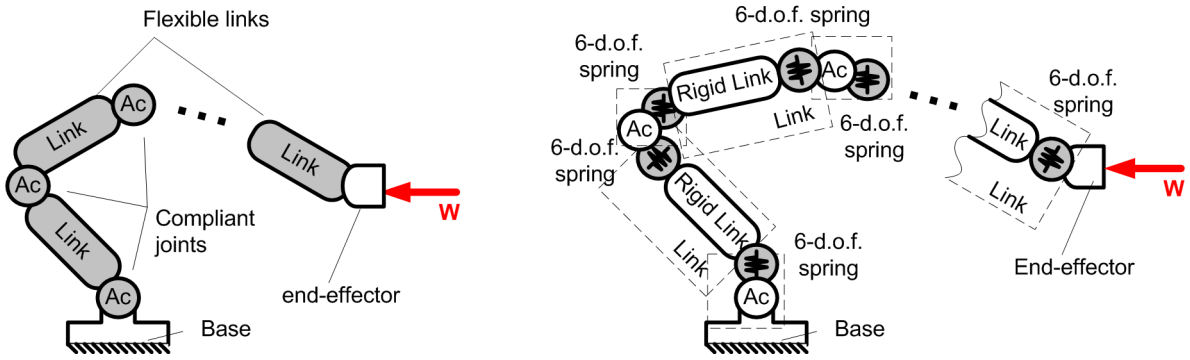

Figure 1.17 Serial industrial robot and its VJM-based stiffness model

(iii) **Virtual Joint Modeling (VJM).** This method is based on the expansion of the traditional rigid-body model of the robotic manipulator, where the links and joints are assumed to be rigid and perfect while their compliances are taken into account by additional virtual springs that are referred to as virtual joints. Geometrically, such approximation is equivalent to adding these joints after the compliant elements (links and joints) whose flexibilities are described by these virtual joints. It is obvious that such lumped presentation of the manipulator stiffness essentially simplifies the model. For this reason, at present it is the most popular stiffness modeling method in robotics. The method has been firstly introduced by Salisbury (Salisbury, 1980) and Gosselin (Gosselin, 1990), who assumed that the manipulator flexibility is localized in the actuator joints only. The derived expression defining relation between the joint and Cartesian stiffness matrices became a basis for the manipulator stiffness analysis in many research works (Chen and Kao, 2002; Majou et al., 2007; Quennouelle, 2009). In the first works, it was strictly assumed that the links are rigid and each actuated joint is presented by a single one-dimensional virtual spring (Gosselin and Zhang, 2002; Pigoski et al., 1998; Zhang, 2000). In recent works, to take into account the links flexibilities, the number of virtual springs was increased up to six for each element (Pashkevich et al., 2009a). In this case, the key issue of this method is how to define the virtual spring parameters. One of the possible solutions has been proposed in (Klimchik, 2011), where the CAD models of the links were used to compute the compliance matrix

via FEA This leads to essential increase of VJM method accuracy that becomes comparable with the FEA approach, but the computational expenses are much lower.

As follows from the above presented review and comparison study, the VJM method is the most attractive one for the considered application area due to its computational efficiency and acceptable accuracy. In the frame of this method, all types of the compliance in the manipulator are localized in the actuated joints and presented by *virtual springs*. Using this approach, the manipulator can be presented as the sequence of rigid links separated by the actuators and virtual joints incorporating all elastic properties of compliant elements. Under these assumptions, the stiffness model of the serial robot can be presented as shown in Figure 1.17.

For VJM model of serial manipulator, the end-effector location $\mathbf{t}$ (that includes both position and orientation) can be defined by the extended geometric model described by the vector function

$$\mathbf{t} = g(\mathbf{q},\ \boldsymbol{\theta}) \tag{1.18}$$

where the vector $\mathbf{q}$ includes the actuator coordinates and $\boldsymbol{\theta}$ denotes the vector of virtual joint coordinates. It can be proved that the static equilibrium equation can be written as (Salisbury, 1980)

$$\mathbf{J}_\theta^T \cdot \mathbf{w} = \mathbf{K}_\theta \cdot \boldsymbol{\theta} \tag{1.19}$$

where $\mathbf{J}_\theta = \partial \mathbf{g}(\mathbf{q},\boldsymbol{\theta}) / \partial \boldsymbol{\theta}$ is the Jacobian matrix, and $\mathbf{K}_\theta$ is the $n \times n$ diagonal matrix

$$\mathbf{K}_\theta = \begin{bmatrix} \mathbf{K}_{\theta_1} & 0 & \cdots & 0 \\ 0 & \mathbf{K}_{\theta_2} & \ddots & \vdots \\ \vdots & \ddots & \ddots & 0 \\ 0 & \cdots & 0 & \mathbf{K}_{\theta_n} \end{bmatrix} \tag{1.20}$$

that aggregates stiffness of all virtual springs (here n is the number of the virtual joints). In order to find the desired stiffness matrix $\mathbf{K}_C$, the wrench-deflection relation $\mathbf{w} \to \Delta\mathbf{t}$ defined by equations (1.18) and (1.19) should be linearized in the neighborhood of the current manipulator configuration $\mathbf{q}$. It can be proved that this relation can be presented in the form

$$\Delta\mathbf{t} = \left(\mathbf{J}_\theta \mathbf{k}_\theta \mathbf{J}_\theta^T\right) \cdot \mathbf{w} \tag{1.21}$$

that yields the following expression for the desired Cartesian stiffness matrix

$$\mathbf{K}_C = \left(\mathbf{J}_\theta \mathbf{k}_\theta \mathbf{J}_\theta^T\right)^{-1} \tag{1.22}$$

which is obtained from the comparison of expressions (1.16) and (1.21). In the literature (Li et al., 2002), (Chen and Kao, 2000), the latter is sometimes presented in a different form as

$$\mathbf{K}_\theta = \mathbf{J}_\theta^T \mathbf{K}_C \mathbf{J}_\theta \tag{1.23}$$

which is also referred to as CCT (Conservative Congruency Transformation).

The above presented conventional formulations (1.22) and (1.23) for the mapping of stiffness matrices between the Cartesian and joint spaces have been found numerous applications and generalizations for different types of robots (Abele et al., 2007; Arumugam et al., 2004; Tyapin and Hovland, 2009; Vertechy and Parenti-Castelli, 2007). However, as it has been pointed out by several researchers, these expressions are only valid if the robotic manipulators are at their unloaded equilibrium configuration, i.e. without essential external forces (Chen and Kao, 2000). For this reason, CCT has been revised to describe the manipulator elastostatic properties in the loaded mode and presented in the form

$$\mathbf{K}_C = \left(\mathbf{J}_\theta^T \left(\mathbf{K}_\theta - \mathbf{K}_w \right)^{-1} \mathbf{J}_\theta \right)^{-1} \tag{1.24}$$

that includes an additional $n \times n$ matrix $\mathbf{K}_w$ induced by external loadings. This matrix is computed in the following way

$$\mathbf{K}_w = \frac{\partial^2}{\partial \boldsymbol{\theta}^2} \left(g^T (\mathbf{q},\, \boldsymbol{\theta}) \cdot \mathbf{w} \right) \tag{1.25}$$

and takes into account changes in the manipulator geometry under the loading via the second derivatives (Hessian) of the function $g^T(\mathbf{q},\, \boldsymbol{\theta}) \cdot \mathbf{w}$. Detailed proofs concerning the derivation and computation of matrix $\mathbf{K}_w$ are given in (Chen and Kao, 2000).

In spite of the fact that the VJM method was originally developed for serial manipulators, it can be also efficiently applied to parallel robots. The basic idea is to obtain the stiffness model for each kinematic chain separately, then to integrate them in a unified model, assuming the corresponding manipulator is strictly parallel (Pashkevich et al., 2008; Xi et al., 2004). However in practice, the kinematic chains are often connected to different points of the end-platform, so the simple summation cannot be directly applied. Another problem arises when the influence of passive joints, which are widely used in over- and under-constrained parallel manipulators, cannot be neglected (Pashkevich et al., 2008; Quennouelle, 2009). Besides, for parallel robots with parallelogram-based links, essential modifications of the VJM method are required. Detailed review for these issues can be found in (Klimchik, 2011).

Hence, for robotic application the VJM method is very attractive for stiffness modeling and provides reasonable trade-off between computational time and model accuracy. However, the main difficulty in this method is related to the evaluation of the parameters of virtual springs (i.e. the stiffness matrix $\mathbf{K}_{\theta_i}$). In the majority of the works, these matrices/coefficients have been obtained via approximations of manipulator links by symmetrical beams. In several works, the compliance matrices have been obtained from CAD models using virtual experiments. However, the latter approach has some limitations because of non-homogeneity and variations in the material properties. So, from engineering point of view, the most reasonable way to obtain reliable stiffness parameters (i.e. elements of the matrix $\mathbf{K}_\theta$) is to apply the model calibration techniques using the data from real experiments. This problem is considered in the following subsection.

1.3.2 Calibration of manipulator elastostatic model

As follows from the previous Subsection, the desired VJM-based model includes a number of elastostatic parameters that are not available in the datasheets provided by robot manufacturers. They can be evaluated using either *virtual experiments* in CAD environment or *real experiments* with measurement devices. First approach has been introduced in (Klimchik et al., 2013b), it is relatively simple but requires rather precise CAD models of the manipulator components. Using this method, it is possible to obtain the compliance matrices $\mathbf{k}_{\theta i}$ for the links, however it is hardly applicable to the identification of joint compliances. The second approach (based on real experiments) is currently used to calibrate the simplified manipulator stiffness model, which includes only the joint compliances as the parameters. It should be mentioned that, theoretically this approach can be also used in a more general case where the link compliances are included in the model as well. However, in practice, there are some difficulties that are typical for simultaneous identification of huge number of parameters that essentially differ in their magnitude and may be mutually dependent. In particular, for a typical 6-dof serial robot, the complete set of the elastostatic parameters consists of 258 elements, whose magnitudes differ by the factor of 10^3 and there are only 32 independent ones (Klimchik et al., 2013a).

On the other hand, in accordance with (Becquet, 1987), the link flexibility is usually lower compared to joint flexibility, and is responsible for less than 5% of the compliance errors. For this reason, in this work, it is assumed that the links are quite rigid comparing to the joints and the stiffness parameters are limited by the actuator joint compliances.

Similar to the manipulator geometric calibration (see Section 1.2), the elastostatic calibration includes four basic steps. However, related numerical techniques should be revised in accordance with the specificities of elastostatic calibration. Let us briefly describe them assuming that the manipulator geometric parameters are already calibrated.

Step 1: Modeling. The aim of first step is to obtain the manipulator elastostatic model that is suitable for calibration. It means that the desired model should be able to take into account not only the changes in the manipulator configuration but also the influence of the external loadings applied to the end-effector, which causes deformations in all links and joints. Besides, the model must take into account the influence of the gravity compensator that are usually used in heavy industrial robots employed in modern machining processes (Ortmeier and Engelhardt, 2002; Rahman et al., 1995; Ulrich and Kumar, 1991). It is clear that the above mentioned problems of the model completeness and irreducibility (see Section 1.2) are also important here in general case, when the full-scale VJM-based model of manipulator is used. However, because of the adapted assumptions concerning the dominating influence of the joint stiffness, the problem of stiffness model reduction does not arise here.

Step 2: Measurement. For the second step, the open-loop methods (end-effector position/location coordinate measurements) that are used in the geometric calibration can be also applied to the case of elastostatic calibration (Meggiolaro et al., 2005). However, in contrast to the geometric calibration, here to obtain the vector of the end-effector deflections, it is required to get measurements for the reference points twice, with two different loadings. In practice, to simplify the experiment setup, one of the measurements is usually performed with zero force (without loadings). In this case, the end-effector deflections is computed using the difference between these two measurements

$$\Delta\mathbf{t}_i = \mathbf{t}(\mathbf{q}_i, \mathbf{w}_i) - \mathbf{t}(\mathbf{q}_i, \mathbf{0}), \quad i = \overline{1,m} \tag{1.26}$$

Besides, in addition to the usual external devices for the end-effector coordinate measurements, the force sensor is required to measure the external forces/torques $\mathbf{w}_i$. For example, in (Wang et al., 2009), a portable coordinate measurement system was used for the measurement of end-effector coordinates and an ATI Omega force sensor was used to measure the external force acting on the robot. It should be mentioned that direct application of the closed-loop methods (point/plane constraints) require essential revision of the corresponding identification algorithm. Besides, in this case, the force sensors may introduce undesired compliance which also affects the identification accuracy.

Step 3: Identification. The third step can be also treated as the best fitting between the given input variables (joint coordinates and external forces) and the measurement output data (the end-effector location) using the developed models. Similar to the geometric calibration, this problem can be solved using the least-square technique

$$\sum \left\| g(\mathbf{q}_i,\ \boldsymbol{\theta}_i) - \mathbf{t}(\mathbf{q}_i, \mathbf{w}_i) \right\|^2 \to \min_{\mathbf{k}_\theta} \quad i = \overline{1,m} \tag{1.27}$$

where $g(.)$ defines the manipulator extended geometric model, $\mathbf{q}_i$ is the vector of actuated coordinates for corresponding manipulator configuration, $\boldsymbol{\theta}_i$ is the vector of robot elastostatic deflections and the function $\mathbf{t}(\mathbf{q},\mathbf{w})$ is the end-effector location obtained by measurements. In this

expression, the vectors $\mathbf{q}_i$ and $\mathbf{t}(\mathbf{q}_i, \mathbf{w}_i)$ are treated as known, while the vectors $\boldsymbol{\theta}_i$ are expressed via the unknown elastostatic parameters $\mathbf{k}_\theta$ using the following equation

$$\boldsymbol{\theta}_i = \mathbf{k}_\theta \cdot \mathbf{J}_{\theta i}^T \cdot \mathbf{w}_i \tag{1.28}$$

where $\mathbf{J}_{\theta i}$ is the Jacobian matrix with respect to the virtual joints $\boldsymbol{\theta}_i$. It should be mentioned that the problem of the least-square objective non-homogeneity also exists here (see subsection 1.2.3) and will be considered in details in the following chapter.

Step 4: Compensation. At the last step, the obtained elastostatic model is applied for the compliance errors compensation. Assuming that the external loadings are given by the prescribed technological process, corresponding technique requires repetitive computations of the manipulator Jacobian $\mathbf{J}_\theta$, which is presented in equation (1.21). This Jacobian highly depends on the robot configuration and varies essentially throughout the workspace. In contrast to the geometric error compensation (see Figure 1.14a), where the identified parameters can be integrated in the robot controller in the on-line mode using built-in geometric model, similar solution for the compliance errors compensation is hardly possible because there is no corresponding model in commercially available controllers. So, the only reasonable way is to apply the off-line error compensation, where the modification should be made in the control program by adjusting the reference trajectory (see Figure 1.18). In literature, there are also relevant compensation techniques that are based on neural networks, fuzzy logic, etc. (Huang et al., 2000; Yoo and Ham, 2000). Another popular method for compensation of compliance errors in the robotic-based machining is the so-called "mirror" technique, where the measurements of loadings and computation of stiffness parameters are not required (Dépincé and Hascoët, 2006; Seo, 1998). In the frame of this technique, the reference and corrupted trajectories (by compliance errors) are symmetrical to the desired one. However, to achieve the desired accuracy, several steps (application of the mirror technique) may be required (Dumas, 2011), more details concerning this method has been described in Section 1.2.3, (see Figure 1.16). So, this approach is only suitable for large-scale production where the manufacturing task and the workpiece location remain the same.

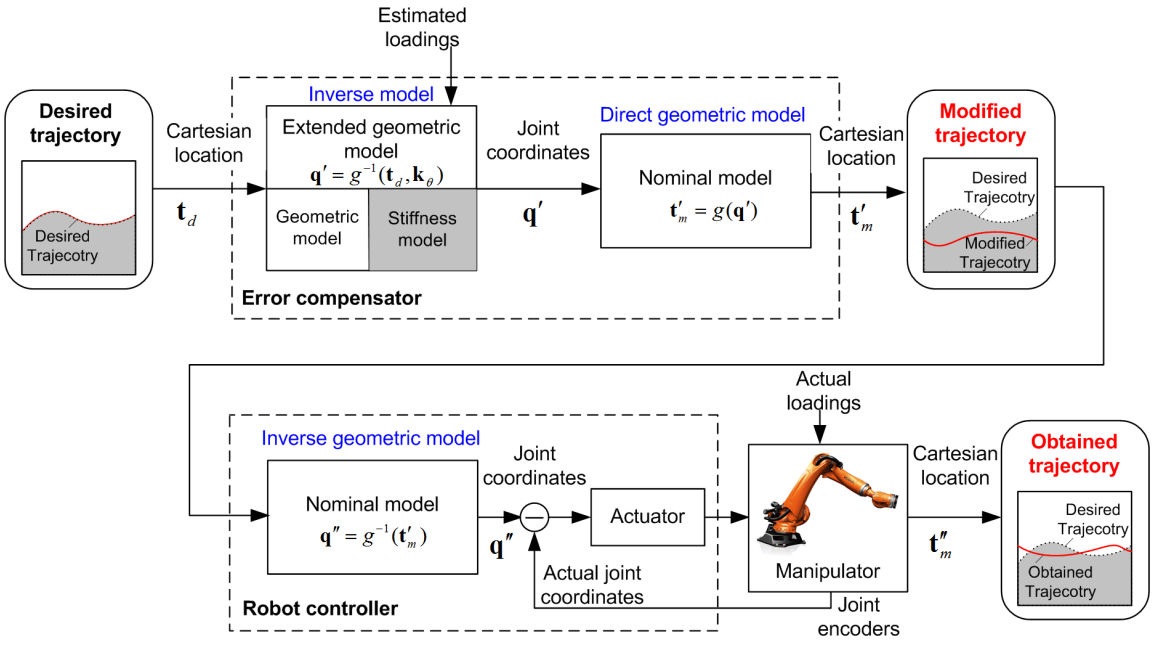

Figure 1.18 Off-line compliance errors compensation strategy

Summary of the above presented calibration steps is presented in Table 1.2, which highlights the main particularities and difficulties of elastostatic calibration. In contrast to the geometric calibration, the elastostatic one is based on both the manipulator extended geometric model and the stiffness model, and requires additional force sensors. The main difficulty is related to the application of force in different directions, whose magnitude is limited by admissible stresses in the manipulator components. The latter essentially affects the identification accuracy, which depends on the force magnitude.

Table 1.2 Particularities and difficulties of the elastostatic calibration

Calibration steps	Particularities	Difficulties
Step 1: Modeling	• Extended geometric model • Lumped stiffness model • Take into account robot configurations and applied forces	• Huge number of parameters • Influence of gravity compensator
Step 2: Measurement	• Measurements with two different loadings • Both position and force sensors are required	• Application of force in different directions • Limited force magnitude
Step 3: Identification	• Large number of parameters must be identified	• Identifiability of stiffness parameter • Non-homogeneity of the least-square objective • Problem of the weights assigning
Step 4: Compensation	• Compensation relies on both geometric and elastostatic models • Application of off-line compensation strategy only • Deflections depend on robot configurations and applied forces	• Evaluation of the machining forces • Influence of the dynamic factors: oscillation and chattering effects

Let us present in more details some previous results and key works in the area of the elastostatic calibration. This problem has been studied since 1980s. In one of the first works, Judd and Knasinski discovered that the flexibility in joints and in links is responsible for about 10% of the end-effector positioning errors (Judd and Knasinski, 1990). However, this conclusion has been made for case when the applied external forces are relatively small, which is not approved for the machining applications. As follows from our experience, in robotic-based machining (milling, for instance) the compliance errors dominate the geometric ones and are responsible for more than 90% of the end-effector deviations. On the other hand, according to the results presented in (Renders et al., 1991), the other error sources (such as gear transmission backlash, thermal expansion of the links, etc.) all together are responsible for less than 1% of the total positioning error. Some other works present an important influence of the thermal effect on the robot accuracy (Cherif et al., 2010; Pritschow et al., 2002) however this effect can be considered negligible if the robot is under similar oprerating condition during identification and machining.

Later, the problem of elastostatic calibration has attracted more attention. In particular, the identification of non-geometric errors was in the focus of the work (Gong et al., 2000), where the authors used a laser tracker to calibrate an advanced model of a 6-dof robot. In the frame of this work, geometric and compliance errors as well as thermal expansions have been taken into account

sequentially. The calibration was based on 30 different measurement configurations; it allowed reducing the positioning error from 1.06mm to 0.08mm. Another contribution in this area has been presented in (Jang et al., 2001), where the authors concentrated on the elastostatic calibration of a 6-dof welding industrial robot Daewoo DR06. It has been based on 112 measurement points *regularly spread* in a limited region of the robot workspace, where the loadings up to 15.2kg have been applied to generate the deformations. Corresponding end-effector locations were measured by a camera-type system Optotrak 6D. In this case, calibration improved the accuracy from 5.51mm to 1.87mm, which was acceptable for the welding application.

A slightly different approach has been presented in (Alici and Shirinzadeh, 2005), where the manipulator elastostatic properties have been described by an enhanced stiffness model (1.24) that takes into account both the first and second order derivatives of the geometric equations (Jacobian and Hessians). The primary goal was to improve the accuracy of a 6-dof robot Motoman SK 120, which contains a parallel five-bar mechanism. To calibrate its elastostatic parameters, 20 *heuristically selected* manipulator configurations have been used. The external forces/torques have been generated using a cable-pully system; the magnitudes varied from 0-50kg and were measured using a wrist force/torque sensor. Relevant experimental setup is presented in Figure 1.19a. Corresponding stiffness parameters have been obtained by solving the non-linear least-square optimization problem, the achieved accuracy is 0.43mm.

Another important works in this area has been devoted to the geometric and elastostatic calibration of medical robots used in patient positioning systems (Meggiolaro et al., 2005). Here, the geometric and elastostatic errors have been integrated in a unique model using polynomial approximation. Relevant calibration experiments have been carried out using 400 measurement configurations with the applied forces from 0-136kg. After calibration, the achieved accuracy was 0.38mm (the authors stressed that the desired accuracy of 0.5mm can be achieved using 125 configurations only).

An alternative approach for geometric and elastostatic errors compensation for the manipulator with closed-loops has been introduced in (Marie and Maurine, 2008). The authors used the MSA-based stiffness model (see Subsection 1.4.1), where the manipulator links were approximated by symmetrical beams whose stiffness parameters have been computed using conventional expressions known from the strength of material theory. This model was used for the error compensation of the industrial robot KUKA IR663 and allowed to achieve the accuracy of 0.3mm, which has been evaluated by direct measurements. Corresponding experimental setup is presented in Figure 1.19c.

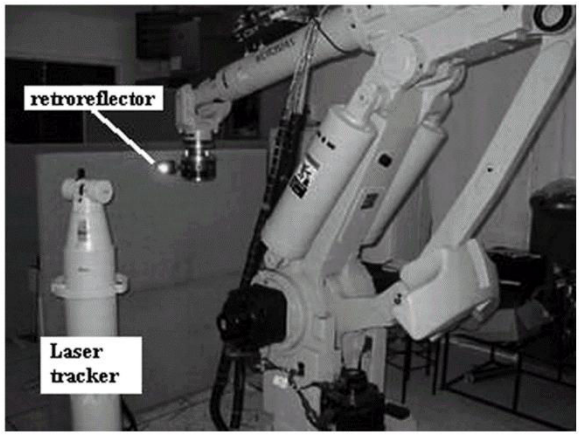

(a) Motoman SK 120 (Alici, 2005)

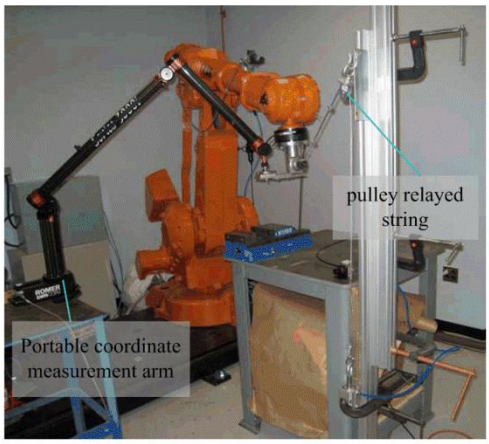

(b) Research Center of ABB Inc., Windsor, ABB IRB4400 (Wang, 2009)

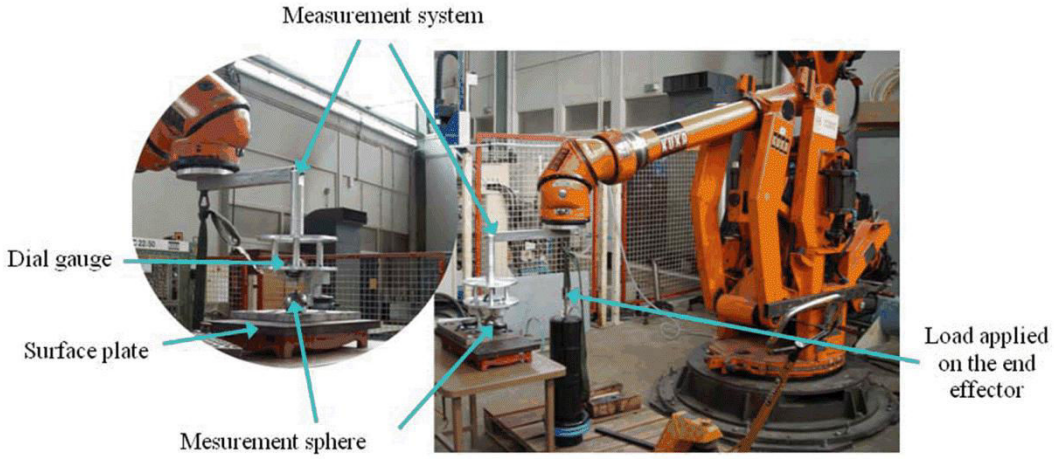

(c) INSA Rennes, KUKA IR663 (Marie, 2008)

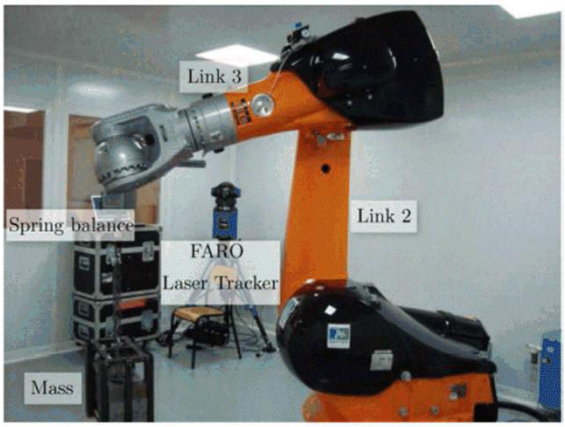

(d) Laboratory LGM2B, Bordeaux, KUKA KR240 (Dumas, 2011)

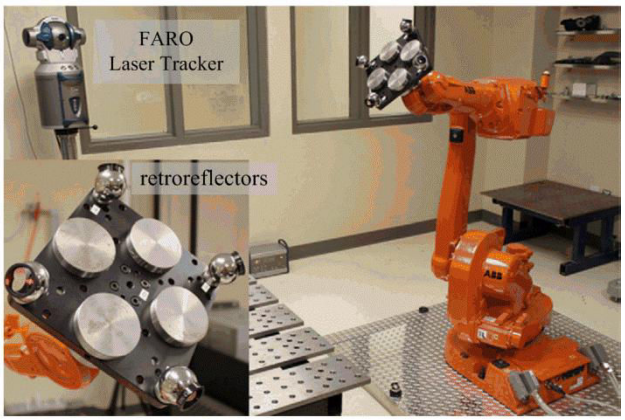

(e) Robotics laboratory, ETS, Montreal, ABB IRB 1600-6/1.45 (Nubiola, 2012)

Figure 1.19 Experimental setups of elastostatic calibration

In the last decade, the interest to the elastostatic calibration has been increased. There are a number of works that differ in manipulator architecture, application area and calibration experiment setups. For example, in (Lightcap et al., 2008), the authors attempted to improve the positioning accuracy of a 6-dof robot Mitsubishi PA10-6CE considering both geometric and elastostatic calibration. They have used the torsional springs to represent the manipulator flexibility and to take

into account the deflection caused by the robot payload. In the calibration experiments, 10 manipulator configurations were used, the applied loadings were up to 90N and the end-effector locations have been evaluated by a coordinates measuring machine. In this study, the calibration allowed to reduce the positioning errors from 2.45mm to 0.71mm.

Another example is the work of Wang *et al.* who focused on the positioning accuracy improvement for a 6-dof industrial robot ABB IRB4400 used for the machining (Wang et al., 2009). The manipulator elastostatic properties have been described by the conventional lumped model assuming that all flexibilities are concentrated in the actuated joints. The model parameters have been identified from six experiments, where the external forces have been generated using an air cylinder through a pulley relayed string. A portable coordinate measurement arm and the ATI Omega force sensor were used to measure the positions and forces respectively (see Figure 1.19b). In this case, the elastostatic calibration allowed reducing the end-effector positioning error from 1.8mm to 0.4mm.

Similar stiffness model has been used in (Dumas et al., 2012), where the authors concentrated on calibration of a 6-dof serial robot KUKA KR240 used in milling application. They also assumed that the manipulator links are rigid and the joints include torsional springs describing the manipulator elasticity, but the model has been enhanced by including the second-order derivative term $\mathbf{K}_w$ in Eq. (1.24) as it has been done by (Alici and Shirinzadeh, 2005). An essential distinct feature of this work is the use of some intuitive approaches for selection of measurement configurations that aim at minimizing the matrix $\mathbf{K}_w$ influence and providing good dexterity, evaluated via the condition number of the kinematic Jacobian. Based on this approach, 23 manipulator configurations were selected for the elastostatic calibration experiments. Corresponding experimental setups are presented in Figure 1.19d, which include a Faro laser tracker, several retroreflectors and a mass connected to the robot end-effector by means of a chain and a spring balance. The authors reported that after calibration the end-effector positioning accuracy was about 0.6 mm.

The most recent contributions in the area of elastostatic calibration belong to Bonev *et al.*, who used an extended geometric model with 29 parameters, both geometric and elastostatic ones (Nubiola and Bonev, 2012). In their experiment study, they dealt with a 6-dof robot ABB IRB 1600-6/1.45 (Figure 1.19e). To identify the desired parameters, 1000 configurations have been used, and for each of them several reference points were measured by a Faro laser tracking system. After calibration, the positioning accuracy was 0.7 mm within the entire workspace and 0.67 mm within certain cube volume.

State of the art in the area of manipulator elastostatic calibration is summarized in Table 1.3. As follows from this table, all of the authors used the open-loop method that relies on the end-effector position/location measurements by means of either laser tacking system or coordinates measurement machine (that provided either 3D or 6D deflections). Since these works deal with different robots whose elastostatic properties differ essentially, the magnitudes of the applied forces vary from 5-250 kg. The major difference in these calibration experiments was related to the number of measurement configurations that differs from one case to another and varies from only 6 configurations up to 1000. In spite of the fact that the authors used different experimental setups, they were able to achieve roughly the same accuracy within the range of 0.3-0.7 mm.

Table 1.3 Summary of the review on elastostatic calibration

Publications	Application: manipulator	Applied forces	Measurement devices	N° of poses	Achieved accuracy
(Alici and Shirinzadeh, 2005)	Motoman SK 120	0-50kg	Laser sensing system Wrist force/torque sensor	20	0.43 mm
(Meggiolaro et al., 2005)	Patient positioning system	0-136kg	Leica 3D laser tracker	125	0.49 mm
(Marie and Maurine, 2008)	KUKA IR663	30-100kg	Three dial indicators	—	0.3 mm
(Lightcap et al., 2008)	Mitsubishi PA10-6CE	0-9.2kg	MicroVal PFX454 touch trigger probe CMM	10	0.71 mm
(Wang et al., 2009)	ABB IRB4400	0-30.6kg	ATI Omega force sensor, Portable coordinate measurement arm	6	0.4 mm
(Dumas et al., 2012)	KUKA KR240	0-250kg	Faro laser tracker Spring balance	23	0.6 mm
(Nubiola and Bonev, 2012)	ABB IRB 1600-6/1.45	1.85-4.8kg	Faro laser tracking system	1000	0.7 mm

It is worth mentioning that in most of the relevant works the authors used the stiffness mode corresponding to strictly serial robotic manipulators, ignoring the fact that some of the considered manipulators include closed-loops created by *gravity compensators* and/or kinematic parallelograms (see Figure 1.19a-d). However, the closed-loops introduce additional elastostatic parameters that should be taken into account in the corresponding model (in contrast, these closed-loops do not effect the geometric model). For this reason, existing calibration techniques for such industrial robots should be enhanced adapting some results from the stiffness modeling of parallel manipulators (Deblaise et al., 2006; Li et al., 2002; Nagai and Liu, 2008; Pashkevich et al., 2009a).

Another important problem that has not yet received enough attention is *optimal selection of measurement configurations* aimed at increasing the calibration accuracy (using terminology from statistics, this problem can be also referred to as the "calibration experiments design"). This technique allows achieving the desired precision using minimum number of calibration experiments, which is important in industrial environment. It is clear that in an industrial workshop, it is not realistic to make 1000 measurements as in the work (Nubiola and Bonev, 2012), this process is very time and energy consuming, so the design of calibration experiments looks as a promising way to improve the calibration efficiency. This issue will be further discussed in the following section and is the primary subject of this work.

1.4 OPTIMAL DESIGN OF EXPERIMENTS IN CALIBRATION OF MANIPULATOR MODELS

In robotics, to achieve good accuracy, adequate model and precise model parameters are required. While in practice, the model structure is usually well known, the identification of the model parameters requires essential experimental work and the accuracy of the calibration results highly depends on the manipulator configurations. For this reason, the design of experiments (Atkinson et al., 2007) is an important problem and an efficient tool that allows to improve the parameter identification accuracy by proper selection of the measurement configurations. Originally, this idea came from the

linear regression analysis, so let us address some basic concepts of linear regression and design of experiment theory, as well as their applications/modifications in robot calibration.

1.4.1 Design of experiments for linear regression models

The linear regression analysis is a statistical approach that allows us to obtain the linear relation between model input and output variables. Under this assumption, a linear regression model (see Figure 1.20) can be presented as

$$\mathbf{y} = \mathbf{A}\mathbf{x} \tag{1.29}$$

where $\mathbf{x}$ is the $n \times 1$ input vector and $\mathbf{y}$ is $k \times 1$ output vector, $\mathbf{A}$ is the $k \times n$ regression matrix that is treated as unknown.

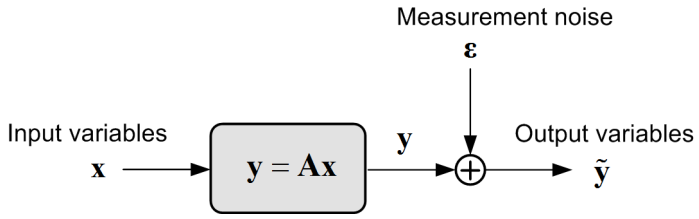

Figure 1.20 The linear regression model

For the identification, such a model is usually transformed into the form where the unknown parameters a_{ij} are extracted from the matrix $\mathbf{A}$ and are collected in a single vector $\boldsymbol{\pi} = [a_{11},...,a_{nk}]^T$. So, the model (1.29) is rewritten as

$$\mathbf{y} = \mathbf{X}\boldsymbol{\pi} \tag{1.30}$$

where $\mathbf{X}$ is $k \times nk$ so-called observation matrix that depends on the input variables:

$$\mathbf{X} = \begin{bmatrix} \mathbf{x}^T & \mathbf{0}_{1\times n} & \cdots & \mathbf{0}_{1\times n} \\ \mathbf{0}_{1\times n} & \mathbf{x}^T & \ddots & \mathbf{0}_{1\times n} \\ \vdots & \ddots & \ddots & \vdots \\ \mathbf{0}_{1\times n} & \mathbf{0}_{1\times n} & \cdots & \mathbf{x}^T \end{bmatrix}_{k\times nk} \tag{1.31}$$

To find the desired parameters $\boldsymbol{\pi}$, the users must carry out several experiments that provides sets of inputs $\left\{\mathbf{x}_i,\ i = \overline{1,m}\right\}$ and output measurements $\left\{\mathbf{y}_i,\ i = \overline{1,m}\right\}$. So, the system of equations that is used for identification can be expressed as

$$\mathbf{y}_i = \mathbf{X}_i\boldsymbol{\pi}, \quad i = 1,...,m \tag{1.32}$$

where m is the number of experiments. To identify the parameters $\boldsymbol{\pi}$, the number of experiments should be high enough to ensure the rank of the aggregated observation matrix to be equal to the number of desired parameters $n_\pi = kn$, i.e.

$$rank\begin{bmatrix} \mathbf{X}_1 \\ \vdots \\ \mathbf{X}_m \end{bmatrix} = n_\pi \tag{1.33}$$

However, in practice, the output measurements often include errors because of the inaccuracy of measurement devices. For this reason, the original model should be rewritten as

$$\tilde{\mathbf{y}}_i = \mathbf{X}_i\boldsymbol{\pi} + \boldsymbol{\varepsilon}_i, \quad i = 1,...,m \tag{1.34}$$

where the vector $\boldsymbol{\varepsilon}_i$ is the measurement error that is usually assumed to be the unbiased i.i.d. (independent and identically distributed) random variables with zero expectation and the standard deviation σ. Because of the measurement errors influence, the system (1.34) (which should be overdetermined to reduce the noise impact) cannot be solved exactly. For this reason, the least square approach is applied, which minimizes the sum of squared residuals. Using this method, the parameter estimation can be expressed as

$$\hat{\boldsymbol{\pi}} = \left(\sum_{i=1}^{m} \mathbf{X}_i^T \mathbf{X}_i \right)^{-1} \left(\sum_{i=1}^{m} \mathbf{X}_i^T \tilde{\mathbf{y}}_i \right) \tag{1.35}$$

It can be proved that this expression provides us with the unbiased estimate of the desired parameters, i.e.,

$$E(\hat{\boldsymbol{\pi}}) = \boldsymbol{\pi} \tag{1.36}$$

but for each set of the experiments providing us with the input-output values $\left\{ \mathbf{x}_i,\ \tilde{\mathbf{y}}_i,\ i = \overline{1,m} \right\}$, the estimated parameters differ from the true value $\boldsymbol{\pi}$. In practice, the degree of this variation is evaluated by the covariance matrix, which in the case of the above adapted assumptions can be expressed as

$$\operatorname{cov}\left(\hat{\boldsymbol{\pi}}\right) = \sigma^2 \left(\sum_{i=1}^{m} \mathbf{X}_i^{\mathrm{T}} \mathbf{X}_i \right)^{-1} \tag{1.37}$$

and where the matrix sum $\sum_{i=1}^{m} \mathbf{X}_i^{\mathrm{T}} \mathbf{X}_i$ is also referred to as the information matrix. It is clear that to achieve the best accuracy, the covariance matrix should be as small as possible and it can be reduced by proper selection of input variables $\left\{ \mathbf{x}_i,\ i = \overline{1,m} \right\}$ as well as by increasing the number of experiments.

The problem of the covariance matrix minimization is the key issue of the dedicated theory (design of experiments), where the notion of the "minimum covariance matrix" is formalized and several practical rules for selection of the input variables $\mathbf{x}_i$ are proposed. In most of the existing works (Franceschini and Macchietto, 2008), the optimal plans of experiments are based on a simple idea that, for the minimum of $\operatorname{cov}\left(\hat{\boldsymbol{\pi}}\right)$, the input variables should differ from each other as much as possible (within allowable limits, of course). This idea is illustrated in Table 1.4, where several optimal plans are shown for two types of the regression models:

(i) one-variable model $y = \pi_1 + \pi_2 x$ with two parameters

(ii) two-variable model $y = \pi_1 x_1 + \pi_2 x_2$ with two parameters

It can be proved that the covariance matrices of these models can be computed using expressions

$$\operatorname{cov}(\boldsymbol{\pi}) = \frac{2}{\sum_{i=1}^{m} \sum_{j=1}^{m} \left(x_i - x_j \right)^2} \begin{bmatrix} \sum_{i=1}^{m} x_i^2 & -\sum_{i=1}^{m} x_i \\ -\sum_{i=1}^{m} x_i & m \end{bmatrix} \tag{1.38}$$

and

$$\operatorname{cov}(\boldsymbol{\pi}) = \frac{1}{\sum_{i=1}^{m} x_{1i}^2 \sum_{i=1}^{m} x_{2i}^2 - \left(\sum_{i=1}^{m} x_{1i} x_{2i} \right)^2} \begin{bmatrix} \sum_{i=1}^{m} x_{2i}^2 & -\sum_{i=1}^{m} x_{1i} x_{2i} \\ -\sum_{i=1}^{m} x_{1i} x_{2i} & \sum_{i=1}^{m} x_{1i}^2 \end{bmatrix} \tag{1.39}$$

respectively. The corresponding covariance matrices are also presented in this table, assuming that the input variables are limited by certain values $x_j \in [-\Delta_j,\ \Delta_j]$.

Table 1.4 Optimal plans of experiments for one- and two-variable models

One-variable model	Two-variable model
Case of two measurement points: $m = 2$	
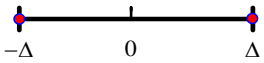 $\text{cov} = \frac{1}{2\Delta^2}\begin{bmatrix}\Delta^2 & 0\\ 0 & 1\end{bmatrix}$	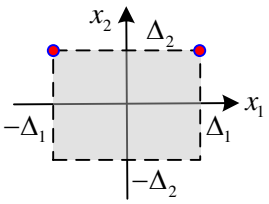 $\text{cov} = \frac{1}{2\Delta_1^2\Delta_2^2}\begin{bmatrix}\Delta_2^2 & 0\\ 0 & \Delta_1^2\end{bmatrix}$
Case of three measurement points: $m = 3$	
Plan 1 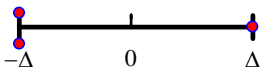 $\text{cov} = \frac{1}{8\Delta^2}\begin{bmatrix}3\Delta^2 & \Delta\\ \Delta & 3\end{bmatrix}$	Plan 1 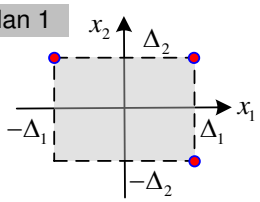 $\text{cov} = \frac{1}{8\Delta_1^2\Delta_2^2}\begin{bmatrix}3\Delta_2^2 & \Delta_1\Delta_2\\ \Delta_1\Delta_2 & 3\Delta_1^2\end{bmatrix}$
Plan 2 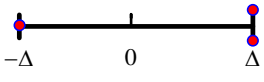 $\text{cov} = \frac{1}{8\Delta^2}\begin{bmatrix}3\Delta^2 & -\Delta\\ -\Delta & 3\end{bmatrix}$	Plan 2 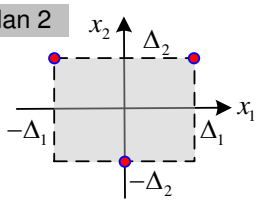 $\text{cov} = \frac{1}{6\Delta_1^2\Delta_2^2}\begin{bmatrix}3\Delta_2^2 & 0\\ 0 & 2\Delta_1^2\end{bmatrix}$
Plan 3 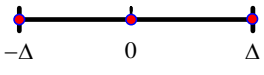 $\text{cov} = \frac{1}{6\Delta^2}\begin{bmatrix}2\Delta^2 & 0\\ 0 & 3\end{bmatrix}$	Plan 3 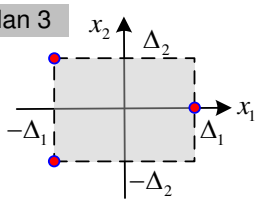 $\text{cov} = \frac{1}{6\Delta_1^2\Delta_2^2}\begin{bmatrix}2\Delta_2^2 & 0\\ 0 & 3\Delta_1^2\end{bmatrix}$
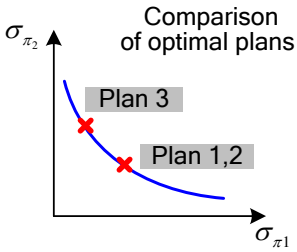	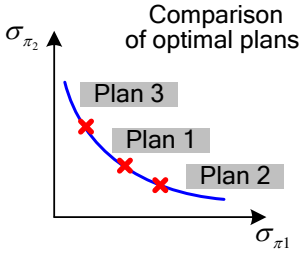
Case of three measurement points: $m = 4$	
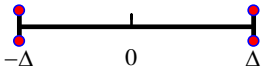 $\text{cov} = \frac{1}{4\Delta_1^2\Delta_2^2}\begin{bmatrix}\Delta_2^2 & 0\\ 0 & \Delta_1^2\end{bmatrix}$	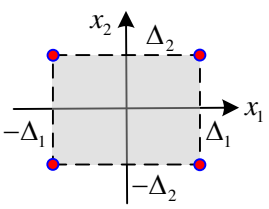 $\text{cov} = \frac{1}{4\Delta_1^2\Delta_2^2}\begin{bmatrix}\Delta_2^2 & 0\\ 0 & \Delta_1^2\end{bmatrix}$

As follows from the presented examples, the above mentioned simple rule (to locate the measurement points as far as possible from each other) usually provides us with reasonably good plan of experiments. Nevertheless, its straightforward application may yield unacceptable results. For instance, in the case of $m=2$ and for the model (ii), maximally distant points (Δ_1,Δ_2) and $(-\Delta_1,-\Delta_2)$ provides infinite covariance matrix. Moreover, in the case of $m=3$, this technique gives us several Pareto optimal solutions, from which the users must select a single one only. Clearly, it is not a trivial problem and requires some numerical criteria to compare these solutions. For this reason, several scalar criteria have been proposed in the related works (Driels and Pathre, 1990; Sun and Hollerbach, 2008a), which operate with different features of the covariance matrix (trace, determinant, eigenvalues, etc.). Using them, the so-called principles of A-, T-, D-, G-, E-optimality have been developed. Let us present them in more details in terms of the definition, advantages and drawbacks.

A- and **T-optimality** operate with the trace of covariance and information matrix respectively. The first one is aimed at minimization on the sum of diagonal elements of the covariance matrix and can be expressed as

$$\operatorname{trace}\left(\left(\sum_{i=1}^{m}\mathbf{X}_i^{\mathrm{T}}\mathbf{X}_i\right)^{-1}\right)\rightarrow\min_{\{\mathbf{x}_1,\ldots,\mathbf{x}_m\}} \tag{1.40}$$

The second approach maximizes the sum of diagonal elements of the information matrix and can be written as

$$\operatorname{trace}\left(\sum_{i=1}^{m}\mathbf{X}_i^{\mathrm{T}}\mathbf{X}_i\right)\rightarrow\max_{\{\mathbf{x}_1,\ldots,\mathbf{x}_m\}} \tag{1.41}$$

These two approaches have almost similar intuitive objectives, aiming at minimizing the average variances of the estimated parameters, however the optimization results might differ. In general, the T-optimality principle is easier to apply since it deals with the information matrix (where the matrix inversion is not required). However, as pointed out by many authors (De Pauw, 2005; Goodwin and Payne, 1977; Vanrolleghem et al., 1995; Zullo, 1991), this approach is unreliable because the off-diagonal elements of the information matrix are not included in the objective function. Besides, both of these criteria are hard to apply if the parameters have different units (in this case, the final results highly depend on their normalization).

D-optimality is targeted at maximizing the determinant of the information matrix (or minimizing the determinant of the covariance matrix) and can be written as

$$\det\left(\sum_{i=1}^{m}\mathbf{X}_i^{\mathrm{T}}\mathbf{X}_i\right)\rightarrow\max_{\{\mathbf{x}_1,\ldots,\mathbf{x}_m\}} \tag{1.42}$$

It tends to give extreme importance to the parameter to which the model is most sensitive. One of the potential problem here is that the volume of the confidence region can be reduced thanks to the decrease in the variance of a particular parameter (Pinto et al., 1990; Zullo, 1991). However, the errors in all the other parameters may remain very large.

G-optimality seeks to minimize the maximal diagonal elements in the covariance matrix and may be presented as the following form

$$\max\left\{\operatorname{diag}\left(\left(\sum_{i=1}^{m}\mathbf{X}_i^{\mathrm{T}}\mathbf{X}_i\right)^{-1}\right)\right\}\rightarrow\min_{\{\mathbf{x}_1,\ldots,\mathbf{x}_m\}} \tag{1.43}$$

where the function diag(·) extracts the diagonal elements of the covariance matrix. It has the effect of minimizing the maximum variance of the estimated parameters and ensures that there is no extremely large difference between the errors of the estimated parameters.

E-optimality intends to minimize the maximum eigenvalue of the covariance matrix and can be expressed as

$$\max\left\{\text{eig}\left(\left(\sum_{i=1}^{m}\mathbf{X}_i^{\mathrm{T}}\mathbf{X}_i\right)^{-1}\right)\right\}\rightarrow\min_{\{\mathbf{x}_1,\ldots,\mathbf{x}_m\}} \tag{1.44}$$

The objective of this approach is to minimize the maximum variance of all possible normalized linear combination of the parameter estimates. It is often used for the purpose of reducing parameter correlations (Franceschini and Macchietto, 2008; Sidoli et al., 2004).The linear regression analysis is a well studied area and the design of experiment techniques for relevant regression models have been properly developed. For this reason, their applications in robotics seem promising for good accuracy improvement in parameter identification. However, because of the non-linearity of the robot models, direct application may cause some problems, which will be presented in the following subsection.

1.4.2 Limitations of conventional techniques for robot calibration

In robotics, the main difficulty of calibration experiment design is that the robot kinematics and elastics cannot be described using linear models (1.29). In contrast, for the robotic manipulators, relevant models are highly non-linear, and the parameters are integrated in expressions in more complex way. So, direct application of the conventional techniques may provide unreasonable calibration results, which are briefly presented below.

For illustrative purposes, let us evaluate the applicability of optimal experiment plans from the previous subsection (see Table 1.3) for the measurement pose selection of a two-link manipulator presented in Figure 1.21. It is assumed that the joint limits of this manipulator are $q_1\in[-180°,180°]$ and $q_2\in[-150°,150°]$, and the manipulator geometry is described by the expressions

$$\begin{cases} p_x=(l_1^0+\Delta l_1)\cos(q_1+\Delta q_1)+(l_2^0+\Delta l_2)\cos(q_1+q_2+\Delta q_1+\Delta q_2)\\ p_y=(l_1^0+\Delta l_1)\sin(q_1+\Delta q_1)+(l_2^0+\Delta l_2)\sin(q_1+q_2+\Delta q_1+\Delta q_2)\end{cases} \tag{1.45}$$

where the variables p_x, p_y define the manipulator end-effector position in Cartesian space, l_1^0, l_2^0 denote the nominal link lengths, q_1, q_2 are the actuated joint coordinates. The unknown parameters to be identified are denoted as $\Delta q_1, \Delta q_2$ and $\Delta l_1, \Delta l_2$, they are respectively the joint offsets and the link length errors. So, here the vector of parameters is defined as $\boldsymbol{\pi}=(\Delta l_1, \Delta l_2, \Delta q_1, \Delta q_2)$.

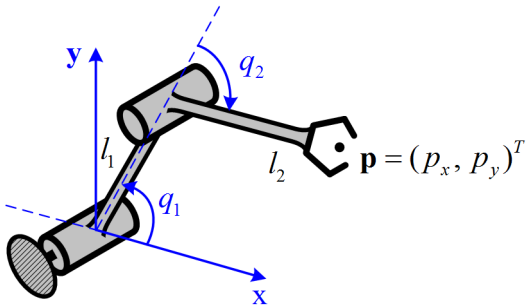

Figure 1.21 Two-link planar manipulator

It can be easily proved that for this case, the minimum number of configurations required for the calibration experiments $m=2$. Corresponding covariance matrix can be computed using Eq.(1.37), where the observation matrix $\mathbf{X}$ should be substituted by the identification Jacobian $\mathbf{J}_\pi$, which is obtained by straightforward differentiation of Eq.(1.45) with respect to the components of the vector $\boldsymbol{\pi}$. Relevant matrix has the following analytical form

$$\operatorname{cov}(\boldsymbol{\pi})=\begin{bmatrix} \frac{1}{1-C_\Delta} & \frac{C_2^{(1)}+C_2^{(2)}}{2\left(C_\Delta-1\right)} & 0 & \frac{S_2^{(1)}+S_2^{(2)}}{2l_2\left(1-C_\Delta\right)} \\ \frac{C_2^{(1)}+C_2^{(2)}}{2\left(C_\Delta-1\right)} & \frac{1}{1-C_\Delta} & \frac{S_2^{(1)}+S_2^{(2)}}{2l_1\left(C_\Delta-1\right)} & \frac{S_2^{(1)}+S_2^{(2)}}{2l_1\left(1-C_\Delta\right)} \\ 0 & \frac{S_2^{(1)}+S_2^{(2)}}{2l_1\left(C_\Delta-1\right)} & \frac{1}{l_1^2\left(1-C_\Delta\right)} & \frac{2l_2+l_1\left(C_2^{(1)}+C_2^{(2)}\right)}{2l_1^2l_2\left(C_\Delta-1\right)} \\ \frac{S_2^{(1)}+S_2^{(2)}}{2l_2\left(1-C_\Delta\right)} & \frac{S_2^{(1)}+S_2^{(2)}}{2l_1\left(1-C_\Delta\right)} & \frac{2l_2+l_1\left(C_2^{(1)}+C_2^{(2)}\right)}{2l_1^2l_2\left(C_\Delta-1\right)} & \frac{l_1^2+l_2^2+l_1l_2\left(C_2^{(1)}+C_2^{(2)}\right)}{l_1^2l_2^2\left(1-C_\Delta\right)} \end{bmatrix} \tag{1.46}$$

where $q_1^{(i)}, q_2^{(i)}$, $i=1,2$ define the measurement configurations $\mathbf{q}^{(i)}=(q_1^{(i)}, q_2^{(i)})$, and C_*, S_* stand for the cosine and sine of the corresponding joint angles: $C_2^{(i)}=\cos(q_2^{(i)})$, $S_2^{(i)}=\sin(q_2^{(i)})$, and $C_\Delta=\cos(q_2^{(1)}-q_2^{(2)})$. In the above matrix, the rows (columns) 1 and 2 correspond to the parameters Δl_1, Δl_2 and the rows (columns) 3 and 4 are related to the parameters Δq_1, Δq_2. It should be noted that this matrix does not include angles $q_1^{(1)}$ and $q_1^{(2)}$, so the calibration results will not vary with their values, and only the variables $q_2^{(1)}$ and $q_2^{(2)}$ are important here.

As it has been mentioned above, to achieve the highest identification accuracy the calibration plans should produce the minimum covariance matrix. It is obviously a multi-objective optimization problem, that cannot be solved unambiguously. For this reason, let us try several intuitive approaches to obtain the plans of experiments. The first group of them arrives *from the conventional design of experiments theory* (see previous subsection) that motivates users to spread the measurement points as much as possible. This yields the following solutions

Plan #1: $\mathbf{q}_1=(-180°,150°)$ and $\mathbf{q}_2=(180°,150°)$

Plan #2: $\mathbf{q}_1=(-180°,150°)$ and $\mathbf{q}_2=(180°,-150°)$

whose covariance matrices are presented in Table 1.5. As follows from these results, plan #1 (which is optimal for the linear regression model) is not acceptable here, because the relevant information matrix is singular and the covariance matrix is infinite (in other words, the desired parameters cannot be obtained from this set of experiments). In contrast, plan #2 (which is unacceptable for the linear regression) can be used in robotics, but its optimality is not clear and relevant covariance matrix should be compared with other ones obtained using different ideas.

The second group of plans can be obtained in a more straightforward way, by *minimizing the diagonal elements of the covariance matrix* (1.46), which represent the variances of the parameters Δl_1, Δl_1, Δq_1, Δq_2 respectively that will be further denoted as $\sigma_1^2,...,\sigma_4^2$. As follows from relevant expressions, corresponding optimality conditions can be written as

(i) The variances σ_1^2, σ_2^2, σ_3^2 are minimal if $C_\Delta=-1$ or equivalently, if $\sum_{i=1}^{2} C_2^{(i)}=0$ and $\sum_{i=1}^{2} S_2^{(i)}=0$;

(ii) The variance σ_4^2 is minimal if $\sum_{i=1}^{2} S_2^{(i)}=0$ and $\sum_{i=1}^{2} C_2^{(i)}=\{-2l_1/l_2 \text{ or } -2l_2/l_1\}$.

Using these optimality conditions, another plan of calibration experiments was obtained

Plan #3: $\mathbf{q}_1 = (0°, 90°)$ and $\mathbf{q}_2 = (0°, -90°)$

that satisfies the first optimality condition. As follows form relevant covariance matrix presented in Table 1.5, in this case, the variances $\sigma_1^2, ..., \sigma_3^2$ are 4 times smaller comparing to those obtained for plan #2. On the contrary, the variance σ_4^2 has been increased almost twice. Finally, for comparison purposes, one more plan was generated in more intuitive way

Plan #4: $\mathbf{q}_1 = (0°, 135°)$ and $\mathbf{q}_2 = (0°, -135°)$.

This plan is intermediate between the plans #2 and #3.

Comparison results for the plans #2, #3 and #4 are presented in Figure 1.22 (plan #1 is not included since it is not acceptable because of the covariance matrix infinity). As follows from this figure, all these solutions can be treated as Pareto-optimal ones, i.e., they are not strictly dominated by each other. For instance, the reduction of the variance σ_3^2 always leads to increasing of σ_4^2, but the variances σ_1^2 and σ_2^2 are reduced in a similar way. Hence, the *selection of a particular plan* from the set of acceptable ones is not a trivial problem that requires some additional efforts. It should be mentioned that most of the existing criteria (used in the A-, T-, G-optimality principles) cannot be applied here since they either sum or compare the matrix elements with different units, which is inconsistent from physical point of view.

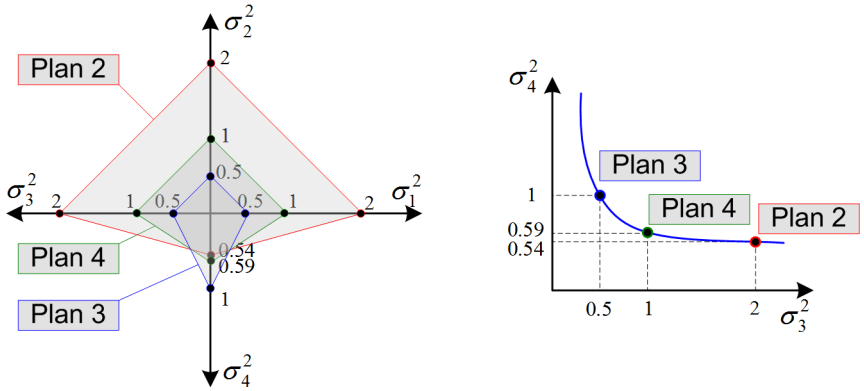

Figure 1.22 The Pareto-optimal solutions (normalized with respect to $\lambda_1\lambda_2$, assuming $\lambda_1 = \lambda_2 = 1$)

Another useful conclusion is related to the *location of the measurement points* within the space of allowable joint variables. It is worth mentioning that for linear regression (see Table 1.4) the measurement points should be spread as much as possible and are located on the boarders of the allowable space. However, for the manipulator studied in this subsection, the Pareto-optimal solutions can be located inside of this space. During our analysis, one more idea has been examined: to evaluate the measurement point location in other spaces (unit circle, sphere, etc.) but it has not produced any reasonable result because the covariance matrix (1.46) is invariant with respect to joint variables $q_1^{(1)}$ and $q_1^{(2)}$.

Therefore, the considered example shows limitations of the conventional design of experiments techniques that came from the linear regression analysis. For this reason, in robotics, there have been developed a number of special techniques and dedicated performance measures for the problem of measurement pose selection, which will be in the focus of following subsections.

Table 1.5 Different plans of calibration experiments and corresponding covariance matrices (case of a two-link manipulator $\lambda_i = 1/l_i,\ i = 1,2$)

Measurement configuration	Covariance matrix
Group 1: conventional design of experiments	
Plan #1: $\mathbf{q}_1 = (-180°, 150°),\ \mathbf{q}_2 = (180°, 150°)$ 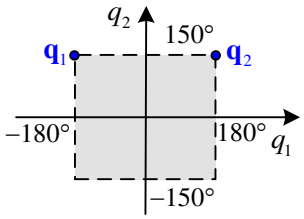	$\mathrm{cov} = \begin{bmatrix} \inf & & & \\ & \inf & & \\ & & \inf & \\ & & & \inf \end{bmatrix}$
Plan #2: $\mathbf{q}_1 = (-180°, 150°),\ \mathbf{q}_2 = (180°, -150°)$ 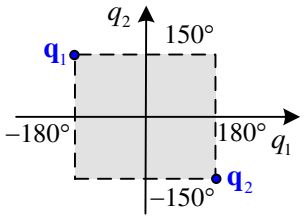	$\mathrm{cov} = \begin{bmatrix} 2 & \sqrt{3} & 0 & 0 \\ \sqrt{3} & 2 & 0 & 0 \\ 0 & 0 & 2\lambda_1^2 & -2\lambda_1^2 + \sqrt{3}\lambda_1\lambda_2 \\ 0 & 0 & -2\lambda_1^2 + \sqrt{3}\lambda_1\lambda_2 & 2(\lambda_1^2 + \lambda_2^2 - \sqrt{3}\lambda_1\lambda_2) \end{bmatrix}$
Group 2: covariance matrix minimization	
Plan #3: $\mathbf{q}_1 = (0°, 90°),\ \mathbf{q}_2 = (0°, -90°)$ 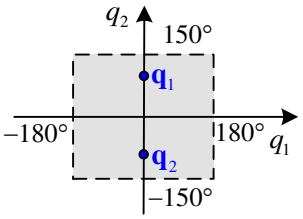	$\mathrm{cov} = \begin{bmatrix} 0.5 & 0 & 0 & 0 \\ 0 & 0.5 & 0 & 0 \\ 0 & 0 & 0.5\lambda_1^2 & -0.5\lambda_1^2 \\ 0 & 0 & -0.5\lambda_1^2 & 0.5(\lambda_1^2 + \lambda_2^2) \end{bmatrix}$
Plan 4: $\mathbf{q}_1 = (0°, 135°),\ \mathbf{q}_2 = (0°, -135°)$ 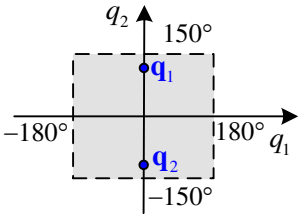	$\mathrm{cov} = \begin{bmatrix} 1 & -\sqrt{2}/2 & 0 & 0 \\ -\sqrt{2}/2 & 1 & 0 & 0 \\ 0 & 0 & \lambda_1^2 & -\lambda_1^2 + \sqrt{2}/2\lambda_1\lambda_2 \\ 0 & 0 & -\lambda_1^2 + \sqrt{2}/2\lambda_1\lambda_2 & \lambda_1^2 + \lambda_2^2 - \sqrt{2}\lambda_1\lambda_2 \end{bmatrix}$

1.4.3 Design of experiments for robot calibration

Taking into account the above mentioned difficulties and the manipulator particularities, the robotic experts have proposed a number of dedicated criteria for the selection of the manipulator measurement configurations. They are mainly based on the singular values of the identification

Jacobian $\mathbf{J}_\pi$, and have been named as the observability indices (Sun and Hollerbach, 2008b). It should be mentioned that the majority of the related works are devoted to the calibration of manipulator geometric parameters. Let us briefly describe these indices

Criterion O_1: *Root of the singular values product.* This criterion is based on the principle of D-optimality (Borm and Meng, 1991), which seeks to maximize the geometric mean of all the singular values

$$\sqrt[n_s]{\sigma_{\min} \cdots \sigma_{\max}} \rightarrow \max_{\{\mathbf{q}_1,\ldots,\mathbf{q}_m\}} \tag{1.47}$$

where $\sigma_{\min}$ and $\sigma_{\max}$ are the minimum and maximum singular value of the identification Jacobian matrix $\mathbf{J}_\pi$ computed for the measurement configurations $\{\mathbf{q}_1,\ldots,\mathbf{q}_m\}$, and n_s is the number of parameters to be identified (which should be equal to the number of non-zero singular values). This performance measure has been used for the calibration of Delta robot (Lintott and Dunlop, 1997).

Criterion O_2: *The inverse condition number*. This criterion has been introduced in (Driels and Pathre, 1990), it deals with the maximization of the function

$$\frac{\sigma_{\min}}{\sigma_{\max}} \rightarrow \max_{\{\mathbf{q}_1,\ldots,\mathbf{q}_m\}} \tag{1.48}$$

which allows us to ensure that no singular value is preferred over another such that the errors are homogenized, so this index is dimensionless. For this reason, this criterion has found wide applications for the problem of measurement pose selection for the manipulator geometric calibration (Huang et al., 2008; Khalil et al., 1991; Zhuang et al., 1994; Zhuang et al., 1996). However, in most of previous works, it was ignored an obvious fact that a good condition number cannot ensure small variances (relevant example is presented in the following subsection).

Criterion O_3: *The minimum singular value*. This criterion aims at maximizing the minimum singular value:

$$\sigma_{\min} \rightarrow \max_{\{\mathbf{q}_1,\ldots,\mathbf{q}_m\}} \tag{1.49}$$

which intends to maximize the worst observability of the parameters errors. In (Nahvi et al., 1994), this index along with the condition number (criterion O_2) have been used simultaneously as the principle indices for the geometric calibration of a parallel robot.

Criterion O_4: *The noise amplification index*. This criterion attempts to maximize the product of the inverse condition number and minimum singular value

$$\frac{\sigma_{\min}^2}{\sigma_{\max}} \rightarrow \max_{\{\mathbf{q}_1,\ldots,\mathbf{q}_m\}} \tag{1.50}$$

It combines indices O_2 and O_3 in order to take into account the advantages of each. It is considered as an indicator of the amplification of the sensor noise and un-modeled errors (Nahvi and Hollerbach, 1996). The bigger this index, the smaller the error impacts. The effectiveness of this index comparing to the others has been confirmed by calibration of a 3-dof parallel-drive robot. In this work, the idea of the noise amplification will be developed further (but using different approach).

Based on the above performance measures, many of the researchers focused on the *associated optimization problems* for the geometric calibration of different types of robot. In particular, Khalil *et al*. (Khalil et al., 1991) used a conjugate-type optimization method. Zhuang *et al*. tried to avoid local minima by using simulated annealing (Zhuang et al., 1994) and genetic algorithm (Zhuang et al.,

1996). Daney *et al.* developed an algorithm called the iterative one-by-one pose search (IOOPS), and applied it to the calibration of a Gaugh platform (Daney, 2002). In spite of the fact that these results are promising and provided rather good convergence for the considered case studies, the problem of the optimization technique efficiency for robot calibration is not solved yet for the general case.

Although the problem of geometric calibration is rather important, the geometric errors are not the only sources of errors that may influence the manipulator end-effector location. For the robots that are used in machining process, the applied cutting forces may cause essential compliance errors that also have significant impacts on the end-effector location. Similar to the geometric calibration, the robot compliance errors also highly depend on the manipulator configurations and differ throughout the workspace. For this reason, the identification of elastostatic parameters becomes a crucial issue. However, few works had addressed this problem (Carbone and Ceccarelli, 2010; Zhou et al., 2010), where the design of experiments can also be obviously applied. So, let us investigate the applicability and limitations of the presented existing techniques for calibration experiments design for this new application area.

1.4.4 Measurement pose selection for geometric and elastostatic calibration

To show the limitations of the existing techniques for simultaneous geometric and elastostatic calibration, let us apply them to the two-link manipulator considered in subsection 1.4.2. To avoid the problem of non-homogeneity, here only the joint offsets $\boldsymbol{\pi} = (\Delta q_1, \Delta q_2)^T$ are considered as the parameters to be identified in *geometric calibration*. In this case, the end-effector position of this manipulator can be expressed as

$$\begin{cases} p_x = l_1 \cos(q_1 + \Delta q_1) + l_2 \cos(q_1 + \Delta q_1 + q_2 + \Delta q_2) \\ p_y = l_1 \sin(q_1 + \Delta q_1) + l_2 \sin(q_1 + \Delta q_1 + q_2 + \Delta q_2) \end{cases} \tag{1.51}$$

and the identification Jacobian (which is also an observation matrix here) can be computed as

$$\mathbf{J}_\pi = \begin{bmatrix} -l_1 \sin(q_1) - l_2 \sin(q_1 + q_2) & -l_2 \sin(q_1 + q_2) \\ l_1 \cos(q_1) + l_2 \cos(q_1 + q_2) & l_2 \cos(q_1 + q_2) \end{bmatrix} \tag{1.52}$$

This matrix allows us to express the end-effector deviations as

$$\Delta \mathbf{p} = \mathbf{J}_\pi \Delta \boldsymbol{\pi} \tag{1.53}$$

and has been used for computing the existing performance measures (see subsections 1.4.1 and 1.4.3) corresponding to different plans of experiments examined below.

For the *elastostatic calibration*, it was assumed that the geometric parameters have been already calibrated, and only the joint compliances $\mathbf{k} = (k_1,\ k_2)^T$ are the parameters to be identified. Under such assumptions and in accordance with (Pashkevich et al., 2009a), the manipulator end-effector displacement caused by external loadings can be written as

$$\Delta \mathbf{p} = \mathbf{J}_\theta \mathbf{k}_\theta \mathbf{J}_\theta^{\mathrm{T}} \mathbf{F} \tag{1.54}$$

where $\Delta \mathbf{p}$ defines the end-effector displacement; $\mathbf{k}_\theta$ is a matrix that aggregates the joint compliances; $\mathbf{J}_\theta$ is the kinematic Jacobian, which can be obtained using Eq.(1.52), and $\mathbf{F} = [F_x,\ F_y]$ is the external forces applied to the end-effector. For identification purposes, this relation can be transformed into the linearized form (1.30) and be expressed as

$$\Delta \mathbf{p} = \mathbf{A}\mathbf{k} \tag{1.55}$$

where matrix $\mathbf{A}$ is the observation matrix here and has the following form

$$\mathbf{A}=\begin{bmatrix} -(l_1S_1+l_2S_{12})\left((l_1C_1+l_2C_{12})F_y-(l_1S_1+l_2S_{12})F_x\right) & -l_2^2S_{12}\left(C_{12}F_y-S_{12}F_x\right) \\ (l_1C_1+l_2C_{12})\left((l_1C_1+l_2C_{12})F_y-(l_1S_1+l_2S_{12})F_x\right) & l_2^2C_{12}\left(C_{12}F_y-S_{12}F_x\right) \end{bmatrix} \tag{1.56}$$

where S_*, C_* stand for the sine and cosine of the corresponding joint angles: $S_1=\sin(q_1)$, $C_1=\cos(q_1)$, $S_{12}=\sin(q_1+q_2)$ and $C_{12}=\cos(q_1+q_2)$. The obtained linear relation has been further used for the identification of the elastostatic parameters using conventional least square approach.

The comparison study has been carried out for this manipulator with the following parameters: the link lengths: $l_1=1\text{m}$, $l_2=0.8\text{m}$, and the force magnitude $F=1\text{N}$. The measurement accuracy has been defined by the parameter $\sigma=0.1\text{mm}$. The corresponding numerical results for the case of one calibration experiment for different optimization objectives are presented in Table 1.6 and Table 1.7 for geometric and elastostatic calibration respectively. They include corresponding optimal measurement poses (obtained by optimization of relevant objectives) and the identification accuracy of the model parameters. To simplify the comparison, the identification accuracy is also presented in Figure 1.23.

Table 1.6 Comparison of measurement poses for geometric calibration

Experiment design principle	Optimal Poses [deg]		Identification Accuracy [rad$\times10^{-3}$]	
	q_1	q_2	$\sigma_{\Delta q1}$	$\sigma_{\Delta q_2}$
Conventional approach				
A-optimality	64.3	114.2	0.110	0.136
T-optimality	87.5	0	inf	inf
D-optimality	-80.3	-90.0	0.100	0.160
G-optimality	55.8	-121.5	0.115	0.133
E-optimality	90.5	-128.7	0.128	0.128
SVD-based approach				
O_1-optimality	-137.3	-90.0	0.100	0.160
O_2-optimality	30.7	-134.6	0.140	0.126
O_3-optimality	90.5	-128.7	0.128	0.128
O_4-optimality	-180.0	131.5	0.133	0.127

As follows from these results, the obtained optimal measurement configurations differ from one criterion to another, and the identification accuracy presented in Figure 1.23. shows that there is no unique optimal solution that satisfies all criteria simultaneously. It should be mentioned that in both cases of calibration (geometric and elastostatic), the results corresponding to the T-optimality principle are not included because unreasonable plans (manipulator singular configurations) were generated, from which the desired parameters cannot be obtained. For the case of geometric calibration, relevant experiment plans provide a set of Pareto-optimal solutions, which do not dominate each other. For the case of elastostatic calibration, the solutions obtained using the principles O_2- and O_4-optimality are dominated by the other ones, and the remaining solutions are also Pareto-optimal. These plans can be all considered as optimal in different senses, and from which the users are not able to choose a single one. In fact, the main disadvantage of these approaches is that their optimization objectives are not directly related to the robot accuracy, which is a critical issue in industry. So, despite that they may

improve the identification accuracy for the model parameters, they cannot provide desired precision for the robot end-effector location.

Table 1.7 Comparison of measurement poses results for elastostatic calibration

Experiment design principle	Optimal Poses [deg]		Identification Accuracy [rad/N×10^{-3}]	
	q_1	q_2	$\sigma_{\Delta k_1}$	$\sigma_{\Delta k_2}$
Conventional approach				
A-optimality	-82.5	98.4	0.1123	0.1948
T-optimality	0	0	inf	inf
D-optimality	45.9	-63.8	0.0765	0.2804
G-optimality	-155.2	-64.9	0.0727	0.3437
E-optimality	-89.2	-108.9	0.1416	0.1840
SVD-based approach				
O_1-optimality	45.9	-63.8	0.0765	0.2804
O_2-optimality	97.5	143.1	0.3187	0.3187
O_3-optimality	-89.2	-108.9	0.1416	0.1840
O_4-optimality	-93.3	118.5	0.1707	0.1840

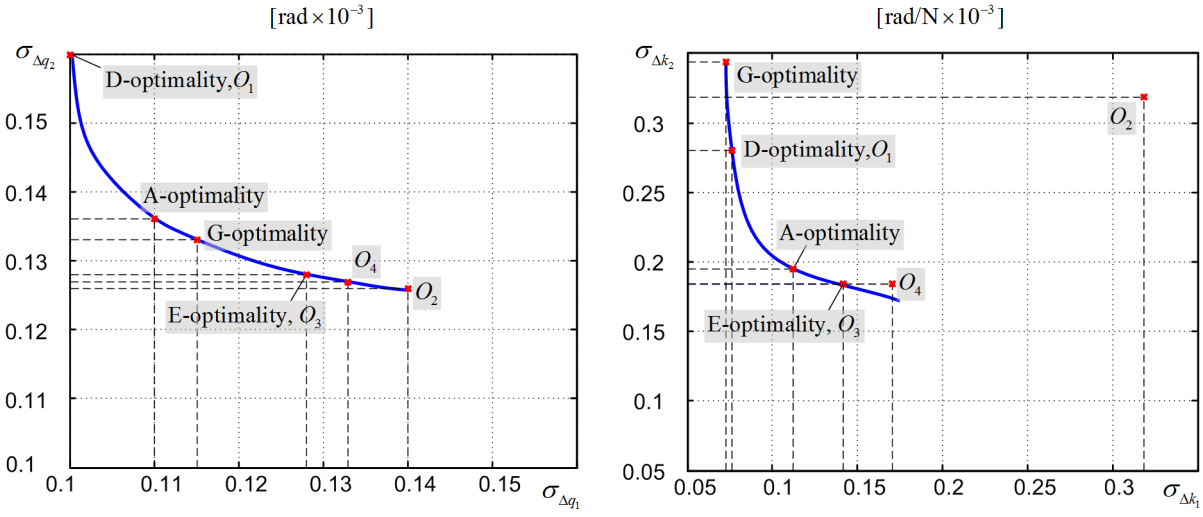

(a) Geometric parameters (b) Elastostatic parameters

Figure 1.23 Identification accuracy for different approaches to calibration experiments design

Hence, in order to achieve high calibration accuracy for the manipulator parameters (both geometric and elastostatic ones), as well as for the end-effector location, it is important to define a proper objective for measurement pose selection. As follows from our experience, an appropriate performance measure should satisfy the following requirements:

(a) it should be able to evaluate the parameters with different units

(b) it should minimize the maximum errors in the identified parameters

(c) it should detect the model parameter errors impact on the end-effector location accuracy.

Based on these requirements, the existing approaches have been evaluated qualitatively, and the corresponding results are presented in Table 1.8.

Table 1.8 Summary of the existing approaches to calibration experiment design

Experiment design principle	Requirement (a)	Requirement (b)	Requirement (c)
A-optimality	—	✔	—
T-optimality	—	✔	—
D-optimality	✔	—	—
G-optimality	—	✔	—
E-optimality	✔	—	—
O_1 -optimality	✔	—	—
O_2 -optimality	✔	—	—
O_3 -optimality	✔	—	—
O_4 -optimality	✔	—	—

As follows from the presented results, all existing principles of experiment design provide solutions for which at least one requirement cannot be satisfied. On the other hand, relevant design objectives are not directly related to the robot accuracy. Hence, taking into account the specificities of the application area studied in this work, it is required to develop a new industry-oriented performance measure for the calibration experiment design, which ensures high positioning accuracy of the robot manipulator under the loading caused by technological process.

1.5 SUMMARY: THESIS GOAL AND RESEARCH PROBLEMS

In machining of large dimensional parts, application of industrial robots looks very attractive since they provide large workspace and more flexibility comparing to conventional CNC-machines. But because of some particularities of robot kinematics, the end-effector positioning errors are accumulated from link to link and affect on the machining accuracy. Besides, in this application, the elastic deflections of the robot transmissions and links become significant and comparable with the geometric errors that are traditionally studied in robotic literature. For this reason, to achieve desired accuracy of the machining process, robot control must rely on the accurate manipulator model that is able to compensate both the geometric errors and the elastic deformations under loadings caused by the machining force/torque and the gravity forces applied to the manipulator components.

However in practice, most of the model parameters are unknown, only nominal values of the principal geometric parameters can be extracted from the manufacturer datasheet, and they often differ from the real ones that should be used in robot controllers. On the other hand, the manipulator elastic parameters can be obtained from the calibration experiments only. So, the identification accuracy for both geometric and elastic parameters becomes critically important.

To reduce the identification errors, it is very attractive to apply to the robot calibration the ideas from the design of experiment theory. Nevertheless in robotics, the problem of optimal calibration experiment design has not got enough attention. In previous works, it has been applied to the problem of geometric calibration only using some abstract performance measures that are not directly related to the robot accuracy in machining applications. Besides, very limited number of works addressed the issue of elastostatic calibration, where measurement configurations have been obtained using intuitive approaches. Therefore, it is required essential revision and enhancement of existing approaches in calibration experiments planning for identification of both geometric and elastostatic parameters of robotic manipulators.

To address the above described problem, the goal of the thesis is formulated as follows: enhancement of robot calibration techniques for geometric and elastostatic parameters in order to increase the accuracy and efficiency of error compensation for robotic-based machining of large dimension parts by means of optimal design of calibration experiments (to reduce the measurement error impact). To achieve this goal, the following problems have to be solved:

Problem 1:

Development of a new problem-oriented performance measure for robot calibration experiment design and related identification algorithms that ensure required accuracy for industrial application studied in this work.

Problem 2:

Development of advanced geometric and elastostatic models for heavy industrial robots employed in machining of large dimensional parts, which allow to take into account the particularities of the manipulators with gravity compensator and coupling between actuated joints.

Problem 3:

Application of the developed calibration technique for the identification of geometric and elastostatic model parameters for robotic work-cell employed in machining of large dimensional parts for aerospace industry.

CHAPTER 2

DESIGN OF EXPERIMENTS FOR CALIBRATION OF MANIPULATOR GEOMETRIC PARAMETERS

2.1 Introduction 51
2.2 Manipulator geometric modeling 54
2.2.1 Complete, irreducible geometric model for serial manipulator 54
2.2.2 Linearization of the manipulator geometric model 58
2.3 Measurement methods in robot calibration 61
2.3.1 Existing measurement methods 62
2.3.2 Enhancing of partial pose measurement method 66
2.4 identification of model parameters 70
2.4.1 Identification algorithm for the enhanced partial pose method 70
2.4.2 Influence of the measurement errors on the identification accuracy 73
2.5 Optimal selection of measurement configurations 74
2.5.1 New approach for calibration experiment design 74
2.5.2 Generalization for the case of multiple test configurations 77
2.5.3 Comparison analysis of proposed and conventional approaches 78
2.6 Efficiency improvement of measurement pose selection 82
2.6.1 Analysis of the conventional numerical optimization techniques 82
2.6.2 Hybrid approach to optimal configuration selection 84
2.6.3 Quasi-optimal solution for measurement configuration selection 86
2.7 Summary 88

This chapter is devoted to the design of experiments for calibration of manipulator geometric parameters. Particular attention is paid to the enhancement of measurement and optimization techniques employed in geometric calibration of serial industrial robots. It presents a complete, irreducible geometric model for serial manipulator, which takes into account different sources of error (link lengths, joint offsets, etc). In contrast to other works, it proposes a new industry-oriented performance measure for optimal measurement configuration selection and improves the partial pose measurement technique via using only the direct measurement data from the external device. This new approach is aimed at finding the calibration configurations that ensure the best robot positioning accuracy after geometric error compensation. In this chapter, several simulation examples illustrate the benefits of the developed pose selection technique and corresponding accuracy improvement

2.1 INTRODUCTION

The standard engineering practice in industrial robotics assumes that the closed-loop control is employed on the level of actuated joint coordinates. On the contrary, the spatial location of the manipulator end-effector is defined by the open-loop control, which is based on computation of direct/inverse transformations that provide the correspondence between joint angles and Cartesian coordinates of the end-effector. So, the robot accuracy highly depends on the validity of the related mathematical expressions used for the computation of the end-effector position and orientation. These transformations of the related geometric model employed in the robot control algorithm include a number of parameters, which often differ from their nominal values due to manufacturing tolerances. Real values of these parameters can be identified from the calibration experiments, where the identification accuracy becomes very important.

In robotic literature, the problem of geometric calibration is already well studied and has been in the focus of the research community for many years (Roth et al., 1987). As reported by a number of authors, the manipulator geometric errors are responsible for about 90% of the total positioning error. Besides the errors in link lengths and joint offsets, they can be also induced by the non-perfect assembling of different links and arise in shifting and/or rotation of the frames associated with different elements, which normally are assumed to be matched and aligned. It is clear that the geometric errors do not vary with the manipulator configuration, while their influence on the positioning accuracy depends on the latter. At present, there exists various calibration techniques that are able to identify these errors using different measurement methods (full/partial pose information measures, line/plane constraints, etc.) for both serial and parallel robots. Moreover, the identified errors can be efficiently compensated either by adjusting the controller input (the target point) or by direct modification of the model parameters used in the robot controller.

Among numerous publications devoted to robot geometric calibration, limited number of works directly address the problem of parameter identification accuracy and reduction of the impact of measurement errors. Despite the fact that the calibration accuracy may be improved by straightforwardly increasing the number of experiments, the measurement configurations may also affect the robot calibration. It has been shown that the latter may significantly improve the identification accuracy (Driels and Pathre, 1990). Intuitively, using diverse manipulator configurations for different experiments seems perfectly corresponds to the basic idea of the classical experiment design theory, which intends to spread the measurements as much distinct as possible. However, the classical results are mostly obtained for very specific models (such as the linear regression) and cannot be applied directly due to non-linearity of the relevant expressions of robot geometric model.

Nevertheless, there are few works where the problem of optimal pose selection for robot calibration has been studied (Daney et al., 2005; Sun and Hollerbach, 2008b). In order to compare the plans of experiments, several quantitative performance measures have been proposed and used as the objectives of the optimization problem associated with the optimal sets of measurement poses. Currently, there exist two main trends in defining the objectives. The first one is based on the conventional optimality criteria that operate with covariance matrix norms. Another one is the observability indices, which are based on the singular values of the identification Jacobian (condition number, for instance). However, these approaches deal with rather abstract notions that do not directly relate to the robot accuracy and may lead to some unexpected results (when the condition number is perfect, but the parameter estimation errors are rather high). Besides, it usually requires very intensive

and time consuming computations caused by a poor convergence of the optimization and high dimension of the search space (number of calibration experiments multiplied by the manipulator joint number). Therefore, for the industrial applications, a new problem-oriented performance measure is required.

Before presenting the developed approach, let us first describe the classical calibration procedure. In general, it is divided into four sequential steps: modeling, measurement, identification and implementation (Bernhardt et al., 1993). The first step focuses on the development of appropriate mathematical model. At the second step, related measurements (calibration experiments) are carried out. The third step deals with identification of the unknown parameters using certain numerical algorithms. And finally, the last step implements the identified parameters in the robot model used in the controller or in relevant compensation technique.

In this work, the *primary goal* is to achieve the desired robot positioning accuracy using minimum number of experiments. Here it is proposed to introduce an additional step, the *design of experiments*, which is performed before measurements and is aimed at obtaining the set of measurements poses that ensures good calibration results (robot accuracy after error compensation). It allows us to improve the efficiency of error compensation and estimate the robot accuracy that is quite important for industrial applications.

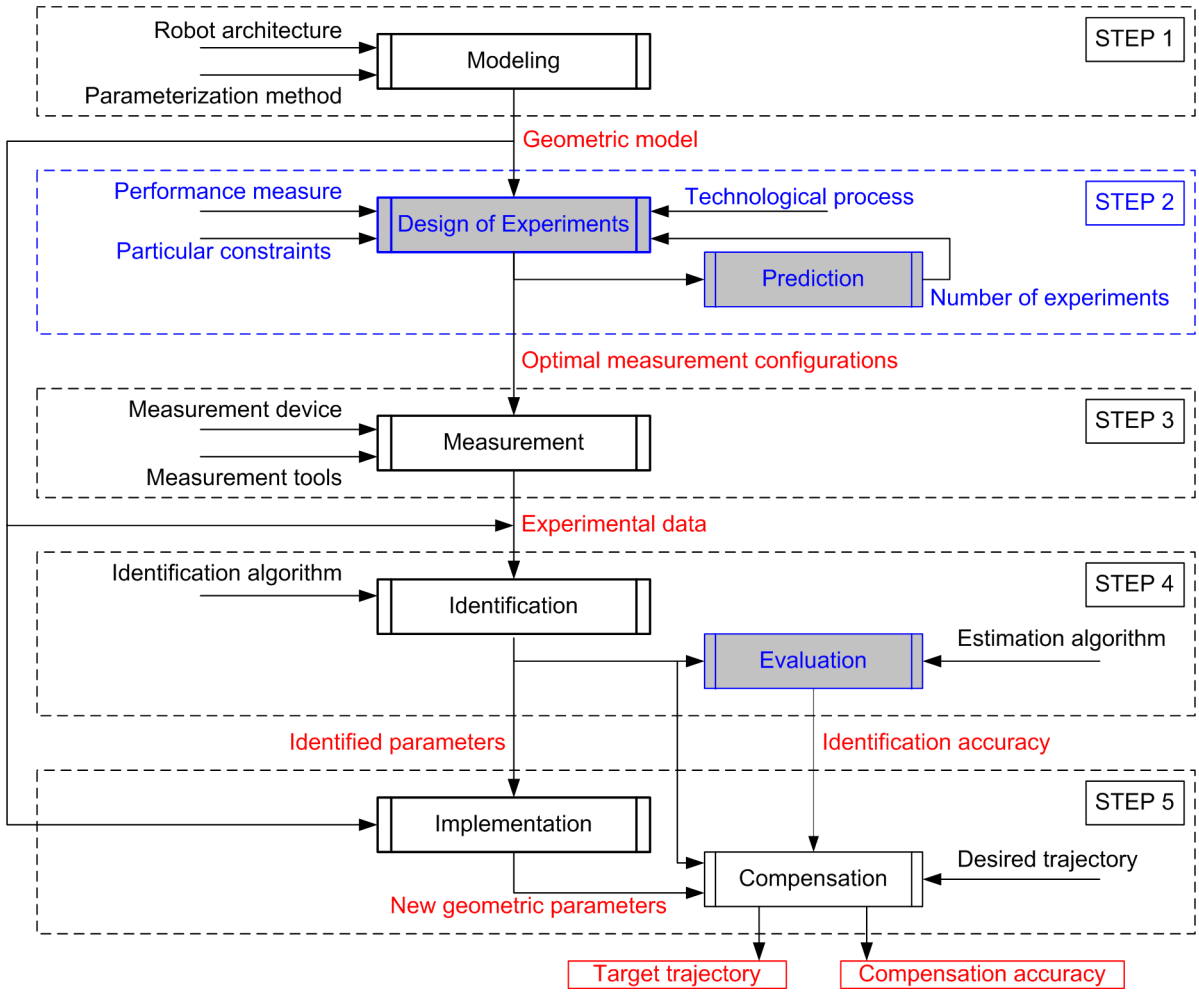

Figure 2.1 The schematic of robot calibration procedure

The modified procedure includes five steps, which are schematically presented in Figure 2.1.

S1: The first step (*modeling*) is aimed at developing a suitable geometric model, which properly describes the relation between the manipulator geometric parameters (link lengths and joint angles) and the end-effector location (position and orientation).

S2: The second step (*design of experiments*) is aimed at choosing optimal measurement configurations. It should rely on an appropriate performance measure, which takes into account the particularities of technological process. It should be also able to obtain solution within the work-cell constraints, and to adjust the number of experiments based on the error estimation.

S3: The third step (*measurements*) deals with carrying out calibration experiments using the obtained configurations. Depending on the measurement methods (measurement tools and devices, marker location, etc.), it may provide different experimental data (the end-effector position/location, etc.). Detail review on the measurement methods is presented in Section 2.3, where comparison study is also provided.

S4: At the fourth step (*identification*) the errors in geometric parameters are computed using the corresponding model and proper identification algorithm. Using the experimental data, it is possible to evaluate identification accuracy for the parameters of interest.

S5: At the last step (*implementation*), the geometric errors are compensated by modification of the geometric parameters embedded in the robot controller. In the case when some errors can not be balanced in the controller, the off-line error compensation technique is required. This technique should compensate the manipulator errors via modification of the target trajectory.

Using the parameters covariance matrix obtained in step 4, it is possible to predict the end-effector positioning accuracy for a given trajectory. It is clear that the proposed scheme of robot calibration procedure allows to improve the calibration efficiency for given number of experiments (or to minimize the number of experiments for given accuracy) and to predict the robot accuracy after error compensation before carrying out experiments.

As follows from the detailed literature analysis in this area, the steps 1, 3, 4 and 5 in the calibration procedure have been almost well studied (Elatta et al., 2004; Roth et al., 1987), while the step 2 still requires essential revision in terms of the applicability to particular manufacturing process where the robot is used. Hence, the goal of this Chapter is the enhancement of calibration technique for manipulator geometric parameters by means of the design of experiments. Particular problems that should be considered here are the following:

(i) Development of an industry-oriented performance measure which has clear physical meaning that is related to robot accuracy, and ensures the best positioning accuracy after error compensation.

(ii) Enhancement of the numerical techniques employed in calibration experiment design (measurement pose selection).

(iii) Validation of the developed technique by application examples that deal with geometric calibration of planar and spatial manipulators.

To address these problems, the remainder of the chapter is organized as follows. Section 2.2 presents a suitable manipulator geometric model for calibration purposes (complete, irreducible model). In Section 2.3, several existing measurement methods are compared and an enhanced partial pose measurement method is proposed. Sections 2.4 deals with dedicated identification algorithms for manipulator geometric parameters. Section 2.5 proposes a new approach for measurement pose

selection and its generalization for the case of complex trajectory. Section 2.6 focuses on efficiency improvement of the developed measurement pose selection technique. And finally, Section 2.7 summarizes the main results and contributions of this chapter.

2.2 MANIPULATOR GEOMETRIC MODELING

2.2.1 Complete, irreducible geometric model for serial manipulator

As follows from the literature review presented in Section 1.2, the standard D-H model may not be suitable for the robot calibration. To avoid this difficulty, some modifications have been proposed that however introduce some redundancy, which may cause non-identifiability of certain parameters. This redundancy can be eliminated by applying either numerical or analytical techniques (Meggiolaro and Dubowsky, 2000; Schröer et al., 1997; Zhuang et al., 1992) that allow us to obtain an appropriate model, which is usually referred to as "complete, irreducible and continuous" one. Let us present one of these techniques, which is described in details in (Pashkevich, 2001).

In the frame of the notations that are defined in Section 1.2 and assuming that the manipulator links are rigid enough and the non-geometric factors are negligible in this level of calibration, the general expression of the geometric model for a n-dof serial manipulator can be described as a sequence of homogeneous transformations

$$\mathbf{T}(\mathbf{q}) = \mathbf{T}_{base}(\boldsymbol{\pi}_b) \cdot \left[\mathbf{T}_{joint}(q_1, \pi_{q1}) \cdot \mathbf{T}_{Link}(\boldsymbol{\pi}_{L1}) \right] \cdot \ldots \cdot \left[\mathbf{T}_{joint}(q_n, \pi_{qn}) \cdot \mathbf{T}_{Link}(\boldsymbol{\pi}_{Ln}) \right] \cdot \mathbf{T}_{tool}(\boldsymbol{\pi}_t) \qquad (2.1)$$

where $\mathbf{T}$ with different indices denote the relevant matrices of size 4×4, $\mathbf{q}$ is the vector of the actuated joint coordinates, while the vectors $\boldsymbol{\pi}_b$, $\boldsymbol{\pi}_t$, $\boldsymbol{\pi}_{Lj}$ and the scalars π_{qj} are the manipulator geometric parameters corresponding to the base, tool, links and joints, respectively. In literature (see subsection 1.3), there are a number of techniques that allows us to obtain the manipulator model of such type, which is definitely complete but includes redundant parameters to be eliminated (methods of Hayati, Whitney-Losinski, etc.). In this work, we will use the model generation technique that is based on dedicated analytical elimination rules and includes the following steps:

Step 1. *Construction* of the complete and obviously reducible model in the form of homogeneous matrices product.

- The base transformation $\mathbf{T}_{base} = \left[\mathbf{T}_x \mathbf{T}_y \mathbf{T}_z \mathbf{R}_x \mathbf{R}_y \mathbf{R}_z \right]_b$
- The joint and link transformations $\mathbf{T}_{joint,j} \cdot \mathbf{T}_{Link,j}$
  - (i) For revolute joint $\mathbf{T}_{joint,j} \cdot \mathbf{T}_{Link,j} = \mathbf{R}_{e,j}\left(q_j, \pi_{qj}\right) \cdot \left[\mathbf{T}_u \mathbf{T}_v \mathbf{R}_u \mathbf{R}_v \right]_{Lj}$
  - (ii) For prismatic joint $\mathbf{T}_{joint,j} \cdot \mathbf{T}_{Link,j} = \mathbf{T}_{e,j}\left(q_j, \pi_{qj}\right) \cdot \left[\mathbf{R}_u \mathbf{R}_v \right]_{Lj}$

  where $\mathbf{e}_j$ is the joint axis, $\mathbf{u}_j$ and $\mathbf{v}_j$ are the axes orthogonal to $\mathbf{e}_j$.
- The tool transformation $\mathbf{T}_{tool} = \left[\mathbf{T}_x \mathbf{T}_y \mathbf{T}_z \mathbf{R}_x \mathbf{R}_y \mathbf{R}_z \right]_t$

Step 2. *Elimination* of non-identifiable and semi-identifiable parameters in accordance with specific rules for different nature and structure of consecutive joints.

- For the case of consecutive revolute joint $\mathbf{R}_{e,j}\left(q_j, \pi_{qj}\right)$
  - (i) if $\mathbf{e}_j \perp \mathbf{e}_{j-1}$, eliminate the term $\mathbf{R}_{u,L_{j-1}}$ or $\mathbf{R}_{v,L_{j-1}}$ that corresponds to $\mathbf{R}_{e,j}$;
  - (ii) if $\mathbf{e}_j \parallel \mathbf{e}_{j-1}$, eliminate the term $\mathbf{T}_{u,L_{j-k}}$ or $\mathbf{T}_{v,L_{j-k}}$ that defines the translation orthogonal to the joint axes, for which k is minimum ($k \geq 1$).

- For the case of consecutive prismatic joint $\mathbf{T}_{e,j}\left(q_j, \pi_{qj}\right)$

  (i) if $\mathbf{e}_j \perp \mathbf{e}_{j-1}$, eliminate the term $\mathbf{T}_{u,L_{j-1}}$ or $\mathbf{T}_{u,L_{j-1}}$ that corresponds to $\mathbf{T}_{e,j}$;

  (ii) if $\mathbf{e}_j \| \mathbf{e}_{j-1}$, eliminate the term $\mathbf{T}_{u,L_{j-k}}$ or $\mathbf{T}_{v,L_{j-k}}$ that defines the translation in the direction of axis $\mathbf{e}_j$, for which k is minimum ($k \geq 1$).

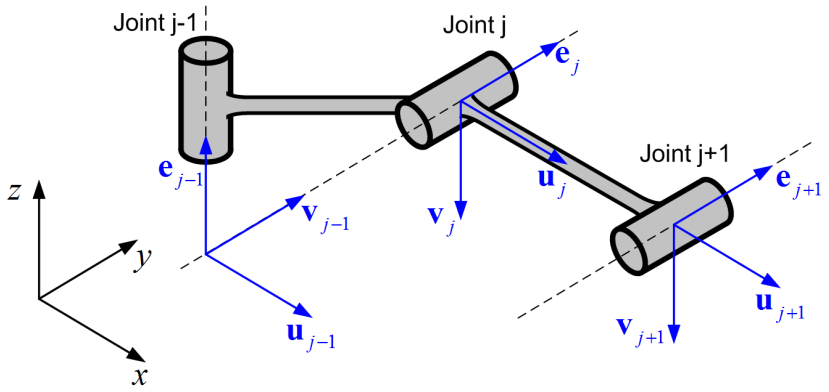

Figure 2.2 Manipulator segment with perpendicular and parallel axes

To demonstrate this technique, let us show how to apply it to the manipulator segment consisting of two links and three successive revolute joints. Figure 2.2 illustrates the corresponding frame assignments, where the joint axis $\mathbf{e}_j$ is perpendicular to $\mathbf{e}_{j-1}$ and parallel to $\mathbf{e}_{j+1}$. For this particular architecture, the joint and link transformations can be written as

$$\mathbf{T} = \mathbf{R}_z(q_{j-1} + \Delta q_{j-1}) \cdot \left[\mathbf{T}_x \mathbf{T}_y \mathbf{R}_x \mathbf{R}_y\right]_{L_{j-1}} \cdot \mathbf{R}_y(q_j + \Delta q_j) \cdot \left[\mathbf{T}_x \mathbf{T}_z \mathbf{R}_x \mathbf{R}_z\right]_{L_j} \cdot \mathbf{R}_y(q_{j+1} + \Delta q_{j+1}) \quad (2.2)$$

where the terms $\mathbf{R}_{y,L_{j-1}}$ and $\mathbf{T}_{z,L_j}$ (or $\mathbf{T}_{x,L_j}$) should be eliminated from the model according to the above presented elimination rules. In more details, since $\mathbf{e}_j \perp \mathbf{e}_{j-1}$ and $\mathbf{e}_j$ is directed along the y-axis, so the term $\mathbf{R}_{y,L_{j-1}}$, which is the rotation around the y-axis in the preceding link, should be eliminated. Similarly, since $\mathbf{e}_j \| \mathbf{e}_{j+1}$, the term $\mathbf{T}_{z,L_j}$ (or $\mathbf{T}_{x,L_j}$), which is the translation in the preceding link that are orthogonal to the y-axis, should be also eliminated. This yields the following irreducible model of this segment:

$$\mathbf{T} = \mathbf{R}_z(q_{j-1} + \Delta q_{j-1}) \cdot \left[\mathbf{T}_x \mathbf{T}_y \mathbf{R}_x\right]_{L_{j-1}} \cdot \mathbf{R}_y(q_j + \Delta q_j) \cdot \left[\mathbf{T}_x \mathbf{R}_x \mathbf{R}_z\right]_{L_j} \cdot \mathbf{R}_y(q_{j+1} + \Delta q_{j+1}) \quad (2.3)$$

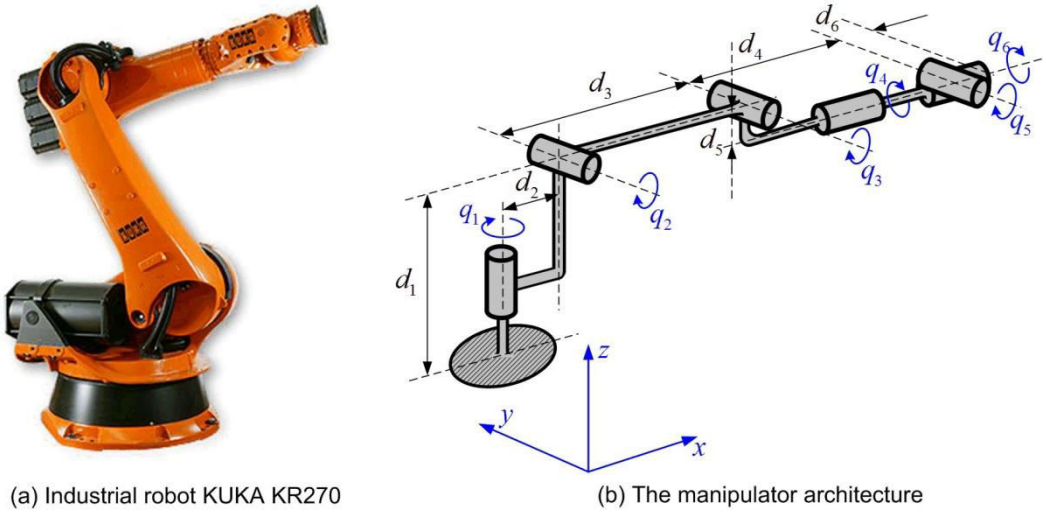

(a) Industrial robot KUKA KR270 (b) The manipulator architecture

Figure 2.3 The industrial serial robot KUKA KR270 and its geometric model.

Let us apply the above presented technique to the industrial robot KUKA KR270 (See Figure 2.3), which is used in experimental validations of this thesis. For this manipulator that includes six revolute joints, the complete (but redundant) model contains 42 parameters and can be presented as

$$\begin{aligned}\mathbf{T} = &\left[\mathbf{T}_x\mathbf{T}_y\mathbf{T}_z\mathbf{R}_x\mathbf{R}_y\mathbf{R}_z\right]_b \cdot \mathbf{R}_z(q_1+\Delta q_1)\cdot\left[\mathbf{T}_x\mathbf{T}_y\mathbf{R}_x\mathbf{R}_y\right]_{L_1}\cdot \mathbf{R}_y(q_2+\Delta q_2)\cdot\left[\mathbf{T}_x\mathbf{T}_z\mathbf{R}_x\mathbf{R}_z\right]_{L_2}\cdot\\ &\cdot \mathbf{R}_y(q_3+\Delta q_3)\cdot\left[\mathbf{T}_x\mathbf{T}_z\mathbf{R}_x\mathbf{R}_z\right]_{L_3}\cdot \mathbf{R}_x(q_4+\Delta q_4)\cdot\left[\mathbf{T}_y\mathbf{T}_z\mathbf{R}_y\mathbf{R}_z\right]_{L_4}\cdot \mathbf{R}_y(q_5+\Delta q_5)\cdot\left[\mathbf{T}_x\mathbf{T}_z\mathbf{R}_x\mathbf{R}_z\right]_{L_5} \quad (2.4)\\ &\cdot \mathbf{R}_x(q_6+\Delta q_6)\cdot\left[\mathbf{T}_y\mathbf{T}_z\mathbf{R}_y\mathbf{R}_z\right]_{L_6}\cdot\left[\mathbf{T}_x\mathbf{T}_y\mathbf{T}_z\mathbf{R}_x\mathbf{R}_y\mathbf{R}_z\right]_t\end{aligned}$$

It should be mentioned that the nominal values of some parameters can be found in the manufacturer datasheets (see Table 2.1), but the remaining ones are assumed to be equal to zero.

Table 2.1 Nominal geometric parameters of KUKA KR270 industrial robot

Parameter	d_1	d_2	d_3	d_4	d_5	d_6
Nominal values (mm)	750	350	1250	1100	-55	230

Applying the elimination rules for the case of consecutive revolute joints, the following parameters are sequentially eliminated from the redundant model (2.4):

$$\begin{aligned}\mathbf{T} = &\left[\mathbf{T}_x\mathbf{T}_y\mathbf{T}_z\mathbf{R}_x\mathbf{R}_y\mathbf{R}_z\right]_b \cdot \mathbf{R}_z(q_1+\cancel{\Delta q_1})\cdot\left[\mathbf{T}_x\mathbf{T}_y\mathbf{R}_x\cancel{\mathbf{R}_y}\right]_{L_1}\cdot \mathbf{R}_y(q_2+\Delta q_2)\cdot\left[\mathbf{T}_x\cancel{\mathbf{T}_z}\mathbf{R}_x\mathbf{R}_z\right]_{L_2}\cdot\\ &\cdot \mathbf{R}_y(q_3+\Delta q_3)\cdot\left[\mathbf{T}_x\mathbf{T}_z\cancel{\mathbf{R}_x}\mathbf{R}_z\right]_{L_3}\cdot \mathbf{R}_x(q_4+\Delta q_4)\cdot\left[\mathbf{T}_y\mathbf{T}_z\cancel{\mathbf{R}_y}\mathbf{R}_z\right]_{L_4}\cdot \mathbf{R}_y(q_5+\Delta q_5)\cdot\left[\cancel{\mathbf{T}_x}\mathbf{T}_z\cancel{\mathbf{R}_x}\mathbf{R}_z\right]_{L_5}\times (2.5)\\ &\cdot \mathbf{R}_x(q_6+\cancel{\Delta q_6})\cdot\left[\cancel{\mathbf{T}_y}\cancel{\mathbf{T}_z}\cancel{\mathbf{R}_y}\cancel{\mathbf{R}_z}\right]_{L_6}\cdot\left[\mathbf{T}_x\mathbf{T}_y\mathbf{T}_z\cancel{\mathbf{R}_x}\cancel{\mathbf{R}_y}\cancel{\mathbf{R}_z}\right]_t\end{aligned}$$

Here, it is worth to make the following remarks:

Remark 1 In the redundant model (2.4), it has been already taken into account that the nominal geometric parameter d_1 (shift of the robot base along z-axis) cannot be identified separately from the base transformation.

Remark 2 For the first and the last joints, which are connected to the robot base and tool respectively, the offsets Δq_1 and Δq_6 are treated as semi-identifiable parameters. So, they are eliminated from the manipulator geometric model and are incorporated in the base and tool parameters. However, the actuated joint variables q_1 and q_6 must be retained in the model.

Remark 3 The geometric parameters of the last link cannot be identified separately from the tool transformation. So, it is reasonable to include these parameters in the tool transformation.

Remark 4 In the case when only position measurements are available, the tool orientations are not known. So, the parameters of the rotational transformations $\{\mathbf{R}_x, \mathbf{R}_y, \mathbf{R}_z\}_t$ corresponding to the tool are treated as non-identifiable.

Remark 5 Six parameters describing the base transformation and three parameters that define tool transformation can be treated as known (there are dedicated techniques to identify them separately).

This finally allows us to obtain the complete and irreducible geometric model for the considered manipulator that includes 18 principle parameters to be identified

$$\begin{aligned}\mathbf{T}_{robot} = \mathbf{R}_z(q_1)\cdot\left[\mathbf{T}_x\mathbf{T}_y\mathbf{R}_x\right]_{L_1}\cdot\mathbf{R}_y(q_2+\Delta q_2)\cdot\left[\mathbf{T}_x\mathbf{R}_x\mathbf{R}_z\right]_{L_2}\cdot\mathbf{R}_y(q_3+\Delta q_3)\cdot\left[\mathbf{T}_x\mathbf{T}_z\mathbf{R}_z\right]_{L_3}\cdot \\ \cdot\ \mathbf{R}_x(q_4+\Delta q_4)\cdot\left[\mathbf{T}_y\mathbf{T}_z\mathbf{R}_z\right]_{L_4}\cdot\mathbf{R}_y(q_5+\Delta q_5)\cdot\left[\mathbf{T}_z\mathbf{R}_z\right]_{L_5}\cdot\mathbf{R}_x(q_6)\end{aligned} \tag{2.6}$$

This model will be further used for geometric calibration of the industrial robot KUKA KR270 and optimal selection of the measurement poses. For the convenience, let us collect these parameters in a single vector

$$\boldsymbol{\pi} = \left\{p_{x1}\ \ p_{y1}\ \ \varphi_{x1}\ \ \Delta q_2\ \ p_{x2}\ \ \varphi_{x2}\ \ \varphi_{z2}\ \ \Delta q_3\ \ p_{x3}\ \ p_{z3}\ \ \varphi_{z3}\ \ \Delta q_4\ \ p_{y4}\ \ p_{z4}\ \ \varphi_{z4}\ \ \Delta q_5\ \ p_{z5}\ \ \varphi_{z5}\right\} \tag{2.7}$$

where Δq_j is the joint offset, p_{xj}, p_{yj}, p_{zj} and $\varphi_{xj}, \varphi_{yj}, \varphi_{zj}$ are the relevant translational and rotational parameters, and j indicates the joint/link number. For these parameters, the corresponding nominal values are

$$\boldsymbol{\pi}_0 = \left\{d_2\ \ 0\ \ 0\ \ 0\ \ d_3\ \ 0\ \ 0\ \ 0\ \ d_4\ \ d_5\ \ 0\ \ 0\ \ 0\ \ 0\ \ 0\ \ 0\ \ 0\ \ 0\right\} \tag{2.8}$$

where the geometric meaning of $d_2,...,d_5$ is illustrated in Figure 2.3 and the numerical values are provided in Table 2.1.

It should be noted that in industrial practice, the end-effector location is usually presented in more compact (but equivalent) form which includes only six values: three Cartesian coordinates $\left\{p_x, p_y, p_z\right\}$ and three orientation angles $\left\{\varphi_x, \varphi_y, \varphi_z\right\}$. For robot KUKA KR270 they are denoted as $\left\{x, y, z\right\}$ and $\left\{a, b, c\right\}$ respectively. Relevant transformation from/to the homogeneous matrix presentation to/from this vector form are described by the following expressions: (Angeles, 2007)

Direct transformation. For a given robot end-effector location $\left\{x, y, z, a, b, c\right\}$, the homogeneous transformation matrix $\mathbf{T}$ is computed as

$$\mathbf{T} = \left[\begin{array}{ccc:c} \cos(b)\cos(a) & \cos(a)\sin(b)\sin(c)-\sin(a)\cos(c) & \sin(c)\sin(a)+\cos(c)\cos(a)\sin(b) & x \\ \cos(b)\sin(a) & \cos(c)\cos(a)+\sin(c)\sin(a)\sin(b) & \cos(c)\sin(b)\sin(a)-\cos(a)\sin(c) & y \\ -\sin(b) & \cos(b)\sin(c) & \cos(b)\cos(c) & z \\ \hdashline 0 & 0 & 0 & 1 \end{array}\right] \tag{2.9}$$

Inverse transformation. For a given homogeneous transformation matrix $\mathbf{T}$, the location vector can be obtained using the following expressions

(i) The position vector is simply:

$$x = \mathbf{T}_{1,4}, \quad y = \mathbf{T}_{2,4}, \quad z = \mathbf{T}_{3,4} \tag{2.10}$$

(ii) The orientation angles vary with different cases:

(a) For the case when $\left|\mathbf{T}_{3,1}\right| \neq 1$

$$\begin{aligned} c &= \text{atan2}(\mathbf{T}_{3,2}, \mathbf{T}_{3,3}) \\ a &= \text{atan2}(\mathbf{T}_{2,1}, \mathbf{T}_{1,1}) \\ b &= \begin{cases} \text{atan2}(\mathbf{T}_{3,1}, \mathbf{T}_{3,3}/\cos(c)), & \text{if } \mathbf{T}_{3,3} \neq 0 \\ \text{atan2}(-\cos(a)\mathbf{T}_{3,1}, \mathbf{T}_{1,1}), & \text{if } \mathbf{T}_{3,3} = 0 \text{ and } \mathbf{T}_{1,1} \neq 0 \\ \text{atan2}(-\sin(a)\mathbf{T}_{3,1}, \mathbf{T}_{2,1}), & \text{if } \mathbf{T}_{3,3} = 0 \text{ and } \mathbf{T}_{2,1} \neq 0 \end{cases} \end{aligned} \tag{2.11}$$

(b) For the case when $\left|\mathbf{R}_{3,1}\right| = 1$, their exist infinite number of solutions for angles c and a due to their dependency, so

$$b = \text{asin}(\mathbf{T}_{3,1})$$
$$\begin{cases} c - a = \text{atan2}(\mathbf{T}_{1,2}, \mathbf{T}_{1,3}), & \text{if } \sin(b) = 1 \\ a + c = \text{atan2}(\mathbf{T}_{1,2}, \mathbf{T}_{1,3}), & \text{if } \sin(b) = -1 \end{cases} \tag{2.12}$$

where one of the rotational angles c or a should be fixed in order to compute the other one.

In the following sections, these direct and inverse transformations will be used for computing end-effector location of robot KUKA KR270 required for some numerical routines employed in parameter identification algorithms.

2.2.2 Linearization of the manipulator geometric model

The geometric model (2.1) presented in the previous subsection allows us to compute the end-effector location for any given values of the actuated coordinates $\mathbf{q}$ (provided that the manipulator parameters $\boldsymbol{\pi}$ are known). However, for calibration purposes, it is usually required a linearized version of this model allowing to evaluate the influence of the small variations of $\mathbf{q}$ and $\boldsymbol{\pi}$. So, let us assume that the geometric model (2.1) can be written as the vector function

$$\mathbf{t} = g(\mathbf{q}, \boldsymbol{\pi}) \tag{2.13}$$

where the vector $\mathbf{t} = (\mathbf{p}, \boldsymbol{\varphi})^T$ defines the manipulator end-effector location (position and orientation), vector $\mathbf{q}$ contains all actuated joint coordinates, and vector $\boldsymbol{\pi} = \boldsymbol{\pi}_0 + \Delta\boldsymbol{\pi}$ collects all geometric parameters and their deviations. Using the general expression defined in Eq. (2.13), the actual location of the manipulator end-effector, which incorporates the geometric errors can be written as

$$\mathbf{t} = g(\mathbf{q}, \boldsymbol{\pi}_0 + \Delta\boldsymbol{\pi}) \tag{2.14}$$

Usually in practice, the geometric errors $\Delta\boldsymbol{\pi}$ are relatively small, so the following linearized model can be used

$$\mathbf{t} = g(\mathbf{q}, \boldsymbol{\pi}_0) + \frac{\partial g(\mathbf{q}, \boldsymbol{\pi}_0)}{\partial \boldsymbol{\pi}} \Delta\boldsymbol{\pi} \tag{2.15}$$

where $\partial g(\mathbf{q}, \boldsymbol{\pi}_0)/\partial \boldsymbol{\pi}$ is defined as the identification Jacobian $\mathbf{J}_\pi$. So, Eq. (2.15) can be rewritten as

$$\mathbf{t} = \mathbf{t}_0 + \mathbf{J}_\pi \Delta\boldsymbol{\pi} \tag{2.16}$$

where $\mathbf{t}_0 = g(\mathbf{q}, \boldsymbol{\pi}_0)$ is the end-effector location computed using the nominal geometric parameters.

There are different ways to compute the identification Jacobian matrix $\mathbf{J}_\pi$, either analytically or numerically (Coleman and Verma, 1996; Khalil and Creusot, 1997). Let us present one of the methods that is based on semi-analytical differentiation (Pashkevich et al., 2009a). In the frame of this method, the general transformation matrix of the manipulator geometric model is presented in the following form

$$\mathbf{T} = \mathbf{T}_{base} \cdot \left[\mathbf{T}_1(\mathbf{q}, \boldsymbol{\pi}) \cdot \mathbf{H}(\boldsymbol{\pi}_\kappa) \cdot \mathbf{T}_2(\mathbf{q}, \boldsymbol{\pi}) \right]_{robot} \cdot \mathbf{T}_{tool} \tag{2.17}$$

where the terms $\mathbf{T}_1(\mathbf{q}, \boldsymbol{\pi})$ and $\mathbf{T}_2(\mathbf{q}, \boldsymbol{\pi})$ are the transformation matrices on the left and right sides of the currently considered parameter $\boldsymbol{\pi}_\kappa$. Besides, here the matrix $\mathbf{H}(\boldsymbol{\pi}_\kappa)$ refers to the elementary homogeneous transformation (which is either a translation or a rotation) related to the parameter $\boldsymbol{\pi}_\kappa$.

Using this presentation, the partial derivatives of $\mathbf{T}$ with respect to the parameter $\boldsymbol{\pi}_\kappa$ can be computed using the matrix product

$$\mathbf{T}'_\kappa = \mathbf{T}_{base} \cdot \left[\mathbf{T}_1(\mathbf{q},\boldsymbol{\pi}) \cdot \mathbf{H}'(\boldsymbol{\pi}_\kappa) \cdot \mathbf{T}_2(\mathbf{q},\boldsymbol{\pi}) \right]_{robot} \cdot \mathbf{T}_{tool} \tag{2.18}$$

where $\mathbf{H}'(\boldsymbol{\pi}_\kappa)$ is the differential transformation matrix, which can be easily obtained analytically (See Table 2.2). It should be mentioned that these derivatives are computed in the neighborhood of the nominal values $\boldsymbol{\pi}_0$. So, taking into account that many of the nominal parameters are equal to zero, additional simplification can be done (see the last column in Table 2.2, where relevant notations $\mathbf{H}'_{Tx},...,\mathbf{H}'_{Rz}$ are introduced).

Table 2.2 Elementary homogeneous transformation matrices and their derivatives

Elementary transformation	Homogeneous matrix $\mathbf{H}(\cdot)$	Matrix derivative $\mathbf{H}'(\cdot)$	Zero-value matrix derivative
		Translation	
$\mathbf{T}_x(p)$	$\begin{bmatrix} 1 & 0 & 0 & p \\ 0 & 1 & 0 & 0 \\ 0 & 0 & 1 & 0 \\ 0 & 0 & 0 & 1 \end{bmatrix}$	$\begin{bmatrix} 0 & 0 & 0 & 1 \\ 0 & 0 & 0 & 0 \\ 0 & 0 & 0 & 0 \\ 0 & 0 & 0 & 0 \end{bmatrix}$	$\mathbf{H}'_{Tx} = \begin{bmatrix} 0 & 0 & 0 & 1 \\ 0 & 0 & 0 & 0 \\ 0 & 0 & 0 & 0 \\ 0 & 0 & 0 & 0 \end{bmatrix}$
$\mathbf{T}_y(p)$	$\begin{bmatrix} 1 & 0 & 0 & 0 \\ 0 & 1 & 0 & p \\ 0 & 0 & 1 & 0 \\ 0 & 0 & 0 & 1 \end{bmatrix}$	$\begin{bmatrix} 0 & 0 & 0 & 0 \\ 0 & 0 & 0 & 1 \\ 0 & 0 & 0 & 0 \\ 0 & 0 & 0 & 0 \end{bmatrix}$	$\mathbf{H}'_{Ty} = \begin{bmatrix} 0 & 0 & 0 & 0 \\ 0 & 0 & 0 & 1 \\ 0 & 0 & 0 & 0 \\ 0 & 0 & 0 & 0 \end{bmatrix}$
$\mathbf{T}_z(p)$	$\begin{bmatrix} 1 & 0 & 0 & 0 \\ 0 & 1 & 0 & 0 \\ 0 & 0 & 1 & p \\ 0 & 0 & 0 & 1 \end{bmatrix}$	$\begin{bmatrix} 0 & 0 & 0 & 0 \\ 0 & 0 & 0 & 0 \\ 0 & 0 & 0 & 1 \\ 0 & 0 & 0 & 0 \end{bmatrix}$	$\mathbf{H}'_{Tz} = \begin{bmatrix} 0 & 0 & 0 & 0 \\ 0 & 0 & 0 & 0 \\ 0 & 0 & 0 & 1 \\ 0 & 0 & 0 & 0 \end{bmatrix}$
		Rotation	
$\mathbf{R}_x(\varphi)$	$\begin{bmatrix} 1 & 0 & 0 & 0 \\ 0 & \cos\varphi & -\sin\varphi & 0 \\ 0 & \sin\varphi & \cos\varphi & 0 \\ 0 & 0 & 0 & 1 \end{bmatrix}$	$\begin{bmatrix} 0 & 0 & 0 & 0 \\ 0 & -\sin\varphi & -\cos\varphi & 0 \\ 0 & \cos\varphi & -\sin\varphi & 0 \\ 0 & 0 & 0 & 0 \end{bmatrix}$	$\mathbf{H}'_{Rx} = \begin{bmatrix} 0 & 0 & 0 & 0 \\ 0 & 0 & -1 & 0 \\ 0 & 1 & 0 & 0 \\ 0 & 0 & 0 & 0 \end{bmatrix}$
$\mathbf{R}_y(\varphi)$	$\begin{bmatrix} \cos\varphi & 0 & \sin\varphi & 0 \\ 0 & 1 & 0 & 0 \\ -\sin\varphi & 0 & \cos\varphi & 0 \\ 0 & 0 & 0 & 1 \end{bmatrix}$	$\begin{bmatrix} -\sin\varphi & 0 & \cos\varphi & 0 \\ 0 & 0 & 0 & 0 \\ -\cos\varphi & 0 & -\sin\varphi & 0 \\ 0 & 0 & 0 & 0 \end{bmatrix}$	$\mathbf{H}'_{Ry} = \begin{bmatrix} 0 & 0 & 1 & 0 \\ 0 & 0 & 0 & 0 \\ -1 & 0 & 0 & 0 \\ 0 & 0 & 0 & 0 \end{bmatrix}$
$\mathbf{R}_z(\varphi)$	$\begin{bmatrix} \cos\varphi & -\sin\varphi & 0 & 0 \\ \sin\varphi & \cos\varphi & 0 & 0 \\ 0 & 0 & 1 & 0 \\ 0 & 0 & 0 & 1 \end{bmatrix}$	$\begin{bmatrix} -\sin\varphi & -\cos\varphi & 0 & 0 \\ \cos\varphi & -\sin\varphi & 0 & 0 \\ 0 & 0 & 0 & 0 \\ 0 & 0 & 0 & 0 \end{bmatrix}$	$\mathbf{H}'_{Rz} = \begin{bmatrix} 0 & -1 & 0 & 0 \\ 1 & 0 & 0 & 0 \\ 0 & 0 & 0 & 0 \\ 0 & 0 & 0 & 0 \end{bmatrix}$

Further, since any homogeneous matrix $\mathbf{T}$ can be represented as $\mathbf{T}=\left[\mathbf{R}, \mathbf{p};\ \mathbf{0},\ 1\right]$, where $\mathbf{R}$ is the corresponding rotation matrix of size 3×3, and $\mathbf{p}$ is the 3×1 translation vector, the desired columns of the identification Jacobian $\mathbf{J}_\pi$ can be extracted from the matrix $\mathbf{T}'_\kappa$ in the following way:

- The position part of the Jacobian column is simply the vector $\mathbf{p}$, so

$$\left[\mathbf{J}_\pi\right]_{1,\kappa}=\left[\mathbf{T}'_\kappa\right]_{1,4},\quad \left[\mathbf{J}_\pi\right]_{2,\kappa}=\left[\mathbf{T}'_\kappa\right]_{2,4},\quad \left[\mathbf{J}_\pi\right]_{3,\kappa}=\left[\mathbf{T}'_\kappa\right]_{3,4} \tag{2.19}$$

- The orientation part can be computed in a similar way but current orientation of the manipulator end-effector must be taken into account:

$$\left[\mathbf{J}_\pi\right]_{4,\kappa}=\left[\mathbf{T}'_\kappa\cdot\mathbf{T}^{-1}\right]_{3,2},\quad \left[\mathbf{J}_\pi\right]_{5,\kappa}=\left[\mathbf{T}'_\kappa\cdot\mathbf{T}^{-1}\right]_{1,3},\quad \left[\mathbf{J}_\pi\right]_{6,\kappa}=\left[\mathbf{T}'_\kappa\cdot\mathbf{T}^{-1}\right]_{2,1} \tag{2.20}$$

To demonstrate this method, let us show how to apply it to a manipulator segment whose geometric model contains the following transformations

$$\mathbf{T}=\mathbf{R}_z(q_1+\Delta q_1)\cdot\mathbf{T}_x\left(p_{x1}\right)\cdot\mathbf{T}_y\left(p_{y1}\right)\cdot\mathbf{R}_x\left(\varphi_{x1}\right)\cdot\mathbf{R}_y(q_2+\Delta q_2) \tag{2.21}$$

and where the geometric parameters are collected in the vector $\boldsymbol{\pi}=\left\{\Delta q_1, p_{x1}, p_{y1}, \varphi_{x1}, \Delta q_2\right\}$. Assuming that their nominal values are $\boldsymbol{\pi}_0=\left\{0, d, 0, 0, 0\right\}$, the derivatives $\left\{\mathbf{T}'_\kappa,\ \kappa=1,...,5\right\}$ can be written as

$$\begin{aligned}
\mathbf{T}'_1&=\mathbf{R}_z(q_1)\ \cdot\ \mathbf{H}'_{Rz}\ \cdot\ \mathbf{T}_x\left(d\right)\mathbf{R}_y(q_2)\\
\mathbf{T}'_2&=\mathbf{R}_z(q_1)\ \cdot\ \mathbf{H}'_{Tx}\ \cdot\ \mathbf{R}_y(q_2)\\
\mathbf{T}'_3&=\mathbf{R}_z(q_1)\mathbf{T}_x\left(d\right)\ \cdot\ \mathbf{H}'_{Ty}\ \cdot\ \mathbf{R}_y(q_2)\\
\mathbf{T}'_4&=\mathbf{R}_z(q_1)\mathbf{T}_x\left(d\right)\ \cdot\ \mathbf{H}'_{Rx}\ \cdot\ \mathbf{R}_y(q_2)\\
\mathbf{T}'_5&=\mathbf{R}_z(q_1)\mathbf{T}_x\left(d\right)\ \cdot\ \mathbf{H}'_{Ry}\ \cdot\ \mathbf{R}_y(q_2)
\end{aligned} \tag{2.22}$$

Using these expressions, the columns of the desired identification Jacobian $\mathbf{J}_\pi$ can be easily extracted from the above matrices using the rules defined in (2.19) and (2.20)

$$\mathbf{J}_\pi=\begin{bmatrix}
-d\sin(q_1) & \cos(q_1) & -\sin(q_1) & 0 & 0\\
d\cos(q_1) & \sin(q_1) & \cos(q_1) & 0 & 0\\
0 & 0 & 0 & 0 & 0\\
0 & 0 & 0 & \cos(q_1) & -\sin(q_1)\\
0 & 0 & 0 & \sin(q_1) & \cos(q_1)\\
1 & 0 & 0 & 0 & 0
\end{bmatrix} \tag{2.23}$$

Now let us apply this method to the computation of the identification Jacobian of robot KUKA KR270 whose geometric model has been presented in previous subsection and which is used in experimental validation of this thesis. This model contains 18 parameters to be identified (see expression (2.6)). Corresponding derivatives $\left\{\mathbf{T}'_\kappa,\ \kappa=1,...,18\right\}$ with respect to these parameters have the following forms that are presented in Table 2.3. To avoid very tedious analytical expressions, it is prudent to compute the matrices $\mathbf{T}'_\kappa$ numerically and to apply to them the extraction rules (2.19) and (2.20) presented above. This allows us to avoid obvious problems related to numerical differentiation and to obtain the desired Jacobian matrix $\mathbf{J}_\pi$ of size 6×18. In the following sections, this matrix will be used for some numerical computations required for the identification of the manipulator geometric parameters of robot KUKA KR270.

Table 2.3 Matrix derivatives for geometric model of robot KUKA KR270

Parameter	Matrix derivative
p_{x1}	$\mathbf{T}_1' = \mathbf{T}_{base} \cdot \left[\mathbf{R}_z(q_1) \cdot \mathbf{H}_{Tx}' \cdot \mathbf{R}_y(q_2)\mathbf{T}_x(d_3)\mathbf{R}_y(q_3)\mathbf{T}_x(d_4)\mathbf{T}_z(d_5)\mathbf{R}_x(q_4)\mathbf{R}_y(q_5)\mathbf{R}_x(q_6) \right] \cdot \mathbf{T}_{tool}$
p_{y1}	$\mathbf{T}_2' = \mathbf{T}_{base} \cdot \left[\mathbf{R}_z(q_1)\mathbf{T}_x(d_2) \cdot \mathbf{H}_{Ty}' \cdot \mathbf{R}_y(q_2)\mathbf{T}_x(d_3)\mathbf{R}_y(q_3)\mathbf{T}_x(d_4)\mathbf{T}_z(d_5)\mathbf{R}_x(q_4)\mathbf{R}_y(q_5)\mathbf{R}_x(q_6) \right] \cdot \mathbf{T}_{tool}$
φ_{x1}	$\mathbf{T}_3' = \mathbf{T}_{base} \cdot \left[\mathbf{R}_z(q_1)\mathbf{T}_x(d_2) \cdot \mathbf{H}_{Rx}' \cdot \mathbf{R}_y(q_2)\mathbf{T}_x(d_3)\mathbf{R}_y(q_3)\mathbf{T}_x(d_4)\mathbf{T}_z(d_5)\mathbf{R}_x(q_4)\mathbf{R}_y(q_5)\mathbf{R}_x(q_6) \right] \cdot \mathbf{T}_{tool}$
Δq_2	$\mathbf{T}_4' = \mathbf{T}_{base} \cdot \left[\mathbf{R}_z(q_1)\mathbf{T}_x(d_2) \cdot \mathbf{H}_{Ry}' \cdot \mathbf{R}_y(q_2)\mathbf{T}_x(d_3)\mathbf{R}_y(q_3)\mathbf{T}_x(d_4)\mathbf{T}_z(d_5)\mathbf{R}_x(q_4)\mathbf{R}_y(q_5)\mathbf{R}_x(q_6) \right] \cdot \mathbf{T}_{tool}$
p_{x2}	$\mathbf{T}_5' = \mathbf{T}_{base} \cdot \left[\mathbf{R}_z(q_1)\mathbf{T}_x(d_2)\mathbf{R}_y(q_2) \cdot \mathbf{H}_{Tx}' \cdot \mathbf{R}_y(q_3)\mathbf{T}_x(d_4)\mathbf{T}_z(d_5)\mathbf{R}_x(q_4)\mathbf{R}_y(q_5)\mathbf{R}_x(q_6) \right] \cdot \mathbf{T}_{tool}$
φ_{z2}	$\mathbf{T}_6' = \mathbf{T}_{base} \cdot \left[\mathbf{R}_z(q_1)\mathbf{T}_x(d_2)\mathbf{R}_y(q_2)\mathbf{T}_x(d_3) \cdot \mathbf{H}_{Rz}' \cdot \mathbf{R}_y(q_3)\mathbf{T}_x(d_4)\mathbf{T}_z(d_5)\mathbf{R}_x(q_4)\mathbf{R}_y(q_5)\mathbf{R}_x(q_6) \right] \cdot \mathbf{T}_{tool}$
φ_{x2}	$\mathbf{T}_7' = \mathbf{T}_{base} \cdot \left[\mathbf{R}_z(q_1)\mathbf{T}_x(d_2)\mathbf{R}_y(q_2)\mathbf{T}_x(d_3) \cdot \mathbf{H}_{Rx}' \cdot \mathbf{R}_y(q_3)\mathbf{T}_x(d_4)\mathbf{T}_z(d_5)\mathbf{R}_x(q_4)\mathbf{R}_y(q_5)\mathbf{R}_x(q_6) \right] \cdot \mathbf{T}_{tool}$
Δq_3	$\mathbf{T}_8' = \mathbf{T}_{base} \cdot \left[\mathbf{R}_z(q_1)\mathbf{T}_x(d_2)\mathbf{R}_y(q_2)\mathbf{T}_x(d_3) \cdot \mathbf{H}_{Ry}' \cdot \mathbf{R}_y(q_3)\mathbf{T}_x(d_4)\mathbf{T}_z(d_5)\mathbf{R}_x(q_4)\mathbf{R}_y(q_5)\mathbf{R}_x(q_6) \right] \cdot \mathbf{T}_{tool}$
p_{x3}	$\mathbf{T}_9' = \mathbf{T}_{base} \cdot \left[\mathbf{R}_z(q_1)\mathbf{T}_x(d_2)\mathbf{R}_y(q_2)\mathbf{T}_x(d_3)\mathbf{R}_y(q_3) \cdot \mathbf{H}_{Tx}' \cdot \mathbf{T}_z(d_5)\mathbf{R}_x(q_4)\mathbf{R}_y(q_5)\mathbf{R}_x(q_6) \right] \cdot \mathbf{T}_{tool}$
p_{z3}	$\mathbf{T}_{10}' = \mathbf{T}_{base} \cdot \left[\mathbf{R}_z(q_1)\mathbf{T}_x(d_2)\mathbf{R}_y(q_2)\mathbf{T}_x(d_3)\mathbf{R}_y(q_3)\mathbf{T}_x(d_4) \cdot \mathbf{H}_{Tz}' \cdot \mathbf{R}_x(q_4)\mathbf{R}_y(q_5)\mathbf{R}_x(q_6) \right] \cdot \mathbf{T}_{tool}$
φ_{z3}	$\mathbf{T}_{11}' = \mathbf{T}_{base} \cdot \left[\mathbf{R}_z(q_1)\mathbf{T}_x(d_2)\mathbf{R}_y(q_2)\mathbf{T}_x(d_3)\mathbf{R}_y(q_3)\mathbf{T}_x(d_4)\mathbf{T}_z(d_5) \cdot \mathbf{H}_{Rz}' \cdot \mathbf{R}_x(q_4)\mathbf{R}_y(q_5)\mathbf{R}_x(q_6) \right] \cdot \mathbf{T}_{tool}$
Δq_4	$\mathbf{T}_{12}' = \mathbf{T}_{base} \cdot \left[\mathbf{R}_z(q_1)\mathbf{T}_x(d_2)\mathbf{R}_y(q_2)\mathbf{T}_x(d_3)\mathbf{R}_y(q_3)\mathbf{T}_x(d_4)\mathbf{T}_z(d_5) \cdot \mathbf{H}_{Rx}' \cdot \mathbf{R}_x(q_4)\,\mathbf{R}_y(q_5)\mathbf{R}_x(q_6) \right] \cdot \mathbf{T}_{tool}$
p_{y4}	$\mathbf{T}_{13}' = \mathbf{T}_{base} \cdot \left[\mathbf{R}_z(q_1)\mathbf{T}_x(d_2)\mathbf{R}_y(q_2)\mathbf{T}_x(d_3)\mathbf{R}_y(q_3)\mathbf{T}_x(d_4)\mathbf{T}_z(d_5)\mathbf{R}_x(q_4) \cdot \mathbf{H}_{Ty}' \cdot \mathbf{R}_y(q_5)\mathbf{R}_x(q_6) \right] \cdot \mathbf{T}_{tool}$
p_{z4}	$\mathbf{T}_{14}' = \mathbf{T}_{base} \cdot \left[\mathbf{R}_z(q_1)\mathbf{T}_x(d_2)\mathbf{R}_y(q_2)\mathbf{T}_x(d_3)\mathbf{R}_y(q_3)\mathbf{T}_x(d_4)\mathbf{T}_z(d_5)\mathbf{R}_x(q_4) \cdot \mathbf{H}_{Tz}' \cdot \mathbf{R}_y(q_5)\mathbf{R}_x(q_6) \right] \cdot \mathbf{T}_{tool}$
φ_{z4}	$\mathbf{T}_{15}' = \mathbf{T}_{base} \cdot \left[\mathbf{R}_z(q_1)\mathbf{T}_x(d_2)\mathbf{R}_y(q_2)\mathbf{T}_x(d_3)\mathbf{R}_y(q_3)\mathbf{T}_x(d_4)\mathbf{T}_z(d_5)\mathbf{R}_x(q_4) \cdot \mathbf{H}_{Rz}' \cdot \mathbf{R}_y(q_5)\mathbf{R}_x(q_6) \right] \cdot \mathbf{T}_{tool}$
Δq_5	$\mathbf{T}_{16}' = \mathbf{T}_{base} \cdot \left[\mathbf{R}_z(q_1)\mathbf{T}_x(d_2)\mathbf{R}_y(q_2)\mathbf{T}_x(d_3)\mathbf{R}_y(q_3)\mathbf{T}_x(d_4)\mathbf{T}_z(d_5)\mathbf{R}_x(q_4) \cdot \mathbf{H}_{Ry}' \cdot \mathbf{R}_y(q_5)\,\mathbf{R}_x(q_6) \right] \cdot \mathbf{T}_{tool}$
p_{z5}	$\mathbf{T}_{17}' = \mathbf{T}_{base} \cdot \left[\mathbf{R}_z(q_1)\mathbf{T}_x(d_2)\mathbf{R}_y(q_2)\mathbf{T}_x(d_3)\mathbf{R}_y(q_3)\mathbf{T}_x(d_4)\mathbf{T}_z(d_5)\mathbf{R}_x(q_4)\mathbf{R}_y(q_5) \cdot \mathbf{H}_{Tz}' \cdot \mathbf{R}_x(q_6) \right] \cdot \mathbf{T}_{tool}$
φ_{z5}	$\mathbf{T}_{18}' = \mathbf{T}_{base} \cdot \left[\mathbf{R}_z(q_1)\mathbf{T}_x(d_2)\mathbf{R}_y(q_2)\mathbf{T}_x(d_3)\mathbf{R}_y(q_3)\mathbf{T}_x(d_4)\mathbf{T}_z(d_5)\mathbf{R}_x(q_4)\mathbf{R}_y(q_5) \cdot \mathbf{H}_{Rz}' \cdot \mathbf{R}_x(q_6) \right] \cdot \mathbf{T}_{tool}$

2.3 MEASUREMENT METHODS IN ROBOT CALIBRATION

In robot calibration, there exist various measurement methods that differ in measurement data structure (the manipulator end-effector position and orientation, position only, distance to the base point, etc.), and relevant equipments for external measurements (laser tracker, ball-bar system and the others) (Mooring et al., 1991). In fact, the structure of the obtained data highly depends on the employed measurement devices, whose precision affects the accuracy of the calibration results. So, in order to achieve high accuracy, proper selection of a measurement method becomes a very important issue. In practice, the evaluation of a good measurement system is based on numerous factors such as the cost, easy-to-use, the set-up time, measurement and tracking performance, accuracy and measurement volume. To find a suitable method for the considered application, several existing (and commonly used) measurement techniques as well as their efficiency are reviewed below.

2.3.1 Existing measurement methods

In the literature, the existing measurement techniques (Figure 2.4) are classified into two categories, the open-loop methods and the closed-loop ones. Let us sequentially investigate these two types of methods.

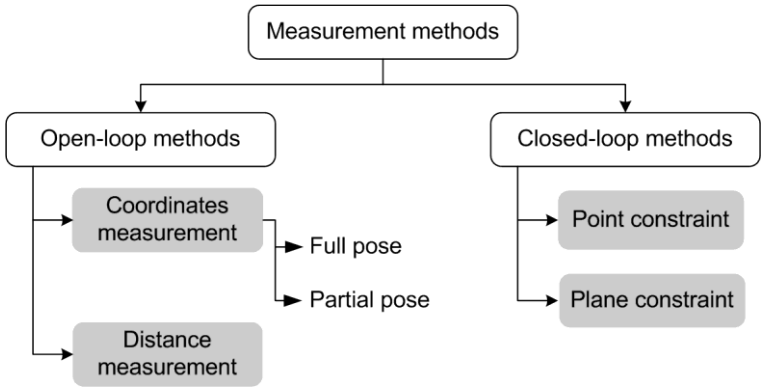

Figure 2.4 Classification of the existing measurement techniques for manipulator calibration

The open-loop methods use external measurement devices to measure the manipulator end-effector pose information for a number of configurations. This class includes the most popular measurement techniques for robot calibration, but there are still some open questions concerning the impact of utilizing different data types (full/partial pose information) on the calibration accuracy. Here, two main approaches are presented, which are based on the absolute end-effector coordinates measurement and the relative distance measurement.

Calibration using the end-effector coordinates. In this method, external device are required (such as a laser tracking system (LTS, Figure 2.5), coordinates measuring machine, inclinometers, etc.) to measure either the manipulator end-effector position or the location with respect to the user defined world frame. Here, the number of measured components can vary from six (full pose information) to only one (partial pose information). Advanced LTS is able to provide either the 6D location coordinates

$$\mathbf{t} = (p_x, p_y, p_z, \varphi_x, \varphi_y, \varphi_z)^T \tag{2.24}$$

or the 3D position

$$\mathbf{p} = (p_x, p_y, p_z)^T \tag{2.25}$$

of the robot end-effector. It should be mentioned that the orientation components $(\varphi_x, \varphi_y, \varphi_z)$ provided by the measurement systems are always computed by some embedded software using Cartesian coordinates of several reference points $\{p_{xj}, p_{yj}, p_{zj} \,|\, j = 1,2,3,...\}$.

The above described measurement techniques have been used in the majority of the proposed calibration methods. For example, such approach has been applied in (Besnard and Khalil, 1999) for calibration of a 6-dof parallel manipulator, where two inclinometers were used to measure the orientation of the moving platform. They concluded that using 80 configurations, 35 geometric parameters can be identified that ensured a robot position accuracy of 0.4mm. In (Zhuang et al., 1998), the authors applied a full pose measurement with a single theodolite for the calibration of Stewart platform. In total, 42 parameters have been identified, including the assembling errors of the platform and U-joints as well as the leg length offsets. The calibration experiments have been carried out using 12 different configurations, and the obtained s.t.d. of position errors is about 0.5mm. According to

(Khalil et al., 2000), it is possible to identify maximum number of parameters for the same parameterization method using 6D measurement. However, this technique is generally very costly and time consuming.

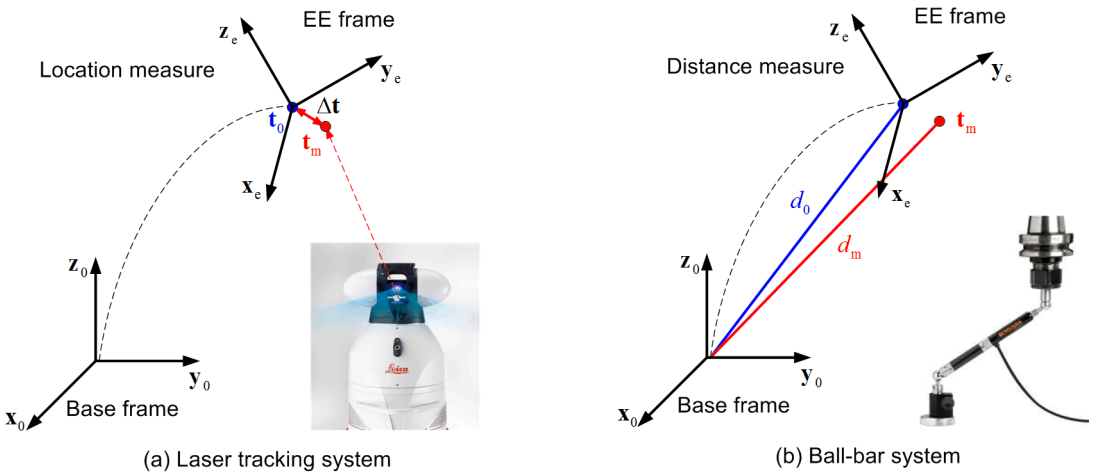

Figure 2.5 Open-loop measurement methods and related external devices.

Calibration using distance measurement. In this method, the calibration is based on the relative pose information of the manipulator end-effector location. Usually, the distance between the robot end-point and the origin of the reference frame (the base frame of measurement system) is measured. This measurement also requires an external device, such as an extendable ball-bar system (Figure 2.5), a linear variable differential transformer, etc. Such distance can be also computed from the model, using the Cartesian coordinates of the end-effector

$$d = \sqrt{(p_x - p_x^r)^2 + (p_y - p_y^r)^2 + (p_z - p_z^r)^2} \tag{2.26}$$

where coordinates (p_x^r, p_y^r, p_z^r) define the position of the reference point. So, the residual is defined as the difference between the measured and computed distances between the end-point of a given robot configuration and user defined reference point (the origin of the frame defined by the measurement device).

Such a method has been used in (Goswami et al., 1993), where the authors presented a calibration system with the ball-bar connected to a steel sphere attached to the robot end-effector and a magnetic chuck mounted on the table. It has been proved that using this approach, it is possible to identify 36 independent geometric parameters for PUMA 560 manipulator. Totally, 800 configurations have been used for the calibration and the s.t.d. of the position errors has been reduced to 0.08mm. Another technique described in (Driels, 1993) also deals with the calibration of PUMA robot, where the measurement data have been obtained from the wire potentiometer attached to the robot end-effector. According to the experimental validations (carried out with 48 configurations), the position error has been reduced from 10mm to 0.5mm.

In contrast to the previous measurement method (providing 6D or 3D end-effector coordinates), the distance measurement requires less expensive equipment and can still be easily implemented. However, the measurement volume is limited by the accessible space of the employed measurement device, and is much smaller comparing with location/position measurement. Besides, since this method provides only one scalar value as output data (the distance), more configurations are required to identify the desired parameters. Consequently, the calibration efficiency is reduced.

The closed-loop methods use physical constraints imposed on the manipulator end-effector instead of external measurements. Usually, they are implemented by attaching the robot end-effector to certain fixed environment (a point or a plane) and forming a mobile closed chain. So, the related calibration is based on the actuator values only that provides the input values for the identification algorithm. Two main approaches are usually used in relevant literature, which are based on point and plane constraints correspondingly.

Calibration using point constraint. In this method, the calibration is based on the values of actuator coordinates for a set of configurations, for which the robot end-effector is attached to a fixed contact point (Bennett et al., 1991). It is assumed that this point is known and defined by either 6D location coordinates

$$\mathbf{t}_0 = (p_{x0}, p_{y0}, p_{z0}, \varphi_{x0}, \varphi_{y0}, \varphi_{z0})^T \tag{2.27}$$

or 3D position coordinates

$$\mathbf{p}_0 = (p_{x0}, p_{y0}, p_{z0})^T, \tag{2.28}$$

and that the manipulator can reach with multiple configurations. In this technique, the residual is defined by the difference between the known position/location of the fixed point and the computed position/location, which is evaluated using the obtained actuator coordinates and nominal parameters.

The effectiveness of this method has been studied in (Meggiolaro et al., 2000), where the authors investigated the so-called "single end-point contact" calibration. The method has been evaluated experimentally for a Schilling Titan II hydraulic manipulator, where 800 measurements have been carried out. As a result, the absolute accuracy of the robot has been increased by the factor of 8 and achieved the level of 5.7mm.

The main advantage of this method is that the external devices are not required. So, the calibration experimental setup is much easier. Moreover, the measurement volume is not constrained by the accessibility of the measurement system. On the other hand, the closed chain must have some redundancy in order to perform self-motion. For instance, for the planar manipulator, at least 3-dof are required and for the spatial manipulator 4-dof are required (Meggiolaro et al., 2000).

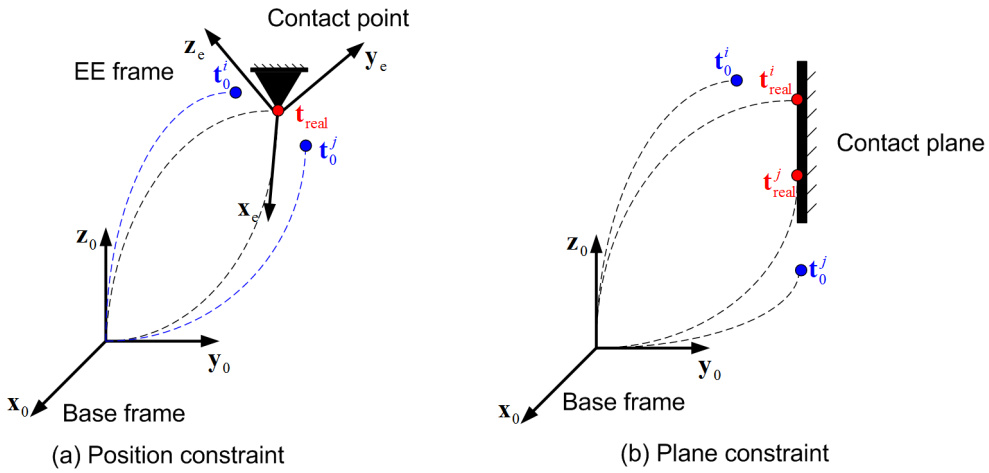

Figure 2.6 Closed-loop measurement methods.

Calibration using plane constraint. In this approach, the calibration is also based on the values of actuator coordinates for a set of configurations, for which the robot end-effector reference point is

constrained to belong the same plane (Zhong and Lewis, 1995). The corresponding set of manipulator end-effector position is defined as follows

$$\mathbf{p}_a = \left\{ \mathbf{p}_1, \mathbf{p}_2, ..., \mathbf{p}_m \middle| \mathbf{a}^T \mathbf{p}_i = c, i = 1, ..., m \right\}, \tag{2.29}$$

where $\mathbf{a}$ is the vector of plane coefficients and c is a scalar constant. For this method, the residual is defined as the difference between the known product $\mathbf{a}^T \mathbf{p}_i = c$ defining the plane and the computed product, which is found using the obtained actuator coordinates and nominal parameters.

One of the first works based on this method (Ikits and Hollerbach, 1997) was devoted to the calibration of robot PUMA 560. Here, 120 configurations were used and the end-effector has been equipped with a special sensor to detect the touching of the plane. For comparison purposes, open-loop method has been also applied, where 60 positions were measured using Optotrak 3D motion tracking system. As a result, the plane constraint method was able to identify 23 independent parameters, while the position measurement can identify 27 parameters. The achieved robot accuracy is about 0.25mm.

Similar to the previous method (point constraint), this technique also requires the values of the manipulator actuator coordinates only, which is an essential advantage in terms of experimental costs. However, the measurement configurations must be carefully selected to avoid collinearities (Ikits and Hollerbach, 1997). Besides, as it has been confirmed by several authors, for this method the number of identifiable parameters is less than for other open-loop methods (Khalil et al., 2000).

Table 2.4 Summary of different measurement methods

	Open-loop methods			Closed-loop methods	
	Location measure	Position measure	Distance measure	Position constraint	Plane constraint
Publications	(Besnard and Khalil, 1999; Zhuang et al., 1998)	(Bai et al., 2003)	(Driels and Swayze, 1994; Goswami et al., 1993)	(Meggiolaro et al., 2000)	(Ikits and Hollerbach, 1997)
Measurement device	Theodolite/ inclinometers	Laser tracker	Ball-bar system/ Wire potentiometer	—	—
Applications	Stewart platform	PUMA 560	PUMA 560	Schilling Titan II	PUMA 560
Number of parameters	35/42*	27	36/24*	—	23
Number of configurations	80/12	40	800/48	800	120
Achieved accuracy	0.4mm/0.5mm	0.1mm	0.08mm/0.5mm	5.7mm	0.25mm

*The number of identified parameters varies with different parameterization methods

Summary of different measurement methods used in manipulator calibration (both open-loop and closed-loop ones) is presented in Table 2.4. As follows from them, the best accuracy has been achieved by using position and distance measurements (about 0.1mm for industrial LTS). However, the latter approach requires 20 times more measurement configurations. The efficiency of the remaining methods is essentially lower (in spite of the fact that they allowed to improve the robot accuracy). For this reason, the end-effector coordinates measurement looks promising for industrial

applications. On the other hand, several essential problems also arise here. For instance, the location measurement should provide both position (p_x, p_y, p_z) and orientation coordinates $(\varphi_x, \varphi_y, \varphi_z)$, but the latter are usually computed using position coordinates of several reference points. Intuitively, these may lead to some loss of the identification accuracy. Besides, the 6D residuals are non-homogeneous to be directly used in the least-square objective, so they should be normalized in relevant identification equations. Therefore, it is required to enhance the measurement techniques in order to overcome these difficulties.

2.3.2 Enhancing of partial pose measurement method

As follows from previous subsection, the most attractive method for industrial applications is the partial pose measurement that requires evaluation of the end-effector Cartesian coordinates only (without orientation). On the other hand, this simplification does not allow user to identify certain manipulator parameters that can be estimated via the end-effector orientation only. For this reason, this subsection proposes an intermediate technique, where the orientation is not computed directly but is incorporated in the identification equations via the Cartesian coordinates of several reference points. Let us present this technique and compare it with the conventional one.

For the *conventional full pose measurement technique*, the desired parameters are identified from the linearized geometric model (2.16), which can be rewritten as

$$\Delta \mathbf{t}_i = \mathbf{J}_{\pi i} \Delta \boldsymbol{\pi}, \quad i = 1, 2, ...m \tag{2.30}$$

where $\Delta \mathbf{t}_i = (\Delta p_{xi}, \Delta p_{yi}, \Delta p_{zi}, \Delta \varphi_{xi}, \Delta \varphi_{yi}, \Delta \varphi_{zi})^T$ is the pose deviation caused by small variation in the model parameters $\Delta \boldsymbol{\pi}$. It is clear that the corresponding system of linear equations can be solved with respect to $\Delta \boldsymbol{\pi}$ if the number of experiments m is sufficiently high and the manipulator configurations $\{\mathbf{q}_i, i = 1, m\}$ are different to ensure non-singularity of relevant observation matrix used in the identification procedure. It is obvious that for this technique, each configuration $\mathbf{q}_i$ produces six scalar equations to be used for the identification. Corresponding optimization problem allowing to compute the desired parameters $\Delta \boldsymbol{\pi}$ is often written as follows

$$\sum_{i=1}^{m} \left\| \Delta \mathbf{t}_i - \mathbf{J}_{\pi i} \Delta \boldsymbol{\pi} \right\|^2 \to \min_{\Delta \boldsymbol{\pi}}, \tag{2.31}$$

without paying attention to the non-homogeneity of the residual components (millimeters and radians). In some cases, the position and orientation components are normalized before computing the squared sum, but it is a non-trivial step affecting the accuracy (in practice, the normalization factors are usually defined intuitively).

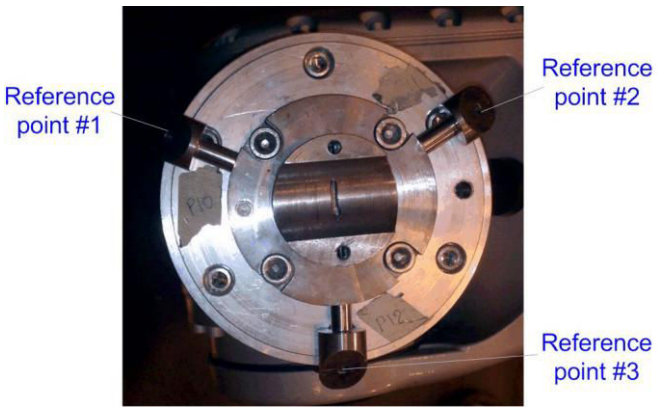

Figure 2.7 Typical manipulator mounting flange with several reference points

The main difficulty with this conventional technique is that the orientation components $(\varphi_{xi}.\varphi_{yi}.\varphi_{zi})^T$ cannot be measured directly. So, these angles are computed using excessive number of measurements for the same configuration $\mathbf{q}_i$, which produce Cartesian coordinates $\{(p_{xi}^j, p_{yi}^j, p_{zi}^j)^T \mid j=\overline{1,n}; n \geq 3\}$ for several reference points of the measurement tool attached to the manipulator mounting flange (Figure 2.7). Hence, instead of using $3mn$ scalar equations, that can be theoretically obtained from the measurement data, this conventional approach uses only $6m$ scalar equations for the identification. This may obviously lead to some loss of the parameter estimation accuracy.

To overcome this difficulty, *the proposed technique* is based on reformulation of the optimization problem (2.31) using only the data directly available from the measurement system, i.e. the Cartesian coordinates of all reference points $\mathbf{p}_i^j$ (see Figure 2.7). This idea allows us to obtain homogeneous identification equations where each residual has the same unit (mm, for instance), and the optimization problem is rewritten as follows

$$\sum_{i=1}^{m}\sum_{j=1}^{n}\left\|\Delta\mathbf{p}_i^j - \mathbf{J}_{\pi i}^{j(p)}\Delta\boldsymbol{\pi}\right\|^2 \rightarrow \min_{\Delta\boldsymbol{\pi}} \tag{2.32}$$

Here, the matrix $\mathbf{J}_{\pi i}^{j(p)}$ with the superscripts "(p)" denotes the position rows of the corresponding identification Jacobian $\mathbf{J}_{\pi i}^{j}$, the index "i" defines the manipulator configuration number, and the index "j" denotes the reference point number. An obvious advantage of this formulation is its simplicity and clarity of the residual vector norm definition (conventional Euclidian norm can be applied here reasonably, the normalization is not required). So, the problem of the weighting coefficient selection does not exist in this case. In fact, under the assumption that measurement errors are modeled as a set of i.i.d. random values (similar for all directions x, y, z and for all measurement configurations), the optimal linear estimator should have equal weights for all equations. Besides, the most important issue is related to the potential benefits in the identification accuracy, since the total number of scalar equations incorporated in the least-square objective increases from $6m$ to $3mn$.

In order to illustrate the benefits of the proposed approach, let us present a numerical example that deals with parameter identification for a 3-link spatial manipulator, whose geometry is described by the following equations

$$\begin{aligned}
p_x &= (l_2\cos q_2 + l_3\cos(q_2+q_3))\cos q_1 \\
p_y &= (l_2\cos q_2 + l_3\cos(q_2+q_3))\sin q_1 \\
p_z &= l_1 + l_2\sin q_2 + l_3\sin(q_2+q_3) \\
\varphi_x &= 0 \\
\varphi_y &= q_2 + q_3 \\
\varphi_z &= q_1
\end{aligned} \tag{2.33}$$

where q_1, q_2, q_3 are the actuated manipulator coordinates and l_1, l_2, l_3 are the link lengths to be identified. Figure 2.8 illustrates the considered manipulator architecture, the placements of measurement points as well as the input data of parameter identification for both approaches. For this case study, the conventional and proposed calibration techniques can be described as follows.

Approach #1 (conventional): The identification is based on the manipulator end-point location (full pose information) $\mathbf{t}_0 = (\mathbf{p}_0, \boldsymbol{\varphi}_0)$, which is computed from the position measurement of three reference points $\{\mathbf{p}_1, \mathbf{p}_2, \mathbf{p}_3\}$. For the considered example, relevant expression for the position component can be presented as

$$\mathbf{p}_0 = \frac{\mathbf{p}_1 + \mathbf{p}_2 + \mathbf{p}_3}{3} \tag{2.34}$$

and the orientation component is computed using the equations

$$\begin{bmatrix} \varphi_{x0} \\ \varphi_{y0} \\ \varphi_{z0} \end{bmatrix} = \begin{bmatrix} 0 \\ \text{atan2}\left(p_{y0}, p_{x0}\right) \\ \text{atan2}\left((p_{x1} - p_{x0})/\|\mathbf{p}_1 - \mathbf{p}_0\|, (p_{z1} - p_{z0})\right) \end{bmatrix} \tag{2.35}$$

So, each identification equation includes six scalar expressions and can be written as

$$\begin{bmatrix} \Delta\mathbf{p}_0 \\ \Delta\boldsymbol{\varphi}_0 \end{bmatrix} = \left[\mathbf{J}_{\pi}^{(p)}|_{\mathbf{p}_0}, \mathbf{J}_{\pi}^{(\varphi)}|_{\mathbf{p}_0} \right]^T \cdot \Delta\boldsymbol{\pi} \tag{2.36}$$

where the notations $\mathbf{J}_{\pi}^{(p)}$ and $\mathbf{J}_{\pi}^{(\varphi)}$ refer to the position and orientation part in the Jacobian matrix computed at the robot end-point $\mathbf{p}_0$.

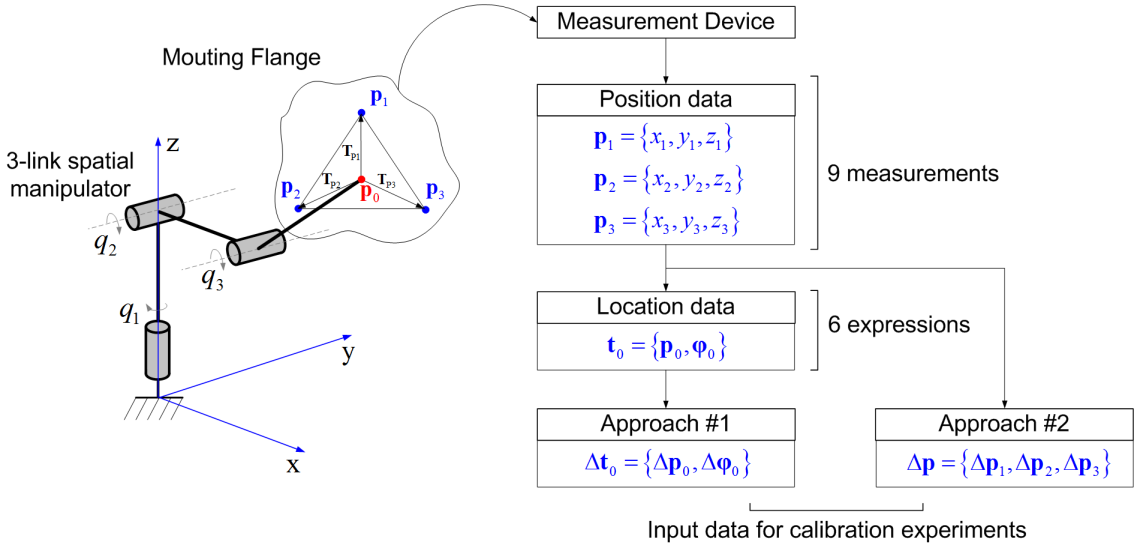

Figure 2.8 Input data for two identification approaches

Approach #2 (proposed): The identification is based on the partial pose information, where three measurement points $\{\mathbf{p}_1, \mathbf{p}_2, \mathbf{p}_3\}$ are directly included in the objective function to be minimized by the identification algorithm. In this case, the identification Jacobian matrix contains only the position part $\mathbf{J}_{\pi}^{(p)}$, and the corresponding identification equations can be written as

$$\begin{bmatrix} \Delta\mathbf{p}_1 \\ \Delta\mathbf{p}_2 \\ \Delta\mathbf{p}_3 \end{bmatrix} = \left[\mathbf{J}_{\pi}^{(p)}|_{\mathbf{p}_1}, \mathbf{J}_{\pi}^{(p)}|_{\mathbf{p}_2}, \mathbf{J}_{\pi}^{(p)}|_{\mathbf{p}_3} \right]^T \cdot \Delta\boldsymbol{\pi} \tag{2.37}$$

where the Jacobian matrices $\mathbf{J}_{\pi}^{(p)}|_{\mathbf{p}_1}$, $\mathbf{J}_{\pi}^{(p)}|_{\mathbf{p}_2}$, $\mathbf{J}_{\pi}^{(p)}|_{\mathbf{p}_3}$ are different and computed at the reference points $\{\mathbf{p}_1, \mathbf{p}_2, \mathbf{p}_3\}$. It should be mentioned that these shifts (from the conventional end-point $\mathbf{p}_0$ to the reference points $\mathbf{p}_1, \mathbf{p}_2, \mathbf{p}_3$) are included in corresponding tool transformations $\mathbf{T}_{tool}^{1}$, $\mathbf{T}_{tool}^{2}$, $\mathbf{T}_{tool}^{3}$ (see equation (2.1)), which must be treated separately. Assuming that the measurement tool geometry is known and the reference points are symmetrical with respect to the tool axes, corresponding transformations from $\mathbf{p}_0$ to $\mathbf{p}_1, \mathbf{p}_2, \mathbf{p}_3$ can be presented as

$$\begin{aligned}\mathbf{T}_{p1} &= \mathbf{T}_z(d)\\ \mathbf{T}_{p2} &= \mathbf{R}_x(\frac{2\pi}{3})\mathbf{T}_z(d)\mathbf{R}_x(-\frac{2\pi}{3})\\ \mathbf{T}_{p3} &= \mathbf{R}_x(-\frac{2\pi}{3})\mathbf{T}_z(d)\mathbf{R}_x(\frac{2\pi}{3})\end{aligned} \tag{2.38}$$

where d is the radius of the circle where the reference points are located (see Figure 2.7).

To compare the efficiency of the above approaches, the simulation study has been carried out. Within this study, the following manipulator parameters have been assigned: $l_1 = 1\text{m}$, $l_2 = 0.8\text{m}$, $l_3 = 0.6\text{m}$. It was assumed that the geometric errors in the link lengths and the actuated joint offsets are respectively $\Delta l_1 = 3.0\text{mm}$, $\Delta l_2 = 2.0\text{mm}$, $\Delta l_3 = 5.0\text{mm}$ and $\Delta q_1 = 1.0\text{deg}$, $\Delta q_2 = 0.5\text{deg}$, $\Delta q_3 = 2.0\text{deg}$. Besides, it was also assumed that the measurements errors are non-biased i.i.d. random variables with the standard deviation $\sigma = 0.01\text{mm}$. The desired parameters were estimated using three measurement configurations, which were generated randomly. To obtain reliable statistics, the calibration experiments have been repeated 1000 times.

Simulation results are summarized in Table 2.5, which presents the standard deviations for the estimates of the parameters Δl_i and Δq_i (corresponding mean values are very close to zero). As follows from these results, the proposed approach ensures the accuracy improvement in the estimation of the link length deviations Δl_i by 125-283%, while the accuracy improvement for the joint offsets estimations Δq_i is slightly less, up to 233%. This confirms advantages of the proposed approach, but it should be mentioned that these numbers are obtained for particular set of the measurement configurations and particular normalization factor utilized in the approach #1. However, as follows from our study, approach #2 always provides better results.

Table 2.5 Comparison of different measurement methods and their influence on the identification accuracy (number of iterations : 1000; number of configurations : 3; $\sigma = 0.01\text{mm}$)

Parameters	Assigned geometric errors	Standard deviations of parameter estimates		Improvement
		Approach #1	Approach #2	
l_1	3 mm	0.069mm	0.018mm	283%
l_2	5 mm	0.019mm	0.006mm	217%
l_3	5 mm	0.009mm	0.004mm	125%
q_1	1 deg	0.187mdeg	0.185mdeg	1%
q_2	0.5 deg	3.742mdeg	1.123mdeg	233%
q_3	2 deg	1.432mdeg	0.866mdeg	65%

Therefore, the proposed approach #2 that is based on partial pose information is rather promising and it will be further used for calibration experiments in this work. In contrast to the conventional methods, the proposed technique uses only direct measurements for several reference points with different tool transformations. It allows us to avoid the problem of non-homogeneity of the relevant optimization objective and does not require any normalization (which arises in the case when full pose residuals are used). It should be mentioned that for the measurement of robot end-effector position coordinates, a laser tracking system Leica AT-901 is available in IRCCyN laboratory.

Corresponding dedicated identification algorithms that employ this measurement technique is presented in the following Section.

2.4 IDENTIFICATION OF MODEL PARAMETERS

Using the manipulator geometric model presented in Section 2.2 and experimental data obtained by measuring end-effector positions (see Section 2.3), it is possible to identify the desired manipulator parameters. This problem can be treated as the best fitting of the measurement results by Eq. (2.1) describing the manipulator geometry. It is clear that, to find the desired parameters, sufficient number of experiments should be performed that provide a set of end-effector position coordinates for different manipulator configurations. Moreover, to reduce the measurement noise impact, number of experiments is usually redundant (i.e. more than sufficient) and relevant system of the identification equations is over-determined. So, its solution can be obtained using the least-square method. Another approach allowing us to increase the identification accuracy is based on enhancing the conventional measurement techniques. This Section presents a dedicated identification algorithm corresponding to the improvement proposed in Subsection 2.3.2 and relevant accuracy analysis.

2.4.1 Identification algorithm for the enhanced partial pose method

In previous works (Bai et al., 2003; Goswami et al., 1993), etc., the parameter identification algorithms are mainly based on the minimization of the least-square objectives that are derived assuming that the measurement tool has a single reference point (see Eq.(2.31)). However, as follows from previous Section, utilization of the enhanced measurement method that operates with several reference points gives some advantages in the identification accuracy. For this reason, it is required to revise the existing identification techniques, taking into account both modification of the objective function and increasing of the number of parameters (because each reference point induces additional parameters).

Let us assume that the measurement tool has n reference points ($n \geq 3$) that are used to estimate relevant vectors of the Cartesian coordinates $\mathbf{p}_i^j = (p_{xi}^j, p_{yi}^j, p_{zi}^j)^T$ for m manipulator configurations $\mathbf{q}_i$. In this notation, the subscript " i " and subscript " j " denote the experiment number and reference point number, respectively. Correspondingly, the manipulator geometric model (2.1) can be rewritten as

$$\mathbf{T}_i^j = \mathbf{T}_{base} \cdot \mathbf{T}_{robot}(\mathbf{q}_i, \boldsymbol{\pi}) \cdot \mathbf{T}_{tool}^j; \quad i = \overline{1,m},\ j = \overline{1,n} \tag{2.39}$$

where the vectors $\mathbf{p}_i^j$ are incorporated in the fourth column of $\mathbf{T}_i^j$, the matrix $\mathbf{T}_{base}$ defines the robot base location, the matrices $\mathbf{T}_{tool}^j$, $j = \overline{1,n}$ describe the locations of the reference points that are observed by the measurement system (see Figure 2.7). Here, the matrix function $\mathbf{T}_{robot}(\mathbf{q}_i, \boldsymbol{\pi})$ describes the manipulator geometry and depends on the current values of the actuated coordinates $\mathbf{q}_i$ and the parameters $\boldsymbol{\pi}$ to be estimated. Taking into account that any homogeneous transformation matrix $\mathbf{T}_a^b$ can be split into the rotational $\mathbf{R}_a^b$ and translational $\mathbf{p}_a^b$ components and presented as

$$\mathbf{T}_a^b = \begin{bmatrix} \mathbf{R}_a^b & \mathbf{p}_a^b \\ \mathbf{0} & 1 \end{bmatrix}, \tag{2.40}$$

the vector of the reference point positions $\mathbf{p}_i^j, j = \overline{1,n}$ (that are measured in calibration experiments) can be expressed in the following form

$$\mathbf{p}_i^j = \mathbf{p}_{base} + \mathbf{R}_{base} \cdot \mathbf{p}_{robot}(\mathbf{q}_i, \boldsymbol{\pi}) + \mathbf{R}_{base} \cdot \mathbf{R}_{robot}(\mathbf{q}_i, \boldsymbol{\pi}) \cdot \mathbf{p}_{tool}^j; \quad i = \overline{1,m},\ j = \overline{1,n}\,. \tag{2.41}$$

This allows us to obtain $3mn$ scalar equations for the calibration purposes, where $n \geq 3$ and m is high enough to ensure identifiability of the desired parameters.

Applying the least-square method, the corresponding optimization problem can be presented as

$$\sum_{i=1}^{m}\sum_{j=1}^{n}\left\|\mathbf{p}_i^j - \mathbf{p}_{base} - \mathbf{R}_{base}\cdot\mathbf{p}_{robot}(\mathbf{q}_i,\boldsymbol{\pi}) - \mathbf{R}_{base}\cdot\mathbf{R}_{robot}(\mathbf{q}_i,\boldsymbol{\pi})\cdot\mathbf{p}_{tool}^j\right\|^2 \rightarrow \min_{\{\mathbf{p}_{base},\mathbf{R}_{base},\mathbf{p}_{tool}^j,\boldsymbol{\pi}\}} \tag{2.42}$$

where the following vectors/matrices are treated as unknowns:

- the 3×1 vector $\mathbf{p}_{base}$ and 3×3 orthogonal matrix $\mathbf{R}_{base}$ defining the position and orientation of the base coordinate system;
- the set of 3×1 vectors $\left\{\mathbf{p}_{tool}^j,\ j=\overline{1,n}\right\}$ defining the reference point positions on the measurement tools;
- the set of manipulator geometric parameters included in the vector $\boldsymbol{\pi}$.

The main difficulty with this optimization problem is that some of the unknowns are included in the objective function in highly non-linear way. So, to solve this problem, numerical optimization technique is required. However in practice, the deviations in the model parameters are relatively small, which allows us to linearize the manipulator geometric model (2.41). This leads to a linear least-square problem, whose solution can be obtained straightforwardly with the matrix pseudo-inverse. However, to simplify computations, here it is proposed to apply the linearization technique sequentially and separately with respect to two different subsets of the model parameters (corresponding to the base/tool transformations and the manipulator geometry). Consequently, the identification procedure is split into two steps. In the frame of this approach, the first step deals with the estimation of $\mathbf{p}_{base}$, $\mathbf{R}_{base}$, $\mathbf{p}_{tool}^j$, which are related to the base and tool transformations (assuming that the manipulator parameters are known). The second step focuses on the estimation of $\boldsymbol{\pi}$ under the assumption that the base and tool components are already identified. In order to ensure that the desired identification accuracy can be achieved, these two steps are repeated iteratively. More details concerning these steps are presented below.

Step 1. For the first step, taking into account that the errors in the base orientation are relatively small, the matrix $\mathbf{R}_{base}$ is presented in the following form

$$\mathbf{R}_{base} = \left[\sim \boldsymbol{\varphi}_{base}\right] + \mathbf{I} \tag{2.43}$$

where $\mathbf{I}$ is a 3×3 identity matrix, vector $\mathbf{r}_{base}$ includes the deviations in the base orientation angles, and the operator "[~]" transforms the vector of these angles $\boldsymbol{\varphi} = (\varphi_x, \varphi_y, \varphi_z)^T$ into the skew symmetric matrix as

$$\left[\sim \boldsymbol{\varphi}\right] = \begin{bmatrix} 0 & -\varphi_z & \varphi_y \\ \varphi_z & 0 & -\varphi_x \\ -\varphi_y & \varphi_x & 0 \end{bmatrix} \tag{2.44}$$

This leads to the following presentation of expression (2.41)

$$\mathbf{p}_i^j = \mathbf{p}_{base} + \mathbf{p}_{robot}^i - \mathbf{p}_{robot}^i\cdot\left[\sim \boldsymbol{\varphi}_{base}\right] + \mathbf{R}_{robot}^i\cdot\mathbf{u}_{tool}^j \tag{2.45}$$

that can also be rewritten in a matrix form as

$$\mathbf{p}_i^j = \mathbf{p}_{robot}^i + \left[\mathbf{I} \;\middle|\; \left[\sim \mathbf{p}_{robot}^i\right]^T \;\middle|\; \mathbf{R}_{robot}^i\right] \begin{bmatrix} \mathbf{p}_{base} \\ \boldsymbol{\varphi}_{base} \\ \mathbf{u}_{tool}^j \end{bmatrix} \tag{2.46}$$

where $\mathbf{p}_{robot}^{i}$ and $\mathbf{R}_{robot}^{i}$ are defined as follows

$$\begin{aligned} \mathbf{p}_{robot}^{i} &= \mathbf{p}_{robot}(\mathbf{q}_i, \boldsymbol{\pi}) \\ \mathbf{R}_{robot}^{i} &= \mathbf{R}_{robot}(\mathbf{q}_i, \boldsymbol{\pi}) \end{aligned} \tag{2.47}$$

and

$$\mathbf{u}_{tool}^{j} = \mathbf{R}_{base}\mathbf{p}_{tool}^{j} \tag{2.48}$$

Here the vectors $\mathbf{p}_{base}$, $\boldsymbol{\varphi}_{base}$ and $\mathbf{u}_{tool}^{j}, j=\overline{1,n}$ are treated as unknowns.

Applying to the linear system (2.46) the linear least-square technique, the desired vectors defining the base and tool transformation parameters can be expressed as follows

$$\left[\mathbf{p}_{base}; \boldsymbol{\varphi}_{base}; \mathbf{u}_{tool}^{1}; ... \mathbf{u}_{tool}^{n}\right] = \left(\sum_{i=1}^{m} \mathbf{A}_i^{j\,T} \mathbf{A}_i^{j}\right)^{-1} \left(\sum_{i=1}^{m} \mathbf{A}_i^{j\,T} \Delta\mathbf{p}_i\right) \tag{2.49}$$

where

$$\mathbf{A}_i^{j} = \begin{bmatrix} \mathbf{I} & \left[\sim \mathbf{p}_{robot}^{i}\right]^{T} & \mathbf{R}_{robot}^{i} & \mathbf{0} & ... & \mathbf{0} \\ \mathbf{I} & \left[\sim \mathbf{p}_{robot}^{i}\right]^{T} & \mathbf{0} & \mathbf{R}_{robot}^{i} & ... & \mathbf{0} \\ ... & ... & ... & ... & ... & ... \\ \mathbf{I} & \left[\sim \mathbf{p}_{robot}^{i}\right]^{T} & \mathbf{0} & \mathbf{0} & ... & \mathbf{R}_{robot}^{i} \end{bmatrix} \tag{2.50}$$

and the residuals are integrated in a single vector $\Delta\mathbf{p}_i = (\Delta\mathbf{p}_i^1, ..., \Delta\mathbf{p}_i^n)^T$. Finally, the variables defining the location to the reference points are computed using expression (2.48) as $\mathbf{p}_{tool}^{j} = \mathbf{R}_{base}^{T} \cdot \mathbf{u}_{tool}^{j}$. This allows us to find the homogeneous transformation matrices $\mathbf{T}_{base}$ and $\mathbf{T}_{tool}^{j}$ that are contained in expression (2.39).

Step 2. On the second step, the manipulator geometric parameters $\boldsymbol{\pi}$ are estimated. For this purpose, the principal system (2.39) is linearized and rewritten in the form

$$\mathbf{p}_i^{j} = \mathbf{p}_{robot}^{i} + \mathbf{J}_{\pi i}^{j(p)} \cdot \Delta\boldsymbol{\pi} \tag{2.51}$$

where the superscript "(p)" denotes the positional components (first three rows) of the corresponding matrices, $\Delta\boldsymbol{\pi}$ is the vector of geometric errors, the matrix $\mathbf{J}_{\pi i}^{j}$ is the identification Jacobian computed for the configuration $\mathbf{q}_i$ with respect to the reference point j. For the computational convenience, expression (2.51) can be presented in the following form

$$\Delta\mathbf{p}_i^{j} = \mathbf{J}_{\pi i}^{j(p)} \cdot \Delta\boldsymbol{\pi} \tag{2.52}$$

where $\Delta\mathbf{p}_i^{j} = \mathbf{p}_i^{j} - \mathbf{p}_{robot}^{i}$ is the residual vector corresponding to the j-th reference point for the i-th manipulator configuration.

Applying to this system the least-square technique, the desired vectors of geometric errors $\Delta\boldsymbol{\pi}$ can be obtained as

$$\Delta\boldsymbol{\pi} = \left(\sum_{i=1}^{m}\sum_{j=1}^{n} \mathbf{J}_{\pi i}^{j(p)T} \mathbf{J}_{\pi i}^{j(p)}\right)^{-1} \left(\sum_{i=1}^{m}\sum_{j=1}^{n} \mathbf{J}_{\pi i}^{j(p)T} \Delta\mathbf{p}_i^{j}\right) \tag{2.53}$$

It should be noted that, to achieve the desired accuracy, the steps 1 and 2 should be repeated iteratively.

Hence, the above presented identification algorithm is able to provide the estimation of the manipulator geometric parameters as well as the matrices of the base and tool transformations. However, the obtained identification results usually include some dispersion caused by the errors that

obviously exist in the experimental data. So, in order to achieve desired identification accuracy, the influence of these errors should be evaluated, which will be in the focus of the following subsection.

2.4.2 Influence of the measurement errors on the identification accuracy

In practice, different sources of error may affect the identification accuracy. They include the measurement errors of the external measurement device providing the end-effector position coordinates (laser tracker in our case), the errors in the actuator encoders (internal measurement devices) giving the manipulator joint coordinates that depend on encoder resolution, etc. Besides, some assumptions concerning the manipulator model (the link rigidity, for instance) also effect the identification accuracy. It is clear that, all these sources of error can be hardly taken into account in calibration. For this reason, only the most significant of the above mentioned sources of error should be considered in the accuracy analysis. As follows from our experience, the inaccuracy of external measurement system has the most significant impact on the robot positioning accuracy, comparing to other sources of error that can be assumed negligible in the frame of geometric calibration.

Under these assumptions, the basic equation of calibration (2.52) should integrate the measurement errors and is expressed as

$$\Delta\mathbf{p}_i^j = \mathbf{J}_{\pi i}^{j(p)} \cdot \Delta\boldsymbol{\pi} + \boldsymbol{\varepsilon}_i^j; \quad i = \overline{1,m},\ j = \overline{1,n} \tag{2.54}$$

where the vectors $\boldsymbol{\varepsilon}_i^j = (\varepsilon_{xi}^j, \varepsilon_{yi}^j, \varepsilon_{zi}^j)^T$ denote the additive random errors, which are usually assumed to be unbiased and independent identically distributed (i.i.d.) with the standard deviation σ. Then, using Eq. (2.53), the estimates of the desired parameters can be presented as

$$\Delta\hat{\boldsymbol{\pi}} = \Delta\boldsymbol{\pi} + \left(\sum_{i=1}^{m}\sum_{j=1}^{n} \mathbf{J}_{\pi i}^{j(p)T} \mathbf{J}_{\pi i}^{j(p)} \right)^{-1} \left(\sum_{i=1}^{m}\sum_{j=1}^{n} \mathbf{J}_{\pi i}^{j(p)T} \boldsymbol{\varepsilon}_i^j \right) \tag{2.55}$$

where the second term describes the stochastic component. As follows from this expression, the considered identification algorithm provides the unbiased estimate of the desired parameters, i.e.,

$$E(\Delta\hat{\boldsymbol{\pi}}) = \Delta\boldsymbol{\pi}$$

where $E(\cdot)$ denotes the mathematical expectation of the random value one. Correspondingly, the covariance matrix of $\Delta\boldsymbol{\pi}$, which defines the identification accuracy, can be computed as

$$\operatorname{cov}(\Delta\hat{\boldsymbol{\pi}}) = \left(\sum_{i=1}^{m}\sum_{j=1}^{n} \mathbf{J}_{\pi i}^{j(p)T} \mathbf{J}_{\pi i}^{j(p)} \right)^{-1} E\left(\sum_{i=1}^{m}\sum_{j=1}^{n} \mathbf{J}_{\pi i}^{j(p)T} \boldsymbol{\varepsilon}_i^j \cdot \sum_{i=1}^{m}\sum_{j=1}^{n} \boldsymbol{\varepsilon}_i^{jT} \mathbf{J}_{\pi i}^{j(p)} \right) \left(\sum_{i=1}^{m}\sum_{j=1}^{n} \mathbf{J}_{\pi i}^{j(p)T} \mathbf{J}_{\pi i}^{j(p)} \right)^{-1} \tag{2.56}$$

Further, after some transformations and taking into account the statistical properties of the measurement errors (which are assumed to be similar for all reference points, all manipulator configurations and all directions, in accordance with expression $E\left(\boldsymbol{\varepsilon}_i \boldsymbol{\varepsilon}_i^T\right) = \sigma^2 \mathbf{I}$), the desired covariance matrix can be simplified to

$$\operatorname{cov}(\Delta\hat{\boldsymbol{\pi}}) = \sigma^2 \left(\sum_{i=1}^{m}\sum_{j=1}^{n} \mathbf{J}_{\pi i}^{j(p)T} \mathbf{J}_{\pi i}^{j(p)} \right)^{-1} \tag{2.57}$$

Hence, the impact of the measurement errors on the identified values of the geometric parameters is defined by the matrix sum $\sum_{i=1}^{m}\sum_{j=1}^{n} \mathbf{J}_{\pi i}^{j(p)T} \mathbf{J}_{\pi i}^{j(p)}$ that in literature is also called the information matrix. It is clear that to achieve the best accuracy, the elements of covariance matrix (2.57) should be as small as possible. This requirement can be satisfied by proper selection of the experiment input data (i.e., the measurement configurations $\{\mathbf{q}_i,\ i = \overline{1,m}\}$) as well as by increasing the number of

experiments m. Since the latter is rather time consuming, it is reasonable to investigate the first approach.

The problem of manipulator measurement pose selection is the key issue of calibration experiments design, where the notion of "optimal measurement pose" is formalized and several scalar criteria are proposed (see Section 1.5). As follows from our analysis, the existing approaches have different effects on the parameter identification accuracy. The main disadvantage of these approaches is that the relevant optimization objectives are not directly related to the manipulator positioning accuracy (they usually focus on the parameter identification accuracy). Hence, in order to achieve simultaneously high accuracy both for the manipulator parameters and for the end-effector position (or to find reasonable trade-off), it is required to define a proper objective for measurement pose selection, taking into account the specificities of the application area studied in this work. This motivates the research direction presented in the following Section.

2.5 OPTIMAL SELECTION OF MEASUREMENT CONFIGURATIONS

The problem of optimal selection of the manipulator measurement configurations has been studied in a number of works (Daney et al., 2005; Huang et al., 2008; Imoto et al., 2009; Zhuang et al., 1996), where several different criteria have been proposed for the corresponding optimization procedure. Using these criteria, relevant plans of experiments (i.e. sets of measurement configurations) may be generated, which improve the identification accuracy comparing to the non-optimal plans obtained randomly or intuitively. However, as it has been shown in Section 1.4, different criteria may provide sets of measurement configurations that are difficult to compare and select the best one of them (usually, they are Pareto-optimal with respect to the identification accuracy of each parameter, see Figure 1.22). Moreover, the conventional optimization criteria operate with some abstract performance measures that are not directly related to the manipulator positioning accuracy after calibration, which is the primary goal for the industrial application studied in this work. For this reason, this Section proposes a new approach for calibration experiments design that has two distinct features compared to the conventional ones: (i) optimization based on a new industrial-oriented performance measure that evaluates the manipulator positioning accuracy after calibration; (ii) utilization of experimental data obtained by means of the enhanced partial pose measurement method. The following Subsections present detailed description of this approach and an illustrative example confirming its advantages.

2.5.1 New approach for calibration experiment design

Generally, the robot calibration allows us to estimate the values of the manipulator parameters using experimental data corrupted by the measurement noise. For this reason, the parameters estimates are not exactly equal to the true values, they vary from one set of experiments to another and can be treated as random variables. As follows from previous Section, relevant identification algorithms provide unbiased estimates (i.e. their expectation is equal to the true values) but their dispersion essentially depends on the set of measurement configurations that provides the experimental data for the identification. Hence, it is reasonable to select the measurement configurations in the best way, in order to ensure the lowest impact of the measurement errors on the parameter estimates. In literature, this problem is known as the "calibration experiments design" and has been studied in a number of works, but existing approaches concentrate on the *accuracy of the parameter estimation* (defined by the relevant covariance matrix (2.57)), while the considered industrial application motivates us to focus on the *manipulator positioning accuracy* after calibration.

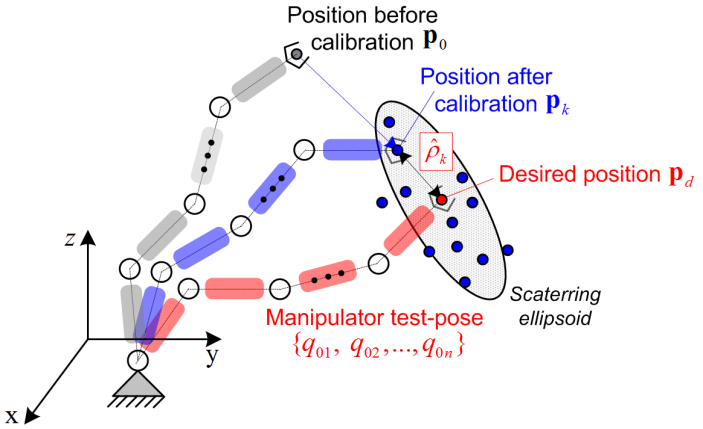

Figure 2.9 Dispersion of the manipulator positioning errors after calibration and performance measure for selection of measurement configurations (for given single target point)

In more details, the notion of manipulator positioning accuracy after calibration is illustrated in Figure 2.9. It is assumed here that the desired end-effector position is $\mathbf{p}_d$, but without calibration, the end-effector is located at the point $\mathbf{p}_0$ (computed using nominal geometric model, i.e., $\mathbf{p}_0 = g(\mathbf{q}_0, \boldsymbol{\pi})$, where $\mathbf{q}_0$ is obtained from equation $\mathbf{p}_d = g(\mathbf{q}_0, \boldsymbol{\pi}_0)$ via the inverse kinematics). For each set of experimental data, calibration yields the parameter estimates $\hat{\boldsymbol{\pi}}_k$ that allow us to partially compensate the positioning errors by computing the joint coordinates $\mathbf{q}_k$ from the equation $\mathbf{p}_d = g(\mathbf{q}_k, \hat{\boldsymbol{\pi}}_k)$ and to locate the end-effector at the point $\mathbf{p}_k = g(\mathbf{q}_k, \boldsymbol{\pi})$. As a result, the end-effector goes closer to the desired position $\mathbf{p}_d$. Evaluating the points $\mathbf{p}_k$ distribution in general, it should be mentioned that they are concentrated around $\mathbf{p}_d$ in such way that

$$\text{mean}(\mathbf{p}_1, \mathbf{p}_2, \ldots) \approx \mathbf{p}_d \tag{2.58}$$

So, the target position can be treated as the center. To evaluate their dispersion with respect to the desired position, relevant distances

$$\rho_k = |\mathbf{p}_k - \mathbf{p}_d|, \quad k = 1, 2, \ldots \tag{2.59}$$

can be used. This leads to the following statistical performance measure

$$\rho_0 = \sqrt{E\left((\mathbf{p}_k - \mathbf{p}_d)^T (\mathbf{p}_k - \mathbf{p}_d)\right)} \tag{2.60}$$

which is the root-mean-square distance between the target position and the end-effector position after calibration. This indicator is used below to describe the geometric errors compensation efficiency. It is clear that the performance measure ρ_0 is directly related to the manipulator accuracy in engineering sense, which justifies its application in this work.

To apply this performance measure to the calibration experiment design, it is necessary to take into account that the influence of the geometric errors on the end-effector position varies from one configuration to another and essentially differs throughout the workspace. So in practice, the desired accuracy is usually required to be achieved for rather limited workspace area (for example, where the workpieces are located in the robotic cell). For this reason, it is proposed to limit the possible manipulator configurations by a single one (the machining configuration, for instance), which will be further referred to as the *manipulator test-pose*. To develop a new approach to calibration experiments design that utilizes the above proposed ideas, let us introduce several basic definitions:

Definition 1. The *plan of experiments* is a set of manipulator configurations $\{\mathbf{q}_i,\ i=\overline{1,m}\}$ that are used for the measurements of the end-effector positions $\{\mathbf{p}_i^j, i=\overline{1,m},\ j=\overline{1,n}\}$ and for further identification of the desired parameters $\boldsymbol{\pi}$.

Definition 2. The *efficiency of manipulator positioning error compensation* ρ_0 is the root-mean-square distance between the desired manipulator end-effector position and the position obtained after application of the error compensation technique (see Figure 2.9).

Definition 3. The *manipulator test-pose* is a particular robot configuration $\mathbf{q}_0$ (that is usually specified in relevant technological process), for which it is required to achieve the best compensation of the positioning errors (i.e. $\rho_0 \to \min$).

In the frame of the adopted notations and assuming that the manipulator geometric model is linearized, the distance $\hat{\rho}_k$ can be computed as the Euclidean norm of the vector $\delta\mathbf{p}_k = \mathbf{J}_{\pi 0}^{(p)}\delta\boldsymbol{\pi}_k$, where the subscript ' 0 ' in the identification Jacobian $\mathbf{J}_{\pi 0}^{(p)}$ is related to the test pose $\mathbf{q}_0$ and $\delta\boldsymbol{\pi}_k = \hat{\boldsymbol{\pi}}_k - \boldsymbol{\pi}$ is the difference between the estimated and true values of the robot geometric parameters. Further, taking into account expression (2.55) and the assumptions concerning the measurement errors that are treated as unbiased and i.i.d. random variables (see Subsection 2.4.2), it can be easily proved that the expectation $E(\delta\mathbf{p}_k)=0$. So, the points $\mathbf{p}_k$ that the end-effector attains after compensation are centred around the desired position $\mathbf{p}_d$, as shown in Figure 2.9.

The dispersion of these points can be evaluated by the variance $E\left(\delta\mathbf{p}_k{}^T\delta\mathbf{p}_k\right)$ which in accordance with the above definition is equal to the square of the performance measure ρ_0. This yields the expression

$$\rho_0^2 = E\left(\delta\boldsymbol{\pi}^T\mathbf{J}_{\pi 0}^{(p)T}\mathbf{J}_{\pi 0}^{(p)}\delta\boldsymbol{\pi}\right) \tag{2.61}$$

which can be rewritten as

$$\rho_0^2 = \operatorname{trace}\left(\mathbf{J}_{\pi 0}^{(p)}E\left(\delta\boldsymbol{\pi}\delta\boldsymbol{\pi}^T\right)\mathbf{J}_{\pi 0}^{(p)T}\right) \tag{2.62}$$

using the identity equation $\delta\mathbf{p}^T\delta\mathbf{p} \equiv \operatorname{trace}(\delta\mathbf{p}\delta\mathbf{p}^T)$. Further, by applying Eq. (2.57) and taking into account that the term $E(\delta\boldsymbol{\pi}\delta\boldsymbol{\pi}^T)$ is the covariance matrix of the geometrical error estimates, i.e., $E(\delta\boldsymbol{\pi}\delta\boldsymbol{\pi}^T) = \operatorname{cov}(\hat{\boldsymbol{\pi}})$, the desired expression can be presented in the final form as

$$\rho_0^2 = \sigma^2 \cdot \operatorname{trace}\left(\mathbf{J}_{\pi 0}^{(p)}\left(\sum_{i=1}^{m}\sum_{j=1}^{n}\mathbf{J}_{\pi i}^{j(p)T}\mathbf{J}_{\pi i}^{j(p)}\right)^{-1}\mathbf{J}_{\pi 0}^{(p)T}\right) \tag{2.63}$$

As follows from this expression, ρ_0^2 can be treated as the weighted trace of the covariance matrix $\operatorname{cov}(\hat{\boldsymbol{\pi}})$, where the weighting coefficients are computed using the test-pose joint coordinates $\mathbf{q}_0$. Hence, the proposed performance measure has obvious advantage compared to the previous ones (see Section 1.4), which operate with "pure" trace of this matrix and involve straightforward summing of its diagonal elements (which may be of different units).

Based on this performance measure, the calibration experiments design can be reduced to the following optimization problem

$$\operatorname{trace}\left(\mathbf{J}_{\pi 0}^{(p)}\left(\sum_{i=1}^{m}\sum_{j=1}^{n}\mathbf{J}_{\pi i}^{j(p)T}\mathbf{J}_{\pi i}^{j(p)}\right)^{-1}\mathbf{J}_{\pi 0}^{(p)T}\right) \to \min_{\{\mathbf{q}_i \dots \mathbf{q}_m\}} \tag{2.64}$$

whose solution gives a set of the desired measurement configurations $\{\mathbf{q}_1,...,\mathbf{q}_m\}$. Hence, in the frame of the proposed approach, the calibration quality (evaluated via the error compensation accuracy ρ_0) is completely defined by the set of Jacobian matrices $\{\mathbf{J}_{\pi 1}^{(p)},...,\mathbf{J}_{\pi m}^{(p)}\}$ that depend on the manipulator configurations $\{\mathbf{q}_1,...,\mathbf{q}_m\}$, while the Jacobian matrix $\mathbf{J}_{\pi 0}^{(p)}$ corresponding the test-pose $\mathbf{q}_0$ defines the weighting coefficients. It is worth mentioning that the conventional approaches based on the A- and T-optimality principles (see Section 1.4) use simplified objective functions where the matrix trace is non-weighted. The efficiency of the proposed approach will be illustrated in the following Subsection (for the case of two-link planar manipulator). In Chapter 4, this approach will be applied to calibration of a 6-dof industrial robot of KUKA family.

2.5.2 Generalization for the case of multiple test configurations

The above presented approach is developed for the accuracy estimation for a single test configuration. However in practice, it is often required to perform machining along rather long and complex trajectories (which is common for aerospace and ship building industries). This type of motions may require significant changes in the manipulator posture and the desired accuracy should be achieved for the whole machining trajectory. For this reason, it is reasonable to extend the test-pose based approach for a more general case, where changes in the manipulator configurations while performing technological task are essential. In this case, the goal of the calibration experiments design is to choose the measurement configurations that minimize the maximum end-effector positioning errors after compensation (evaluated as the root-mean-square distance) for the entire trajectory.

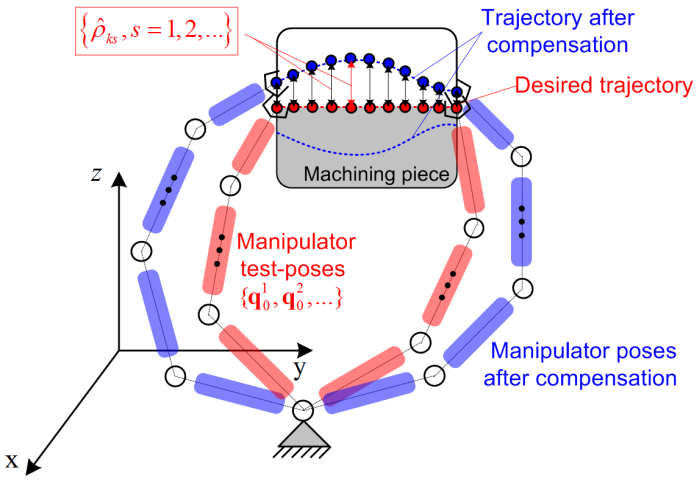

$$\max_s \left\{ E(|\hat{\rho}_{ks}|^2) \right\} \to \min_{\{\mathbf{q}_1,...,\mathbf{q}_m\}}$$

Figure 2.10 Performance measure for selection of measurement configurations that ensure high precision along the given trajectory

This idea is illustrated in Figure 2.10, where the desired trajectory and the trajectory after compensation are presented. It is assumed that the compensation is based on the parameter estimates $\hat{\boldsymbol{\pi}}_k$ obtained using the k-th set of measurement data. The desired trajectory is defined by a set of node points $\{\mathbf{p}_{ds},\ s=1,2,...\}$, corresponding manipulator configurations can be found from $\mathbf{p}_{ds} = g(\mathbf{q}_{0s}, \boldsymbol{\pi}_0)$ via the inverse kinematics. The distances between corresponding points of two trajectories are denoted as $\{\hat{\rho}_{ks},\ k,s=1,2,...\}$. This allows us to define a set of manipulator test-poses $\{\mathbf{q}_{0s},\ s=\overline{1,n_s}\}$ and to introduce the following performance measure

$$\rho_{0\max} = \max_s \left\{ E(|\hat{\rho}_{ks}|^2) \right\} \tag{2.65}$$

that evaluates the highest positioning accuracy along the trajectory. It is clear that this definition perfectly corresponds engineering practice, where the quality of the machining is usually evaluated by the highest machining error.

Definition 4. The *efficiency of manipulator positioning error compensation during machining trajectory* is the maximum root-mean-square distance $\rho_{0\max}$ between the desired manipulator end-effector position and the position obtained after application of the error compensation technique.

Definition 5. The *multiple manipulator test-poses* is a set of particular robot configurations $\{\mathbf{q}_{0s},\ s=1,.2,...\}$ along the machining trajectory, where the desired end-effector positions $\{\mathbf{p}_{ds},\ s=1,2,...\}$ are used as the reference points and for which the highest efficiency of error compensation should be achieved (i.e. $\rho_{0\max}\to\min$).

Using these definitions and applying the technique from Subsection 2.5.1, the generalized performance measure for multiple test configurations can be presented as

$$\rho_{0\max}^2=\sigma^2\cdot\max_s\left\{\operatorname{trace}\left(\mathbf{J}_{\pi 0s}^{(p)}\left(\sum_{i=1}^{m}\sum_{j=1}^{n}\mathbf{J}_{\pi i}^{j(p)T}\mathbf{J}_{\pi i}^{j(p)}\right)^{-1}\mathbf{J}_{\pi 0s}^{(p)T}\right)\right\},\quad s=1,2,... \tag{2.66}$$

where the matrix $\mathbf{J}_{\pi 0s}^{(p)}$ is computed for the test-pose joint coordinates $\mathbf{q}_{0s}$, the superscript "(p)" denotes the positional components of the corresponding matrices, the subscript "$0s$" indicates the s-th test configurations, the subscript "i" and superscript "j" refer to the measurement configuration number and the reference point number. Using this performance measure, the calibration experiment design (i.e., optimal selection of measurement configurations) reduces to the following min-max problem

$$\max_s\left\{\operatorname{trace}\left(\mathbf{J}_{\pi 0s}^{(p)}\left(\sum_{i=1}^{m}\sum_{j=1}^{n}\mathbf{J}_{\pi i}^{j(p)T}\mathbf{J}_{\pi i}^{j(p)}\right)^{-1}\mathbf{J}_{\pi 0s}^{(p)T}\right)\right\}\to\min_{\{\mathbf{q}_1,...,\mathbf{q}_m\}} \tag{2.67}$$

whose solution provides a set of the desired manipulator configurations $\{\mathbf{q}_1,...,\mathbf{q}_m\}$. It is clear that the problem (2.67) is numerically more complicated compared to the previous one (2.64), but it suits better to the notion of machining accuracy studied in this work.

It is also worth mentioning that the performance measure (2.65) can be easily adapted to other applications that differ from the machining. For example, for the pick-and-place operation, where the robot performs its task at two target positions only, two test-poses are enough to achieve the best accuracy after geometric error compensation. Similarly, for machining of large-dimensional workpieces, several reference points can be introduced corresponding to different machining areas. To demonstrate the efficiency of the proposed approach, following subsection contains an illustrative example that deals with experiment design of geometric calibration of 2-dof. manipulator (more complicated examples are presented in Section 2.6 and Chapter 4).

2.5.3 Comparison analysis of proposed and conventional approaches

Let us illustrate the advantages of the test-pose based approach by an example of the geometrical calibration of two-link planar manipulator. It is assumed that the nominal link lengths differ from the real ones, and these deviations should be identified by means of calibration. In this case, the manipulator end-effector position can be expressed as

$$\begin{aligned} p_x &= (l_1 + \Delta l_1)\cos q_1 + (l_2 + \Delta l_2)\cos(q_1 + q_2) \\ p_y &= (l_1 + \Delta l_1)\sin q_1 + (l_2 + \Delta l_2)\sin(q_1 + q_2) \end{aligned} \tag{2.68}$$

where p_x and p_y define the end-effector position, l_1, l_2 and $\Delta l_1, \Delta l_2$ are the nominal link lengths and their deviations (which should be identified), q_1, q_2 are the joint coordinates that define the manipulator configuration. It can be proved that in this case the parameter covariance matrix does not depend on the angles q_{1i} and is expressed as

$$\mathrm{cov}(\Delta\boldsymbol{\pi}) = \frac{\sigma^2}{m^2 - \left(\sum_{i=1}^{m}\cos q_{2i}\right)^2}\begin{bmatrix} m & -\sum_{i=1}^{m}\cos q_{2i} \\ -\sum_{i=1}^{m}\cos q_{2i} & m \end{bmatrix} \tag{2.69}$$

where the vector $\Delta\boldsymbol{\pi} = (\Delta l_1, \Delta l_2)$ denotes the parameters of interest, m is the number of experiments and σ is the s.t.d. of the measurement noise.

For comparison purposes, the plans of experiments have been obtained using three different strategies:

(i) the measurement configurations are generated randomly;

(ii) the measurement configurations are obtained using the conventional approach based on D-optimality principle;

(iii) the measurement configurations are obtained using the proposed test-pose based approach (see Subsection 2.5.1).

For the first approach (i), the measurement configurations are obtained in a trivial way, using random generator scaled within the joint limits. For the conventional approach (ii), where the D-optimality principle was used (that has been proved to be efficient in many applications), the performance measure is equal to the determinant of the covariance matrix (2.69) and can be easily derived as

$$\det\left(\mathrm{cov}(\Delta\boldsymbol{\pi})\right) = \frac{\sigma^2}{m^2 - \left(\sum_{i=1}^{m}\cos q_{2i}\right)^2} \tag{2.70}$$

As follows from this expression, this criterion leads to the minimization of the term $(\sum_{i=1}^{m}\cos q_{2i})^2$. So, the minimum value of the determinant (2.70) is equal to σ^2/m^2 and it is reached when

$$\sum_{i=1}^{m}\cos q_{2i} = 0, \quad i = 1,...,m \tag{2.71}$$

It should be mentioned that this condition is also valid for the application of A- and G-optimality principle.

For the proposed approach (iii), it is assumed that the application of a single test configuration (q_{10}, q_{20}) is considered. In this case, the basic expression for the performance measure ρ_0^2 (2.63) can be presented as

$$\rho_0^2 = 2\sigma^2 \cdot \frac{m - \cos q_{20}\sum_{i=1}^{m}\cos q_{2i}}{m^2 - \left(\sum_{i=1}^{m}\cos q_{2i}\right)^2} \tag{2.72}$$

Hence, the minimum value of ρ_0^2 is equal to

$$\rho^2_{0\min} = \frac{\sigma^2}{m} \cdot \frac{\cos^2 q_{20}}{1-\left|\sin q_{20}\right|} \tag{2.73}$$

and it is achieved when

$$\sum_{i=1}^{m} \cos q_{2i} = m \cdot \frac{1-\left|\sin q_{20}\right|}{\cos q_{20}} \tag{2.74}$$

It should be mentioned that general solution of equation (2.74) for m configurations can be replaced by the decomposition of the whole configuration set by the subsets of 2 and 3 configurations (while providing the same identification accuracy). This essentially reduces computational complexity and allows user to reduce number of different measurement configurations without loss of accuracy.

Using the above presented expressions, the proposed and conventional approaches can be compared analytically and numerically. In particular, the test pose (q_{10}, q_{20}), the conventional approach (ii) ensures the positioning accuracy after compensation $\rho_c^2 = 2\sigma^2/m$, while for the proposed one (iii), similar performance measure is equal to $\rho^2_{0\min} = \sigma^2/m \cdot \cos^2 q_{20} \big/ (1-\left|\sin q_{20}\right|)$. Corresponding values are compared in Table 2.6, which proves that using the proposed approach for the calibration experiment design allows us to improve the positioning accuracy up to 41%.

Table 2.6 Accuracy comparison of the proposed and conventional approaches

Test-pose (q_{20}), [deg]	0°	30°	60°	90°	120°	150°	180°
$\rho_0^2 \,/\, \rho_c^2$	0.5	0.75	0.83	1	0.83	0.75	0.5
Accuracy improvement	41%	15%	10%	0%	10%	15%	41%

To illustrate advantages of the proposed approach, Figure 2.11 presents simulation results for manipulator position errors after compensation corresponding to three different sets of measurement configurations employed in calibration. It is assumed that the manipulator parameters are $l_1 = 1\,\text{m}, l_2 = 0.8\,\text{m}$; the number of measurement configurations $m = 2$; the test configuration is defined by the vector $\mathbf{q}_0 = (-45^\circ, 20^\circ)$, and the s.t.d. of the measurement errors is $\sigma = 1\,\text{mm}$. In accordance with the above presented optimality conditions (see equations (2.71) and (2.74)), the following measurement configurations have been found:

Plan #1: $\mathbf{q}_1 = (0^\circ, -10^\circ)$ and $\mathbf{q}_2 = (0^\circ, 10^\circ)$, which is randomly generated;

Plan #2: $\mathbf{q}_1 = (0^\circ, -90^\circ)$ and $\mathbf{q}_2 = (0^\circ, 90^\circ)$, which satisfies Eq. (2.71);

Plan #3: $\mathbf{q}_1 = (0^\circ, -46^\circ)$ and $\mathbf{q}_2 = (0^\circ, 46^\circ)$, which satisfies Eq. (2.74).

To obtained reliable statistics, the calibration experiments have been repeated 100 times. Corresponding results presented in Figure 2.11 show that the proposed approach allows us to increase accuracy of the end-effector position on average by 18% comparing to the D-optimal plan and by 48% comparing to the randomly generated plan.

In the frame of this example, a more complicated case has been studied when the set of parameters to be calibrated includes both the link length deviations $\{\Delta l_1, \Delta l_2\}$ and the joint offsets $\{\Delta q_1, \Delta q_2\}$. In this case, the calibration was based on three measurements configurations ($m = 3$) and the following plans of experiment have been generated:

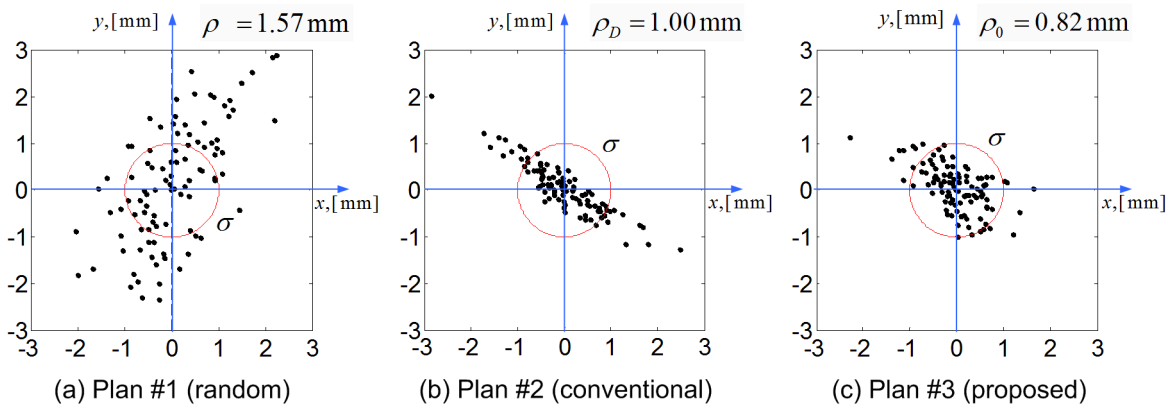

Figure 2.11 Dispersion of manipulator positioning errors after calibration for different plans of experiments: case of tuning two parameters $\{\Delta l_1, \Delta l_2\}$

Plan #1: $\mathbf{q}_1 = (0^\circ, -10^\circ)$, $\mathbf{q}_2 = (0^\circ, 0^\circ)$ and $\mathbf{q}_3 = (0^\circ, 10^\circ)$;

Plan #2: $\mathbf{q}_1 = (0^\circ, -120^\circ)$, $\mathbf{q}_2 = (0^\circ, 0^\circ)$ and $\mathbf{q}_3 = (0^\circ, 120^\circ)$;

Plan #3: $\mathbf{q}_1 = (0^\circ, -57^\circ)$, $\mathbf{q}_2 = (0^\circ, 0^\circ)$ and $\mathbf{q}_3 = (0^\circ, 57^\circ)$.

Simulation results corresponding to this case study are presented in Figure 2.12. As follows from them, the proposed approach allows us to increase the manipulator positioning accuracy by 18% compared to the D-optimal plan and by 56% comparing to the randomly generated plan.

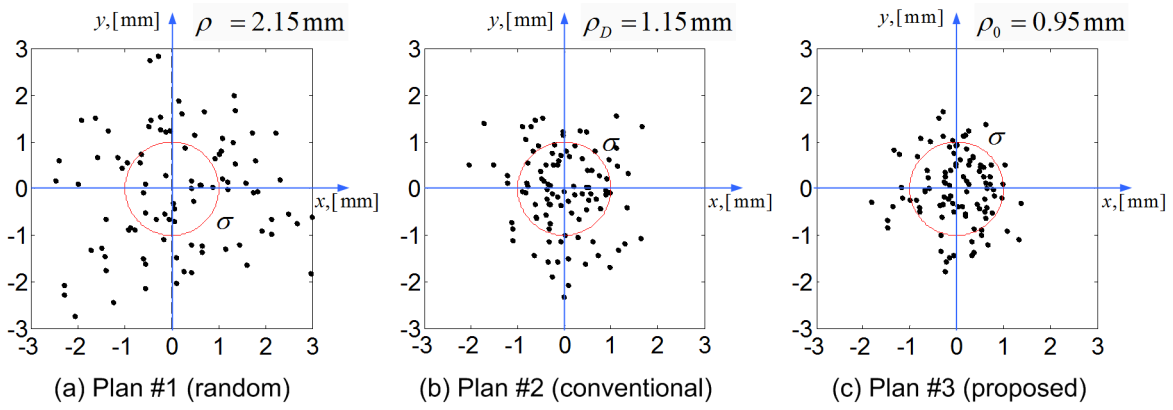

Figure 2.12 Dispersion of manipulator positioning errors after calibration for different plans of experiments: case of tuning four parameters $\{\Delta l_1, \Delta l_2, \Delta q_1, \Delta q_2\}$

Hence, the presented results confirm that the proposed performance measure is attractive for practicing engineers and allows us to avoid the multi-objective optimization problem that arises while minimizing all elements of the covariance matrix (2.57) simultaneously. In addition, using this approach, it is possible to find a balance between the accuracy of different geometrical parameters whose influence on the final robot accuracy is unequal.

Summarizing Section 2.5 in general, it is worth mentioning that the proposed approach allows essential improvement of the calibration efficiency and to achieve the best manipulator positioning accuracy for the user-defined test configurations related to the manufacturing task (in contrast to the conventional approaches that are targeted at the best parameter identification accuracy). However, for typical industrial robots whose model includes very high number of parameters (over 25, see Section 2.2), relevant optimization becomes extremely time consuming. For this reason, the next

Section focuses on the efficiency improvement of the numerical routines employed in the selection of optimal measurement configurations.

2.6 EFFICIENCY IMPROVEMENT OF MEASUREMENT POSE SELECTION

Using the test-pose based approach for calibration experiment design proposed in the previous Section, it is possible to find the optimal set of measurement configurations that ensures the best manipulator end-effector positioning accuracy after calibration. It is clear that analytical solutions of relevant optimization problems (2.64) and (2.67) can hardly be obtained (for example, when the number of parameters to be identified is very high, the analytical computations of the matrix inversion in these expressions are hardly possible). So, applying a numerical optimization technique is the only reasonable way, but the convergence rate, the total computational time and ability to attain the global minimum become key issues. For this reason, several conventional optimization techniques are examined below, where comparison studies are presented. In order to improve their efficiency, two techniques that are adapted to the test-pose based approach have been proposed: (i) application of parallel and hybrid computations; (ii) generation of quasi-optimal solutions using lower-dimensional calibration plans. The following Subsections present detailed presentations of these issues.

2.6.1 Analysis of the conventional numerical optimization techniques

The simplest way to solve the optimization problem (2.64) for the measurement pose selection is to apply conventional optimization techniques incorporated in commercial mathematical software (MathWorks.com). It is clear that the straightforward search with regular grid is non-acceptable because of high complexity and enormous number of solutions to be compared. For this reason, three other algorithms have been examined: (i) random search, (ii) gradient search, and (iii) genetic algorithm. Their comparison study is presented below and summarized in Table 2.7 and Table 2.8, where two criteria have been used: the computational time and the ability to find optimal solution (evaluated via the manipulator accuracy after calibration ρ_0, see Subsection 2.5.1). The computational experiments have been carried out using Matlab optimization toolbox, which was run on a computer with 3.46GHz processor (12MB Cache L2). For all computational experiments, it was assumed that the s.t.d. of the measurement errors is equal to 0.03 mm (which corresponds to the accuracy of the *Leica* laser tracker used in our industrial experiments).

The benchmark example deals with the calibration experiments design for 6-dof industrial manipulator, whose geometric model has been presented in Section 2.2. As follows from relevant Eq.(2.6), this model includes 18 principle geometric parameters as well as 9 parameters corresponding to the base and tool transformations that should be identified via calibration. But for the benchmark example, to reduce the computational efforts and evaluate the algorithm capability before applying to the problem of real dimension, only nine of the most essential parameters were identified (which have major impact on the positioning accuracy). They include the link lengths $\{d_2,...,d_5\}$ whose nominal values are known and the joint offsets $\{\Delta q_1,...,\Delta q_5\}$ (see Figure 2.3). This allowed us to obtain realistic assessments of the conventional optimization techniques capabilities with respect to the considered problem where the number of design variables is very high (72 for 12 measurement configurations).

The first of the examined algorithm (i) is based on the straightforward selection of the best solution from the set of ones generated in a random way. For this study, 10,000 solutions were obtained for different numbers of measurement configurations $m \in \{3,4,6,12\}$. As follows from the

results (see Table 2.7 and Table 2.8), this algorithm is very fast and requires less than 2 minutes to find the best solution. However, the optimal solution provided by this method is essentially worse than those obtained using other algorithms (by 15-30%).

The second algorithm (ii) employs the gradient search with built-in numerical evaluation of the derivatives that is available in Matlab. The starting points were generated randomly and, to avoid convergence to the local minima, the optimization search has been repeated 5000 times (starting from different points). In this case, the best result in terms of the desired objective ρ_0 was obtained, but computational cost was very high (it can reach a hundred hours). So, this technique is hardly acceptable in practice. It is worth mentioning that reduction of the iteration number is rather dangerous here, because there are a number of local minima that the algorithm can converge to (see Table 2.7 that includes the minimum, maximum and average values of ρ_0 obtained for randomly generated starting points). Moreover, as follows from our experience, 5000 iterations are also not enough here.

Table 2.7 Accuracy of conventional optimization techniques (case of 6-dof manipulator, initial points are random)

Algorithm	Performance measure, [mm]	Number of measurement configurations			
		$m=3$	$m=4$	$m=6$	$m=12$
Random Search	$\rho_0^{\min}$	0.0825	0.0607	0.0519	0.0360
	ρ_0^{mean}	1.9155	0.1939	0.0905	0.0500
	$\rho_0^{\max}$	29.8780	14.9746	0.5608	0.0804
Gradient Search	$\rho_0^{\min}$	0.0637	0.0521	0.0426	0.0302
	ρ_0^{mean}	0.0862	0.0610	0.0477	0.0335
	$\rho_0^{\max}$	0.6534	0.2333	0.1319	0.0681
Genetic Algorithm	$\rho_0^{\min}$	0.0638	0.0521	0.0427	0.0301
	ρ_0^{mean}	0.0689	0.0529	0.0433	0.0305
	$\rho_0^{\max}$	0.0802	0.0615	0.0446	0.0309

Table 2.8 Computational time of examined optimization techniques (case of 6-dof manipulator)

Algorithm	Number of measurement configurations			
	$m=3$	$m=4$	$m=6$	$m=12$
Random Search	41 sec	47 sec	1.0 min	1.7 min
Gradient Search	24.2 h	37.5 h	56.3 h	103.6 h
Genetic Algorithm	6.5 h	8.3 h	10.5 h	15.4 h

The third of the examined techniques (iii) applies genetic algorithm (the built-in GA function in Matlab) that is based on adaptive heuristic search. The optimization has been repeated 100 times with population size 50 and 20 generations (initial populations were randomly generated). For illustrative purposes, Figure 2.13 presents the efficiency of this algorithm for selection of three measurement configurations ($m=3$). It shows the algorithm convergence as well as divergence of the optimal

solutions with respect to computing time. As follows from this figure, the optimization results are highly sensitive to the selection of initial population. In particular, the diversity of the optimal solutions got from sequential GA runs is about 25%. So, to achieve the global minimum, the GA should be repeated many times, which leads to essential increase of the computational efforts (more than 6 hours of computations for the considered example). However, compared to gradient search, GA provides acceptable accuracy (only 2% worse) while the computational time is 4 times less.

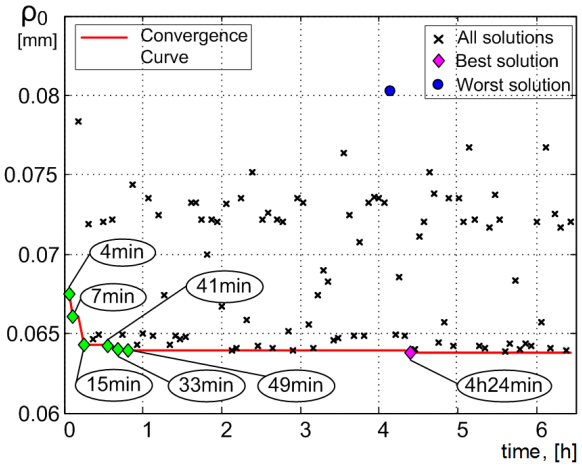

Figure 2.13 Efficiency of genetic algorithm for selection of three measurement poses for 6-dof manipulator (population size 50, generation number 20)

As follows from the obtained results, the random search is rather fast but inefficient here, since it may produce non-acceptable solutions. In contrast, the gradient search is able to find the global minimum provided that it is repeated many times with different starting points (which is very expensive from computational point of view). As a compromise, the genetic algorithm provides intermediate results in terms of accuracy and computational time. However, for problems of the real industrial size, the performances of the GA are also not sufficient. For this reason, the following Subsections are devoted to the improvement of the numerical optimization techniques employed in selection of optimal measurement configurations.

2.6.2 Hybrid approach to optimal configuration selection

Since the considered problem requires numerous repetitions of the optimization with different initial values, applying parallel computing looks attractive to speed up the design process and to take advantage of multi-core architecture available in modern computers. To evaluate benefits of the parallel computing, the same benchmark example has been considered and two algorithms have been examined: (ii)' parallel gradient search, and (iii)' parallel GA with the same parameter settings. The computations were carried out on a workstation with 12 cores (processors with 3.46GHz 12MB Cache L2) The obtained results are presented in Table 2.9, which gives the computational time for different number of measurement poses (the attained value of the objective function ρ_0 is very close to those presented in Table 2.7).

The obtained results are quite expected and confirm essential reduction of computational efforts. For both optimization methods, the consumed time has been decreased by the factor of 10-12 (compared to the results in Table 2.8). However, it is not enough yet to solve the problem of real industrial size, where several dozen of parameters should be identified, instead of nine in the benchmark example.

Table 2.9 Reduction of computational time using parallel computing

Algorithm	Number of measurement configurations			
	$m=3$	$m=4$	$m=6$	$m=12$
Parallel (vs Sequential) Gradient Search	2.1 h (24.2 h)	3.2 h (37.5 h)	4.9 h (56.3 h)	8.9 h (103.6 h)
Parallel (vs Sequential) Genetic Algorithm	36 min (6.5 h)	41 min (8.3 h)	52 min (10.5 h)	1.5 h (15.4 h)

To take the advantages of both examined algorithms (the gradient search and GA) and efficiency of the parallel implementation, a hybrid technique has been developed. It should be mentioned that some software packages (Matlab, etc.) already implement this idea and use the final solution from GA as the initial point of gradient search. However, since the randomly generated initial populations in GA may cause high diversity of the optimal solutions, the selection of these initial values is also an important issue. For this reason, the embedded hybrid option in GA cannot be directly used and requires additional modifications. To improve the efficiency of the existing technique, the starting point selection strategy for the gradient search has been modified. To ensure better convergence to the global minimum, it has been proposed to use the best half of final points obtained from GA as the starting points for the gradient search. From our point of view, it ensures better diversity of the starting points and allows us to avoid convergence to the local minima.

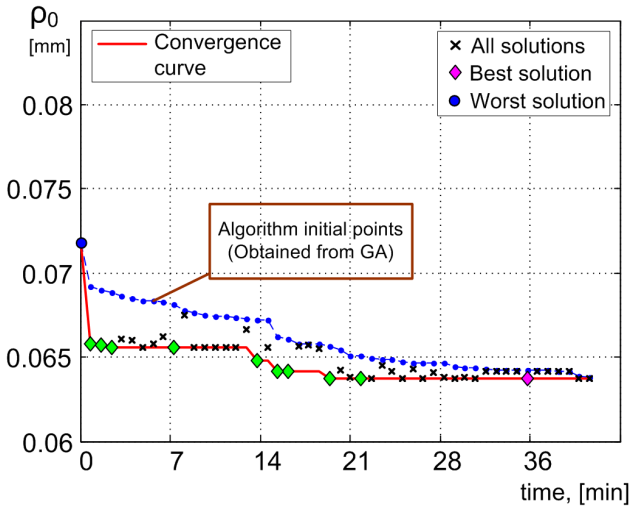

Figure 2.14 Efficiency of the hybrid approach for selection of three measurement poses for 6-dof manipulator (combination of parallel gradient search and parallel genetic algorithm)

The proposed modification has been evaluated using the same benchmark example. For comparison purposes, Figure 2.14 presents the convergence of the hybrid method for the problem of optimal selection of three measurement configurations studied in the previous Subsection (see Figure 2.13). It shows the initial points (obtained from GA), optimal solutions as well as the solution improvement with respect to time. As follows from the figure, the hybrid algorithm converges much faster (computing time is less than 2 min for $m=3$), but if the number of measurement poses is increased up to 12, the computational time is over 1.6 hour that is still unacceptable for industrial problems.

2.6.3 Quasi-optimal solution for measurement configuration selection

Generally, as follows from the identification theory, the only way to improve calibration accuracy is to increase the number of measurements (provided that the reduction of the measurement errors is not possible). However, for the manipulator calibration problem, each measurement is associated with a certain robot configuration that also has influence on the final accuracy. It is clear that the best result is achieved if all measurement poses are different and have been optimized during the calibration experiment design. On the other hand, as follows from our experiences, the diversity of the measurement poses does not contribute significantly to the accuracy improvement if m (the total number of measurements) is high enough. This allows us to propose an alternative technique, which uses the same measurement configurations several times (allowing to simplify and speed up the measurements). This approach can be also referred to as the "reduction of problem dimension".

To explain the proposed approach in more details, let us assume that the problem of the optimal pose selection has been solved for the number of different configurations that is equal to m, and the obtained calibration plan ensures the positioning accuracy ρ_0^m. Using these notations, let us evaluate the calibration accuracy for two alternative strategies that employ total number of experiments $k \times m$:

Strategy #1 (*conventional*): the measurement configurations are found from the full-scale optimization of size $k \times m$.

Strategy #2 (*proposed*): the measurement configurations are obtained by simple repetition of the configurations got from the low-dimensional optimization problem of size m (i.e. at each configuration, the measurements are repeated k times).

It is clear that the calibration accuracy ρ_0^{km} for the strategy #1 is better than the accuracy corresponding to the strategy #2 that can be expressed as $\rho_0^m / \sqrt{k}$. However, as follows from our study, this difference is quite small if the total number of measurements is high enough ($km = 12$, in this case), while the number of different configurations m is larger than 3. This allows us to essentially reduce the size of optimization problem employed in the optimal selection of measurement poses without significant impact on the positioning accuracy.

To demonstrate the validity of the proposed approach, the benchmark example from Subsection 2.6.1 has been solved using the strategies #1 and #2, assuming that the total number of measurements is equal to 12 (i.e. using different factorizations such as 12×1, 6×2, 4×3, 3×4). Relevant results are presented in Table 2.10 and Figure 2.15, where the first lines of the table give the accuracy ρ_0 and the last line shows the computational time. As follows from them, the factorization 12×1, where all measurement poses are different, is only 6% better comparing to the factorization 3×4 where measurements are repeated 4 times in 3 different configurations. At the same time, the factorizations 6×2 and 4×3 give almost the same results as the factorization 12×1. On the other hand, the computational time of the optimal pose generation for $m = 3$ is much lower than for $m = 12$. Hence, as follows from these results, repeating experiments with optimal plans obtained for the lower number of configurations provides almost the same performance as "full-dimensional" optimal plan. Obviously, this reduction of the measurement pose number is very attractive from an engineering viewpoint. This technique will be used for the selection of optimal measurement configurations in the following chapters.

Table 2.10 Efficiency of the quasi-optimal solutions (evaluated via ρ_0) for calibration experiment design problem: case of a 6-dof manipulator, repetitions of measurements

Number of measurements	Accuracy [mm]	Number of different configurations			
		$m=3$	$m=4$	$m=6$	$m=12$
$km=3$	$\rho_0^{\min}$	0.0637 (3×1)			
$km=4$	$\rho_0^{\min}$		0.0521 (4×1)		
$km=6$	$\rho_0^{\min}$	0.0450 (3×2)		0.0426 (6×1)	
$km=12$	$\rho_0^{\min}$	0.0319 (3×4)	0.0301 (4×3)	0.0301 (6×2)	0.0301 (12×1)
Computational time		38min	45min	56min	1.6h

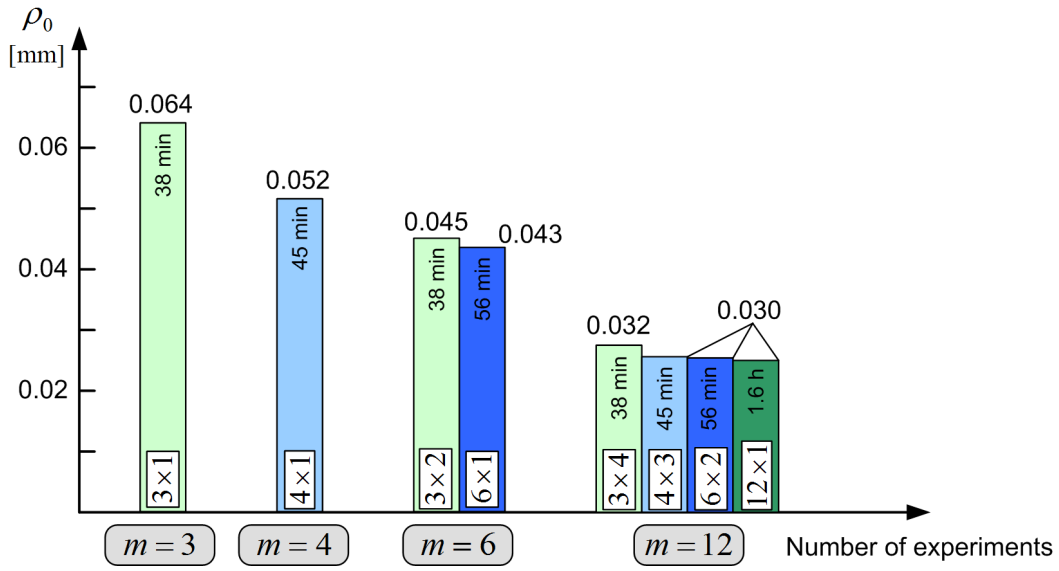

Figure 2.15 Comparison of quasi-optimal and optimal solutions for selection of measurement configurations for robot calibration

Summarizing Section 2.6, it can be concluded that the proposed enhancements of the dedicated numerical routines allows us to improve essentially the efficiency of the measurement pose selection procedure for calibration. In particular, the application of parallel and hybrid approaches significantly reduce the computational time (by the factor of 65 for the considered benchmark example). However, the most essential result has been achieved by replacing the strictly optimal solutions by quasi-optimal ones, obtained by simple repetition of measurement configurations corresponding to the lower-dimensional case. For instance, repeating three times the configurations obtained for $m=4$ leads to the accuracy loss by 0.32% only comparing to the optimal solution for $m=12$ (while the computational time reduces more than twice). This idea gives us very efficient way of simplification of the measurement pose selection procedure, which is attractive for practice engineers.

2.7 SUMMARY

The chapter is devoted to the enhancement of measurement and optimization techniques employed in geometric calibration of serial industrial robots. The main contributions are in the area of calibration experiments design, i.e. selection of the optimal measurement configurations. In contrast to other works, the developed approach is based on a new industry-oriented performance measure, which evaluates the robot positioning accuracy after geometric error compensation.

In more details, the contributions of Chapter 2 can be formulated as follows

(i) Enhanced partial pose measurement method that allows us to increase the identification accuracy and to avoid straightforward computation of the manipulator end-effector orientation, which causes the non-homogeneity in relevant performance measure used for the identification and corresponding numerical difficulties.

(ii) New approach for the calibration experiment design that employs a new industry-oriented performance measure, which evaluates the quality of calibration plan via the manipulator positioning accuracy after errors compensation, and takes into account the industrial requirements of the prescribed manufacturing task (using one or several test-poses).

(iii) Efficient measurement poses selection technique that is based on the reduction of the relevant optimization problem dimension (and replication of the measurement poses) and computation of the optimal measurement configurations using parallel and hybrid algorithms, which allow us to decrease the computational time while achieving the desired accuracy.

The main results of Chapter 2 have been presented in international conferences (Klimchik et al., 2013f), (Klimchik et al., 2012b), (Wu et al., 2013b) (Klimchik et al., 2011),(Wu et al., 2013a), and have been submitted to international journal (Klimchik et al., 2013g).

It should be mentioned that the developed techniques can be generalized for the case of elastostatic calibration. However, some modifications are required to take into account the differences in corresponding manipulator models and experimental setup. These issues will be considered in Chapter 3.

CHAPTER 3

DESIGN OF EXPERIMENTS FOR CALIBRATION OF MANIPULATOR ELASTOSTATIC PARAMETERS

3.1 Introduction 91
3.2 Manipulator elastostatic modeling 93
3.2.1 Stiffness modeling background 93
3.2.2 Stiffness model suitable for calibration 96
3.3 Measurement methods for elastostatic calibration 99
3.3.1 Conventional measurement methods 99
3.3.2 Enhanced partial pose measurement method in elastostatic calibration 102
3.4 Identification of elastostatic parameters 106
3.4.1 Identification algorithm for the enhanced partial pose method 106
3.4.2 Influence of the measurement errors on the identification accuracy 109
3.4.3 Weighted least square technique for elastostatic calibration 110
3.5 Optimal selection of measurement configurations 112
3.5.1 Extension of the test-pose based approach for elastostatic calibration 112
3.5.2 Generalization for the case of multiple test configurations 115
3.5.3 Evaluation of the test-pose based approach for elastostatic calibration 116
3.5.4 Efficiency improvement of measurement pose selection 119
3.6 Elastostatic calibration for heavy industrial robots with gravity compensators 121
3.6.1 Mechanics of gravity compensator 122
3.6.2 Identification of gravity compensator geometric parameters 123
3.6.3 Identification of gravity compensator elastostatic parameters 128
3.7 Summary 132

This chapter focuses on the design of experiments for calibration of manipulator elastostatic parameters. Particular attention is paid to the enhancement of modeling, measurement and identification methods employed in the elastostatic calibration of heavy industrial robot of serial architecture, taking into account the particularity of the close-loop chain created by the gravity compensator. It presents the enhanced partial pose measurement method for the case of elastostatic calibration and applies the weighted least square technique for corresponding parameter identification. In this Chapter, the proposed performance measure is extended for the case of optimal measurement configurations selection in elastostatic calibration experiments. In contrast to previous works, the developed manipulator stiffness model is able to take into account the impact of the gravity compensator.

3.1 INTRODUCTION

In robotic-based machining, the manipulators are required to perform certain tasks, where essential forces are applied to the end-effector, and create non-negligible deformations in links and joints. As follows from our experiences, these deformations may be responsible for over 90% of the end-effector positioning errors in machining applications. Usually, these errors can be compensated by adjusting the controller input program (describing the target trajectory), which requires knowledge of exact values of the elastostatic parameters. In contrast to geometric parameters, the elastostatic ones are usually not provided by robot manufacturers. Therefore, the only way is to identify them from experiments, either virtual experiments in CAD environment or real experiments in robotic work-cell. It should be noted that the accuracy of the identified parameters highly depends on the precision of measurement system and the *set of robot configurations used for calibration*, which consequently affects the quality of the machining process. This Chapter focuses on the robotic manipulator accuracy improvement via optimization of measurement configurations used in elastostatic calibration.

The problem of elastostatic calibration has increasingly attracted attention of robot experts in the last decades (Duelen and Schröer, 1991; Gong et al., 2000). In the early studies, it was claimed that the non-geometric errors are responsible for only 10% of total positioning inaccuracy (Renders et al., 1991). Later, it was discovered by several researchers that the compliance errors have major impacts on the robot accuracy in the case when the external loadings are essential (Meggiolaro et al., 2005). Since then, many approaches have been developed for calibration of elastostatic parameters that differ in modeling methods, measurement setups and application areas (see Section 1.4). There are also several works devoted to simultaneous calibration of both geometric and non-geometric parameters, where extended models have been proposed to include different error sources such as gear transmission backlash, thermal expansion, etc (Gong et al., 2000; Judd and Knasinski, 1990; Renders et al., 1991). Similar to geometric parameters, the elastostatic ones are also assumed to be constant and do not vary with the robot configurations. However, the Cartesian stiffness matrix, which influences the end-effector positioning accuracy under the loadings, highly depends on the robot poses.

In the majority of related works devoted to manipulator elastostatic calibration, the measurement configurations have been determined either randomly or were regularly spread in the robot workspace. To our knowledge, only a single work addressed the problem of measurement configuration selection for elastostatic calibration, using some intuitive approaches based on manipulator kinematic performance (Dumas et al., 2012). However, it is not evident that the kinematic criteria are able to provide the optimal measurement configurations for elastostatic calibration, which provide the desired positioning accuracy. For this reason, this problem requires additional study, where the particularities of elastostatic model must be taken into account.

It should be mentioned that elastostatic calibration differs from the geometric ones in many aspects. Therefore, relevant calibration procedure introduced in Chapter 2 should be revised. The modified procedure includes five steps, which are schematically presented in Figure 3.1 and briefly described below.

S1: The first step (*modeling*) is aimed at developing suitable (i.e. complete and non-redundant) stiffness model for elastostatic calibration and extended geometric model, which properly describe the manipulator elastostatic properties and the end-effector deflections.

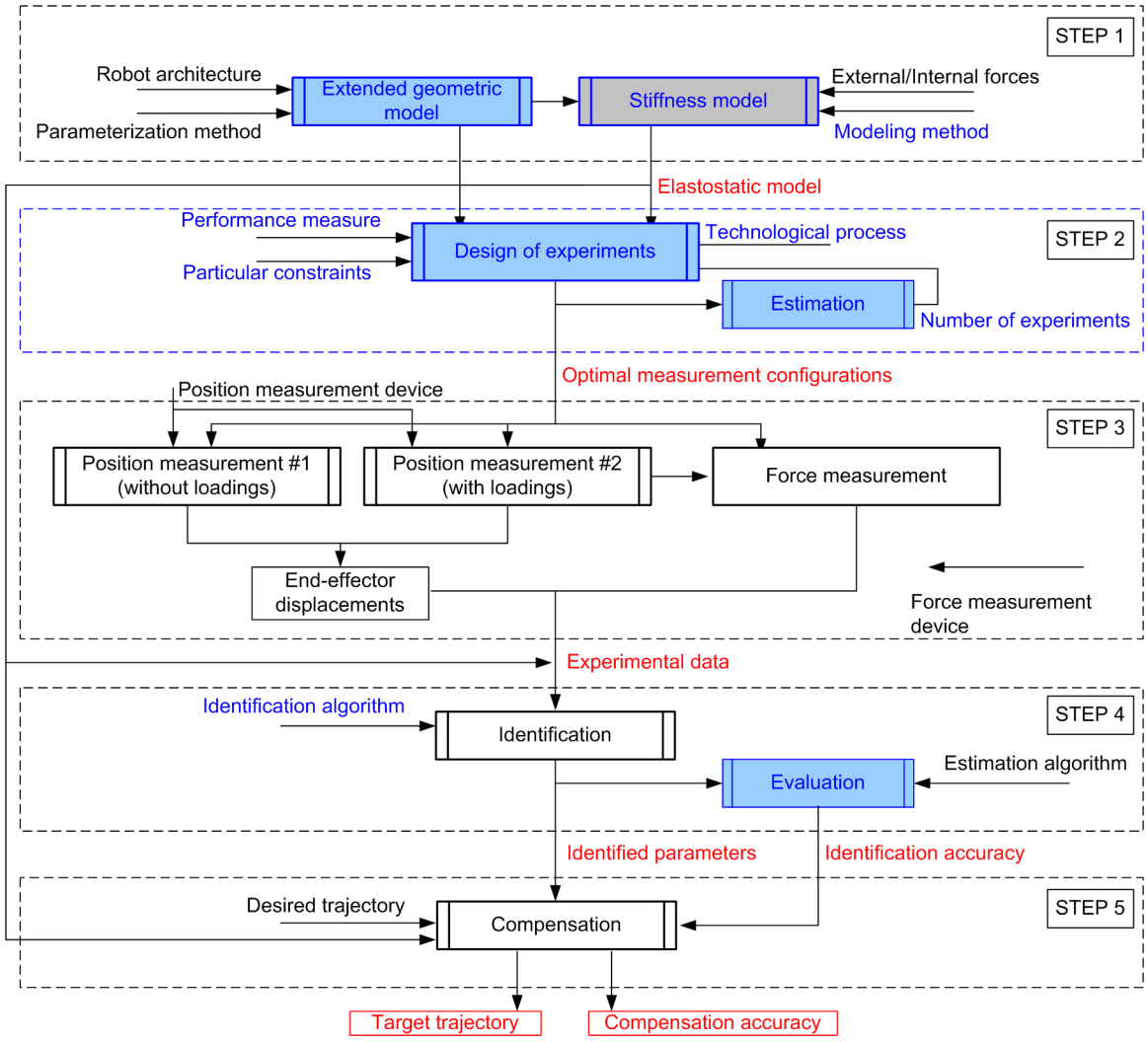

Figure 3.1 Schematics of robot elastostatic calibration procedure

S2: The second step (*design of experiments)* is aimed at choosing optimal measurement configurations and corresponding external forces causing elastostatic deflections. It should rely on an appropriate performance measure, which takes into account specificities of the technological process. and work-cell geometric and physical constraints. The primary goal here is to achieve the desired positioning accuracy using minimum number of calibration experiments (for given statistical properties of the measurement noise).

S3: The third step (*measurement)* deals with carrying out calibration experiments using the obtained configurations. In contrast to geometric calibration, here the end-effector position should be measured twice for each robot configuration: before and after applying the loading. The required end-effector displacements are computed as their difference. In addition, the applied loadings should be measured using the force sensor. The output of this step is the set of the end-effector deflections and corresponding loadings.

S4: At the fourth step (*identification)*, the desired elastostatic parameters are computed using extended geometric and elastostatic models, measured deflections and forces, and proper identification algorithm. At this step, the identification accuracy for the model parameters as well as the expected positioning accuracy are also evaluated.

S5: At the last step (*implementation*), the elastostatic errors are compensated by adjusting the controller input program (describing the target trajectory) using the identified parameters. Here, the on-line compensation strategy is hardly applicable since it is usually impossible to integrate the manipulator elastostatic model in industrial robot controller.

As follows from the detailed literature analysis presented in Section 1.4, there are still a number of open questions in elastostatic calibration that require further investigation. Among them, there is a problem of *enhancement of elastostatic calibration techniques by means of the design of experiments,* which is the goal of this Chapter. It is clear that some results presented in Chapter 2 can be adapted for elastostatic calibration. So, particular problems to be addressed here can be specified as follows

(i) Extension of the test-pose based approach and corresponding performance measure for elastostatic calibration experiment design, which allows achieving the highest positioning accuracy after compliance errors compensation.

(ii) Adapting the developed measurement pose selection technique, enhanced partial pose measurement method and corresponding identification algorithm to the case of elastostatic calibration.

(iii) Development of methodology for modeling and elastostatic calibration of heavy industrial robots with gravity compensators.

To address these problems, the remainder of the chapter is organized as follows: Section 3.2 presents a suitable manipulator elastostatic model for calibration proposes. In Section 3.3, the enhanced partial pose measurement method is extended for the elastostatic case. Section 3.4 focuses on identification algorithms for manipulator elastostatic parameters (which employs the weighted square technique). Section 3.5 deals with optimal selection of measurement poses for elastostatic calibration based on an extension of the proposed test-pose approach. In Section 3.6, a new approach is developed for calibration of heavy industrial robots with gravity compensator. Finally, Section 3.7 summarizes the main results and contributions of this chapter.

3.2 MANIPULATOR ELASTOSTATIC MODELING

As follows from the literature review presented in Section 1.3, the virtual joint method (VJM) is the most attractive method for manipulator stiffness modeling (Chen and Kao, 2000; Majou et al., 2007; Quennouelle, 2009). In the frame of this approach, there has been proposed several alternative techniques for manipulator stiffness modeling that differ in number of parameters and dimensions of virtual springs describing the link/joint elastostatic properties (Gosselin and Zhang, 2002; Pashkevich et al., 2009a; Zhang, 2000). This Section presents the stiffness modeling background for a general serial manipulator, justifies the utilization of one-dimensional springs for milling robots and focuses on the identifiability issues.

3.2.1 Stiffness modeling background

Let us consider the *elastostatic model* of a general serial manipulator, which consists of a fixed "Base", a serial chain of flexible "Links", a number of flexible actuated joints "Ac" and an "End-effector" (Figure 3.2). In this work, it is assumed that all links are separated by either rotational or translational joints. Such architecture can be found in most of industrial serial robots.

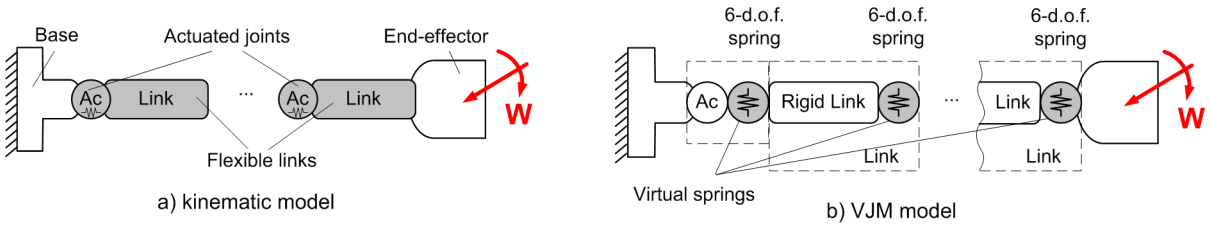

Figure 3.2 Serial manipulator and its VJM-based elastostatic model

To evaluate the stiffness of the considered manipulator, let us apply the virtual joint method (Gosselin, 1990), which is based on the lump modeling approach. According to this approach, the original rigid model should be extended by adding virtual joints (localized springs), which describe elastic deformations of the links. Besides, virtual springs are included in the actuated joints, in order to take into account the stiffness of the transmission and control loop. Under these assumptions, the kinematic chain can be described by the following serial architecture (Pashkevich et al., 2009a):

(a) a rigid link between the manipulator base and the first actuated joint described by the constant homogeneous transformation matrix $\mathbf{T}_{\text{Base}}$;

(b) several flexible actuated joints described by the homogeneous matrix function $\mathbf{T}^{j}_{\text{Joint}}(q^{j}+\theta^{j}_{\text{Ac}})$, which depends on the actuated joint variable q^{j} and the virtual joint variable θ^{j}_{Ac} that takes into account the joint compliances;

(c) a set of rigid links, which are described by the constant homogeneous transformation matrices $\mathbf{T}^{j}_{\text{Link}}$;

(d) a set of 6-d.o.f. virtual joints that take into account the link flexibility and are described by the homogeneous matrix function $\mathbf{T}_{\text{VJM}}(\boldsymbol{\theta}^{j}_{\text{Link}})$ which depends on the virtual joint variables $\boldsymbol{\theta}^{j}_{\text{Link}}=(\theta^{j}_{\text{x}},\theta^{j}_{\text{y}},\theta^{j}_{\text{z}},\theta^{j}_{\varphi\text{x}},\theta^{j}_{\varphi\text{y}},\theta^{j}_{\varphi\text{z}})$ corresponding to the translation/rotation deflections in/around the axes x, y, z;

(e) a rigid link from the last joint to the end-effector, described by the constant homogeneous matrix transformation $\mathbf{T}_{\text{Tool}}$.

In the frame of these notations, the extended kinematic expression defining the end-effector location subject to variations of all joint coordinates can be described as a sequence of homogeneous transformations

$$\mathbf{T}=\mathbf{T}_{\text{Base}}\cdot\left[\mathbf{T}_{\text{Joint}}(q^{1}+\theta^{1}_{\text{Ac}})\cdot\mathbf{T}^{1}_{\text{Link}}\cdot\mathbf{T}_{\text{VJM}}(\boldsymbol{\theta}^{1}_{\text{Link}})\right]\cdot\ldots\cdot\left[\mathbf{T}_{\text{Joint}}(q^{n}+\theta^{n}_{\text{Ac}})\cdot\mathbf{T}^{n}_{\text{Link}}\cdot\mathbf{T}_{\text{VJM}}(\boldsymbol{\theta}^{n}_{\text{Link}})\right]\cdot\mathbf{T}_{\text{Tool}} \quad (3.1)$$

where n is the number of links/joints, and the components $\mathbf{T}_{\text{Base}}$, $\mathbf{T}^{j}_{\text{Joint}}(.)$, $\mathbf{T}^{j}_{\text{Link}}$, $\mathbf{T}^{j}_{\text{VJM}}(.)$ and $\mathbf{T}_{\text{Tool}}$ may be factorized with respect to the terms including the joint variables (in order to simplify the computation of the derivatives). It should be mentioned that here the transformation matrices $\mathbf{T}_{\text{Base}}$, $\mathbf{T}^{j}_{\text{Link}}$ and $\mathbf{T}_{\text{Tool}}$ are treated as knowns and they depend on the geometric parameters $\boldsymbol{\pi}_{\text{Base}}$, $\boldsymbol{\pi}_{\text{Link}}$, $\boldsymbol{\pi}_{\text{Tool}}$ that have been already calibrated (see Chapter 2).

Using this expression, the manipulator end-effector location $\mathbf{t}=(\mathbf{p},\boldsymbol{\varphi})^{T}$ (position $\mathbf{p}=(p_x,p_y,p_z)^{T}$ and orientation $\boldsymbol{\varphi}=(\varphi_{\text{x}},\varphi_{\text{y}},\varphi_{\text{z}})^{T}$) can be extracted from the homogeneous matrix $\mathbf{T}$ using the technique proposed in (Pashkevich et al., 2009a) and described as

$$\mathbf{t}=g(\mathbf{q},\boldsymbol{\theta}) \quad (3.2)$$

where the function $g(.)$ defines the manipulator *extended geometric model*, including the vector $\mathbf{q}=(q_1,q_2,\ldots,q_{\text{n}})^{T}$ that aggregates all actuated coordinates, and the vector $\boldsymbol{\theta}=(\theta_1,\theta_2,\ldots,\theta_{\text{n}\theta})^{T}$ that

collects all virtual joint coordinates, n_θ is the total number of the virtual joints. It should be noted that here the values of coordinates $\mathbf{q}$ are completely defined by the robot controller, while the values of virtual joint coordinates $\boldsymbol{\theta}$ depend on the external loading $\mathbf{w}$ applied at the robot end-effector.

To take into account manipulator stiffness properties, let us assume that variations in the virtual joint variables $\boldsymbol{\theta}$ generate the reaction forces/torques applied to the corresponding links that are evaluated by the following linear equation (that can be treated as a generalized Hooke's law for the manipulator in virtual joint space)

$$\boldsymbol{\tau}_\theta = \mathbf{K}_\theta \cdot \boldsymbol{\theta} \tag{3.3}$$

where the vector $\boldsymbol{\tau}_\theta = (\tau_\theta^{(1)}, \tau_\theta^{(2)}, ..., \tau_\theta^{(n\theta)})^T$ aggregates the virtual joint reactions, $\mathbf{K}_\theta = diag(\mathbf{K}_\theta^{(1)}, \mathbf{K}_\theta^{(2)}, ..., \mathbf{K}_\theta^{(n\theta)})$ is the aggregated virtual spring stiffness matrix, and $\mathbf{K}_\theta^{(i)}$ is the spring stiffness matrix of the corresponding link/joint. It should be noted that the size of this matrix varies with the dimension of corresponding virtual springs, usually, 1×1 for joint stiffness and 6×6 for link stiffness.

Further, let us apply the principle of virtual work assuming that the joints are given small, arbitrary virtual displacements $\Delta\boldsymbol{\theta}$ in the equilibrium neighbourhood. Then, the virtual work of the external wrench $\mathbf{w}$ applied to the end-effector along the corresponding displacement $\Delta\mathbf{t}$ is equal to

$$\delta w = (\mathbf{w}^T \cdot \mathbf{J}_\theta) \cdot \Delta\boldsymbol{\theta} \tag{3.4}$$

where $\mathbf{J}_\theta = \partial g(\mathbf{q},\boldsymbol{\theta}) / \partial\boldsymbol{\theta}$ is the Jacobian with respect to the virtual joints $\boldsymbol{\theta}$, which can be computed analytically or semi-analytically, using the factorization technique presented in Section 2.2. On the other hand, for the internal forces $\boldsymbol{\tau}_\theta$, the virtual work is equal to

$$\delta w = -\boldsymbol{\tau}_\theta^{\,T} \cdot \Delta\boldsymbol{\theta} \tag{3.5}$$

Therefore, since in the static equilibrium the total virtual work is equal to zero for any virtual displacement, the equilibrium conditions can be derived as

$$\boldsymbol{\tau}_\theta = \mathbf{J}_\theta^{\,T} \cdot \mathbf{w} \tag{3.6}$$

This gives additional expressions describing the force/torque propagation from the joints to the end-effector that should be considered simultaneously with the extended geometric equation (3.2).

Combining the virtual joint reaction equation (3.3), the equilibrium condition (3.6) and the linearized geometric model $\Delta\mathbf{t} = \mathbf{J}_\theta \cdot \boldsymbol{\theta}$, it is possible to write static equations

$$\Delta\mathbf{t} = \mathbf{J}_\theta \cdot \boldsymbol{\theta}; \qquad \mathbf{J}_\theta^{\,T} \cdot \mathbf{w} - \mathbf{K}_\theta \cdot \boldsymbol{\theta} = 0 \tag{3.7}$$

describing elastostatic properties of the considered manipulator. In these equations, the end-effector displacement $\Delta\mathbf{t}$ is treated as the model input and the external wrench $\mathbf{w}$ is the model output, which corresponds to the representation of the manipulator stiffness matrix in the following form

$$\mathbf{w} = \mathbf{K}_C \cdot \Delta\mathbf{t} \tag{3.8}$$

where $\mathbf{K}_C$ is the desired Cartesian stiffness matrix of the considered manipulator for given robot configuration $\mathbf{q}$. To find this matrix, equation (3.7) can be presented in the matrix form

$$\begin{bmatrix} \mathbf{0} & \mathbf{J}_\theta \\ \mathbf{J}_\theta^{\,T} & -\mathbf{K}_\theta \end{bmatrix} \cdot \begin{bmatrix} \mathbf{w} \\ \boldsymbol{\theta} \end{bmatrix} = \begin{bmatrix} \Delta\mathbf{t} \\ \mathbf{0} \end{bmatrix} \tag{3.9}$$

Solving this system of equations for $\mathbf{w}$, yields the following force-deflection relation

$$\Delta\mathbf{t} = \mathbf{J}_\theta \cdot \mathbf{K}_\theta^{-1} \cdot \mathbf{J}_\theta^{\,T} \cdot \mathbf{w} \tag{3.10}$$

that allows us to express the manipulator Cartesian stiffness matrix as

$$\mathbf{K}_{\mathrm{C}} = \left(\mathbf{J}_{\theta} \cdot \mathbf{K}_{\theta}^{-1} \cdot \mathbf{J}_{\theta}^{T} \right)^{-1} \tag{3.11}$$

where the matrix $\mathbf{K}_{\theta}^{-1}$ is usually denoted as $\mathbf{k}_{\theta}$ and so-called the compliance matrix.

In engineering practice, the Cartesian stiffness matrix $\mathbf{K}_{\mathrm{C}}$ is treated as the most detailed description of manipulator elastostatic properties at given workspace point, but it varies from one configuration to another. To compute this matrix, it is required to have the manipulator elastostatic parameters $\mathbf{k}_{\theta}$ that should be identified via relevant calibration experiments. It should be mentioned that that force-deflection relation (3.10) is not yet suitable for identification of the elastostatic parameters. Therefore, the following Subsection focuses on driving stiffness model suitable for calibration.

3.2.2 Stiffness model suitable for calibration

Similar to the geometric calibration, suitability of the stiffness model for the elastostatic calibration is related to the notions of completeness and irreducibility. Here, to be complete, the model should contain a sufficient number of the elastostatic parameters that are able to describe all possible end-effector deflections caused by the external loadings. The irreducibility means that the model includes a minimum set of independent parameters that ensures its completeness. To obtain the desired stiffness model that satisfy these two requirements, the corresponding force-deflection relation (3.10) should be presented in a more convenient form and should be analyzed using the algebraic tools developed for geometric calibration (see Section 2.2). First, let us address this problem in the general case, assuming that both the link and joint stiffness are essential.

To estimate the desired matrices describing the elasticity of the manipulator components (i.e., compliances of the virtual springs presented in Figure 3.2), the corresponding elastostatic model (3.8) should be rewritten as

$$\Delta \mathbf{t} = \sum\nolimits_{i=1}^{n} \left(\mathbf{J}_{\theta}^{(\mathrm{i})} \cdot \mathbf{k}_{\theta}^{(\mathrm{i})} \cdot \mathbf{J}_{\theta}^{(\mathrm{i})T} \right) \cdot \mathbf{w} \tag{3.12}$$

where $\Delta \mathbf{t}$ is the vector of the end-effector deflection under the loading $\mathbf{w}$, the matrices $\mathbf{k}_{\theta}^{(\mathrm{i})}$ denote the link/joint compliances that should be identified via calibration experiments, and the matrices $\mathbf{J}_{\theta}^{(\mathrm{i})}$ are corresponding sub-Jacobians obtained by fractioning of the aggregated Jacobian $\mathbf{J}_{\theta} = [\mathbf{J}_{\theta}^{(1)}, \mathbf{J}_{\theta}^{(2)}, ...]$. Further, to be in agreement with conventional identification techniques, the model (3.12) should be presented as a linear function with respect to the desired parameters (i.e., the elements of the matrices $\mathbf{k}_{\theta}^{(\mathrm{i})}$), which are convenient to collect in a single vector $\mathbf{k} = (k_{\theta,1}, k_{\theta,2}, ... k_{\theta,\mathrm{n}\theta})^{T}$. This yields the following expression

$$\Delta \mathbf{t} = \mathbf{A}_{k}(\mathbf{q}, \mathbf{w}) \cdot \mathbf{k} \tag{3.13}$$

where $\mathbf{A}_{k}(.)$ is so-called observation matrix that defines the mapping between the unknown compliance vector $\mathbf{k}$ and the end-effector deflections $\Delta \mathbf{t}$ under the loading $\mathbf{w}$ for the manipulator configuration $\mathbf{q}$. It can be proved that the matrix $\mathbf{A}_{k}$ can be expressed via the columns of the Jacobian $\mathbf{J}_{\theta}$ and the external wrench $\mathbf{w}$ in the following way

$$\mathbf{A}_{k} = \left[\mathbf{J}_{\theta,1} \mathbf{J}_{\theta,1}^{T} \mathbf{w}, \ \ldots, \mathbf{J}_{\theta,i} \mathbf{J}_{\theta,i}^{T} \mathbf{w}, \ldots, \mathbf{J}_{\theta,\mathrm{n}\theta} \mathbf{J}_{\theta,\mathrm{n}\theta}^{T} \mathbf{w} \right] \tag{3.14}$$

where $\mathbf{J}_{\theta,i}$ is the i-th column vector of the aggregated Jacobian matrix.

In practice, to estimate the manipulator elastostatic parameters, the user must carry out sufficient number of experiments that provide sets of input variables $\{\mathbf{q}_i, \mathbf{w}_i, i = \overline{1,m}\}$ and output

variables $\{\Delta\mathbf{t}_i, i=\overline{1,m}\}$. Corresponding system of identification equations can be presented in an aggregated form as

$$\Delta\mathbf{t}_a = \mathbf{A}_{ka}\cdot\mathbf{k} \tag{3.15}$$

where the vector $\Delta\mathbf{t}_a = (\Delta\mathbf{t}_1, \Delta\mathbf{t}_2, ..., \Delta\mathbf{t}_m)^T$ collects the end-effector deflections of all experiments, $\mathbf{A}_{ka} = \left[\mathbf{A}_{k1};\ \mathbf{A}_{k2}; ...; \mathbf{A}_{km}\right]$ denotes the aggregated observation matrix, m is the number of experiments, and the subscript 'a' is referred to the operation of aggregation. To be suitable for the identification, the system of equations (3.15) should be non-singular, i.e., the rank of the matrix $\mathbf{A}_{ka}$ should be equal to the number of parameters to be identified n_θ. This condition may be satisfied only when the manipulator elastostatic model is irreducible and number of measurement configurations is high enough. If the stiffness model includes redundant parameters, i.e., $rank(\mathbf{A}_{ka}) < n_\theta$, it is possible to apply the model reduction technique presented in geometric modeling part of this work (see Sections 1.2 and 2.2), but the matrix $\mathbf{A}_{ka}$ should be used for the analysis instead of the aggregated Jacobian matrix $\mathbf{J}_{\pi a}$. It allows us to separate the set of the desired parameters into three groups of identifiable, non-identifiable or semi-identifiable ones (using SVD decomposition technique, for instance).

One of the essential particularities of elastostatic calibration is that the dimension of the desired parameter vector $\mathbf{k}$ is very high in general case (because each compliance matrix $\mathbf{k}_\theta^{(i)}$ includes 21 elements). For example, the elastostatic properties of a 6-dof serial manipulator with revolute joints can be descried using 1-dimensional spring for each actuated joint and 6-dof spring for each link. In total, it gives 258 parameters whose identifiability requires further study. However, as follows from our experiences, for serial industrial robots employed in machining, the links are usually quite rigid. So, the link compliances are dominated by the actuated joints compliances. For this reason, in this work, it is possible to use six 1-dof virtual springs localized at the joints to represent the manipulator elastostatic properties. It is clear that such a model is complete in geometric sense because it allows us to describe any end-effector deflections (expect some singular configurations that are usually out of the workspace suitable for machining application). It can be also proved that the model is irreducible and includes only identifiable parameters (six joint compliances); here, the rank of the relevant matrix $\mathbf{A}_{ka}$ is equal to six. In the remainder of this work, such representation will be further used to describe the elastostatic properties of a serial industrial robot employed in a machining work-cell.

Using this approach, let us derive the elastostatic model of the robotic manipulator KUKA KR270, which is used for experimental verification. Corresponding VJM-based presentation is shown in Figure 3.3, where the manipulator compliance is taken into account by one-dimensional virtual springs localized at the actuated joints. In this case, the extended geometric model of the manipulator includes sequentially

(a) a rigid link between the manipulator base and the first actuated joint q_1 described by the constant homogeneous transformation matrix $\mathbf{T}_{\text{Base}}$, whose geometric parameters has been already identified;

(b) six 1-dof flexible actuated joints with additional virtual springs describing the joint stiffness in the control loop, which are defined by the homogeneous matrix functions $\left\{\mathbf{T}_{\text{Joint}}(q_j + \theta_j),\ j=\overline{1,6}\right\}$, where q_j are the actuated joint coordinates and θ_j are the virtual joint variables;

(c) a set of rigid links described by the constant homogeneous transformation matrices $\left\{\mathbf{T}_{\text{Link}}^j,\ j=\overline{1,6}\right\}$, which integrate the identified geometric parameters;

(d) a rigid link from the last joint q_6 to the end-effector, described by the constant homogeneous transformation matrix $\mathbf{T}_{\text{Tool}}$.

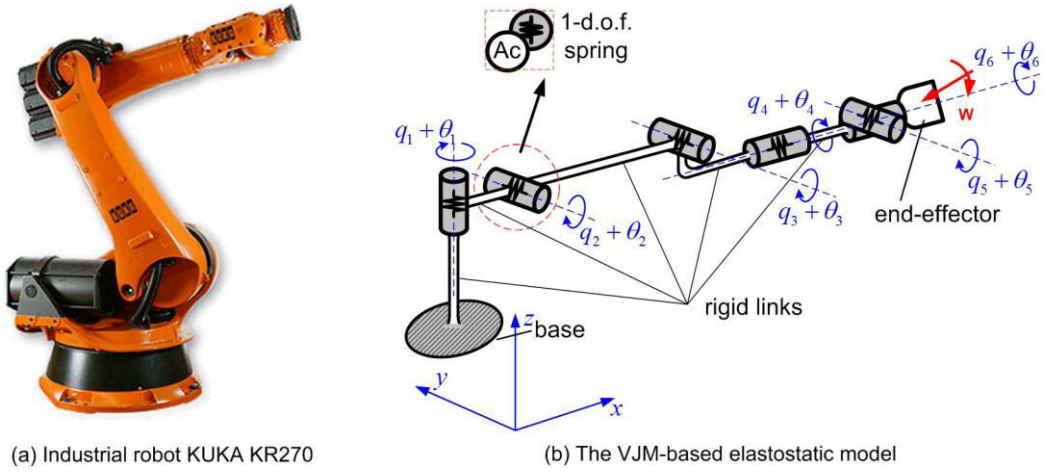

(a) Industrial robot KUKA KR270 (b) The VJM-based elastostatic model

Figure 3.3 Serial industrial robot KUKR KR270 and its VJM-based stiffness model

For this manipulator, the end-effector location subject to variations of all joint coordinates can be extracted from the following homogeneous transformation

$$\mathbf{T} = \mathbf{T}_{\text{Base}} \cdot \left[\prod_{j=1}^{6} \mathbf{T}_{\text{Joint}}(q_j + \theta_j) \cdot \mathbf{T}_{\text{Link}}^{j} \right] \cdot \mathbf{T}_{\text{Tool}} \tag{3.16}$$

that is further used for computing the Jacobian matrices in the calibration equation (3.13). It should be noted that this kinematic model includes 12 variables: 6 actuated joint coordinates $\mathbf{q} = (q_1, q_2, ..., q_6)$ defining the robot configuration, and 6 virtual joint coordinates $\boldsymbol{\theta} = (\theta_1, \theta_2, ..., \theta_6)$ defining deflections in the actuated joints. Using equations (3.7), relevant force-deflection relation can be presented as

$$\boldsymbol{\theta} = \mathbf{k}_{\theta} \cdot \mathbf{J}_{\theta}^{T} \cdot \mathbf{w} \tag{3.17}$$

which allows us to compute the joint deflections $\boldsymbol{\theta}$ assuming that the joint compliance matrix $\mathbf{k}_{\theta}$ is known. Combining equations (3.16) and (3.17), one can obtain desired elastostatic model in the form (3.11), which is used for identification. So, here the parameters of interest are the diagonal elements of the 6×6 compliance matrix $\mathbf{k}_{\theta} = diag(k_{\theta 1}, k_{\theta 2}, ..., k_{\theta 6})$, which are collected in a single vector $\mathbf{k}$ that should be identified via calibration based on expression (3.13). It can be proved that the observation matrix $\mathbf{A}_k$ for the considered manipulator has the following form

$$\mathbf{A}_k = \begin{bmatrix} \mathbf{J}_{\theta,11}(\sum_{i=1}^{6}\mathbf{J}_{\theta,i1}w_i) & \mathbf{J}_{\theta,12}(\sum_{i=1}^{6}\mathbf{J}_{\theta,i2}w_i) & \cdots & \mathbf{J}_{\theta,16}(\sum_{i=1}^{6}\mathbf{J}_{\theta,i6}w_i) \\ \mathbf{J}_{\theta,21}(\sum_{i=1}^{6}\mathbf{J}_{\theta,i1}w_i) & \mathbf{J}_{\theta,22}(\sum_{i=1}^{6}\mathbf{J}_{\theta,i2}w_i) & \cdots & \mathbf{J}_{\theta,26}(\sum_{i=1}^{6}\mathbf{J}_{\theta,i6}w_i) \\ \vdots & \vdots & \vdots & \vdots \\ \mathbf{J}_{\theta,61}(\sum_{i=1}^{6}\mathbf{J}_{\theta,i1}w_i) & \mathbf{J}_{\theta,62}(\sum_{i=1}^{6}\mathbf{J}_{\theta,i2}w_i) & \cdots & \mathbf{J}_{\theta,66}(\sum_{i=1}^{6}\mathbf{J}_{\theta,i6}w_i) \end{bmatrix}_{6\times6} \tag{3.18}$$

where $\mathbf{J}_{\theta,ij}$ is the ij-th element of the Jacobian matrix $\mathbf{J}_{\theta}$. It should be noted that in the above equation, the Jacobian matrix $\mathbf{J}_{\theta}$ is equivalent to the kinematic Jacobian $\mathbf{J}_{\text{q}}$ (since all the virtual springs are localized at the actuated joints). In the following Sections, this model will be further used for numerical computations required for the elastostatic calibration of KUKA KR270 robot as well as in the corresponding calibration experiments design.

Summarizing this Section in general, it is worth mentioning that the presented modeling technique for elastostatic calibration is based on both the extended geometric model and lumped stiffness model. It is shown that the model with six one-dimensional localized virtual springs at actuated joints is irreducible and suitable for calibration. More details concerning relevant measurement methods and identification algorithms are in the focus of the following Sections.

3.3 MEASUREMENT METHODS FOR ELASTOSTATIC CALIBRATION

For the elastostatic calibration, the measurement system must provide a set of end-effector deflections corresponding to certain external forces/torques. To measure the deflections, the same technique can be applied as in geometric calibration, including replacing the orientation components by the position ones corresponding to several reference points (enhance partial pose measurement technique, as it has been called in Section 2.3). However, to measure the force/torque magnitude and direction, some additional devices are required. In addition, in the manipulator elastostatic calibration, a crucial issue in the measurement procedure is related to the force application. These problems are sequentially discussed in the following subsections.

3.3.1 Conventional measurement methods

One major difference between the measurement methods for geometric and elastostatic calibration is that the latter requires two types of measurements: (i) measurement of the manipulator pose (the end-effector coordinates), and (ii) measurement of the external force/torque applied to the end-effector (the magnitude and the direction). Figure 3.4 presents a classification of measurement methods for manipulator pose data and external force/torque components. Similar to the previous chapter (see Section 2.3), these methods are divided into two main groups (open-loop and closed-loop ones) that differ in experimental setup that may include or not include some mechanical constraints.

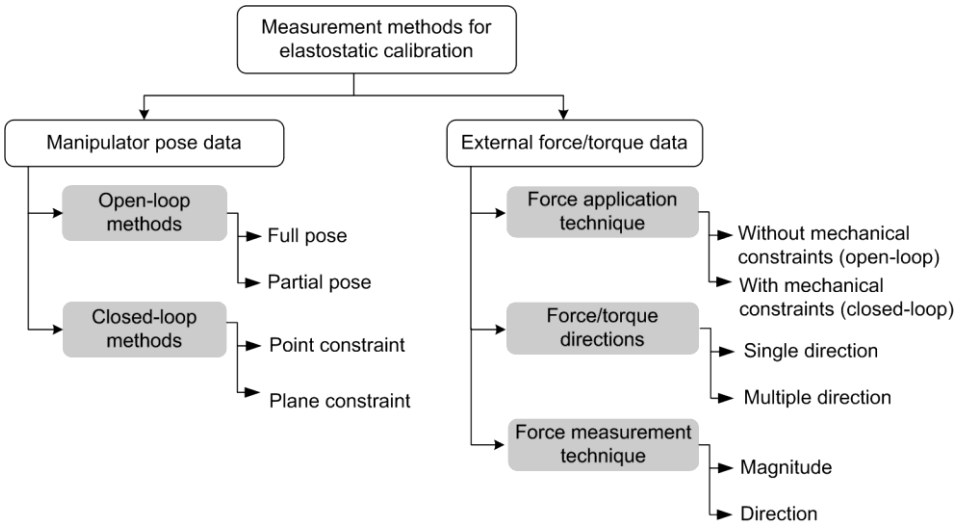

Figure 3.4 Measurement methods for elastostatic calibration

In the case of elastostatic calibration, the *closed-loop* measurement employs the idea of using physical constraints imposed between the manipulator end-effector and certain fixed environment (a rigid table fixed on the work-cell floor, for instance). When robot approaches corresponding target points, the reaction force is generated due to the resistance of the rigid obstacle, and causes joint deflections. To measure the generated forces/torques at the contact point, some special force sensors

are required, which allow to obtain one- or multi-dimensional force components. These sensors may be located at the robot base, at the end-effector or at the robot wrist, depending on particular experimental setup. Corresponding experimental data include both the measured forces $\mathbf{w}_i$ and the obtained joint deflections $\Delta\mathbf{q}_i$. It should be stressed that here, in contrast to geometric calibration, user can define several target points for the controller to generate different forces/torques for the same physical constraint.

This technique has clear advantage in terms of the simplicity of force application, where no additional loading setup is required. However, the calibration results highly depend on the sensitivity and flexibility of the force measurement device employed in the measurement setup. Besides, in addition to the difficulty of implementation of the mechanical constraints within the work-cell environment, it essentially reduces the calibration workspace to a quite limited area (the surface of the table, for instance). This also induces some limitations in selection of optimal measurement configurations for calibration.

On the other hand, the *open-loop* measurement methods can be easily adapted to elastostatic calibration. Similar to the geometric case, some external devices for measuring the manipulator end-effector position/location coordinates are required. However here, the same reference points on the end-effector should be measured twice, before and after applying test loadings. To measure the Cartesian coordinates of these reference points, different measurement devices can be used. For example, (Alici and Shirinzadeh, 2005), (Meggiolaro et al., 2005) and (Nubiola and Bonev, 2012) used the laser-based sensing system; (Wang et al., 2009) and (Lightcap et al., 2008) utilized the coordinates measurement machine. It is clear that in all cases the calibration results are highly influenced by the precision of the corresponding measurement device and the location of the reference points. These issues require additional investigations and will be discussed in the following sections.

An evident advantage of the open-loop technique is that the diversity of measurement configurations is higher than the closed-loop methods. However, the force application procedure is more complicated. To generate the elastostatic deflections, different experimental setup can be used, which usually include some mounting tools and weights. It should be stressed that these experimental setups introduce additional limitations for measurement configuration selection. Nevertheless, usually these limitations do not affect significantly the calibration accuracy and the workspace suitable for calibration is still larger than in the case of the closed-loop methods. For this reason, this approach is widely used in the area of elastostatic parameters identification.

In engineering practice, applying of vertical gravity force is the most attractive solution. Such a force can be generated using the weights attached to the robot end-effector, the corresponding experimental setup is presented in Figure 3.5(a). It should be mentioned that using such simple arrangement and a specific tool, it is possible to generate both force and torque at the reference points. This approach has been used in (Dumas et al., 2012) where the authors connected some weights to the robot end-effector with a chain. Similarly, in (Lightcap et al., 2008), a weight rack was directly mounted on the end-effector. However in some cases, applying only the vertical force may be not sufficient for the identification of the desired stiffness parameters. For instance, if any actuated joint axis is parallel to the force direction, the corresponding joint compliances cannot be identified. For this reason, several researchers attempted to change the force direction at the robot end-effector using the so-called cable pulley system. This simple mechanism is illustrated in Figure 3.5(b) and allows us to alter the force direction from the vertical one, while applying the gravity force only. In addition, here it is possible to generate any desired external loadings (force and torque within the allowable limits) without additional expensive devices (Alici and Shirinzadeh, 2005; Wang et al., 2009). A typical

example of such experimental setup was given in (Wang et al., 2009), where the authors used an air cylinder with a pulley relayed string, where the force magnitude can be adjusted by changing the air pressure, and the force direction can be altered by changing the pulley position.

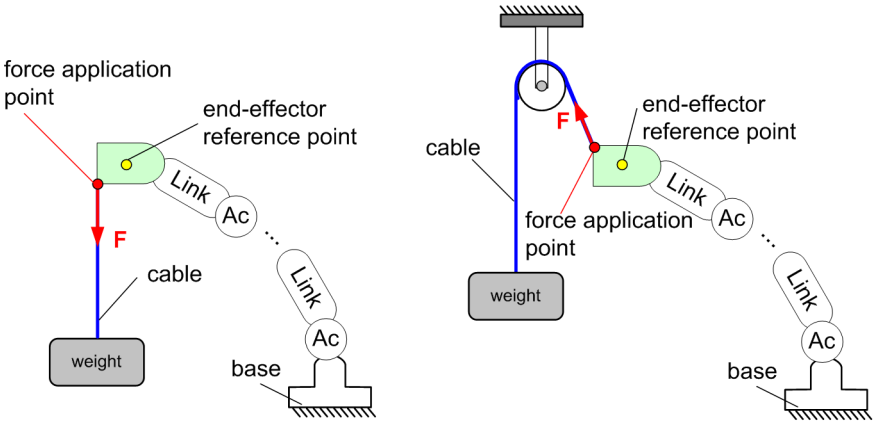

Figure 3.5 Mechanisms for the force/torque application using the gravity force

To obtain the required experimental data, the magnitude and direction of the applied loading must be carefully measured. In general, they can be measured using multi-directional force sensor or a dynamometer and position measurement system. In the case where the gravity force is applied without the pulley system, it is required to measure the force magnitude only while the force direction is already known (Dumas et al., 2012). In order to measure 3-dimensional force, in the work (Alici and Shirinzadeh, 2005) a wrist force/torque sensor was used. In another work (Wang et al., 2009), the authors have used ATI Omega force sensor and avoid utilization of the torque measurement since it has rather low accuracy. In contrast, in (Meggiolaro et al., 2005), a 6-dimensional force/torque sensor was used, but the precision of the measurement system and its possible influences on the final identification accuracy were not reported. The above described force application methods and the related measurement setups used in the existing works are summarized in Table 3.1.

Table 3.1 Force application methods and measurement equipments used in existing works

Publication	Robot	Force application method	Force measurement equipment
(Dumas et al., 2012)	KUKA KR240-2	Connecting chain	Spring balance (1D)
(Lightcap et al., 2008)	Mitsubishi PA10-6CE	Weight rack	Known (1D)
(Wang et al., 2009)	ABB IRB4400	Pulley relayed string	ATI Omega force sensor (3D)
(Alici and Shirinzadeh, 2005)	Motoman SK120	Cable-pulley system	Wrist force/torque sensor (3D)
(Meggiolaro et al., 2005)	Patient positioning system	—	6-axis force/torque sensor (6D)

As follows from the presented review, the closed-loop measurement methods are simpler in terms of force application, but provide rather limited choices of measurement configurations. While

the open-loop methods have more complicated loading setup, however, wider range of calibration workspace. Taking into account the importance of optimal selection of measurement configurations and to simplify the experimental setup, in this work, the open-loop technique is used with the gravity force only. However, to improve the elastostatic calibration accuracy, the enhanced partial pose measurement technique proposed in the previous chapter for geometric calibration (see Section 2.3) can be also adapted here. This issue is discussed in details in the following Subsection.

3.3.2 Enhanced partial pose measurement method in elastostatic calibration

Similar to geometric calibration, the equations for the elastostatic parameters identification include both position and orientation components of the residuals. In engineering practice, the position residuals are obtained directly from conventional measurement equipment that usually provide the Cartesian coordinates of the reference point. On the other hand, the orientation residuals are evaluated indirectly via relevant trigonometric computations, using position residuals of several additional reference points. To avoid these computations that may provoke loss of accuracy and the problem of non-homogeneity in relevant optimization objective, in Section 2.3 it has been proposed the enhanced partial pose measurement method. Its basic idea is the following: (i) exclude from the original system the identification equations corresponding to the orientation residuals; (ii) include in it auxiliary identification equations corresponding to the position residuals of the additional reference points. Let us apply this idea to the case of elastostatic calibration and present some details.

For the conventional full pose measurement technique, the desired elastostatic parameters $\mathbf{k}$ are identified from the system of equations

$$\Delta\mathbf{t}_i = \mathbf{A}_k(\mathbf{q}_i, \mathbf{w}_i)\cdot\mathbf{k}, \quad i = 1,2,...m \tag{3.19}$$

that are based on linearized model (3.13). Here, $\Delta\mathbf{t}_i = (\Delta p_{xi}, \Delta p_{yi}, \Delta p_{zi}, \Delta\varphi_{xi}, \Delta\varphi_{yi}, \Delta\varphi_{zi})^T$ is the 6-dimensional end-effector deflection vector that includes both position $\Delta\mathbf{p}_i = (\Delta p_{xi}, \Delta p_{yi}, \Delta p_{zi})^T$ and orientation $\Delta\boldsymbol{\varphi}_i = (\Delta\varphi_{xi}, \Delta\varphi_{yi}, \Delta\varphi_{zi})^T$ components. It is clear that this system of linear equations can be solved with respect to vector $\mathbf{k}$ if the number of experiments m is high enough and the measurement configurations defined by the input variables $\{\mathbf{q}_i, \mathbf{w}_i, i = 1,m\}$ ensure non-singularity of relevant aggregated observation matrix $\mathbf{A}_{ka}$ (assuming that all model parameters are identifiable, see subsection 3.2.2). For this technique, each set of input variables (including the manipulator configuration $\mathbf{q}_i$ and the applied wrench $\mathbf{w}_i$) produces six scalar equations to be used for the identification. Corresponding least-square optimization problem that allows us to obtain the desired parameters $\mathbf{k}$ can be expressed as

$$\sum_{i=1}^{m} \left\| \Delta\mathbf{t}_i - \mathbf{A}_k(\mathbf{q}_i, \mathbf{w}_i)\cdot\mathbf{k} \right\|^2 \to \min_{\mathbf{k}} \tag{3.20}$$

where the residual components are obviously non-homogeneous (for example, millimeters and radians). In some cases, these components are normalized before computing the squared sum, but the weight assigning procedure is a non-trivial step that also affects the identification accuracy.

Similar to geometric calibration, the main difficulty with the conventional method is that the orientation components $(\varphi_{xi}.\varphi_{yi}.\varphi_{zi})^T$ cannot be measured directly, and they are computed using excessive number of position measurements for the same configuration. In addition to the problem of non-homogeneity in the optimization objective function, this also causes some loss of accuracy. So, to overcome this difficulty, let us adapt the proposed technique of enhanced partial pose measurement to the case of elastostatic calibration. In the frame of this method, the optimization problem (2.31) is reformulated using only the data directly available from the measurement system, i.e. the Cartesian

coordinates of all reference points $\mathbf{p}_i^j$ (see Figure 2.7). This idea allows us to obtain homogeneous identification equations where each residual has the same unit (millimeter, for instance). The corresponding optimization problem is rewritten as follows

$$\sum_{i=1}^{m}\sum_{j=1}^{n}\left\|\Delta\mathbf{p}_i^j - \mathbf{A}_k^{j(p)}(\mathbf{q}_i,\mathbf{w}_i)\cdot\mathbf{k}\right\|^2 \to \min_{\mathbf{k}} \tag{3.21}$$

Here, the matrix $\mathbf{A}_k^{j(p)}(.)$ with the superscripts "(p)" denotes the position rows of the corresponding observation matrix $\mathbf{A}_k^j(.)$, the index "i" defines the manipulator configuration number, and the index "j" denotes the reference point number. It should be mentioned that comparing to geometric calibration, where only partial Jacobian matrix $\mathbf{J}_\pi^{j(p)}$ is used, computation of matrix $\mathbf{A}_k^j$ requires the complete Jacobian matrix $\mathbf{J}_0^j$ (see Eq.(3.18)). More detailed presentation of the above matrices will be given in the following Section. It is intuitively clear that this approach is promising with respect to the identification accuracy and the level of improvement is comparable with the case of geometric calibration (for particular case study presented in Section 2.3, the accuracy has been improved by 283%).

Comparing to the geometric calibration, there exist some particularities in elastostatic calibration concerning the experimental setup. One important issue is related to obtaining the end-effector deflections, where the measurement of reference point position must be carried out twice for each robot configuration (before and after applying external loadings). Another problem is related to the magnitude and direction of the applied force/torque as well as their measurements. Besides, the measurement setup in the case of elastostatic calibration includes not only the device for end-effector coordinate measurement (i.e. laser tracker), but also some special calibration tools for force application and corresponding sensors for measuring its magnitude and direction. It should be noted that the magnitude of end-effector deflections should be higher than resolution/precision of position measurement device and robot repeatability. For this reason, maximum robot payload is preferable to be used in the calibration experiments. In more details, the measurement procedure for manipulator elastostatic calibration is given below:

Step 0 Move the manipulator to a pre-selected configuration $\mathbf{q}_i$;

Step 1 Measure the positions of several reference points $\mathbf{p}_{0i}^j$ located at the manipulator end-effector using coordinates measurement system (without external loading);

Step 2 Apply external loadings at the robot end-effector with a given magnitude (within the allowable robot payload) and predefined direction;

Step 3 Measure the positions of the same reference points $\mathbf{p}_i^j$ using coordinates measurement system (with external loadings);

Step 4a Measure the directions of applied forces/torques $\mathbf{w}_i$ using either the coordinates measurement system or multi-directional force sensor;

Step 4b Measure the magnitudes of applied forces/torques $\mathbf{w}_i$ using the force sensor;

Step 5 Collect the experimental data $\left\{\Delta\mathbf{p}_i^j, \mathbf{w}_i\right\}$;

Step 6 Repeat steps from 0 to 5 for m robot configurations.

Corresponding experimental setup and measurement devices used in this work are shown in Figure 3.6. They include two main components:

(i) a laser tracker for the position coordinates measurement of references point #1-#3 before and after applying external loading (in steps 1 and 3, respectively), as well as the position of the force application point (in step 4a);

(ii) a dynamometer for the measurement of force magnitude (in step 4b).

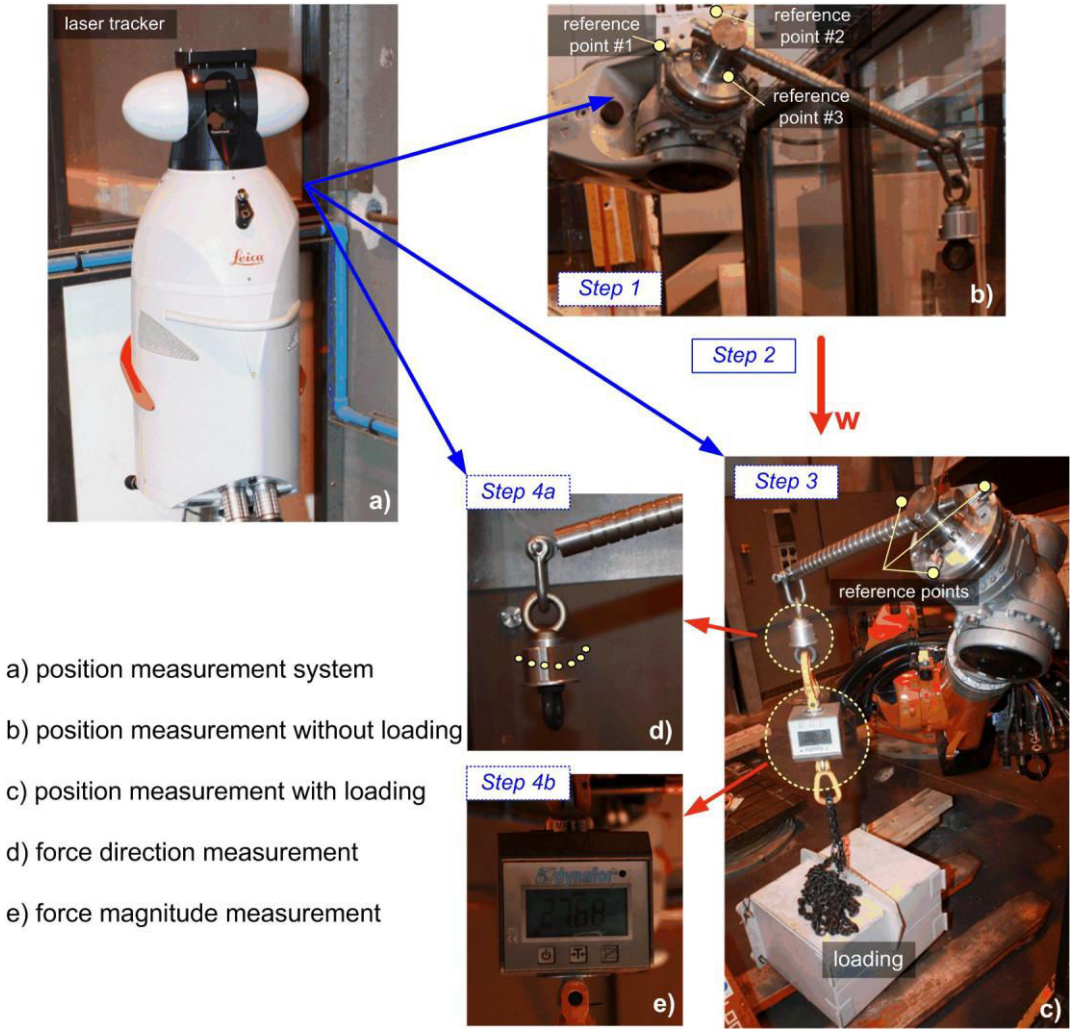

Figure 3.6 Measurement steps for elastostatic calibration (steps 1 to 4)

As follows from the relevant review (see previous Subsection), applying forces in different directions is often limited by the experimental environment. For this reason, for calibration of an industrial machining robot, the gravity force is preferable. However, it should be mentioned that applying only the gravity force may be not sufficient for identification of the desired set of manipulator elastostatic parameters. For instance, in serial industrial robots, the first actuated joint usually has a strictly vertical axis. In this case, to identify the joint compliance, the forces/torques applied to the robot end-effector must have horizontal (non-vertical) component. Nevertheless, this requirement can still be satisfied by using some additional mechanical equipment (see Figure 3.5), which changes the external force direction.

The end-effector used in our elastostatic calibration experiments is presented in Figure 3.7 (it is also referred to as "calibration tool"). It includes four markers whose coordinates are measured by the

laser tracker. The gravity force is applied at the end-point $\mathbf{p}_{wi}$ of this tool, allowing us to generate both external force and torque simultaneously. It should be stressed that the force/torque application point is different from the reference points $\mathbf{p}_i^j$ used for the deflection evaluation. So, the tool transformations should be different in corresponding equations for computing the wrench $\mathbf{w}_i$ and the position residuals $\Delta\mathbf{p}_i^j$. It is also worth mentioning that the calibration tool flexibility is not critical here, since the deflections are measured at the base of this tool.

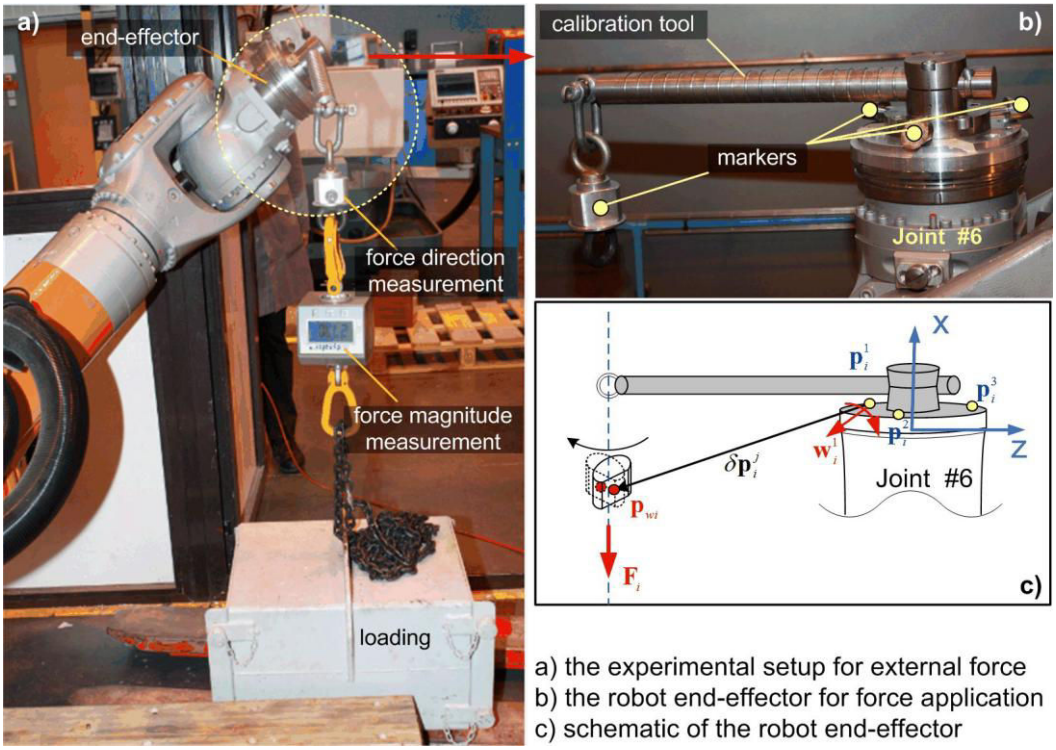

Figure 3.7 End-effector and force measurement device used for elastostatic calibration experiments

To compute the external wrench $\mathbf{w}_i^j$ generated by the gravity force, it is necessary to take into account the calibration tool geometry (see Figure 3.7c). Assuming that the gravity force is applied at point $\mathbf{p}_{wi}$, the original wrench at this point can be presented as the combination of the force $\mathbf{F}_i = (0,\ 0,\ F_{zi})^T$ and the torque $\mathbf{M}_i = (0,\ 0,\ 0)^T$. Taking into account that the deflections are measured at the reference points $\mathbf{p}_i^j$, corresponding forces and torques at these points should be recomputed as

$$\mathbf{F}_i^j = \mathbf{F}_i; \quad \mathbf{M}_i^j = \mathbf{F}_i \times (\mathbf{p}_{wi} - \mathbf{p}_i^j) \tag{3.22}$$

where the position coordinates $\mathbf{p}_{wi}$ are provided by the laser tracker (using the position measurements for a set of points on an arc, whose center point is $\mathbf{p}_{wi}$). This yields the following expression for the torque components

$$\mathbf{M}_i^j = \begin{bmatrix} 0 & -F_z & 0 \\ F_z & 0 & 0 \\ 0 & 0 & 0 \end{bmatrix} \cdot \begin{bmatrix} \delta p_{xi}^j \\ \delta p_{yi}^j \\ \delta p_{zi}^j \end{bmatrix} \tag{3.23}$$

where the vector $\delta\mathbf{p}_i^j = \mathbf{p}_{wi} - \mathbf{p}_i^j$ describes the offset between the force application point and the reference point used for deflection evaluation. Finally, the recomputed wrench at each reference point can be presented as

$$\mathbf{w}_i^j = \begin{pmatrix} 0 & 0 & F_z & -F_z \delta p_{yi}^j & F_z \delta p_{xi}^j & 0 \end{pmatrix}^T \tag{3.24}$$

As follows from this expression, the component δp_{zi}^j does not influence on the wrench $\mathbf{w}_i^j$. It means that the z-coordinate of $\mathbf{p}_{wi}$ is not important and can be defined arbitrarily.

Summarizing this Section in general, it is worth mentioning that the enhanced partial pose measurement method can be well-adapted to elastostatic calibration, where the same level of accuracy improvement can be potentially achieved as in the geometric calibration. The presented measurement setup has some advantages in terms of its simplicity and allows us to avoid using expensive multi-dimensional force/torque measurement equipment. Some experimental results based on this measurement setup will be presented in Chapter 4.

3.4 IDENTIFICATION OF ELASTOSTATIC PARAMETERS

Using the manipulator elastostatic model presented in Section 3.2 and the experimental data obtained by the enhanced partial pose measurement method (the end-effector position deflections and corresponding external forces/torques), it is possible to identify the desired elastostatic parameters. This section presents the dedicated identification algorithm and relevant accuracy analysis.

3.4.1 Identification algorithm for the enhanced partial pose method

Let us present basic equations allowing us to compute desired elastostatic parameters from experimental data obtained using the partial pose measurement method. In the frame of this method, the coordinates of several reference points for a given configuration are used directly without computing the orientation angles. Similar to geometric calibration, it should also give essential advantages in terms of identification accuracy. However, the structure of the input data for the identification algorithm is different. Here, instead of the absolute position of reference points, the relative deflections $\Delta\mathbf{p}$ and corresponding external loadings $\mathbf{w}$ should be used; the actuated joint coordinates are required as well. Another particularity is related to the geometric model that should be extended to take into account both the actuated joint coordinates $\mathbf{q}$ and the virtual spring coordinates $\boldsymbol{\theta}$. It should be stressed that at this step, elastostatic calibration, the manipulator geometric parameters $\boldsymbol{\pi}$, the base $\mathbf{T}_{\text{base}}$ and tool $\mathbf{T}_{\text{tool}}^j$ transformations are known and obtained via geometric calibration.

In general case, the manipulator extended geometric model can be presented as the product of the following homogeneous transformation matrices

$$\mathbf{T}^j = \mathbf{T}_{\text{base}} \cdot \mathbf{T}_{\text{robot}}(\mathbf{q},\, \boldsymbol{\theta}) \cdot \mathbf{T}_{\text{tool}}^j \tag{3.25}$$

where index j corresponds to the reference point number, the matrix function $\mathbf{T}_{\text{robot}}(\mathbf{q},\, \boldsymbol{\theta})$ describes the manipulator geometry with respect to the actuated joint coordinates $\mathbf{q}$ and the virtual joint coordinates $\boldsymbol{\theta}$. To identify the desired elastostatic parameters, it is required to have the manipulator end-effector deflection caused by two different loadings, one of which can be assigned to zero. In this case, it is possible to distinguish two manipulator modes: (i) *unloaded mode* when the external wrench $\mathbf{w} = 0$ and (ii) *loaded mode* when $\mathbf{w} \neq 0$. It should be stressed that in the unloaded mode, the joint deflections are equal to zero, so the matrix function $\mathbf{T}_{\text{robot}}(\mathbf{q},\, \boldsymbol{\theta})$ can be replaced by $\mathbf{T}_{\text{robot}}(\mathbf{q},\, \mathbf{0})$. Using these notations, the deflection matrix for the j-th reference point can be expressed as

$$\Delta\mathbf{T}^j = \mathbf{T}_{\text{base}} \cdot \left(\mathbf{T}_{\text{robot}}(\mathbf{q},\, \boldsymbol{\theta}) - \mathbf{T}_{\text{robot}}(\mathbf{q},\, \mathbf{0})\right) \cdot \mathbf{T}_{\text{tool}}^j \tag{3.26}$$

Since any homogeneous transformation matrix can be split into rotational $\mathbf{R}_a^b$ and translational $\mathbf{p}_a^b$ parts (see Eq.(2.40)), the latter equation can be rewritten in the following form

$$\begin{aligned}\Delta\mathbf{p}^j &= \mathbf{p}_{\text{base}} + \mathbf{R}_{\text{base}} \cdot \Delta\mathbf{p}_{\text{robot}}\left(\mathbf{q},\ \boldsymbol{\theta}\right) + \mathbf{R}_{\text{base}} \cdot \Delta\mathbf{R}_{\text{robot}}\left(\mathbf{q},\ \boldsymbol{\theta}\right) \cdot \mathbf{p}_{\text{tool}}^j \\ \Delta\mathbf{R}^j &= \mathbf{R}_{\text{base}} \cdot \Delta\mathbf{R}_{\text{robot}}\left(\mathbf{q},\ \boldsymbol{\theta}\right) \cdot \mathbf{R}_{\text{tool}}^j\end{aligned} \tag{3.27}$$

where the vector $\Delta\mathbf{p}_{\text{robot}}$ and the matrix $\Delta\mathbf{R}_{\text{robot}}$ are defined by the expression

$$\mathbf{T}_{\text{robot}}\left(\mathbf{q},\ \boldsymbol{\theta}\right) - \mathbf{T}_{\text{robot}}\left(\mathbf{q},\ \mathbf{0}\right) = \begin{bmatrix} \Delta\mathbf{R}_{\text{robot}} & \Delta\mathbf{p}_{\text{robot}} \\ \mathbf{0} & 0 \end{bmatrix} \tag{3.28}$$

It is worth mentioning that here the joint deflections $\boldsymbol{\theta}$ depend on the applied external wrench $\mathbf{w}$, the vector of the actuated joint coordinates $\mathbf{q}$ and the elastostatic parameters matrix $\mathbf{k}_\theta$ to be identified (see Eq.(3.17)).

It should be mentioned that Eq.(3.27) is not suitable for calibration straightforwardly since the desired parameters $\mathbf{k}_\theta$ are integrated in the matrix functions $\Delta\mathbf{p}_{\text{robot}}(.)$ and $\Delta\mathbf{R}_{\text{robot}}(.)$. To solve this problem, this equation should be linearized with respect to the set of desired compliance parameters $\mathbf{k}$ and presented in the following form

$$\begin{bmatrix} \Delta\mathbf{p}^j \\ \Delta\boldsymbol{\varphi}^j \end{bmatrix} = \begin{bmatrix} \mathbf{A}_k^{j(p)} \\ \mathbf{A}_k^{j(\varphi)} \end{bmatrix} \cdot \mathbf{k} \tag{3.29}$$

where $\Delta\mathbf{p}^j$ and $\Delta\boldsymbol{\varphi}^j$ are the end-effector position and orientation deflections, the matrices $\mathbf{A}_k^{j(p)}$ and $\mathbf{A}_k^{j(\varphi)}$ correspond to the position and orientation parts of the observation matrix $\mathbf{A}_k^j$. According to expression (3.14), the c-th column vector of this matrix can be presented as

$$\mathbf{A}_{k,c}^j = \mathbf{J}_{\theta,c}^j \mathbf{J}_{\theta,c}^{j\ T} \mathbf{w} \tag{3.30}$$

where the 6×1 column vector of the Jacobian $\mathbf{J}_{\theta i,c}$ contains the position part $\mathbf{J}_{\theta i,c}^{(p)}$ and orientation part $\mathbf{J}_{\theta i,c}^{(\varphi)}$; the external wrench $\mathbf{w}$ includes the external 3×1 force vector $\mathbf{F}$ and 3×1 torque vector $\mathbf{M}$. So, the above expression can be rewritten as

$$\mathbf{A}_{k,c}^j = \begin{bmatrix} \mathbf{J}_{\theta,\text{c}}^{j(p)} \\ \mathbf{J}_{\theta,\text{c}}^{j(\varphi)} \end{bmatrix} \cdot \begin{bmatrix} \mathbf{J}_{\theta,\text{c}}^{j(p)T} & \mathbf{J}_{\theta,\text{c}}^{j(\varphi)T} \end{bmatrix} \cdot \begin{bmatrix} \mathbf{F} \\ \mathbf{M} \end{bmatrix} \tag{3.31}$$

After some transformations, the matrix columns $\mathbf{A}_{ki,c}^{j(p)}$ and $\mathbf{A}_{ki,c}^{j(\varphi)}$ can be presented as

$$\begin{aligned}\mathbf{A}_{k,c}^{j(p)} &= \mathbf{J}_{\theta,\text{c}}^{j(p)} \cdot \mathbf{J}_{\theta,\text{c}}^{j(p)T} \cdot \mathbf{F} + \mathbf{J}_{\theta,\text{c}}^{j(p)} \cdot \mathbf{J}_{\theta,\text{c}}^{j(\varphi)T} \cdot \mathbf{M} \\ \mathbf{A}_{k,c}^{j(\varphi)} &= \mathbf{J}_{\theta,\text{c}}^{(\varphi)} \cdot \mathbf{J}_{\theta,\text{c}}^{j(p)T} \cdot \mathbf{F} + \mathbf{J}_{\theta,\text{c}}^{j(\varphi)} \cdot \mathbf{J}_{\theta,\text{c}}^{j(\varphi)T} \cdot \mathbf{M}\end{aligned} \tag{3.32}$$

and finally, the matrices $\mathbf{A}_k^{j(p)}$ and $\mathbf{A}_k^{j(\varphi)}$ are computed using the above derived expressions and presented as the following form

$$\begin{aligned}\mathbf{A}_k^{j(p)} &= \left[\mathbf{A}_{k,1}^{j(p)}, ..., \mathbf{A}_{k,c}^{j(p)}, ..., \mathbf{A}_{k,n_\theta}^{j(p)}\right] \\ \mathbf{A}_k^{j(\varphi)} &= \left[\mathbf{A}_{k,1}^{j(\varphi)}, ..., \mathbf{A}_{k,c}^{j(\varphi)}, ..., \mathbf{A}_{k,n_\theta}^{j(\varphi)}\right]\end{aligned} \tag{3.33}$$

where "n_θ" refers to the total number of virtual joints. It should be stressed that here, in contrast to geometric calibration, the matrices $\mathbf{A}_k^{j(p)}$ and $\mathbf{A}_k^{j(\varphi)}$ depend on both position and orientation parts of the Jacobian.

In the frame of enhanced partial pose measurement method, each calibration experiment produces a set of vectors $\{\Delta\mathbf{p}_i^j, \mathbf{q}_i, \mathbf{w}_i \,|\, j=\overline{1,n}\}$, which define the position deflections of the robot end-effector, the corresponding actuator coordinates and the external wrenches respectively. So, the calibration procedure is treated as the best fitting of the experimental data $\left\{\Delta\mathbf{p}_i^j, \mathbf{q}_i, \mathbf{w}_i, i=\overline{1,m}, j=\overline{1,n}\right\}$

by the stiffness model that can be solved using the standard least-square technique. Corresponding system of equations for elastostatic identification can be presented as

$$\Delta\mathbf{p}_i^j = \mathbf{A}_k^{j(p)}(\mathbf{q}_i, \mathbf{w}_i)\cdot\mathbf{k} \qquad i=\overline{1,m},\ j=\overline{1,n} \tag{3.34}$$

where $\Delta\mathbf{p}_i^j$ is the end-effector deflection for the i-th configuration that is computed using the measurement data of j-th reference point before and after loading. In this case, only the positioning part of the observation matrix $\mathbf{A}_{ki}^{j(p)}$ is required, and it can be computed using equations (3.32) and (3.33); here vector $\mathbf{k}$ aggregates the desired joint compliances, which are the parameters to be identified.

Applying the least-square technique to the system of equations (3.34), corresponding optimization problem can be expressed as

$$\sum_{i=1}^{m}\sum_{j=1}^{n}\left(\mathbf{A}_{ki}^{j(p)}\mathbf{k}-\Delta\mathbf{p}_i^j\right)^T\left(\mathbf{A}_{ki}^{j(p)}\mathbf{k}-\Delta\mathbf{p}_i^j\right)\rightarrow\min_{\{\mathbf{q}_i,\mathbf{w}_i\}} \tag{3.35}$$

whose solution provides the estimates of the desired vector of compliances parameters

$$\mathbf{k}=\left(\sum_{i=1}^{m}\sum_{i=1}^{n}\mathbf{A}_{ki}^{j(p)T}\mathbf{A}_{ki}^{j(p)}\right)^{-1}\cdot\left(\sum_{i=1}^{m}\sum_{j=1}^{n}\mathbf{A}_{ki}^{j(p)T}\Delta\mathbf{p}_i^j\right) \tag{3.36}$$

Using the above presented expressions, the elastostatic parameters can be identified via the three-step identification algorithm presented in Figure 3.8. At the first step, the manipulator base $\mathbf{T}_{\text{base}}$ and tool $\mathbf{T}_{\text{tool}}^j$ transformations are identified, using dedicated algorithm presented in Subsection 2.4.1. It provides the input data for the second step, where the manipulator geometric parameters $\boldsymbol{\pi}$ are estimated using Eq.(2.53), based on the obtained optimal measurement configurations. To achieve the desired accuracy, these two steps should be repeated iteratively. At the last step, the compliance parameters $\mathbf{k}$ are obtained via Eq.(3.36), based on preselected measurement configurations (which differ from the ones in geometric calibration) and corresponding external loading.

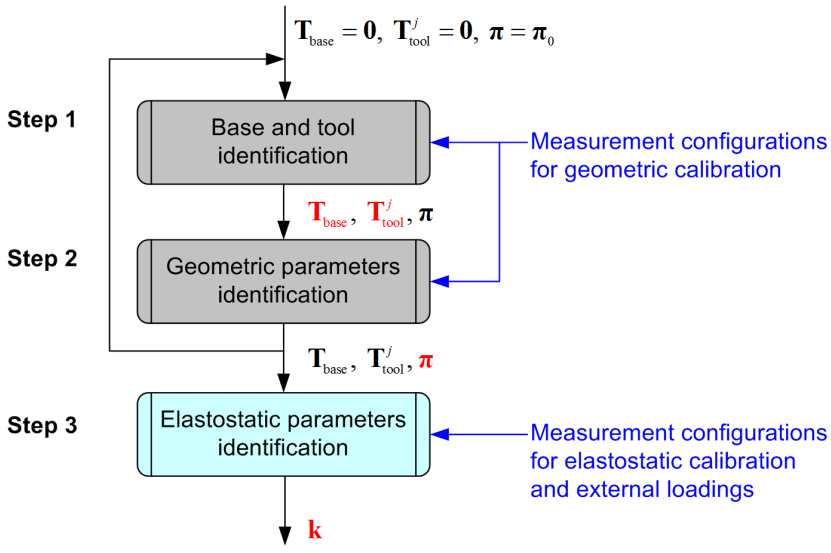

Figure 3.8 Three-step algorithm for manipulator elastostatic parameters identification

The above presented algorithm is able to provide good estimation of the desired parameters, in the case when the experimental data provided in the measurement step are perfect. However, in

practice, the measurement data are corrupted by noise that is usually non-negligible. Its impact is estimated in the following subsection.

3.4.2 Influence of the measurement errors on the identification accuracy

It is obvious that errors cannot be avoided in the calibration experiments. In practice, the calibration results can be affected by different types of errors: the measurement errors induced by the precision of external devices, providing the reference point position coordinates; the errors caused by the precision of relevant force sensors that give the measurement of force components, etc. As follows from our experience, if the joint encoder resolution is higher than 0.01deg and the force measurement error is less than 0.5%, their influences are negligible compared to the precision of position measurement system, which in practice is about 0.05mm. Therefore, it is reasonable to evaluate the calibration accuracy under the influence of the position measurement errors only. Below, these errors will be treated as independent identically distributed (i.i.d.) random values with zero expectation and standard deviation σ.

Taking into account the above mentioned measurement errors properties, corresponding position deflections at the reference points can be expressed as

$$\Delta \mathbf{p}_i^j = \mathbf{A}_{ki}^{j(p)} \cdot \mathbf{k} + \boldsymbol{\varepsilon}_i^j \tag{3.37}$$

where $\mathbf{k}$ is the true value of the unknown parameter and $\boldsymbol{\varepsilon}_i^j$ is the measurement errors at the j-th reference point in the i-th experiment. Using expression (3.36), the estimates of the compliance parameter vector $\hat{\mathbf{k}}$ can be presented as

$$\hat{\mathbf{k}} = \mathbf{k} + \left(\sum_{i=1}^{m} \sum_{i=1}^{n} \mathbf{A}_{ki}^{j(p)T} \mathbf{A}_{ki}^{j(p)} \right)^{-1} \cdot \left(\sum_{i=1}^{m} \sum_{j=1}^{n} \mathbf{A}_{ki}^{j(p)T} \boldsymbol{\varepsilon}_i^j \right) \tag{3.38}$$

where the second term describes the stochastic component. As follows from this equation, expression (3.36) provides the unbiased estimates of the desired parameters, i.e.,

$$E(\hat{\mathbf{k}}) = \mathbf{k} \tag{3.39}$$

where $E(.)$ denotes the mathematical expectation of the random values. It can be also proved that the covariance matrix of $\hat{\mathbf{k}}$ that defines the identification accuracy can be computed as

$$\operatorname{cov}(\hat{\mathbf{k}}) = \left(\sum_{i=1}^{m} \sum_{j=1}^{n} \mathbf{A}_{ki}^{j(p)T} \mathbf{A}_{ki}^{j(p)} \right)^{-1} E\left(\sum_{i=1}^{m} \sum_{j=1}^{n} \mathbf{A}_{ki}^{j(p)T} \boldsymbol{\varepsilon}_i^j \sum_{i=1}^{m} \sum_{j=1}^{n} \boldsymbol{\varepsilon}_i^{jT} \mathbf{A}_{ki}^{j(p)} \right) \left(\sum_{i=1}^{m} \sum_{j=1}^{n} \mathbf{A}_{ki}^{j(p)T} \mathbf{A}_{ki}^{j(p)} \right)^{-1} \tag{3.40}$$

Taking into account statistical properties of the measurement errors, i.e.,

$$E\left(\boldsymbol{\varepsilon}_i^j \boldsymbol{\varepsilon}_k^{jT} \right) = \begin{cases} \mathbf{0}, & \text{if } i \neq k \\ \sigma^2 \mathbf{I}, & \text{if } i = k \end{cases} \tag{3.41}$$

the intermediate term in Eq.(3.40) can be written as

$$E\left(\sum_{i=1}^{m} \sum_{j=1}^{n} \mathbf{A}_{ki}^{j(p)T} \boldsymbol{\varepsilon}_i^j \sum_{i=1}^{m} \sum_{j=1}^{n} \boldsymbol{\varepsilon}_i^{jT} \mathbf{A}_{ki}^{j(p)} \right) = \sigma^2 \left(\sum_{i=1}^{m} \sum_{j=1}^{n} \mathbf{A}_{ki}^{j(p)T} \mathbf{A}_{ki}^{j(p)} \right) \tag{3.42}$$

So finally, the desired covariance matrix can be simplified to

$$\operatorname{cov}(\hat{\mathbf{k}}) = \sigma^2 \left(\sum_{i=1}^{m} \sum_{i=1}^{n} \mathbf{A}_{ki}^{j(p)T} \mathbf{A}_{ki}^{j(p)} \right)^{-1} \tag{3.43}$$

Hence, for the considered problem, the impact of the measurement errors is defined by the matrix sum $\sum_{i=1}^{m}\sum_{j=1}^{n}\mathbf{A}_{ki}^{j(p)T}\mathbf{A}_{ki}^{j(p)}$ that is also called the information matrix. The obtained covariance matrix can be used for both the accuracy evaluation of the identified parameters and for the design of calibration experiments. On the other hand, this matrix is derived using the assumption that the measurement errors statistical properties are similar for all directions and for all robot configurations. However in practice, this assumption is not always valid and in some cases the properties of the measurement noise depend on robot configuration and vary from one direction to another. This issue is in the focus of the following subsection.

3.4.3 Weighted least square technique for elastostatic calibration

To identify the desired parameters, most of the robot calibration procedures employ the ordinary least-square technique (Rao and Toutenburg, 1999), where all identification equations are treated similarly, with the same weights. This approach perfectly suits to the measurement systems that provide roughly the same precision in all directions and in all workspace points. Mathematically, it corresponds to the i.i.d.-hypothesis concerning the measurement noise, such that the calibration results can be treated as unbiased estimates of the desired parameters. However, as follows from our experience, at least one of these assumptions may be violated because the precision of the position measurement system (laser tracker, for instance) used in the calibration experiments essentially depends on the direction and the target marker location in the manipulator workspace.

To overcome this difficulty, the weighted least-square technique can be applied (Sheather, 2009). As known from literature, for the linear regression it gives rather good improvement and allows essentially reducing the measurement errors impact. In the frame of this technique, it is assumed that the measurement noise varies from one configuration to another. In this case, to improve the identification accuracy, it is reasonable to modify the optimization function (3.35) and rewrite it in the following form

$$\sum_{i=1}^{m}\sum_{j=1}^{n}\left(\mathbf{A}_{ki}^{j(p)}\mathbf{k}-\Delta\mathbf{p}_i^j\right)^T\cdot\mathbf{W}_i^{j2}\cdot\left(\mathbf{A}_{ki}^{j(p)}\mathbf{k}-\Delta\mathbf{p}_i^j\right)\rightarrow\min_{\{\mathbf{q}_i,\mathbf{w}_i\}} \tag{3.44}$$

where the matrix $\mathbf{W}_i^j=diag(w_{xi}^j,w_{yi}^j,w_{zi}^j)$ defines the corresponding weighting coefficients. This leads to a slightly different expression for the parameters estimates

$$\hat{\mathbf{k}}=\left(\sum_{i=1}^{m}\sum_{i=1}^{n}\mathbf{A}_{ki}^{j(p)T}\mathbf{W}_i^{j2}\mathbf{A}_{ki}^{j(p)}\right)^{-1}\cdot\left(\sum_{i=1}^{m}\sum_{j=1}^{n}\mathbf{A}_{ki}^{j(p)T}\mathbf{W}_i^{j2}\Delta\mathbf{p}_i^j\right) \tag{3.45}$$

and the covariance matrix that can be computed as

$$\mathrm{cov}(\hat{\mathbf{k}})=\left(\sum_{i=1}^{m}\sum_{j=1}^{n}\mathbf{A}_{ki}^{j(p)T}\mathbf{W}_i^{j2}\mathbf{A}_{ki}^{j(p)}\right)^{-1}\sum_{i=1}^{m}\sum_{j=1}^{n}\mathbf{A}_{ki}^{j(p)T}\mathbf{W}_i^{j2}\boldsymbol{\Sigma}_i^{j2}\mathbf{W}_i^{j2}\mathbf{A}_{ki}^{j(p)}\left(\sum_{i=1}^{m}\sum_{j=1}^{n}\mathbf{A}_{ki}^{j(p)T}\mathbf{W}_i^{j2}\mathbf{A}_{ki}^{j(p)}\right)^{-1} \tag{3.46}$$

where the matrix $\boldsymbol{\Sigma}_i^{j2}=E\left(\boldsymbol{\varepsilon}_i^j\boldsymbol{\varepsilon}_i^{jT}\right)$ denotes the measurement errors covariance and has the following structure

$$E\left(\boldsymbol{\varepsilon}_i^j\boldsymbol{\varepsilon}_k^{jT}\right)=\begin{cases}\mathbf{0}, & \text{if } i\neq k\\ diag\left(\sigma_{xi}^{j2},\sigma_{yi}^{j2},\sigma_{zi}^{j2}\right), & \text{if } i=k\end{cases} \tag{3.47}$$

More detailed analysis of expressions (3.46) and (3.47) shows that the best selection of the weighting coefficients corresponds to the equation $\mathbf{W}_i^{j2}\cdot\boldsymbol{\Sigma}_i^{j2}=\mathbf{I}$ that gives the following solution

$$w_i^j = 1/\sigma_i^j \tag{3.48}$$

where σ_i^j is the standard deviation of the measurement error at the j-th reference point in the i-th identification expression. Corresponding covariance matrix is expressed as

$$\mathrm{cov}(\hat{\mathbf{k}}) = \left(\sum_{i=1}^{m} \sum_{i=1}^{n} \mathbf{A}_{ki}^{j(p)T} \left(\boldsymbol{\Sigma}_i^{j2} \right)^{-1} \mathbf{A}_{ki}^{j(p)} \right)^{-1} \tag{3.49}$$

Hence, to assign the weighting coefficients, the measurement noise variance should be known. However, in practice, exact values of σ_{xi}^j, $\sigma_{yi}^j, \sigma_{zi}^j$ are unknown and the estimates can be used only. On the other hand, as follows from practical experience, small variations in the weighting coefficients are not critical and they do not affect significantly the identification accuracy. Nevertheless, if the weights are assigned using small number of experiments, the identification results can be unpredictably affected. Therefore, the problem of computing the weighting coefficients that are able to ensure robustness of the identification algorithm is important.

It should be mentioned that computing σ_i^j based on a few measurements may have opposite effect, which decreases the identification accuracy. For this reason, relevant experiments should be carried out using a sufficient number of points in the vicinity of the same robot configuration that allows us to estimate s.t.d. of measurement noise for x-, y- and z-directions with a quite good precision. As follows from our experience, the obtained values of σ_i^j can be considerably higher than the claimed accuracy of the measurement system (0.01mm for the laser tracker used in our experiments). For this reason, it is proposed to introduce constant component in the σ_i^j that is equal to the claimed precision of measurement system σ_0. This idea leads to the following expression for the weighting coefficients

$$w_i^j = \frac{\sigma_0}{\sigma_0 + \lambda \cdot \hat{\sigma}_i^j} \tag{3.50}$$

where λ is a scalar factor that allows us to tune the impact of the variance estimate $\hat{\sigma}_i^j$, σ_0 is normalization component that also allows us to avoid division by zero. It should be noted that this approach can be also applied to geometric calibration, corresponding accuracy improvement of calibration results will be illustrated in Chapter 4.

As follows from above presented expressions, in order to have the smallest dispersion of the identification errors, it is required to have all elements in the covariance matrix as small as possible. This is obviously a multi-objective optimization problem, and the minimization of one element may increase others. In the literature, to reduce this problem to a mono-objective one, numerous scalar criteria have been proposed and provide rather different optimal solutions. Hence, it is quite important to select a proper optimization objective that ensures the best positioning accuracy of the manipulator under the loading. For this reason, the next section focuses on adapting the proposed test-pose based approach (see Chapter 2) for optimal measurement configuration selection in the case of elastostatic calibration, and ensures the best end-effector accuracy under external loadings. It is worth mentioning that the above described weighted least square technique can be only applied after obtaining real experiments data for the estimation of σ_i^j. So, the design of calibration experiments should be based on the covariance matrix (3.43) obtained under the assumption of the i.i.d. measurement noise.

3.5 OPTIMAL SELECTION OF MEASUREMENT CONFIGURATIONS

The problem of optimal measurement configurations selection for elastostatic calibration has been studied in very limited number of works. (Carbone and Ceccarelli, 2010; Zhou et al., 2010). On the other hand, numerous results in design of experiments for geometric calibration can be hardly applied here in straightforward way (due to essential difference between the manipulator geometric and elastostatic models). So, it is reasonable to extend the test-pose based approach developed in Chapter 2 for the case of elastostatic calibration. This approach is aimed at improving the manipulator positioning accuracy after calibration that perfectly suits to the industrial application considered in this work. This section presents detailed description of the test-pose based approach in elastostatic calibration as well as the efficiency improvement techniques for optimal measurement pose selection.

3.5.1 Extension of the test-pose based approach for elastostatic calibration

As follows from the previous study devoted to experiment design in geometric calibration, proper selection of the measurement configurations allows us to achieve an essential reduction of the measurement error impact. However, there exists an open question related to the numerical evaluation of this impact. Corresponding performance measure can be treated as the objective function in relevant optimization problem, which produces the desired plan of experiments. In the literature, the conventional approaches focus on minimizing the parameter identification errors based on evaluation of the corresponding covariance matrix. In contrast, the proposed test-pose based approach aims at improving the manipulator positioning accuracy, which obviously suits better the industrial applications. The benefits of this approach in terms of calibration efficiency have been demonstrated for the geometric case. So, it is reasonable to adapt the proposed approach and corresponding performance measure to elastostatic calibration.

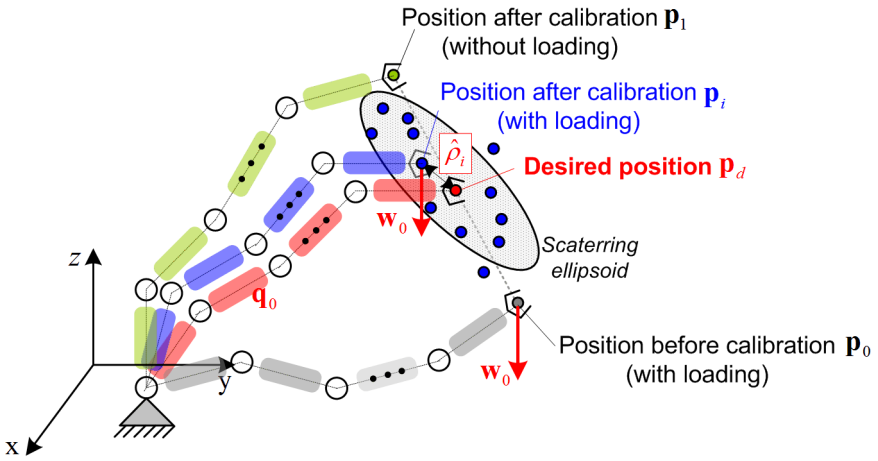

Figure 3.9 Dispersion of the manipulator positioning errors after calibration (for a given machining configuration and test loading)

The notion of manipulator positioning accuracy in elastostatic calibration is illustrated in Figure 3.9, where four manipulator configurations are presented (the desired one, the configuration under loading before calibration, as well as the configurations after calibration with and without loadings). Here, it is assumed that the desired end-effector position $\mathbf{p}_d$ is given or can be computed for given configuration $\mathbf{q}_0$ using manipulator direct geometric model, i.e., $\mathbf{p}_d = g(\mathbf{q}_0, \mathbf{0})$. Since the external test loading $\mathbf{w}_0$ causes the end-effector deflection $\Delta\mathbf{p}$, the end-effector position before calibration differs from the desired one and corresponds to the point $\mathbf{p}_0 = g(\mathbf{q}_0, \boldsymbol{\theta})$. For each set of

experimental data, calibration yields the parameters estimate vector $\hat{\mathbf{k}}_i$ that allows us to compensate the positioning errors by computing the deflection $\Delta\mathbf{p}_i$ and locate the end-effector at the point $\mathbf{p}_1$, which is symmetrical to the point $\mathbf{p}_0$ with respect to the target position $\mathbf{p}_d$ (i.e. $\mathbf{p}_1 = 2\mathbf{p}_d - \mathbf{p}_0$). Then, after applying the same test loading, the end-effector is located at position $\hat{\mathbf{p}}_i$, which goes closer to the target position $\mathbf{p}_d$ but slightly differs from it.

It should be noted that the obtained position $\hat{\mathbf{p}}_i$ highly depends on particular measurement noise and in practice, the points $\{\hat{\mathbf{p}}_i, i = 1,2,...\}$ are distributed around the target position $\mathbf{p}_d$. These points define the dispersion of the positioning errors after compensation $\hat{\mathbf{p}}_i - \mathbf{p}_d$. This vector varies with each particular set of experimental data, so it is reasonable to estimate it from statistical point of view taking into account measurement noise properties. This allows us to introduce the performance measure ρ_0, which is the root-mean-square distance between the desired position and the end-effector position after calibration, i.e.

$$\rho_0 = E\left(\left|\hat{\rho}_i\right|^2\right) \tag{3.51}$$

where $\hat{\rho}_i = \left|\hat{\mathbf{p}}_i - \mathbf{p}_d\right|$ corresponds to the dispersion distance for each set of experiment data. This statistical performance measure is used below to describe the elastostatic errors compensation efficiency and is treated as the objective function for corresponding optimization problem. To apply this performance measure to calibration experiment design, it is necessary to take into account that the influence of the compliance errors on the end-effector position varies with the manipulator configuration and throughout the workspace. So, an important idea of the test-pose based approach is that the desired accuracy is required to be achieved for rather limited workspace area, which allows us to limit the possible manipulator configurations by a single one (the machining configuration). Using these ideas, the problem of interest here is formulated as follows

Problem: To find an optimal plan of experiments, providing the measurement configurations and corresponding external loadings $\{\mathbf{q}_i, \mathbf{w}_i,\ i = \overline{1,m}\}$, which allows us to achieve the best compensation of positioning errors (evaluated via ρ_0) for a given manipulator test-pose and test-loading $\{\mathbf{q}_0, \mathbf{w}_0\}$ defined in relevant technological process.

In the frame of the adapted notations and assuming that the manipulator elastostatic model is linearized, the distance $\hat{\rho}_i$ can be computed as the Euclidean norm of the vector $\delta\mathbf{p}_i = \mathbf{A}_{k0}^{(p)}\delta\mathbf{k}_i$, where the subscript '0' in the observation matrix $\mathbf{A}_{k0}^{(p)}$ is related to the test pose $\mathbf{q}_0$ and $\delta\mathbf{k}_i = \hat{\mathbf{k}}_i - \mathbf{k}_0$ is the difference between the estimated and true values of the robot compliance parameters. Further, taking into account expression (3.38) and the assumptions concerning the measurement errors that are treated as unbiased and i.i.d. random variables (see Subsection 3.4.2), it can be easily proved that the expectation $E\left(\delta\mathbf{p}_i\right) = 0$. So, the points $\mathbf{p}_k$ that the end-effector attains after compensation are centred around the desired position $\mathbf{p}_d$, as shown in Figure 3.9.

The dispersion of these points can be evaluated by the variance $E\left(\delta\mathbf{p}_i{}^T\delta\mathbf{p}_i\right)$ which in accordance with the above definition is equal to the square of the performance measure ρ_0. This yields the expression

$$\rho_0^2 = E\left(\delta\mathbf{k}^T\mathbf{A}_{k0}^{(p)T}\,\mathbf{A}_{k0}^{(p)}\delta\mathbf{k}\right) \tag{3.52}$$

which can be rewritten as

$$\rho_0^2 = \mathrm{trace}\left(\mathbf{A}_{k0}^{(p)}E\left(\delta\mathbf{k}\delta\mathbf{k}^T\right)\mathbf{A}_{k0}^{(p)T}\right) \tag{3.53}$$

using the identity equation $\delta\mathbf{p}^T\delta\mathbf{p} \equiv \mathrm{trace}(\delta\mathbf{p}\delta\mathbf{p}^T)$. Further, by applying Eq. (3.43) and taking into account that the term $E(\delta\mathbf{k}\delta\mathbf{k}^T)$ is the covariance matrix of the compliance parameters estimates, i.e., $E(\delta\mathbf{k}\delta\mathbf{k}^T) = \mathrm{cov}(\hat{\mathbf{k}})$, the desired expression can be presented in the final form as

$$\rho_0^2 = \sigma^2 \cdot \mathrm{trace}\left(\mathbf{A}_{k0}^{(p)} \left(\sum_{i=1}^{m}\sum_{j=1}^{n} \mathbf{A}_{ki}^{j(p)T} \mathbf{A}_{ki}^{j(p)} \right)^{-1} \mathbf{A}_{k0}^{(p)T} \right) \tag{3.54}$$

As follows from this expression, ρ_0^2 can be treated as the weighted trace of the covariance matrix $\mathrm{cov}(\hat{\mathbf{k}})$, where the weighting coefficients are computed using the test-pose joint coordinates $\mathbf{q}_0$. Hence, the proposed performance measure has obvious advantage compared to the previous ones (see Section 1.4), which operate with "pure" trace of this matrix and involve straightforward summing of its diagonal elements (which may be of different units).

Based on this performance measure, the calibration experiments design can be reduced to the following optimization problem

$$\mathrm{trace}\left(\mathbf{A}_{k0}^{(p)} \left(\sum_{i=1}^{m}\sum_{j=1}^{n} \mathbf{A}_{ki}^{j(p)T} \mathbf{A}_{ki}^{j(p)} \right)^{-1} \mathbf{A}_{k0}^{(p)T} \right) \to \min_{\{\mathbf{q}_i, \mathbf{w}_i,\ i=\overline{1,m}\}} \tag{3.55}$$

whose solution gives a set of the desired measurement configurations $\{\mathbf{q}_1,...,\mathbf{q}_m\}$ and corresponding external loadings $\{\mathbf{w}_1,...,\mathbf{w}_m\}$. Hence, in the frame of the proposed approach, the calibration quality (evaluated via the error compensation accuracy ρ_0) is completely defined by the set of the observation matrices $\{\mathbf{A}_{k1}^{(p)},...,\mathbf{A}_{km}^{(p)}\}$ that depend on the manipulator configurations $\{\mathbf{q}_1,...,\mathbf{q}_m\}$, while the matrix $\mathbf{A}_{k0}^{(p)}$ corresponding to the test-pose $\mathbf{q}_0$ defines the weighting coefficients. A typical example of machining and measurement configurations is shown in Figure 3.10. It is obvious that they can be quite different from each other and the manipulator can be equipped with different end-effectors.

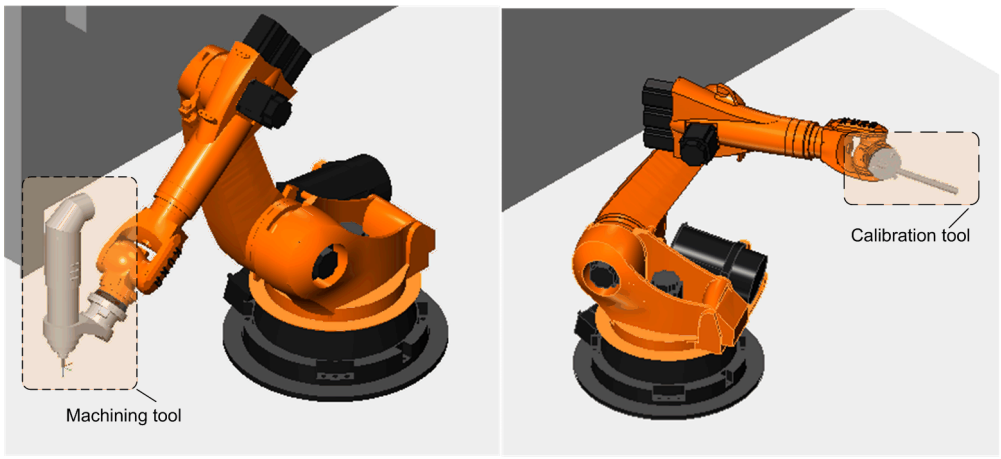

(a) Machining configuration (b) Measurement configuration

Figure 3.10 A typical machining configuration and a measurement configuration

To find the optimal set of measurement configurations, it is necessary to take into account particular constraints in the optimization problems (2.63) and (2.67). Assuming that these problems are solved subject to

$$\mathbf{C}_i(\mathbf{q}_i, \mathbf{w}_i) \le 0, \quad i = \overline{1,r} \tag{3.56}$$

where matrices $\mathbf{C}_i(\mathbf{q}_i, \mathbf{w}_i)$ describe constraints, which vary with different calibration cases and corresponding experiment environment. In particular, these constraints are imposed by the work-cell

design particularities and usually include the manipulator joint limits, the work-cell space limits, measurement equipment limitations, upper boundary of the applied forces and torques, etc. It should be also mentioned that some constraints are imposed to avoid collisions between the work-cell components and the manipulator. Besides, some directions of the applied loading are preferable for the reason of practical implementation. For instance, for the case of elastostatic calibration, they can be expressed as

$$\mathbf{C}_1 = \begin{bmatrix} q_i - q_i^{\max} \\ q_i^{\min} - q_i \end{bmatrix}, \quad \mathrm{C}_2 = \left\| \mathbf{F}^i \right\| - F_{\max}$$
$$\mathbf{C}_3 = \begin{bmatrix} p_z^{\min} - p_z \\ r^{\min} - r \\ \varphi^{\min} - |\varphi| \end{bmatrix}, \quad \mathbf{C}_4 = \begin{bmatrix} \mathbf{p}_i - \mathbf{p}_i^{\max} \\ \mathbf{p}_i^{\min} - \mathbf{p}_i \end{bmatrix} \tag{3.57}$$

where $q_i^{\min}$ and $q_i^{\max}$ are the joint limits, $F_{\max}$ is the robot maximum payload, $p_z^{\min}$ is the minimum height between the end-point of the calibration tool and the work-cell floor, $r^{\min}$ is the minimum radius to avoid collisions between the applied loading and robot body, $\varphi^{\min}$ is the minimum angle between the direction of calibration tool and z-axis of robot base frame to ensure that the vertical loading can be applied, $\mathbf{p}_i^{\min}$ and $\mathbf{p}_i^{\max}$ are the boundaries of work-cell space. The efficiency of the proposed approach will be illustrated in Subsection 3.5.3 (for the case of a two-link planar manipulator). In Chapter 4, this approach will be applied to the calibration of a 6-dof industrial robot of KUKA family.

3.5.2 Generalization for the case of multiple test configurations

The above presented approach is developed for the accuracy evaluation based on a single test configuration. However, in engineering practice, it is often required to perform machining along rather long and complex trajectories. This type of motions may require significant changes in the manipulator configuration and the desired accuracy should be achieved for the whole machining trajectory. For this reason, it is reasonable to generalize the test-pose based approach for the case where changes in the manipulator configurations are essential during the machining process. In this case, the goal of the calibration experiments design is to choose the optimal measurement configurations that minimize the maximum end-effector positioning errors after compensation (evaluated via ρ_0) for the entire trajectory.

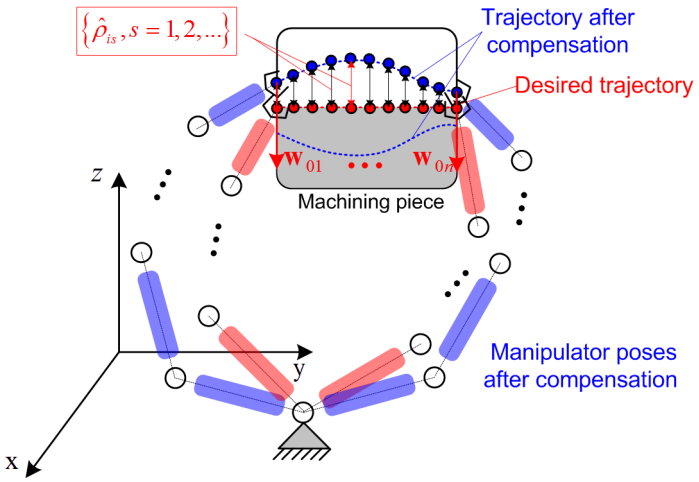

Figure 3.11 Definition of the performance measure for selection of measurement configurations that ensures high precision along the given trajectory

This idea is illustrated in Figure 2.10, where the desired trajectory and the trajectory after compensation are presented. It is assumed that the compensation is based on the parameter estimates $\hat{\mathbf{k}}_i$ obtained using the i-th set of measurement data. The desired trajectory is defined by a set of node points $\{\mathbf{p}_{ds},\ s=1,2,...\}$, corresponding manipulator configurations can be found from $\mathbf{p}_{ds}$ via the inverse kinematics. The distances between corresponding points of two trajectories are denoted as $\{\hat{\rho}_{is},\ i,s=1,2,...\}$. This allows us to define a set of manipulator test-poses $\{\mathbf{q}_{0s},\ s=\overline{1,n_s}\}$ and to introduce the following performance measure

$$\rho_{0\max}=\max_s\left\{E(|\hat{\rho}_{is}|^2)\right\} \tag{3.58}$$

that evaluates the highest positioning accuracy along the trajectory. It is clear that this definition perfectly corresponds to the engineering practice, where the quality of the machining is usually evaluated by the highest machining error. Hence, in this case, the problem of interest can be defined as follows

Problem: To find an optimal set of measurement configurations and corresponding external loadings $\{\mathbf{q}_i,\mathbf{w}_i,\ i=\overline{1,m}\}$, which allow us to achieve the best compensation of positioning errors (evaluated via the maximum root-mean-square distance $\rho_{0\max}$), during the entire machining trajectory that is defined using multiple manipulator test-poses and test-loadings $\{\mathbf{q}_{0s},\mathbf{w}_{0s},\ s=1,.2,...\}$.

Using the above presented ideas and applying the technique from Subsection 3.5.1, the generalized performance measure for multiple test configurations can be presented as

$$\rho^2_{0\max}=\sigma^2\cdot\max_s\left\{\text{trace}\left(\mathbf{A}^{(p)}_{k0s}\left(\sum_{i=1}^{m}\sum_{j=1}^{n}\mathbf{A}^{j(p)T}_{ki}\mathbf{A}^{j(p)}_{ki}\right)^{-1}\mathbf{A}^{(p)T}_{k0s}\right)\right\},\quad s=1,2,... \tag{3.59}$$

where the matrix $\mathbf{A}^{(p)}_{k0s}$ is computed for the test-pose joint coordinates $\mathbf{q}_{0s}$ and corresponding test-loading $\mathbf{w}_{0s}$, the superscript "(p)" denotes the positional components of the corresponding matrices, the subscript "$0s$" indicates the s-th test configuration, the subscript "i" and superscript "j" refer to the measurement configuration number and the reference point number, respectively. Using this performance measure, the calibration experiment design (i.e., optimal selection of measurement configurations) reduces to the following min-max problem

$$\max_s\left\{\text{trace}\left(\mathbf{A}^{(p)}_{k0s}\left(\sum_{i=1}^{m}\sum_{j=1}^{n}\mathbf{A}^{j(p)T}_{ki}\mathbf{A}^{j(p)}_{ki}\right)^{-1}\mathbf{A}^{(p)T}_{k0s}\right)\right\}\rightarrow\min_{\{q_i,w_i,\ i=\overline{1,m}\}}$$

subject to (3.60)

$$\mathbf{C}_i(\mathbf{q}_i,\mathbf{w}_i)\le 0,\qquad i=\overline{1,r}$$

whose solution provides a set of the desired manipulator configurations $\{\mathbf{q}_1,...,\mathbf{q}_m\}$ and corresponding external loadings $\{\mathbf{w}_1,...,\mathbf{w}_m\}$. It is clear that the problem (2.67) is numerically more complicated compared to the previous one (2.64), but it suits better to the notion of machining accuracy studied in this work. To demonstrate the efficiency of the proposed approach, following subsection contains an illustrative example that deals with experiment design of elastostatic calibration of a 2-dof manipulator, more complicated examples are presented in Chapter 4.

3.5.3 Evaluation of the test-pose based approach for elastostatic calibration

Let us illustrate the benefits of the test-pose based approach by an example of the elastostatic calibration of a two-link manipulator. It is assumed that the geometric parameters are already calibrated and only the joint compliances $\mathbf{k}=\left(k_{\theta1},k_{\theta2}\right)^T$ are unknown, which should be identified by

means of calibration. Under these assumptions, the basic expression for elastostatic identification can be written as follows

$$\begin{bmatrix} \Delta p_x \\ \Delta p_y \end{bmatrix} = \mathbf{A}_k^{(p)}(\mathbf{q},\mathbf{w}) \cdot \begin{bmatrix} k_1 \\ k_2 \end{bmatrix} \tag{3.61}$$

where the position part of the observation matrix $\mathbf{A}_k^{(p)}$ can be computed using Eq.(3.32) and Eq.(3.33), which yield the matrix column expression in the following form $\mathbf{A}_{k,c}^{(p)} = \mathbf{J}_{\text{q,c}}\mathbf{J}_{\text{q,c}}{}^T\mathbf{F}$. In addition, it can be proved that one of the variables describing the force direction and joint angle q_1 is redundant, so it is reasonable to fix the measurement force direction and to consider only q_1 as a variable. This allows us to reduce the number of design variables for the corresponding optimization problem. Besides, since here each measurement provides two deflections $(\Delta p_x, \Delta p_y)$ and exactly two parameters $(k_{\theta 1}, k_{\theta 2})$ should be identified, it is possible to calibrate them from a single measurement pose. So, taking into account all above mentioned properties and some basic expressions from previous subsections, corresponding optimization problem can be formulated as follows

$$\text{trace}\left(\mathbf{A}_{k0}^{(p)} \left(\mathbf{A}_k^{(p)T} \mathbf{A}_k^{(p)} \right)^{-1} \mathbf{A}_{k0}^{(p)T} \right) \to \min_{\{q_1, q_2\}} \tag{3.62}$$

where matrix $\mathbf{A}_{k0}^{(p)}$ is defined by the given test-pose and test-loading.

The simulation results for this case study have been obtained for the following parameters: the link lengths $l_1 = 1$ m, $l_2 = 0.8$ m, the force magnitude $F = 1$ N, measurement noise parameter $\sigma = 0.1$ mm. It is assumed that the manipulator test configuration is $\mathbf{q}_0 = (60°, 30°)$, corresponding optimal measurement configurations have been obtained by solving the optimization problem (3.62) and presented in Figure 3.12.

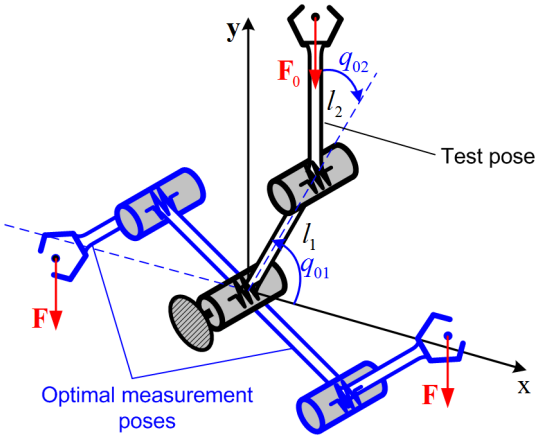

Figure 3.12 The test pose and corresponding optimal measurement configurations for 2-dof planar manipulator

As follows from this figure, the optimal measurement configurations are quite different from the test configuration and are located rather far from it in the workspace. For illustration purposes, all possible solutions have been also obtained using a grid (since relevant optimization problem contains only two variables). This allows us to compare different measurement pose "quality" from the manipulator accuracy point of view (evaluated via ρ_0). Relevant plots are presented in Figure 3.13, which also shows the accuracy improvement factor $\chi = \rho_0^{test} / \rho_0$ that compares the calibration results with the case when the test pose and measurement pose are identical. For this particular example, accuracy improvement factor is equal to 5.4, but it is worth mentioning that it varies with the defined test-pose.

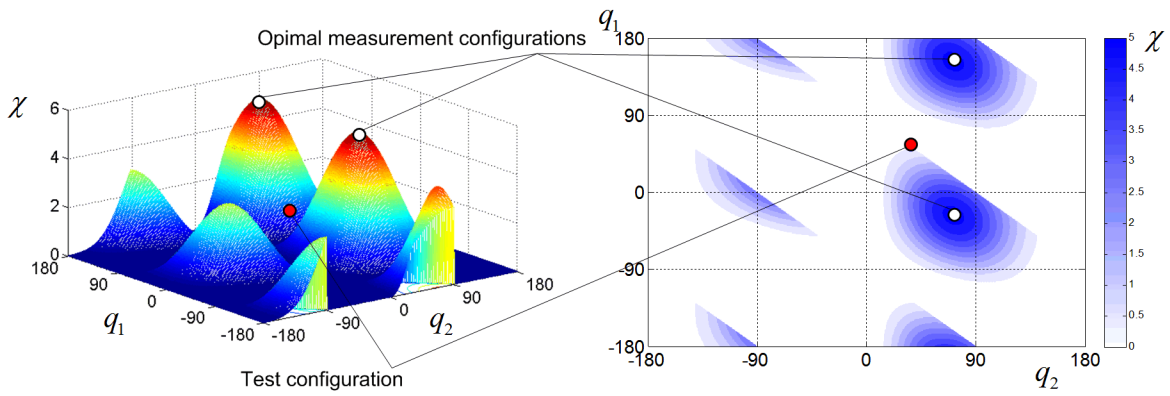

Figure 3.13 Selection of optimal measurement configuration for a given test pose (case of 2-dof planar manipulator, identification of two parameters $k_{\theta 1}, k_{\theta 2}$ from a single measurement providing deflections $\Delta p_x, \Delta p_y$)

To demonstrate the advantages of the proposed approach, several different plans of calibration experiments have been compared, taking into account both identification accuracy for the parameters $k_{\theta 1}, k_{\theta 2}$ and the manipulator positioning accuracy after calibration ρ_0. The examined calibration plans have been obtained both in straightforward way (i.e. using the test pose as the measurement pose) and also via optimization using different criteria. Relevant data are presented in Table 3.2 and in Figure 3.14, where σ_{k_1} and σ_{k_2} denote the identification accuracy for the stiffness parameters $k_{\theta 1}, k_{\theta 2}$ respectively.

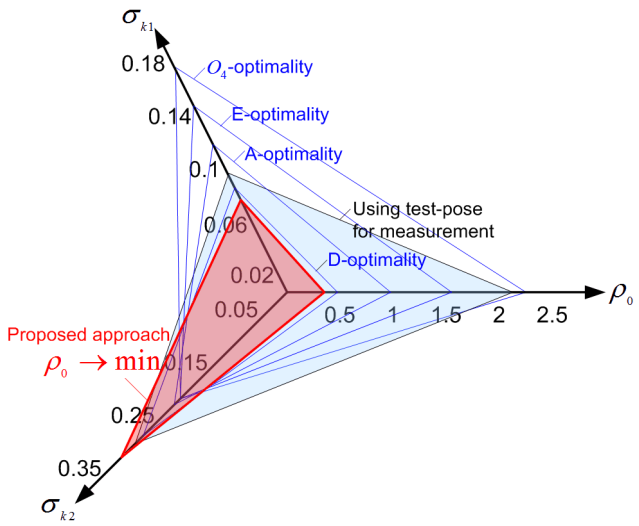

Figure 3.14 The Pareto-optimal solutions with respect to the criteria $\sigma_{k_1}, \sigma_{k_2}$ and ρ_0

As follows from these results, all examined calibration plans are Pareto-optimal with respect to the set of criteria ($\sigma_{k_1}, \sigma_{k_2}, \rho_0$). In particular, A-, D-, and E-optimality principles yield rather good solutions from the identification accuracy point of view, providing non-equal but rather low σ_{k_1} and σ_{k_2}; however, corresponding positioning accuracy after calibration ρ_0 is very moderate (nevertheless, they are better than the straightforward solution by the factors of 2.2, 4.8 and 1.4, respectively). In contrast, O_4-optimality gives almost the same values of σ_{k_1} and σ_{k_2}, but the manipulator positioning accuracy is the worst among all plans. It is worth mentioning that from an engineering point of view it is not reasonable to try to achieve the same accuracy for the parameters $k_{\theta 1}$ and $k_{\theta 2}$ because it is evident that the precision of k_1 has higher influence on the end-effector positioning accuracy than the

one of k_2. This idea is indirectly implemented in the proposed test-pose approach, which provides the lowest value of σ_{k_1} and the best positioning accuracy ρ_0, which is 5.4 times better than the straightforward solution where the test pose is used for the measurement.

Table 3.2 Comparison of manipulator accuracy after calibration for different principles for the measurement pose selection (2-dof manipulator, measurement noise $\sigma = 0.1\,\text{mm}$)

Experiment design principle	Identification accuracy [rad/N$\times 10^{-3}$]		Manipulator accuracy ρ_0 [mm]	Improvement factor $\chi = \rho_0^{test} / \rho_0$
	σ_{k_1}	σ_{k_2}		
Using test-pose as measurement pose	0.0888	0.2818	2.1265	1.0
A-optimality	0.1123	0.1948	0.9544	2.2
D-, O_1-optimality	0.0765	0.2804	0.4425	4.8
E-, O_3-optimality	0.1416	0.1840	1.5167	1.4
O_4-optimality	0.1707	0.1840	2.2061	0.9
Measurement pose selection via minimization of ρ_0	0.0719	0.3175	0.3915	5.4

Hence, the presented results confirm that the proposed approach is attractive for industry and provides the highest end-effector positioning accuracy. In contrast to conventional ones, it allows us to balance the influence of each compliance parameter on the robot accuracy. It is worth mentioning that for the above presented example, relevant optimization problem contains only two variables. However, in practice, for a problem of real dimension, the number of variables can be huge, which increases the computational complexity and computing time. So, the next subsection deals with efficiency improvement of the optimization routines employed in the measurement configuration selection.

3.5.4 Efficiency improvement of measurement pose selection

The procedure of solving the optimization problems (2.64) and (2.67) could be very tedious for the case when numerous measurement configurations are required for the calibration experiments. For this reason, the problem of interest is to find reasonable number of different measurement configurations and to improve the efficiency of optimization routines employed in the measurement pose selection. To achieve this goal, several heuristic techniques considered in Section 2.6 can be applied here in order to reduce the computational time while achieving acceptable accuracy:

(i) Fixing the measurement loading. In general case, the loadings $\left\{\mathbf{w}_i, i = \overline{1,m}\right\}$ applied in calibration experiments should be considered as the design variables of the optimization problems. In fact, to ensure high calibration accuracy, the maximum allowable loading should be applied in order to distinguish better the end-effector deflection from measurement noise. On the other hand, the force direction may vary but it is usually limited by the experimental environment. So in this work, it is proposed to fix the measurement loading and eliminate the variables $\mathbf{w}_i$ from the optimization problem, which obviously allows us to reduce considerably the computational efforts (for instance, for serial 6-dof manipulator, number of variables has been reduced from 12 to 6 for each configuration).

(ii) Applying parallel computations. In order to obtain the global optimum for the considered problem, it is required numerous repetitions of the optimization with different starting points. As follows from our experience, even using thousands of them may be not enough for finding the global optimum but the required computational time could overcome hundreds of hours. So, it is reasonable to apply parallel computing technique to speed up the design process and to take advantage of multi-core architecture in modern computers. Relevant computations in this work are carried out on a workstation with 12 cores, which allows us to decrease the computational time by the factor of 10-12.

(iii) Using hybrid approach. As follows from our study of optimization algorithms, the gradient search based method is able to find global minimum, however, it requires numerous repetitions with different initial values, which is very expensive from computational point of view. On the other hand, another examined technique, genetic algorithm, provides slightly lower accuracy but less computation time. For this reason, to take the advantages of both algorithms, it has been proposed a hybrid approach that combines these two techniques. The idea is to modify the starting point selection strategy for the gradient search in order to improve the algorithm efficiency. To ensure better convergence to the global minimum, it has been proposed to use the best half of final solutions obtained from GA as the starting points for gradient search. This hybrid approach has been proved to be quite efficient in terms of computational time (improved by a factor of 5) and allows us to avoid convergence to the local minima.

(iv) Reducing the problem dimension. In engineering practice, to improve the calibration accuracy, the conventional approach is to increase the number of experiments and solve the corresponding full-scale optimization problem for measurement poses selection. However from our experience, the diversity of the measurement configurations does no contribute essentially to the accuracy improvement if the total number of experiments is high enough. So, it is proposed to repeat the calibration experiments using several times the same measurement configurations, which allows us to simplify the optimization process (with lower dimension) and speed up the measurements. To demonstrate the efficiency of this technique, a comparison of quasi-optimal and optimal solutions for measurement pose selection for elastostatic calibration is presented in Table 3.3. Here, it is assumed that the total number of measurements $m = 12$. The last column in this table presents the manipulator accuracy corresponding to the solution of full-scale optimization problem (using 12 different configurations), while the other columns show the accuracy achieved using the quasi-optimal solutions associated with lower-dimensional optimizations.

Table 3.3 Comparison of quasi-optimal and optimal solutions for measurement pose selection for elastostatic calibration (case of 6-dof manipulator, total number of measurements $m = 12$)

	Number of different poses × number of repetitions ($m \times k$)				
Factorization	**2**×6	**3**×4	**4**×3	**6**×2	**12**×1
$\rho_0^{\min}$, [mm×10^{-3}]	2.445	2.338	2.335	2.283	2.282
Loss of accuracy	7.14%	2.45%	2.32%	<0.01%	0%
Computational time	25min	48min	1.0h	1.3h	1.7h

As follows from the table, the achieved manipulator accuracy for calibration using only 3 different measurement configurations (repeated the experiment for 4 times) is only 2.45% less than using 12 different configurations. It is clear that using the quasi-optimal solutions for selection of

measurement configurations allows us to reduce essentially the computational efforts but without significant impact on the manipulator positioning accuracy.

The contributions of above presented techniques (i),...,(iv) to the efficiency improvement for measurement pose selection are summarized in Table 3.4. The improvement factors for these techniques vary from 2 to 12 in terms of the computational time. As a result, the computational time can be decreased from over 200 hours to 48 minutes, which corresponds to the total improvement factor 250.

Table 3.4 Efficiency improvement factors for applying different heuristic techniques (case of optimal pose selection with 12 measurements)

Efficiency improvement technique	Computational time	Improvement factor
Conventional optimization technique	>200h	
Proposed heuristic techniques		
(i) Fixing the measurement loading	99.3h	2.0
(ii) Parallel computing	8.5h	11.7
(iii) Hybrid approach	1.7h	5.0
(iv) Quasi-optimal solutions	48min	2.2
Total	>200h $\rightarrow$ 48min	250.0

Summarizing Section 3.5 in general, it is worth mentioning that the proposed test-pose based approach and corresponding efficiency improvement techniques are well-adapted for optimal measurement configurations selection in elastostatic calibration. It allows us to increase essentially the calibration efficiency (in terms of computational time for solving relevant optimization problem) and to achieve the highest manipulator positioning accuracy after compensation. It should be mentioned that the obtained results are based on the assumption that the considered manipulator is strictly serial. However in practice, the industrial serial manipulators may include closed-loop chain (induced by gravity compensator, for instance). In this case, corresponding stiffness modeling approach and calibration method should be revised, which is in the focus of the next section.

3.6 ELASTOSTATIC CALIBRATION FOR HEAVY INDUSTRIAL ROBOTS WITH GRAVITY COMPENSATORS

For most of the heavy industrial robots used for high-precision and high-speed machining, to enhance robot stiffness, manufacturers tend to increase the manipulator link cross-sections that obviously leads to an increase of the robot mass. For this reason, the gravity forces applied to the manipulator components become non-negligible and also contribute to the position errors. To overcome this difficulty, the robots are usually equipped with different types of gravity compensators, which, however, considerably complicate the stiffness modeling of those heavy manipulators. To our knowledge, the problem of stiffness modeling and identification for the heavy manipulators with gravity compensators has not been studied in detail yet. Currently, the main activity in this area focuses on the gravity compensator design, which differs in kinematics and/or may also employ some software tools embedded in the robot controller (De Luca and Flacco, 2011; Takesue et al., 2011). This Section presents a VJM-based stiffness model for a serial manipulator with a compensator

attached to the second joint. The main attention is paid to the identification of the model parameters and calibration experiment planning.

3.6.1 Mechanics of gravity compensator

The mechanical structure of the gravity compensator under study is presented in Figure 3.15. The compensator incorporates a passive spring attached to the first and second links, which creates a closed loop that generates the torque applied to the second joint of the manipulator. This design allows us to limit the stiffness model modification by incorporating in it the compensator torque M_c and adjusting the virtual joint stiffness matrix $\mathbf{K}_0$ that here depends on the second joint variable q_2 only.

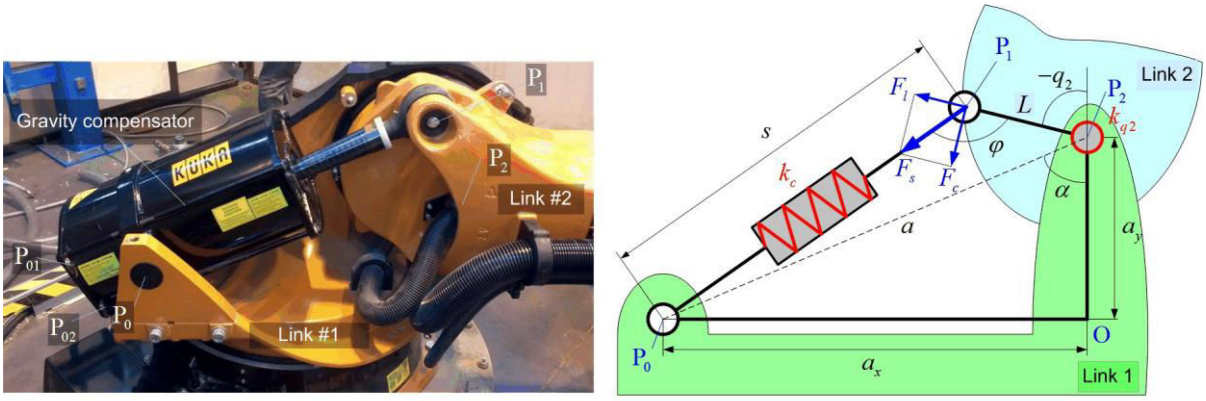

(a) gravity compensator of KUKA KR-270 robot (b) model of gravity compensator

Figure 3.15 Gravity compensator and its model

The compensator geometrical model includes three node points P_0, P_1, P_2, where two distances $|P_1,P_2|$, $|P_0,P_2|$ are constants and the third one $|P_0,P_1|$ varies and depends on q_2. Let us denote them $L=|P_1,P_2|$, $a=|P_0,P_2|$, $s=|P_0,P_1|$. Besides, let us introduce the angles α, φ and the distances a_x and a_y, whose geometrical meaning is clear from Figure 3.15b. Using these notations, the variable s describing the compensator spring deflection can be computed from the expression

$$s^2 = a^2 + L^2 + 2\,a\,L\cos(\alpha - q_2) \tag{3.63}$$

which defines the function $s(q_2)$. This mechanical design allows to balance the manipulator weight for any given configuration by adjusting the compensator spring preloading. It can be taken into account by introducing the zero-value of the compensator length s_0 corresponding to the unloaded spring. Under this assumption, the compensator force applied to the node P_1 can be expressed as follows

$$F_s = K_c\,(s - s_0) \tag{3.64}$$

where K_c is the compensator spring stiffness. Further, the angle φ between the compensator links P_0P_1 and P_1P_2 (see Figure 3.15) can be found from the expression

$$\sin\varphi = a/s\sin(\alpha - q_2) \tag{3.65}$$

which allows us to compute the compensator torque M_c applied to the second joint

$$M_c = K_c\,(1 - s_0 / s)\,a\,L\sin(\alpha - q_2) \tag{66}$$

Upon differentiation of the latter expression with respect to q_2, the equivalent stiffness of the second joint (comprising both the manipulator and compensator stiffnesses) can be expressed as:

$$K_{\theta_2} = K_{\theta_2}^0 + K_c \, a L \, \eta_{q_2} \tag{3.67}$$

where the coefficient η_{q_2} is expressed as follows

$$\eta_{q_2} = \frac{s_0}{s}\left(\frac{aL}{s^2}\sin^2(\alpha - q_2) + \cos(\alpha - q_2) \right) - \cos(\alpha - q_2) \tag{3.68}$$

and highly depends on the joint variable q_2 and the initial preloading in the compensator spring described by s_0. To illustrate this property, Figure 3.16 presents a set of curves $\eta(q_2)$ obtained for different values of s_0 (the remaining parameters α, a, L correspond to robot KUKA KR-270 studied in the experimental part of this work, see Chapter 4).

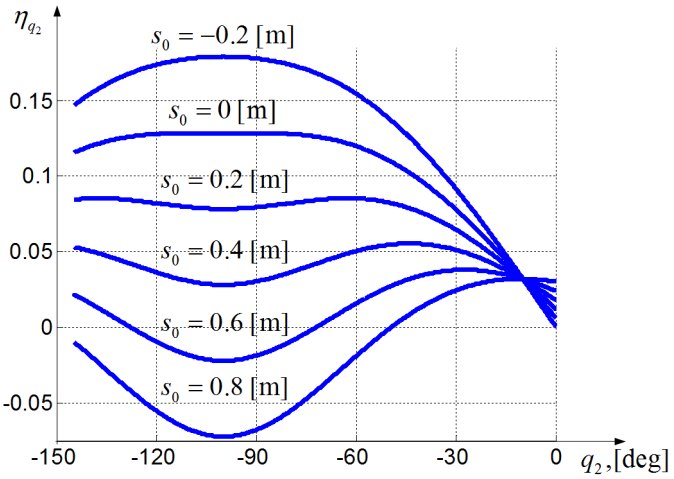

Figure 3.16 Variation of the gravity compensator impact on the equivalent stiffness of the second joint

Hence, using expression (3.67), it is possible to extend the classical stiffness model of the serial manipulator presented in Section 3.2 by modifying the virtual spring parameters in accordance with the compensator properties. While in this work, such an approach is used for the particular compensator type (spring-based, acting on the second joint), the similar idea can be applied to other compensator types. It should be mentioned that the geometrical and elastostatic models of a heavy manipulator with a gravity compensator should include some additional parameters (α, a, L and K_c, s_0 for the presented case) that are usually not included in datasheets. For this reason, the following subsections focus on the identification of the extended set of manipulator parameters.

3.6.2 Identification of gravity compensator geometric parameters

In contrast to strictly serial manipulator that can be treated as a principal mechanism of the considered robots (whose geometry is usually defined in datasheets and can be perfectly tuned by means of calibration), the geometric parameters concerning gravity compensators are usually not included in the technical documentation provided by the robot manufacturers. For this reason, this Subsection focuses on the identification of the geometrical parameters for the described compensator mechanism presented above.

A. Methodology

The geometric structure of the considered gravity compensator is presented in Figure 3.17. Its main parameters are denoted as L, a_x, a_y, where $a_x = a \cdot \sin\alpha$, $a_y = a \cdot \cos\alpha$ (see notations defined in

previous Subsection). As follows from the figure, the identification problem can be reduced to the determination of relative locations of points P_0 and P_1 with respect to P_2.

It is assumed that the measurement data are provided by the laser tracker whose "world" coordinate system is located at the intersection of the first and second actuated manipulator joints. The axes Y, Z of this system are aligned with the axes of joints #1 and #2 respectively, while the axis X is directed to ensure right-handed orthogonal basis. To obtain required data, there are several markers attached to the compensator mechanism (see Figure 3.17). The first one is located at point P_1, which is easily accessible and perfectly visible (the center of the compensator axis P_1 is exactly ticked on the fixing element). In contrast, for the point P_0, it is not possible to locate the marker precisely. For this reason, several markers P_{0i} are used that are shifted with respect to P_0, but located on the rigid component of the compensator mechanism (these markers are rotating around P_0 while the joint coordinate q_2 is actuated). It should be noted that for the adapted compensator geometric model (which is in fact a planar one), the marker location relative to the plane XY is not significant, since the identification algorithm presented in the following Subsections will ignore Z-coordinate.

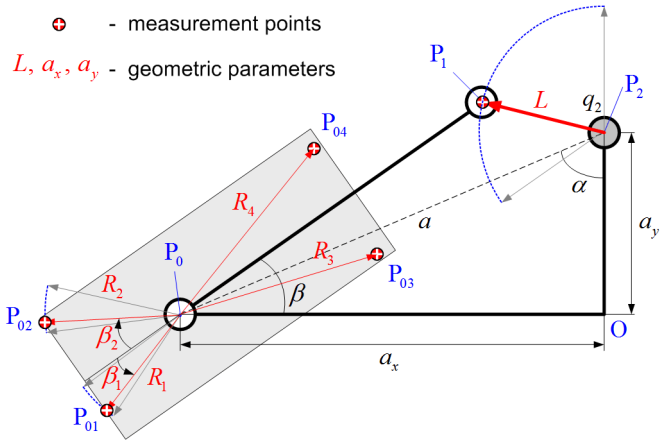

Figure 3.17 Geometric parameters of the gravity compensator and location of the measurement points labeled with markers

Using this setting, the identification problem is solved in two steps. The first step is devoted to the identification of the relative location of points P_1 and P_2. Here, for different values of the manipulator joint coordinates $\{q_{2i},\ i=\overline{1,m}\}$, the laser tracker provides the set of vectors $\{\mathbf{p}_1^i\}$ describing the points that are located in an arc of the circle. After matching these points with a circle, one can obtain the desired value of L (circle radius) and the Cartesian coordinates $\mathbf{p}_2$ of point P_2 (circle center) with respect to the laser tracker coordinate system.

The second step deals with the identification of the relative location of points P_0 and P_2. Relevant information is extracted from two data sets $\{\mathbf{p}_{01}^i\}$ and $\{\mathbf{p}_{02}^i\}$ that are provided by the laser tracker while targeting at the markers P_{01} and P_{02}. Here, the points are matched to two circle arcs with the same center (explicitly assuming that the compensator model is planar), which yields the Cartesian coordinates $\mathbf{p}_0$ of the point P_0, also with respect to the laser tracker coordinate system. Finally, the desired values a_x, a_y are computed as a projection of the difference vector $\mathbf{a}=\mathbf{p}_2-\mathbf{p}_0$ on the corresponding axis of the coordinate system.

As follows from the presented methodology, a key numerical problem in the presented approach is the matching of the experimental points with a circle arc. It looks like a classical problem, however, there is a particularity here caused by availability of additional data $\{q_{2i}\}$ describing relative locations

of points $\left\{\mathbf{p}_1^i\right\}$. This feature allows us to reformulate the identification problem and to achieve higher accuracy compared with the traditional approach.

B. Identification algorithms

The above presented methodology requires solution of two identification problems. The first one is aimed at approximating of a given set of points (with additional arc angle argument) with an arc circle, which provides the circle center and the circle radius. The second problem deals with an approximation of several sets of points by corresponding number of circle arcs with the same center. Let us consider them sequentially.

Algorithm #1 To match the given set of points $\left\{\mathbf{p}_i\right\}$ with additional set of angles $\left\{q_i\right\}$ with a circle arc, let us define the affine mapping

$$\mathbf{p}_i = \mu \mathbf{R} \mathbf{u}_i + \mathbf{t} \tag{3.69}$$

where $\mathbf{u}_i = [\cos q_i,\ \sin q_i,\ 0]^T$ denotes the set of reference points located on the unit circle whose distribution on the arc is similar to $\mathbf{p}_i$, μ is the scaling factor that defines the desired circle radius, $\mathbf{R}$ is the orthogonal rotation matrix, $\mathbf{t}$ is the vector of the translation that defines the circle center. It is worth mentioning that such formulation has an advantage (in terms of accuracy) comparing to a traditional circle approximation and it is a generalization of Procrustes problem known from the matrix analysis.

Using equation (3.69), the identification can be reduced to the following optimization problem

$$F = \sum_{i=1}^{m} \left(\mathbf{p}_i - \mu \mathbf{R} \mathbf{u}_i - \mathbf{t}\right)^T \left(\mathbf{p}_i - \mu \mathbf{R} \mathbf{u}_i - \mathbf{t}\right) \to \min_{\mu, \mathbf{R}, \mathbf{t}} \tag{3.70}$$

which should be solved subject to the orthogonality constraint $\mathbf{R}^T \mathbf{R} = \mathbf{I}$. After differentiation with respect to $\mathbf{t}$, the latter variable can be expressed as

$$\mathbf{t} = m^{-1} \sum_{i=1}^{m} \mathbf{p}_i - \mu m^{-1} \mathbf{R} \sum_{i=1}^{m} \mathbf{u}_i \tag{3.71}$$

and leads to the simplification of (3.70) to

$$F = \sum_{i=1}^{m} \left(\hat{\mathbf{p}}_i - \mu \mathbf{R} \hat{\mathbf{u}}_i\right)^T \left(\hat{\mathbf{p}}_i - \mu \mathbf{R} \hat{\mathbf{u}}_i\right) \to \min_{r, \mathbf{R}} \tag{3.72}$$

where

$$\hat{\mathbf{p}}_i = \mathbf{p}_i - m^{-1} \sum_{i=1}^{m} \mathbf{p}_i; \qquad \hat{\mathbf{u}}_i = \mathbf{u}_i - m^{-1} \sum_{i=1}^{m} \mathbf{u}_i \tag{3.73}$$

Further, differentiation with respect to μ yields to

$$\mu = \sum_{i=1}^{m} \hat{\mathbf{p}}_i^T \mathbf{R} \hat{\mathbf{u}}_i \Big/ \sum_{i=1}^{m} \hat{\mathbf{u}}_i^T \hat{\mathbf{u}}_i \tag{3.74}$$

Finally, after relevant substitutions the objective function can be presented as

$$F = \sum_{i=1}^{m} \hat{\mathbf{p}}_i^T \hat{\mathbf{p}}_i - \left(\sum_{i=1}^{m} \hat{\mathbf{u}}_i^T \hat{\mathbf{u}}_i \right)^{-1} \left(\sum_{i=1}^{m} \hat{\mathbf{p}}_i^T \mathbf{R} \hat{\mathbf{u}}_i \right)^2 \to \min_{\mathbf{R}} \tag{3.75}$$

where the unknown matrix $\mathbf{R}$ must satisfy the orthogonality constraint $\mathbf{R}^T \mathbf{R} = \mathbf{I}$. Since the matrix $\mathbf{R}$ is included in the second term only, the problem can be further simplified to

$$F' = \sum_{i=1}^{m} \hat{\mathbf{p}}_i^T \mathbf{R} \hat{\mathbf{u}}_i = \operatorname{trace}\left(\mathbf{R} \sum_{i=1}^{m} \hat{\mathbf{u}}_i \hat{\mathbf{p}}_i^T \right) \to \max_{\mathbf{R}} \tag{3.76}$$

and can be solved using SVD-decomposition of the matrix

$$\sum_{i=1}^{m} \widehat{\mathbf{u}}_i \widehat{\mathbf{p}}_i = \mathbf{U}\boldsymbol{\Sigma}\mathbf{V}^T \tag{3.77}$$

where the matrices $\mathbf{U}, \mathbf{V}$ are orthogonal and $\boldsymbol{\Sigma}$ is the diagonal matrix of the singular values. Further, using the same approach as for the Procrustes problem, it can be proved that the desired rotation matrix can be computed as

$$\mathbf{R} = \mathbf{V}\mathbf{U}^T \tag{3.78}$$

which sequentially allows us to find the scaling factor μ defining the arc radius and the vector $\mathbf{t}$ defining the arc center.

Algorithm #2. The second problem aims at approximating several point sets $\left\{\mathbf{p}_i^1\right\},...,\left\{\mathbf{p}_i^k\right\}$ by corresponding number of concentric circle arcs with the same center $\mathbf{p}_0$. It should be noted that here the data set $\left\{q_i\right\}$ is not useful, since the required angles $\left\{\beta_i\right\}$ are not measured directly and cannot be computed without having exact compensator geometry. In this case, the objective function can be written in a straightforward way

$$F = \sum_{j=1}^{k} \sum_{i=1}^{m} \left(R_j^2 - \left(\mathbf{p}_i^j - \mathbf{p}_0\right)^T \left(\mathbf{p}_i^j - \mathbf{p}_0\right) \right)^2 \to \min_{\mathbf{p}_0, R_j} \tag{3.79}$$

where R_j denotes the *j*-th ark radius and $\mathbf{p}_0^j$ is the corresponding center point. However, for this formulation it can be easily proved that the optimization problem (3.79) does not lead to a unique solution. In fact, it gives the rotation axis passing through the center points $\mathbf{p}_0^j$, which can be expressed as

$$\mathbf{p}_0^j = \mathbf{p}_c + \xi_j \mathbf{n} \tag{3.80}$$

where $\mathbf{n}$ is the axis direction vector, $\mathbf{p}_c$ is a point belonging to the axis, and ξ_j are corresponding scalar factors.

To solve problem (3.79), first the objective function F can be differentiated with respect to R_j^2 that yields the following expression for the arc radius

$$R_j^2 = m^{-1} \sum_{i=1}^{m} \left(\mathbf{p}_i^j - \mathbf{p}_0^j\right)^T \left(\mathbf{p}_i^j - \mathbf{p}_0^j\right) \tag{3.81}$$

Further, after relevant substitution, the objective fuction can be rewritten as

$$F = \sum_{j=1}^{k} \sum_{i=1}^{m} \left(2\left(\mathbf{p}_c + \xi_j \mathbf{n}\right)^T \widehat{\mathbf{p}}_i^j - \widehat{s}_i^j \right)^2 \to \min \tag{3.82}$$

where

$$\widehat{\mathbf{p}}_i^j = \mathbf{p}_i^j - m^{-1} \sum_{l=1}^{m} \mathbf{p}_l^j; \qquad \widehat{s}_i^j = \mathbf{p}_i^{jT} \mathbf{p}_i^j - m^{-1} \sum_{l=1}^{m} \mathbf{p}_i^{jT} \mathbf{p}_i^j \tag{3.83}$$

To solve the above mentioned ambiguity, additional objectives should be considered

$$R_j^2 \to \min_{R_j} \tag{3.84}$$

which leads to the following solution for the scalar parameter

$$\xi_j = \left(-\mathbf{p}_c + m^{-1} \sum_{i=1}^{m} \mathbf{p}_i^j \right)^T \mathbf{n} \tag{3.85}$$

Further, after differentiation (3.82) with respect to $\mathbf{p}_c$

$$\left(\sum_{j=1}^{k} \sum_{i=1}^{m} \widehat{\mathbf{p}}_i^j \widehat{\mathbf{p}}_i^{jT} \right) \mathbf{p}_c = \frac{1}{2} \sum_{j=1}^{k} \sum_{i=1}^{m} \widehat{s}_i^j \widehat{\mathbf{p}}_i^j \tag{3.86}$$

one can compute the point on the desired rotational axis as

$$\mathbf{p}_c = \frac{1}{2}\left(\sum_{j=1}^{k}\sum_{i=1}^{m}\hat{\mathbf{p}}_i^j\hat{\mathbf{p}}_i^{jT}\right)^{-1}\sum_{j=1}^{k}\sum_{i=1}^{m}\hat{s}_i^j\hat{\mathbf{p}}_i^j \tag{3.87}$$

The remaining unknown vector $\mathbf{n}$ can be obtained from the orthogonality constraints $\left(\mathbf{p}_i^j - \mathbf{p}_0^j\right)^T\mathbf{n} = 0$, $i = \overline{1,m}$, $j = \overline{1,k}$ that leads to the following optimization problem

$$f = \sum_{j=1}^{k}\sum_{i=1}^{m}\left(\left(\mathbf{p}_i^j - \mathbf{p}_0^j\right)^T\mathbf{n}\right)^2 \to \min_{\mathbf{n}} \tag{3.88}$$

that after substitution in it (3.80), (3.85) and (3.87) gives

$$f = \sum_{j=1}^{k}\sum_{i=1}^{m}\left(\hat{\mathbf{p}}_i^{jT}\mathbf{n}\right)^2 \to \min_{\mathbf{n}} \tag{3.89}$$

Further, differentiation (3.89) with respect to $\mathbf{n}$, the optimization problem reduces to the solving following homogeneous linear equation system

$$\sum_{j=1}^{k}\sum_{i=1}^{m}\hat{\mathbf{p}}_i^j\,\hat{\mathbf{p}}_i^{jT}\,\mathbf{n} = \mathbf{0} \tag{3.90}$$

Non-trivial solution of this system can be found using the singular value decomposition of the matrix $\sum_{j=1}^{k}\sum_{i=1}^{m}\hat{\mathbf{p}}_i^j\,\hat{\mathbf{p}}_i^{jT}$

$$\sum_{j=1}^{k}\sum_{i=1}^{m}\hat{\mathbf{p}}_i^j\,\hat{\mathbf{p}}_i^{jT} = \mathbf{U}\boldsymbol{\Sigma}\mathbf{V}^T \tag{3.91}$$

where the vector $\mathbf{n}$ is the last column of the matrix $\mathbf{V}$. It should be mentioned that practical application of the latter expression is essentially simplified by the adapted assumption concerning orientation of the reference coordinate system (see previous subsection), the direction of the identified rotation axis is close to Z-direction.

Hence, the developed algorithms allow us to identify the compensator geometrical parameters L, a_x, a_y that are directly related to the above mentioned rotation center points P_0, P_2 and corresponding radii. In Chapter 4 these algorithms will be applied to the processing of the experimental data.

C. Design of calibration experiments

For the considered identification problem, the design variables are the set of angles $\{\mathbf{q}_{2i}\}$ and the marker locations. The objective functions to be minimized are computed via the covariance matrix that describes the identification errors for the geometrical parameters L and a to be estimated. Since the two identification algorithms are independent, selection of the optimal configurations $\{\mathbf{q}_{2i}\}$ and marker locations can be considered sequentially.

Assuming that each experiment includes the additive measurement errors in the Cartesian coordinates $\boldsymbol{\varepsilon}_i$, expression (3.74) allows us to present the variance of the parameter μ in the following way

$$\mathrm{var}(\mu) = E\left(\sum_{i=1}^{m}\hat{\mathbf{u}}_i^T\mathbf{R}^T\boldsymbol{\varepsilon}_i\sum_{i=1}^{m}\boldsymbol{\varepsilon}_i^T\mathbf{R}\hat{\mathbf{u}}_i\right)\Big/\left(\sum_{i=1}^{m}\hat{\mathbf{u}}_i^T\hat{\mathbf{u}}_i\right)^2 \tag{3.92}$$

where $E(.)$ denotes the expectation and the orthogonal matrix $\mathbf{R}$ defines the orientation of the base coordinate system. Following usual assumption concerning the measurement errors (independent identically distributed, with zero expectation and standard deviation σ^2 for each coordinate) that allows us to present the covariance error matrix as $E\left(\boldsymbol{\varepsilon}_i\,\boldsymbol{\varepsilon}_i^T\right) = \sigma^2\mathbf{I}$, the above expression (3.92) reduces to

$$\mathrm{var}(\mu) = \sigma^2\Big/\left(\sum_{i=1}^{m}\hat{\mathbf{u}}_i^T\hat{\mathbf{u}}_i\right) \tag{3.93}$$

Further, it can be proved that $\sum_{i=1}^{m} \hat{\mathbf{u}}_i^T \hat{\mathbf{u}}_i = m$. So, the variance (3.93) does not depend on the angles q_{2i}. Thus, the identification accuracy for the parameter L depends on the number of experiments only.

For the remaining geometrical parameter a, the identification error depends on the estimation precision of relative location of the points P_2 and P_0. Since relevant identification algorithms employ independent measurement data, the variance $\mathrm{var}(a)$ can be computed as the sum of the traces of $\mathrm{cov}(\mathbf{t}_2)$ and $\mathrm{cov}(\mathbf{t}_0)$, where $\mathbf{t}_2$ and $\mathbf{t}_0$ are the vectors of Cartesian coordinates for the points P_2 and P_0.

For point P_2, expression (3.71) leads to the following covariance matrix

$$\mathrm{cov}(\mathbf{t}_2) = m^{-2} E\left(\sum_{i=1}^{m} \boldsymbol{\varepsilon}_i \sum_{i=1}^{m} \boldsymbol{\varepsilon}_i^T + \mu^2 \mathbf{R} \sum_{i=1}^{m} \mathbf{u}_i \sum_{i=1}^{m} \mathbf{u}_i^T \mathbf{R}^T \right) \tag{3.94}$$

which can be further simplified to

$$\mathrm{cov}(\mathbf{t}_2) = m^{-1}\sigma^2 \left(\mathbf{I} + m^{-2} \sum_{i=1}^{m} \mathbf{u}_i \sum_{i=1}^{m} \mathbf{u}_i^T \right) \tag{3.95}$$

This simplification is based on the above derived expressions $E\left(\sum_{i=1}^{m} \boldsymbol{\varepsilon}_i \sum_{i=1}^{m} \boldsymbol{\varepsilon}_i^T \right) = m\sigma^2 \mathbf{I}$ and $E(\mu^2) = \sigma^2 / m$ and on the assumption that z-axis of the coordinate system is directed along the second joint axis. Hence, for the point P_2, the optimization problem that is related to the design of calibration experiment, can be formulated as

$$F = \left(\sum_{i=1}^{m} \cos q_{2i} \right)^2 + \left(\sum_{i=1}^{m} \sin q_{2i} \right)^2 \to \min_{q_{2i}} \tag{3.96}$$

This problem should be solved taking into account joint limits of the industrial robot. In the case when the range of angles q_2 is over π, it is possible to achieve zero value of this objective since equations $\sum_{i=1}^{m} \cos q_{2i} = 0$ and $\sum_{i=1}^{m} \sin q_{2i} = 0$ are solvable. It should be noted similar equations arise in calibration experiment design for some robots without gravity compensators and have been studied in details in a previous work (Klimchik, 2011).

For the point P_0, similar expression includes a set of the angles β_i that can be recomputed to the joint angles q_{2i} requires for the manipulator control (see Figure 3.17). Here, it is reasonable to find optimal marker locations on the rigid part of the gravity compensator. It can be proven that using these assumptions, the design of experiment reduces to the following optimization problem

$$F = \left(\sum_{j=1}^{k} \cos \beta_j \right)^2 + \left(\sum_{j=1}^{k} \sin \beta_j \right)^2 \to \min_{\beta_j} \tag{3.97}$$

where β_j are the angles around the point P_0 between the compensator spring and the j-th marker location. It is clear that in this case the best solution is produced by similar equations $\sum_{j=1}^{k} \cos \beta_j = 0$ and $\sum_{j=1}^{k} \sin \beta_j = 0$, but contrary to (3.96), this problem can be easily solved by locating the markers on the opposite sides of the compensator rotation axis.

Thus, the calibration experiment design that produces the sets of the optimal manipulator configurations and the marker locations described by the variables $\{q_{2i}\}$ and $\{\beta_j\}$ respectively, is reduced to the solution of the above presented trigonometric equations that allows us essentially increase the calibration accuracy.

3.6.3 Identification of gravity compensator elastostatic parameters

In contrast to geometrical calibration, where the manipulator and compensator can be considered independently, in elastostatic calibration the corresponding equations cannot be separated and the model parameters should be identified simultaneously. This Subsection gives general ideas of

the developed methodology and identification algorithms, as well as the relevant calibration experiment design.

A. Methodology

In the frame of the adapted VJM-based modeling approach the desired stiffness parameters describe elasticity of the virtual springs located in the actuated joints of the manipulator, and also the elasticity and preloading of the compensator spring (see Subsection 3.6.1 for details). Let us denote them as k_{θ_j}, $j=\overline{1,6}$ for the manipulator joint compliances and k_c, s_0 for the compliance and preloading of the compensator.

To find these parameters, the manipulator sequentially passes through several measurement configurations where the external loading is applied to the special end-effector described in Figure 3.18 (it allows to generate both forces and torques applied to the manipulator, see Section 3.3 for detailed description for this end-effector). Using the laser tracker, the Cartesian coordinates of the reference points are measured twice, before and after loading. To increase identification accuracy, it is preferable to use several reference points (markers) and to apply the loading of the maximum allowed magnitude. It is worth mentioning that in order to avoid numerical singularities, the direction of the external loading should not be the same for all experiments (in spite of the fact that the gravity-based loading is the most attractive from the practical point of view). Thus, the calibration experiments yield the dataset that includes values of the manipulator joint coordinates $\{\mathbf{q}_i\}$, applied wrenches $\{\mathbf{w}_i\}$ and corresponding deflections of the reference points $\{\Delta\mathbf{p}_i\}$. Using these data, the elastostatic parameters k_{θ_j}, $j=\overline{1,6}$ and k_c, s_0 should be identified.

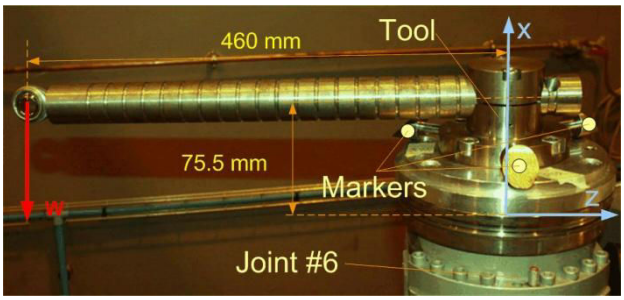

Figure 3.18 End-effector used for elastostatic calibration experiments

B. Identification algorithm

To take into account the compensator influence while retaining our previous approach developed for serial robots without compensator, it is proposed to include in the second joint an equivalent virtual spring with non-linear stiffness depending on the joint variable q_2 (see Eq.(3.67)). Using this idea, it is convenient to consider several independent parameters $k_{\theta_{2i}}$ corresponding to each value of q_2. This allows us to obtain linear form of the identification equations that can be easily solved using the standard least-square technique.

Let us denote the set of desired parameters $k_1,(k_{21},k_{22}...),k_3,...,k_6$ as the vector $\mathbf{k}$, which allows us to present the relevant force-deflection relations in the form

$$\Delta\mathbf{p}_i=\mathbf{B}_i^{(p)}\mathbf{k} \tag{3.98}$$

where matrices $\mathbf{B}_i^{(p)}$ are composed of the elements of the observation matrix

$$\mathbf{A}_{ki}=\left[\mathbf{J}_{\theta,1i}\mathbf{J}_{\theta,1i}{}^T\mathbf{w}_i,...,\mathbf{J}_{\theta,n\theta i}\mathbf{J}_{\theta,n\theta i}{}^T\mathbf{w}_i\right]\quad(i=\overline{1,m}) \tag{3.99}$$

that is usually used in stiffness analysis of serial manipulators (See Section 3.2). Here, $\mathbf{J}_{0,n0i}$ denotes the manipulator Jacobian column, $\mathbf{w}_i$ is the applied external force, and superscript '(p)' stands for the Cartesian coordinates (position without orientation). It is clear that transformation from $\mathbf{A}_{ki}$ to $\mathbf{B}_i^{(p)}$ is rather trivial and is based on the extraction from $\mathbf{A}_{ki}$ the first three lines and inserting in it several zero columns.

Using these notations, the elastostatic parameters identification can be reduced to the following optimization problem

$$F = \sum_{i=1}^{m} (\mathbf{B}_i^{(p)}\mathbf{k} - \Delta\mathbf{p}_i)^T (\mathbf{B}_i^{(p)}\mathbf{k} - \Delta\mathbf{p}_i) \to \min_{k_j, k_c, \rho_0} \tag{3.100}$$

which leads to the following solution

$$\mathbf{k} = \left(\sum_{i=1}^{m} \mathbf{B}_i^{(p)^T} \mathbf{B}_i^{(p)} \right)^{-1} \cdot \left(\sum_{i=1}^{m} \mathbf{B}_i^{(p)^T} \Delta\mathbf{p}_i \right) \tag{3.101}$$

where the parameters $k_1, k_3, ..., k_6$ describe the compliance of the virtual joints #1,#3,...#6, while the other parameters k_{21}, k_{22}... present an auxiliary dataset allowing to separate the compliance of the joint #2 and the compensator parameters k_c, ρ_0. Using Eq.(3.67), the desired expressions can be written as

$$\left[K_{\theta_2}^0 \quad K_c \quad s_0 \cdot K_c \right]^T = \left(\sum_{i=1}^{m_q} \mathbf{C}_i^T \mathbf{C}_i \right)^{-1} \left(\sum_{i=1}^{m_q} \mathbf{C}_i^T K_{\theta_{2i}} \right) \tag{3.102}$$

where m_q is the number of different angles q_2 in the experimental data,

$$\mathbf{C}_i = \left[1 \quad -aL \cdot \cos\gamma_i \quad aL/s \cdot \left(aL/s^2 \cdot \sin^2\gamma_i + \cos\gamma_i \right) \right] \tag{3.103}$$

here $\gamma_i = \alpha - q_{2i}$. Thus, the proposed modification of the previously developed calibration technique allows us to find the manipulator and compensator parameters simultaneously. An open question, however, is how to find the set of measurement configurations that ensure the lowest impact of the measurement noise.

C. Design of calibration experiments

The main idea of the calibration experiment design is to select a set of robot configurations $\{\mathbf{q}_i\}$ (and corresponding external loadings $\{\mathbf{w}_i\}$) that ensure the best identification accuracy. The key issue here is the ranging of different plans in accordance with the prescribed performance measure. In this work, it is proposed to use the industry oriented performance measure that evaluates the calibration plan quality. Its physical meaning is the robot positioning accuracy (under the loading), which is achieved after compliance error compensation based on the identified elastostatic parameters.

Using the above adapted notations and assuming that each experiment includes the additive measurement error $\boldsymbol{\varepsilon}_i$, it can be proved that the covariance matrix for the desired parameters estimates $\hat{\mathbf{k}}$ can be expressed as

$$\mathrm{cov}(\hat{\mathbf{k}}) = \left(\sum_{i=1}^{m} \mathbf{B}_i^{(p)^T} \mathbf{B}_i^{(p)} \right)^{-1} E\left(\sum_{i=1}^{m} \mathbf{B}_i^{(p)^T} \boldsymbol{\varepsilon}_i^T \boldsymbol{\varepsilon}_i \mathbf{B}_i^{(p)} \right) \left(\sum_{i=1}^{m} \mathbf{B}_i^{(p)^T} \mathbf{B}_i^{(p)} \right)^{-1} \tag{3.104}$$

Following also usual assumption concerning the measurement errors (independent identically distributed, with zero expectation and standard deviation σ^2 for each coordinate), the above equation can be simplified to

$$\mathrm{cov}(\hat{\mathbf{k}}) = \sigma^2 \left(\sum_{i=1}^{m} \mathbf{B}_i^{(p)^T} \mathbf{B}_i^{(p)} \right)^{-1} \tag{3.105}$$

Hence, the impact of the measurement errors on the accuracy of the identified parameters $\mathbf{k}$ is defined by the matrix $\sum_{i=1}^{m} \mathbf{B}_i^{(p)T} \mathbf{B}_i^{(p)}$.

It is obvious that in practice the most essential is not the accuracy of the parameters identification, but the accuracy of the robot positioning achieved using these parameters in control system. Taking into account that this accuracy highly depends on the robot configuration (and varies throughout the workspace), it is proposed to evaluate the calibration accuracy in a certain given "test-pose" provided by the user. For the considered application, the test pose is related to the typical machining configuration $\mathbf{q}_0$ and corresponding external loading $\mathbf{w}_0$ related to the technological process. Let us denote the mean square value of the mentioned positioning error as ρ_0^2 and the matrix $\mathbf{A}_i^{(p)}$ (see Eq.(3.99)) corresponding to this test pose as $\mathbf{A}_0^{(p)}$.

It should be noted that that the proposed approach operates with a specific structure of the parameters included in the vector $\mathbf{k}$, where the second joint is presented by several components $k_{21}, k_{22}...$ while the other joints are described by a single parameters $k_1, k_3 ... k_6$. This motivates further re-arrangement of the vector $\mathbf{k}$ and replacing it by several vectors $\mathbf{k}_j = (k_1, k_{2j}, k_3, ... k_6)$ of size 6×1 . Using this notation, the above mentioned performance measure can be expressed as

$$\rho_0^2 = \sum_{j=1}^{m_q} \mathrm{E}\left(\delta \mathbf{k}_j{}^T \mathbf{A}_0^{(p)T} \mathbf{A}_0^{(p)} \delta \mathbf{k}_j \right) \tag{3.106}$$

where $\delta \mathbf{k}_j$ is the elastostatic parameters estimation error caused by the measurement noise for q_{2j} . Further, after substituting $\delta \mathbf{p}^T \delta \mathbf{p} = \mathrm{trace}\left(\delta \mathbf{p} \delta \mathbf{p}^T \right)$ and taking into account that $\mathrm{E}(\delta \mathbf{k}_j \delta \mathbf{k}_j{}^T) = \mathrm{cov}(\mathbf{k}_j)$, the performance measure ρ_0^2 can be presented as

$$\rho_0^2 = \sigma^2 \mathrm{trace}\left(\mathbf{A}_0^{(p)} \sum_{j=1}^{m_q} \left(\sum_{i=1}^{m} \mathbf{A}_i^{j(p)T} \mathbf{A}_i^{j(p)} \right)^{-1} \mathbf{A}_0^{(p)T} \right) \tag{3.107}$$

Based on this performance measure, the calibration experiment design can be reduced to the following optimization problem

$$\mathrm{trace}\left(\mathbf{A}_0^{(p)} \sum_{j=1}^{m_q} \left(\sum_{i=1}^{m} \mathbf{A}_i^{j(p)T} \mathbf{A}_i^{j(p)} \right)^{-1} \mathbf{A}_0^{(p)T} \right) \to \min_{\{\mathbf{q}_i, \mathbf{w}_i\}} \tag{3.108}$$

whose solution gives a set of the desired manipulator configurations and corresponding external loadings. It is evident that its analytical solution can hardly be obtained and a numerical approach is the only reasonable one. More detailed description of the efficient technique providing optimal measurement configurations can be found in subsection 3.5.4.

Summarizing this Section in general, it is worth mentioning that its main contributions lie in the development of the modeling methods and identification algorithms for both geometric and elastostatic parameters of the gravity compensator. To increase the calibration accuracy, the design of experiments has been used that deals with proper selection of the measurement configurations and marker point locations. Both geometric and elastostatic parameters identification results as well as relevant accuracy analysis will be provided in the following chapter. The advantages of the developed approach will be illustrated by experimental study of a KUKA KR-270 industrial robot.

3.7 SUMMARY

The chapter is devoted to the enhancement of modeling, measurement and identification methods employed in the elastostatic calibration of heavy industrial robot of serial and quasi-serial architecture. The main contributions are in the area of calibration experiments design, which is aimed at the manipulator positioning accuracy improvement using limited number of measurements. Compared to the previous Chapter, it is assumed that the manipulator is subject of external and/or internal loadings that cause non-negligible deflections in links/joints. In contrast to other works, the developed approach is based on the proposed industry-oriented performance measure and is able to take into account the influence of the gravity compensator on the manipulator elastostatic properties. To avoid the problem of least-square objective non-homogeneity, the calibration experiments are based on the enhanced partial pose measurement method.

In more details, the contributions of Chapter 3 can be summarized as

(i) Efficient technique for optimal measurement configurations selection in elastostatic calibration, which is based on the industry-oriented performance measure that evaluates the robot positioning accuracy after the compliance errors compensation. Corresponding optimal measurement configurations are obtained using dedicated numerical procedures that are able to take into account physical constraints and to use advantages of hybrid and parallel computing. It has been also shown that in practice, it is reasonable to replace a strictly optimal solution by a set of quasi-optimal ones generated by simple repetition (or superposition) of measurement configurations obtained for lower-dimensional cases.

(ii) Stiffness modeling approach for quasi-serial manipulators with gravity compensators creating closed-loop chains, which is based on extension of conventional stiffness model of serial manipulator by including in it some configuration dependent parameters (that are usually treated as constants).

(iii) Methodology for calibration of the gravity compensator models that is able to identify both geometric and elastostatic parameters, which in contrast to other works, is based on the singular value decomposition and uses measurement information obtained from both position and joint sensors.

Among limitations of the obtained results that give directions for future works, it should be mentioned the model completeness issues, which in this work has been not studied in full-scale (it was assumed that the manipulator stiffness can be described by a set of one-dimensional virtual springs localized in the actuated joints). Nevertheless, for the robot studied in this work, the considered model allowed us to compensate more than 90% of the compliance errors.

The main results of Chapter 3 have been presented in international conferences (Wu et al., 2012), (Klimchik et al., 2013d), (Klimchik et al., 2013e) (Klimchik et al., 2014), and have been published in the international journals , (Klimchik et al., 2012a; Klimchik et al., 2012c).

CHAPTER 4

EXPERIMENTAL VALIDATIONS OF DEVELOPED OPTIMAL POSE SELECTION TECHNIQUES FOR ROBOT CALIBRATION

4.1 The experimental work-cell environment 135
4.2 Geometric calibration experiments for KUKA KR-270 industrial robot 137
4.2.1 Experimental setup and measurement procedure 137
4.2.2 Optimal measurement pose selection for geometric calibration 140
4.2.3 Identification of manipulator geometric parameters 144
4.2.4 Analysis of the identification results for geometric calibration 147
4.3 Elastostatic calibration experiments for KUKA KR-270 industrial robot 149
4.3.1 Experimental setup and measurement procedure 149
4.3.2 Identification of the gravity compensator geometry 153
4.3.3 Identification of manipulator elastostatic parameters using the gravity force 156
4.3.4 Identification of manipulator elastostatic parameter using work-cell constraints 161
4.3.5 Analysis of the identification results for elastostatic calibration 164
4.4 Validation of the developed pose selection technique 167
4.4.1 Validation methodology 167
4.4.2 Validation of the developed technique for geometric calibration 170
4.4.3 Validation of the developed technique for elastostatic calibration 171
4.5 Summary 174

This chapter deals with experimental validation of the developed optimal pose selection technique employed in the calibration procedure, where particular attention is paid to the positioning accuracy improvement of KUKA KR-270 industrial robot (that includes a gravity compensator). It presents the work-cell environment where the calibration experiments are carried out. For both the manipulator geometric and elastostatic calibration, the experimental setups and measurement procedures, optimal measurement configurations and relevant identification results as well as the accuracy analysis are provided. In contrast to other works, the manipulator accuracy is evaluated not only for the measurement configurations, but also for a wider set of configurations (different from those used for calibration)

4.1 THE EXPERIMENTAL WORK-CELL ENVIRONMENT

As follows from previous chapters, efficiency of manipulator geometric and elastostatic calibration can be essentially improved by means of proper selection of measurement configurations used in calibration experiments. In this work, a number of numerical techniques have been proposed that allow us to reduce the measurement noise impact and to compensate the robot positioning errors in the best way. To show the benefits of these techniques and their attractiveness for industrial applications, this chapter presents some experimental results that deal with geometric and elastostatic calibration of industrial robot KUKA KR-270 and employ theoretical contributions of this thesis.

The manufacturing cell where the examined robot has been installed is presented in Figure 4.1, it is located at IUT de Nantes, Carquefou. The work-cell includes a 6-dof industrial serial robot KUKA KR-270 with six revolute joints, a machining table, a vertical tool for mounting the pieces. Their relative locations as well as the main dimensions of the work-cell are shown in Figure 4.1. It should be noted that for geometric calibration, the above mentioned equipment (that can be also treated as the obstacles) cause some limits for the external measurement device placement. In the case of elastostatic calibration, they may also affect the possibility of force application (mounting the weight without collisions with these objects).

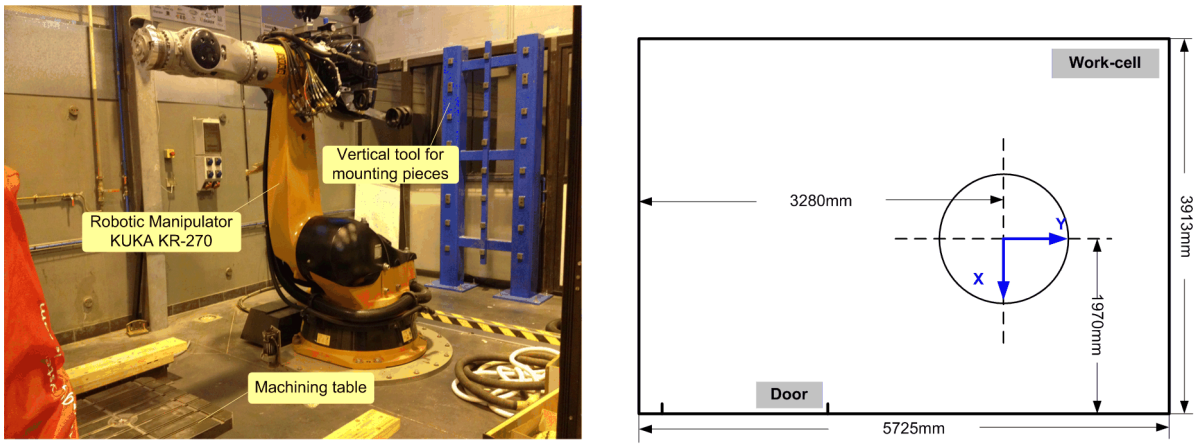

(a) General view (b) Main dimensions

Figure 4.1 The experimental work-cell environment: (a) general view; (b) main dimensions

Taking into account particularities of the technological process considered in this work (see Section 1.1 for details), the manipulator test-pose (configuration $\mathbf{q}_0$) has been defined in the location where the best robot positioning accuracy should be achieved:

$$\mathbf{q}_0 = (76.7°, -56.9°, 89.3°, 45.1°, 76°, 57.2°) \tag{4.1}$$

It is worth mentioning that similar configuration has been used in previous work (Dumas, 2011) to evaluate the quality of the robot-based machining. Corresponding machining wrench used in this process can be computed as

$$\mathbf{w}_0 = (0,\ 280\text{N},\ -180\text{N},\ 0,\ 0,\ 0) \tag{4.2}$$

Below, it will be considered as the test-loading. From the identification theory point of view, these two vector define the input parameters for the calibration experiment design using the proposed test-pose based approach. Corresponding graphic presentation generated using robotic CAD system

Robotmaster is shown in Figure 4.2. It illustrates the defined test-pose, the workpiece location and the machining tool that is used in the milling application. It should be noted that for the considered problem, the geometry of the particular machining tool (including a spindle and milling tool) should be taken into account in relevant experiment design.

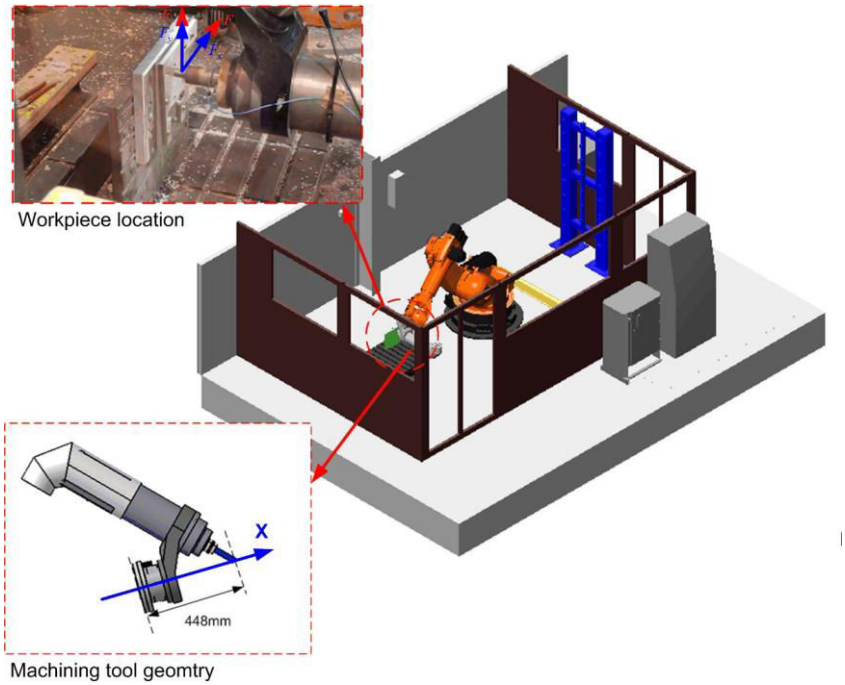

Figure 4.2 The machining configuration (test-pose) and the workpiece location

To achieve the highest robot positioning accuracy for the above defined test pose, corresponding calibration experiments design should take into account the particularities in robot kinematics and work-cell constraints. As shown in the above described experimental environment, relevant optimization problems of finding the optimal measurement configurations should be solved subject to the robot joint limits, the work-cell space limits, and particularly, the collisions between the force application equipment and work-cell obstacles in the case of elastostatic calibration. Another important problem is related to the manipulator gravity compensator, whose elastostatic properties are described by highly non-linear function. For this reason, relevant experiment design should employ sophisticated elastostatic model that takes into account the gravity compensator impact, aiming at identifying its configuration dependent compliance parameters.

Using this robotic cell, a number of experiments has been carried out in order to calibrate manipulator models employed in the error compensation algorithms. For all experiments, the manipulator measurement configurations have been optimized by applying techniques developed in Chapters 2 and 3. Relevant results are presented in Sections 4.2-4.4 that sequentially addresses the following problems:

(i) Calibration of the manipulator geometric parameters using the set of optimal measurement configurations obtained by means of techniques presented in Chapter 2.

(ii) Calibration of the manipulator elastostatic parameters using the set of optimal measurement configurations obtained by means of techniques presented in Chapter 3.

(iii) Validation of the identified manipulator parameters by evaluating the achieved robot positioning accuracy.

While presenting the experimental results, special attention will be also given to applicability of the developed techniques in real industrial environment.

4.2 GEOMETRIC CALIBRATION EXPERIMENTS FOR KUKA KR-270 INDUSTRIAL ROBOT

To confirm the applicability of the calibration techniques proposed in Chapter 2 and demonstrate their benefits from engineering point of view, this Section presents the experimental procedure, the identification results as well as the accuracy analysis for geometric calibration of the industrial robot KUKA KR-270.

4.2.1 Experimental setup and measurement procedure

To identify the desired geometric parameters, the manufacturing cell is equipped with some additional measuring devices that provide us with Cartesian coordinates of the references points for each manipulator configuration. Besides, the manipulator joint angles required for the identification procedure are obtained from the robot control system. So, entire experimental setup includes the following units:

- 6-dof KUKA KR-270 robotic manipulator whose geometric parameters should be identified (repeatability of this robot is 60 μm (Kuka), details concerning its kinematics are presented in Section 2.2);
- Robot control system KR-C2, which is used for changing the manipulator configurations and measuring the corresponding joint angles with precision ±0.0001°;
- Special measurement tool with three reference points located on the circle of radius 104 mm, this tool is attached to the manipulator mounting flange;
- Laser tracker Leica AT-901 that is used to measure the Cartesian coordinates of the reference point with a precision of 10 μm (Leica-geosystems);
- Laser tracker reflector that is sequentially attached to the reference points (with precision about 1 μm), it allows the measurement device to estimate the distances and compute the required Cartesian coordinates;
- Personal computer with dedicated software connected to the laser tracker, which is used for data logging and their transformation in the required form.

The experimental setup for manipulator geometric calibration is shown in Figure 4.3. It is worth mentioning that the calibration experiments are carried out in a limited area (smaller than the robot entire workspace) caused by the work-cell size limitation and different obstacles. For this reason, some of the manipulator configurations cannot be reached during the experiments (therefore, they are not included in the optimal plan).

Another practical issue is related to the reference point visibility with respect to the laser tracker. For this reason, several different laser tracker locations should be used to observe the measurement tool in different manipulator configurations. In this experimental study, minimum number of the laser tracker placements have been found intuitively and verified practically. It is clear that minimization of the laser tracker locations is an important issue. It influences the identification accuracy since each placement introduces six additional parameters describing the laser tracker base location (they should be identified before the robot calibration). In this work, two placements for the laser tracker were used.

They have been defined in accordance with the optimal measurement configurations (details will be presented in Subsection 4.2.2). Their placements in the work-cell are presented in Figure 4.4.

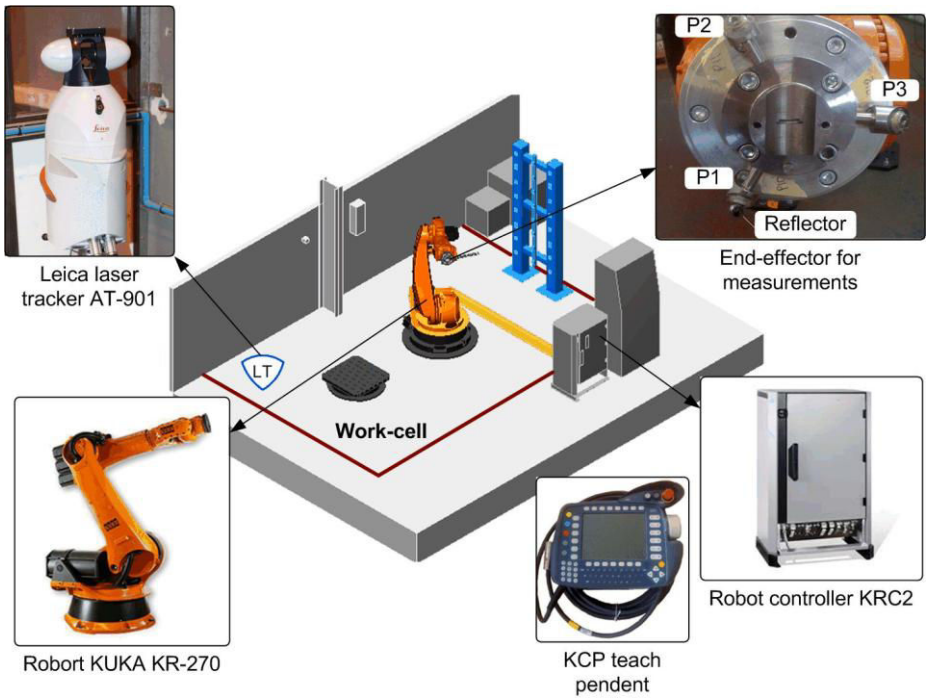

Figure 4.3 Experimental setup for manipulator geometric calibration

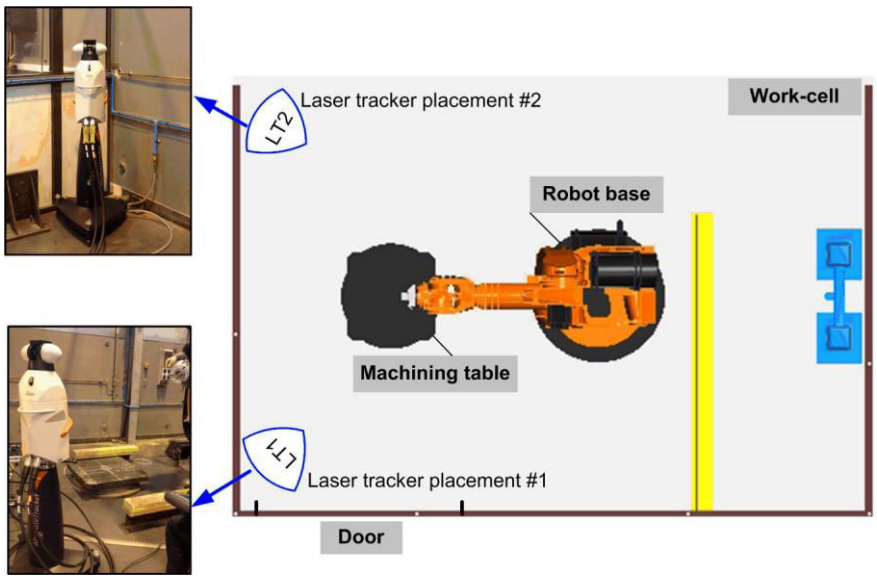

Figure 4.4 Locations of the laser tracker in the work-cell (LT1 and LT2)

To find the parameters describing the laser tracker location with respect to the manipulator base, it is applied an additional calibration technique. This technique uses several auxiliary reference points that are fixed in the work-cell environment and whose coordinates with respect to the robot base are known (Figure 4.5). So, measuring their positions by means of the laser tracker, it is possible to obtain the transformation between the robot base frame and the laser tracker frame. It should be noted that the laser tracker software performs this transformation automatically, so measurement output is expressed

directly with respect to the robot base frame, as it is assumed in all calibration algorithm presented in previous Chapters.

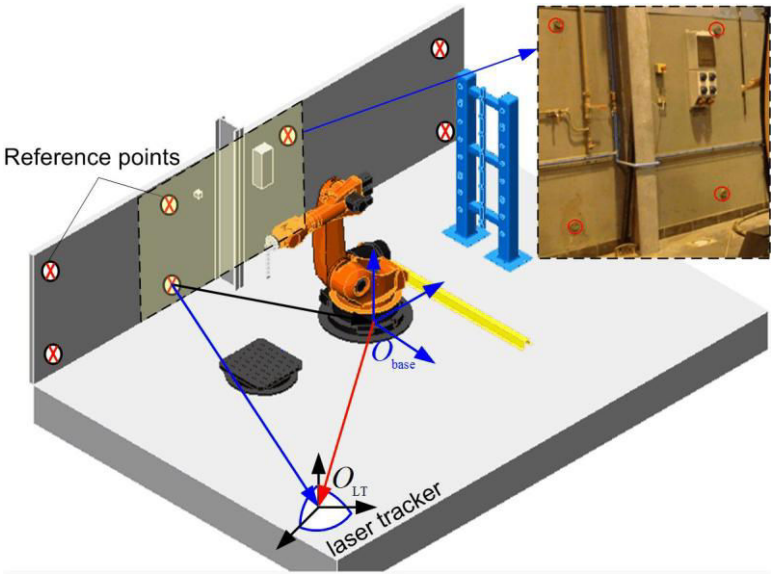

Figure 4.5 Manipulator base frame calibration using work-cell environment

To obtain required data for the manipulator geometric calibration while using the above described experimental setup, the measurement procedure includes the following steps:

Step 1 Attach the measurement tool to the manipulator mounting flange and place the laser tracker at the first location LT1;

Step 2 Calibrate the laser tracker base location by measuring the Cartesian coordinates of the work-cell reference points;

Step 3 Move the manipulator to the first configuration Conf.#1 and measure the Cartesian coordinates of the end-effector reference points (providing that the reflector is visible, otherwise this point is measured from another laser tracker location);

Step 4 Move the manipulator to the next configuration and repeat measurements (similar to Step 3)

Step 5 Change laser tracker placement to LT2, calibrate its base frame and repeat Steps 3, 4 for the end-effector reference points that were not visible from the previous laser tracker location.

To reduce the influence of the non-geometric factors, the measurements were repeated several times for each configuration, with additional movements of the manipulator end-effector from a current location to its neighbourhood and back. As a result of this procedure, the measurement data of each manipulator configuration contain 27 position coordinates (p_x, p_y, p_z for each measurement, which is performed for three end-effector reference points P1, P2, P3, and is repeated three times denoted as #1, #2, #3). An example of the measurement data structure for a single manipulator configuration is presented in Table 4.1.

Table 4.1 Example of measurement data structure (for a single manipulator configuration)

Manipulator configuration, [deg]	Measurement number	Reference point	Cartesian coordinates, [mm]		
			p_x	p_y	p_z
(89.5, −39.4, 98.0, 28.9, −79.6, −97.7) 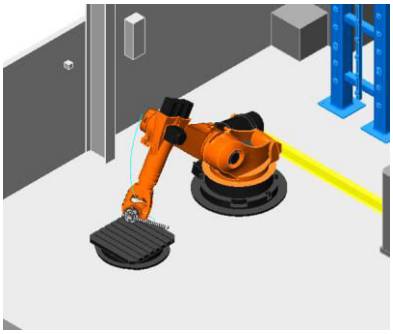	#1	P1	233.76	-2041.18	-148.10
		P2	69.05	-2128.94	-126.26
		P3	148.99	-2037.09	6.12
	#2	P1	233.79	-2041.18	-148.14
		P2	69.09	-2128.94	-126.27
		P3	149.04	-2037.07	6.10
	#3	P1	233.79	-2041.19	-148.16
		P2	69.08	-2128.95	-126.29
		P3	149.06	-2037.08	6.08

It is worth mentioning that the whole data set obtained in experiments presented in this Section contains 432 coordinates p_x, p_y, p_z corresponding to three sets of manipulator configurations (6 different configurations for each set). More detail concerning selection of optimal measurement configurations and laser tracker placements are presented in the following subsection.

4.2.2 Optimal measurement pose selection for geometric calibration

While selecting the minimum number of measurement configurations, it is necessary to take into account that each manipulator pose produces only 6 independent equations that are used for identification (in spite of the fact that relevant data structure includes 27 coordinates, see Table 4.1). On the other hand, the set of geometric parameters to be identified includes 33 unknowns:

(i) 18 principal parameters of the KUKA KR-270 robotic manipulator (see Section 2.2);

(ii) 6 parameters describing the laser tracker location with respect to the robot base (both position and orientation);

(iii) 9 parameters describing locations of the end-effector reference points with respect to the manipulator mounting flange (positions only for three points).

Therefore, at least six different measurement configurations are required to ensure non-singularity of the identification Jacobian and ability to estimate the desired values. For this reason, relevant optimization problem aiming at determining optimal measurement poses has been solved for the configuration number $m = 6$.

To take into account the work-cell constraints and the manipulator joint limits, the optimization problem for selection of measurement configurations has been formulated as follows

$$\operatorname{trace}\left(\mathbf{J}_{\pi 0}^{(p)} \left(\sum_{i=1}^{6} \mathbf{J}_{\pi i}^{(p)T} \mathbf{J}_{\pi i}^{(p)} \right)^{-1} \mathbf{J}_{\pi 0}^{(p)T} \right) \rightarrow \min_{\{\mathbf{q}_j, j=\overline{1,6}\}} \tag{4.3}$$

subject to

$$\begin{aligned} &\mathbf{q}^{\min} \le \mathbf{q}_i \le \mathbf{q}^{\max} \\ &\mathbf{p}^{\min} \le g^{(p)}(\mathbf{q}_i) \le \mathbf{p}^{\max} \end{aligned}, \quad i = \overline{1,6} \tag{4.4}$$

where the notations are taken from Section 2.5. In particular, $\{\mathbf{q}_i \ i=\overline{1,6}\}$ denote the measurement configurations, the function $g^{(p)}(\mathbf{q}_i)$ describes the manipulator geometric model and returns the end-effector position coordinates of the current configuration, $\mathbf{J}_{\pi i}^{(p)}$ is the upper half-part of the relevant identification Jacobian (corresponding to the position coordinates) that is computed for the configuration $\mathbf{q}_i$. Besides, $\mathbf{q}_0$ denotes the manipulator test-pose that produces the weighting coefficients introduced via the Jacobian matrix $\mathbf{J}_{\pi 0}^{(p)}$. The optimization constraints (4.4) take into account the manipulator joint limits $[\mathbf{q}^{\min}, \mathbf{q}^{\max}]$ and the work-cell boundaries $[\mathbf{p}^{\min}, \mathbf{p}^{\max}]$, whose values are given in Table 4.2 and Table 4.3, respectively (the intersection of these two constraints is shown in Figure 4.6). This optimization problem should be solved with respect to six measurement configurations that are described by 36 joint coordinates in total.

Table 4.2 The joint limits of robot KUKA KR-270

	q_1	q_2	q_3	q_4	q_5	q_6
$\mathbf{q}^{\min}$, [deg]	-180	-145	-110	-180	-125	-180
$\mathbf{q}^{\max}$, [deg]	180	0	155	180	125	180

Table 4.3 The work-cell space boundaries with respect to the robot base frame

	p_x	p_y	p_z
$\mathbf{p}^{\min}$, [mm]	-1400	-3000	300
$\mathbf{p}^{\max}$, [mm]	1800	2200	3500

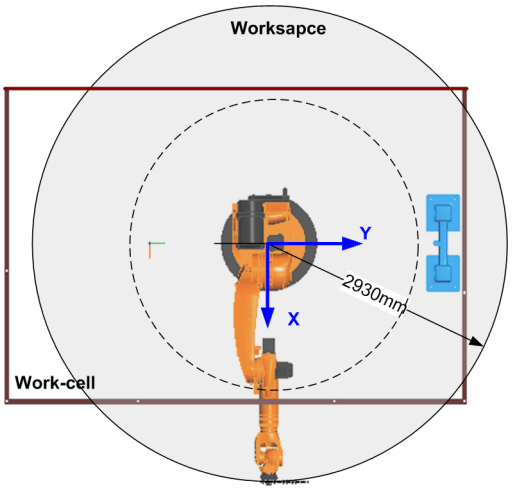

Figure 4.6 Intersection of manipulator workspace and work-cell boundaries

This optimization problem has been solved using the MATLAB software with the built-in optimization functions "ga" and "fmincon", which are required for the proposed hybrid approach that employs the genetic algorithm and the gradient search (see Section 2.6 for details). Corresponding solution minimizes the objective function ρ_0 (the proposed performance measure), which describes the manipulator positioning accuracy after calibration

$$\rho_0 = \sqrt{\sigma^2 \cdot \mathrm{trace}(\mathbf{J}_{\pi 0}^{(p)} (\sum_{i=1}^{6} \mathbf{J}_{\pi i}^{(p)T} \mathbf{J}_{\pi i}^{(p)})^{-1} \mathbf{J}_{\pi 0}^{(p)T})} \tag{4.5}$$

where σ is the measurement noise parameter that has been taken from the technical specification of the laser tracker and is equal to $10\,\mu\mathrm{m}$. It should be mentioned that, in order to reduce the computational efforts and, to pay more attention to the parameters that can be tuned in the robot controller, only nine the most essential geometric parameters were considered while computing the Jacobian matrices $\mathbf{J}_{\pi 0}^{(p)}$ and $\mathbf{J}_{\pi i}^{(p)}$. They include the link lengths $\{d_2,...,d_5\}$ whose nominal values are known and the joint offsets $\{\Delta q_1,...,\Delta q_5\}$ that are nominally equal to zero.

In order to find a solution as close as possible to the global minimum, the optimization problem (4.3) has been solved several times with different starting points. Nevertheless, three different solutions have been obtained that ensure almost the same value of the considered performance measure ρ_0 ($\approx 13.6\,\mu\mathrm{m}$). Corresponding solutions are presented in Table 4.4.

Table 4.4 Optimal measurement configurations for geometric calibration

Configuration number	Joint angle coordinates, [deg]					
	q_1	q_2	q_3	q_4	q_5	q_6
Set I: Solution #1						
Conf.# I.1	89.50	-39.37	98.01	28.95	-79.64	-97.70
Conf.# I.2	60.85	-41.51	90.02	59.30	91.78	-80.24
Conf.# I.3	86.13	-38.57	86.49	82.02	51.20	81.14
Conf.# I.4	72.51	-53.01	80.06	-27.98	79.69	106.77
Conf.# I.5	109.15	-50.67	98.86	37.53	96.14	-89.65
Conf.# I.6	73.99	-145	78.59	-18.83	-101.44	85.08
Set II: Solution #2						
Conf.# II.1	-63.31	-39.00	62.25	59.95	54.71	80.34
Conf.# II.2	117.55	-23.03	40.25	79.09	-124.99	104.42
Conf.# II.3	92.26	-78.34	118.79	22.39	63.06	79.51
Conf.# II.4	126.97	-77.85	117.48	-2.42	-107.03	93.28
Conf.# II.5	66.08	-33.86	54.47	53.00	56.71	103.85
Conf.# II.6	100.05	-62.30	99.77	29.88	100.47	-90.13
Set III: Solution #3						
Conf.# III.1	176.34	-109.40	90.57	8.08	-112.02	95.69
Conf.# III.2	103.55	-31.48	88.03	66.55	-124.99	106.19
Conf.# III.3	79.91	-49.56	88.16	51.71	57.13	84.31
Conf.# III.4	125.36	-50.00	87.09	56.15	56.62	81.98
Conf.# III.5	64.40	-56.37	94.21	36.49	59.40	91.04
Conf.# III.6	128.24	-50.18	87.63	45.04	95.51	-86.18

For comparison purposes, these solutions have been evaluated both separately and in different combinations, assuming that the measurements are performed 18 times in the following way: (i)

repeating three times the measurements in configurations from a single set; (ii) using twice configurations from one set and only once from the second set; (iii) using all configurations from three sets simultaneously (but only once). Corresponding values of ρ_0 are presented in Table 4.5. As follows from this table, the diversity of manipulator configurations has almost negligible contribution to the improvement of robot accuracy (it is about $13.6/\sqrt{3}$ μm, the difference is less than 0.2%). This confirms the results from Section 2.6, which claims that using simple repetition of the optimal plan with lower number of measurement configurations essentially reduces the experimental complexity while the same calibration accuracy can be achieved.

Table 4.5 Comparison of calibration plans with different diversity of measurement configurations

	Calibration plans	Robot accuracy ρ_0 ,[μm]
(i)	{Sol. #1 × 3}	7.85
	{Sol. #2 × 3}	7.84
	{Sol. #3 × 3}	7.83
(ii)	{Sol. #1 × 2, Sol. #2}	7.84
	{Sol. #1 × 2, Sol. #3}	7.84
	{Sol. #1, Sol. #2 × 2}	7.83
	{Sol. #2 × 2, Sol. #3}	7.83
	{Sol. #1, Sol. #3 × 2}	7.83
	{Sol. #2, Sol. #3 × 2}	7.83
(iii)	{Sol. #1, Sol. #2, Sol. #3}	7.83

The obtained measurement configurations have been used for calibration experiments for KUKA KR-270 industrial robot. It is worth mentioning that, in accordance with the measurement procedure described in previous subsection, each manipulator configuration provides 27 values of the position coordinates. These coordinates have been obtained using two different locations of the laser tracker, as it is shown in Table 4.6. However, at certain configurations, some of the reference points were not visible for both laser tracker locations (points P2, P3 for configurations Conf.#I.6, #III.6; points P3 for configurations Conf.# II.3, III.4). This problem can be solved by increasing number of laser tracker locations, but in practice such solution is limited by the experimental time as well as the work-cell constraints. On the other hand, since the calibration experiment employs two laser tracker placements, 6 additional parameters describing the second laser tracker location should be also identified. In total, the system of identification equations contains 432 expressions that can be used to identify the whole set of 39 geometric parameters. To achieve the highest identification accuracy, here it is proposed to use all measurements corresponding to 18 manipulator configurations simultaneously for calibration of the geometric parameters. Corresponding results and detailed accuracy analysis will be given in the following subsections.

Table 4.6 Laser tracker placements for different reference points and measurement configurations

Configuration number	Reference points		
	P1	P2	P3
Set I			
Conf.# I.1	LT1	LT1	LT1
Conf.# I.2	LT2	LT1	LT1
Conf.# I.3	LT1	LT2	LT2
Conf.# I.4	LT1	LT1	LT2
Conf.# I.5	LT1	LT2	LT2
Conf.# I.6	LT2	—	—
Set II			
Conf.# II.1	LT1	LT1	LT1
Conf.# II.2	LT1	LT1	LT1
Conf.# II.3	LT2	LT1	—
Conf.# II.4	LT2	LT1	LT1
Conf.# II.5	LT1	LT1	LT2
Conf.# II.6	LT1	LT2	LT2
Set III			
Conf.# III.1	LT1	LT1	LT1
Conf.# III.2	LT1	LT1	LT1
Conf.# III.3	LT1	LT1	LT2
Conf.# III.4	LT2	LT1	—
Conf.# III.5	LT1	LT1	LT2
Conf.# III.6	LT1	—	—

LT1: Reference point position measured by laser tracker placement #1

LT2: Reference point position measured by laser tracker placement #2

"—": Reference point position cannot be measured by both laser tracker placements

4.2.3 Identification of manipulator geometric parameters

Using the obtained measurement data, the two-step identification procedure has been applied (see Section 2.4). On the first step, the base and tool transformations have been computed, corresponding results are presented in Table 4.7 and Table 4.8. On the second step, these transformations have been used for the identification of the manipulator geometric parameters, which are presented in Table 4.9. It should be mentioned that in order to increase the identification accuracy, this two-step procedure has been repeated iteratively (280 iterations, computing time was less than two minutes).

Table 4.7 Identification results for manipulator base transformations (for geometric calibration)

Laser tracker placement #1					
	Value, [mm]	CI		Value, [deg]	CI
p_x	-0.023	±0.045	φ_x	-0.004	±0.001
p_y	0.010	±0.032	φ_y	0.001	±0.002
p_z	0.057	±0.044	φ_z	-0.017	±0.001
Laser tracker placement #2					
	Value, [mm]	CI		Value, [deg]	CI
p_x	-0.099	±0.122	φ_x	-0.009	±0.004
p_y	-0.098	±0.053	φ_y	0.006	±0.004
p_z	-0.076	±0.121	φ_z	-0.013	±0.003

Table 4.8 Identification results for manipulator tool transformations (for geometric calibration)

	Reference point #1 (P1)		**Reference point #2 (P2)**		**Reference point #3 (P3)**	
	Value, [mm]	CI	Value, [mm]	CI	Value, [mm]	CI
p_x	277.23	±0.05	276.49	±0.05	278.44	±0.05
p_y	-46.53	±0.04	-48.25	±0.04	103.73	±0.05
p_z	-93.87	±0.04	94.05	±0.05	-2.17	±0.05

As follows from the identification results, among the two base transformations, the first base location that corresponds to the laser tracker placement #1 (LT1) is identified more accurate than the one corresponding to the placement #2 (LT2). This is due to the fact that the number of reference points measured by LT1 is nearly 3 times higher than those measured using LT2 (306 and 126 expressions respectively). It should be mentioned that the DH parameter d_1 has been excluded from the calibration since the laser tracker base frame was located at the intersection of the axis #1 and axis #2. In contrast, the tool transformations have been identified using the complete set of 432 equations. So, the desired geometric parameters have been identified with high accuracy, which has been evaluated using two different techniques (based on the statistical properties extracted from the covariance matrix and using the Gibbs sampling).

The results presented in Table 4.9 include 18 parameters, some of them cannot be modified in the robot control software. So, it is interesting to examine the effect of reducing the number of these parameters by setting them to their nominal values. Relevant analysis shows that the manipulator end-effector positioning error impact (because of such simplification) essentially differs from one parameter to another, and they can be split into the following groups:

- Parameters $\{p_{x1}, p_{y1}, p_{x2}, p_{x3}, p_{z3}, p_{y4}, \Delta q_2, \Delta q_3, \varphi_{z2}, \varphi_{z3}, \varphi_{z4}\}$, the loss of accuracy caused by neglecting them varies from 0.10 mm to 1.03 mm;

- Parameters $\{p_{z4}, p_{z5}, \Delta q_5, \varphi_{x1}, \varphi_{x2}, \varphi_{z5}\}$, the loss of accuracy caused by neglecting them varies from 0.02 mm to 0.09 mm;
- Parameter Δq_4, the loss of accuracy caused by neglecting it is equal to 4 μm.

Comparing to the milling accuracy required for the considered milling process (0.05-0.25 mm), the above listed positioning error impacts are not negligible for the most of the geometric parameters. So, their deviations should be compensated either in geometric model embedded in the robot controller or at the step of generation of the machining trajectory.

Table 4.9 Identification results for manipulator geometric parameters

Parameter	Unit	Value	Confidence interval	
			Using covariance matrix	Using Gibbs sampling
$p_{x1} \equiv \Delta d_2$	[mm]	-0.353	±0.086	±0.102
p_{y1}	[mm]	0.426	±0.272	±0.421
φ_{x1}	[deg]	0.015	±0.005	±0.005
Δq_2	[deg]	-0.007	±0.005	±0.004
$p_{x2} \equiv \Delta d_3$	[mm]	0.458	±0.082	±0.060
φ_{x2}	[deg]	0.022	±0.014	±0.022
φ_{z2}	[deg]	-0.023	±0.005	±0.005
Δq_3	[deg]	-0.023	±0.019	±0.013
$p_{x3} \equiv \Delta d_4$	[mm]	-0.214	±0.089	±0.093
$p_{z3} \equiv \Delta d_5$	[mm]	-0.508	±0.363	±0.259
φ_{z3}	[deg]	-0.011	±0.017	±0.022
Δq_4	[deg]	0.001	±0.008	±0.009
p_{y4}	[mm]	-0.167	±0.113	±0.044
p_{z4}	[mm]	-0.018	±0.073	±0.044
φ_{z4}	[deg]	0.025	±0.015	±0.010
Δq_5	[deg]	-0.011	±0.027	±0.009
p_{z5}	[mm]	0.016	±0.104	±0.041
φ_{z5}	[deg]	-0.008	±0.018	±0.007

For comparison purposes, the manipulator accuracy improvement due to calibration has been studied based on the residual analysis before and after calibration (computed using the nominal and identified values of geometric parameters respectively). Here, two types of residuals have been examined, the coordinate-based and distance-based ones. Corresponding results are presented in Table 4.10, which includes the maximum and root mean square (RMS) values of the relevant residuals. As follows from the results, both types of the residuals have been essentially reduced after calibration.

In particular, the maximum values have been reduced by a factor of 4 and 3.5, while the RMS values of these two criteria have been decreased by a factor of 5.3 and 5.5, respectively.

Table 4.10 Evaluation of the manipulator accuracy improvement based on residual analysis

Criterion		Before calibration	After calibration	Improvement factor
Coordinate-based residuals, [mm]	max	1.25	0.32	4.0
	RMS	0.54	0.10	5.3
Distance-based residuals, [mm]	max	1.31	0.39	3.5
	RMS	0.94	0.17	5.5

Hence, the obtained results allow us to achieve good manipulator accuracy at the measurement configurations. So, it is reasonable to expect that using the geometric model, which integrates the identified parameters, the desired positioning accuracy for the given test configuration can be also achieved. More detailed analysis concerning the parameter identification accuracy and its impact on the robot positioning accuracy will be discussed in the next Subsection.

4.2.4 Analysis of the identification results for geometric calibration

In order to evaluate the calibration results, first let us analyze the residuals computed from the identification equations for each coordinate separately. Their distributions for each configuration are presented in Figure 4.7, corresponding histograms are shown in Figure 4.8. As follows from detailed analysis, the residuals tend to follow the normal probability distributions with zero mean and almost the same parameter σ, which is equal to 0.10 mm, 0.09 mm, and 0.11 mm for X-, Y-, and Z- direction, respectively. The latter justifies the utilization of ordinary least square technique (with equal weights) for the parameter identification and allows us to conclude that the measurement noise parameter σ in our experiment is equal to 0.1 mm. This value will be used below to evaluate the manipulator accuracy after calibration.

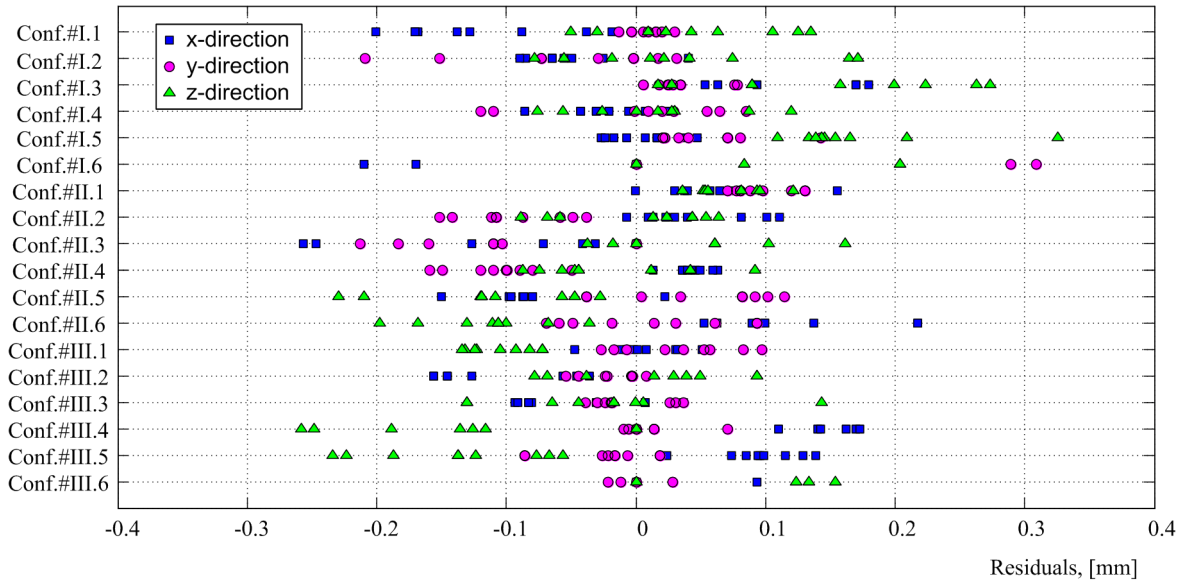

Figure 4.7 Residual distribution after geometric calibration for different measurement configurations

It is worth mentioning that the noise parameter σ estimated from the residual analysis is essentially higher than the precision of the laser tracker measurement system, which is defined in the technical specifications as 0.01 mm. This difference can be caused by limitations of the geometric model, which does not take into account a number of essential features such as the elastostatic deformations due to gravity forces, the friction/backlash in joints and other factors that influence on the robot repeatability (±0.06 mm, as specified in the data sheets). Nevertheless, as it is shown below, geometric calibration ensures essential improvement of the robot accuracy.

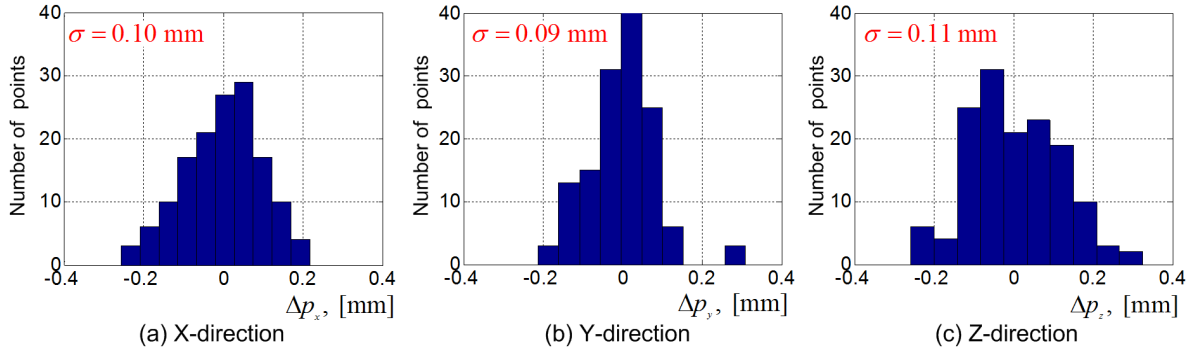

Figure 4.8 Histograms of residual distribution along X-, Y-, and Z-directions after geometric calibration

To evaluate the robot accuracy after geometric calibration, expression (2.62) has been applied separately for each measurement configuration and each end-effector reference point. It allows us to compute a number of performance measures

$$\hat{\rho}_i^j = \sqrt{\text{trace}\left(\mathbf{J}_{ei}^{j(p)}\,\text{cov}(\boldsymbol{\pi}_e)\,\mathbf{J}_{ei}^{j(p)T}\right)} \qquad i=\overline{1,18},\ j=\overline{1,3} \tag{4.6}$$

where i denotes the manipulator configuration number, j is the reference point number, the vector $\boldsymbol{\pi}_e$ collects all 39 identified parameters (i.e. 12 parameters for two base transformations, 9 parameters for three tool transformations and 18 manipulator geometric parameters), the matrix $\mathbf{J}_{ei}^{j(p)}$ aggregates the observation matrix $\mathbf{A}_i^{j(p)}$ (for base and tool calibration) and the geometric Jacobian matrix $\mathbf{J}_{\pi i}^{j(p)}$ of the manipulator, i.e., $\mathbf{J}_{ei}^{j(p)} = [\mathbf{A}_i^{j(p)};\ \mathbf{J}_{\pi i}^{j(p)}]$. The covariance matrix $\text{cov}(\boldsymbol{\pi}_e)$ of size 39×39 is computed as

$$\text{cov}(\boldsymbol{\pi}_e) = \sigma^2 \left(\sum_{i=1}^{m}\sum_{j=1}^{n} \mathbf{J}_{ei}^{j(p)T}\mathbf{J}_{ei}^{j(p)} \right)^{-1} \tag{4.7}$$

where the noise parameter $\sigma = 0.1$ mm has been estimated from the experimental data. Table 4.11 summarizes the manipulator positioning errors evaluated using the geometric model and residuals after calibration for each measurement configuration separately. It also provides the residuals from minimum to maximum values of all the measurement points for each configuration. It should be noted that the number of measurements varies from 3 to 9 due to the visibility issue of the laser tracker.

As follows from the numerical results presented in Table 4.11, the positioning errors evaluated using the model are in good agreement with the ones obtained via residual analysis (based on experimental data). So, the geometric model is able to provide quite reasonable estimates of the end-effector positioning errors for all manipulator configurations, including the test-pose. Relevant computations show that for the considered test-pose defined by the joint coordinate vector $\mathbf{q}_0$ (see Eq. (4.1)), it is possible to achieve a positioning accuracy of about 0.04 mm that is acceptable for the

considered technological process. It is worth mentioning that the positioning accuracy evaluated via residuals perfectly follows the Maxwell-Boltzmann distribution (with the standard deviation of 0.07 mm). Hence, the geometric calibration experiment gives acceptable results with accuracy improvement by a factor of 5 compared to non-calibrated robot, but the statistical limits have not been achieved because of the model limitations. To overcome these difficulties, it is required to extend the geometric model and to consider the manipulator elastostatic errors, which will be in the focus of next section.

Table 4.11 Positioning errors after geometric calibration for each measurement configuration

Measurement configuration	Number of measurements	Residuals	Positioning error evaluated using residuals	Positioning error evaluated using the model
		[mm]	[mm]	[mm]
Conf.# I.1	9	{-0.20,...,0.14}	0.06	0.06
Conf.# I.2	9	{-0.21,...,0.17}	0.06	0.05
Conf.# I.3	9	{0.01,...,0.27}	0.11	0.05
Conf.# I.4	9	{-0.12,...,0.12}	0.03	0.06
Conf.# I.5	9	{-0.03,...,0.33}	0.07	0.05
Conf.# I.6	3	{-0.21,...,0.31}	0.19	0.09
Conf.# II.1	9	{-0.01,...,0.15}	0.03	0.06
Conf.# II.2	9	{-0.15,...,0.11}	0.05	0.06
Conf.# II.3	6	{-0.26,...,0.16}	0.12	0.06
Conf.# II.4	9	{-0.16,...,0.10}	0.02	0.06
Conf.# II.5	9	{-0.23,...,0.11}	0.04	0.05
Conf.# II.6	9	{-0.20,...,0.22}	0.06	0.05
Conf.# III.1	9	{-0.13,...,0.10}	0.03	0.06
Conf.# III.2	9	{-0.16,...,0.10}	0.04	0.05
Conf.# III.3	9	{-0.13,...,0.14}	0.05	0.04
Conf.# III.4	6	{-0.25,...,0.17}	0.13	0.05
Conf.# III.5	9	{-0.23,...,0.14}	0.06	0.04
Conf.# III.6	3	{-0.02,...,0.15}	0.08	0.05

4.3 ELASTOSTATIC CALIBRATION EXPERIMENTS FOR KUKA KR-270 INDUSTRIAL ROBOT

To demonstrate the advantages of the calibration techniques presented in Chapter 3 and justify their attractiveness for industrial application, this Section presents the experimental procedure, the identification results and corresponding accuracy analysis for elastostatic calibration of KUKA KR270 industrial robot under the loading.

4.3.1 Experimental setup and measurement procedure

In addition to the experimental devices used in geometric calibration, some extra tools for relevant force application and measurements are used in elastostatic calibration. Corresponding experimental setup is presented in Figure 4.9 and corresponding equipment is listed below:

- 6-dof KUKA KR-270 robotic manipulator whose elastostatic parameters should be identified (relevant stiffness model is presented in Section 3.2);
- Robot control system KR-C2, which is used for changing the manipulator configurations and measuring the corresponding joint angles;
- Special measurement tools with three reference points located on the circle of radius 104 mm, this tool is attached to the manipulator mounting flange;
- Special calibration tool attached to the manipulator mounting flange for force application, with an additional reference point for force direction measurement;
- Dynamometer for measurement of force magnitude with precision 2.0 N;
- Laser tracker Leica AT-901 that is used to measure the reference points Cartesian coordinates with precision 10 μm;
- Laser tracker reflector that is sequentially attached to the reference points (with precision about 1 μm), it allows the measurement device to estimate the distances and compute the required Cartesian coordinates;
- Personal computer with dedicated software connected to the laser tracker, which is used for data logging and their transformation in the required form.

Compared to the geometric case, here the calibration workspace is further limited due to the force application equipment and safety reasons. To apply the loading, it is required certain volume in order to avoid collisions between the robot body and work-cell obstacles (the machining table, for instance). These limitations are quite essential and should be taken into account in the optimization problem of the measurement configurations selection. It is also worth mentioning that the problem of the laser tracker visibility can be solved by tuning the joint angle q_1, which does not influence on the optimization objective. So here, only one laser tracker location is enough for implementing all desired measurements.

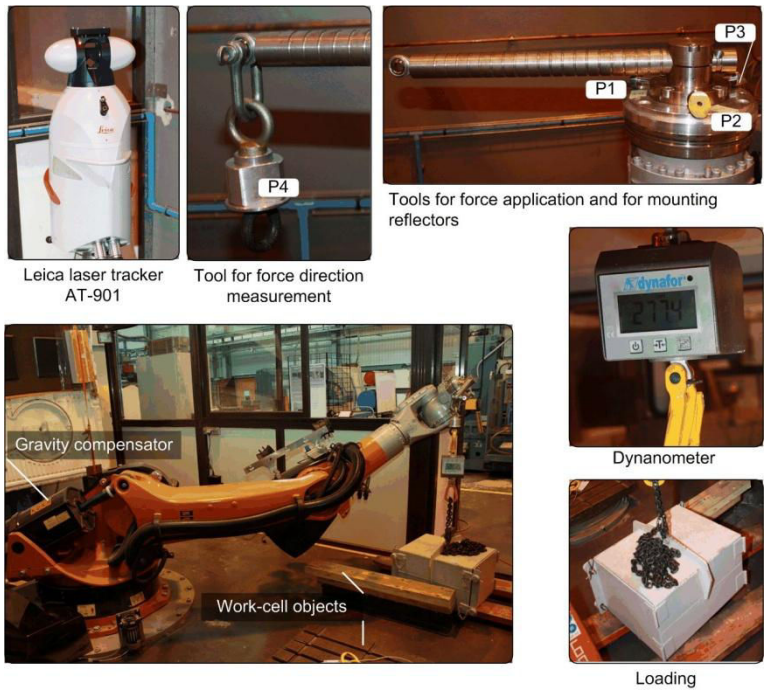

Figure 4.9 Experimental setup for manipulator elastostatic calibration

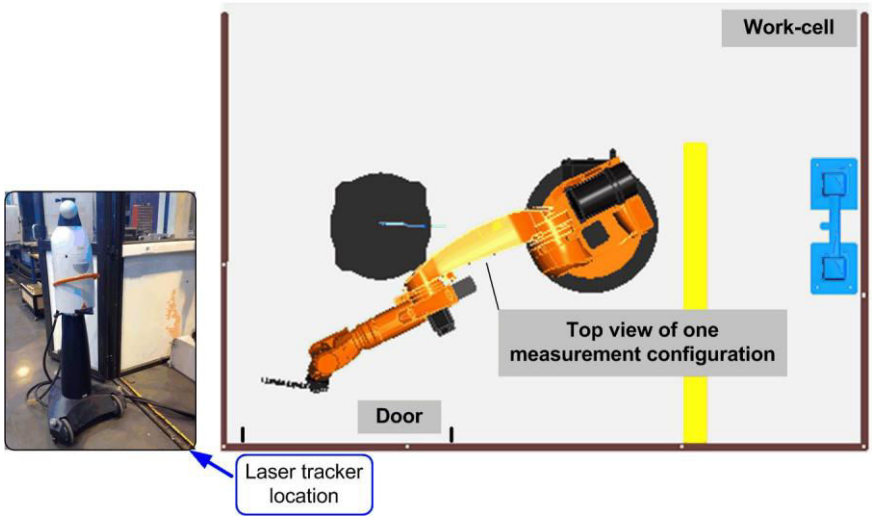

Figure 4.10 Laser tracker placement used in elastostatic calibration

In the case of elastostatic calibration, the laser tracker location has been calibrated using an alternative technique compared to the geometric calibration. This approach is based on robot movements that allow us to identify separately the directions of joint axis #1 and axis #2 (that correspond to Z- and Y-axes of the robot base). The method includes the following steps:

Step 1 Rotate the manipulator around the axis #1 within the reflectors vision of the laser tracker. For such motion, the joint coordinate q_1 varies while the coordinates $q_2,...,q_6$ remain constant. The obtained measurement data (a set of points on a circle) allow us to define the center of rotation O_1, and the direction of the axis #1 (coinciding with the Z-axis of the manipulator). The latter is computed as the normal vector with respect to the plane defined by the measurement points. It should be noted that to increase the identification accuracy, the circle radius should be as large as possible.

Step 2 Rotate the manipulator around the axis #2 within the reflectors vision of the laser tracker. For such motion, the joint coordinate q_2 varies while the coordinates $q_1,q_3,...,q_6$ remain constant. The obtained measurement data (a set of points on a circle) allow us to define the center of rotation O_2, and the direction of the axis #2 (which is parallel to the Y-axis of the manipulator).

Step 3 Define the Y-axis of the manipulator that is parallel to joint axis #2 and intersects with its Z-axis, the intersecting point defines the origin of the manipulator base O_{base}.

Step 4 Define the X-axis using the right-hand rule for the directions X, Y, Z.

More details concerning this method are shown in Figure 4.11. Similar to the geometric case, the laser tracker base frame is located at the intersection of the joint axis #1 and axis #2, which is shifted along the Z-axis by the distance corresponding to the DH parameter d_1 (see Figure 2.3 in Chapter 2).

According to the developed algorithms for the manipulator elastostatic calibration presented in Section 3.4 (which takes into account the gravity compensator impact), the experimental procedure can be divided into three sequential stages: (i) calibration of the gravity compensator geometry; (ii) calibration of the manipulator elastostatic parameters $k_2,...,k_6$; and (iii) calibration of the manipulator elastostatic parameter k_1. These stages include several procedures briefly described below:

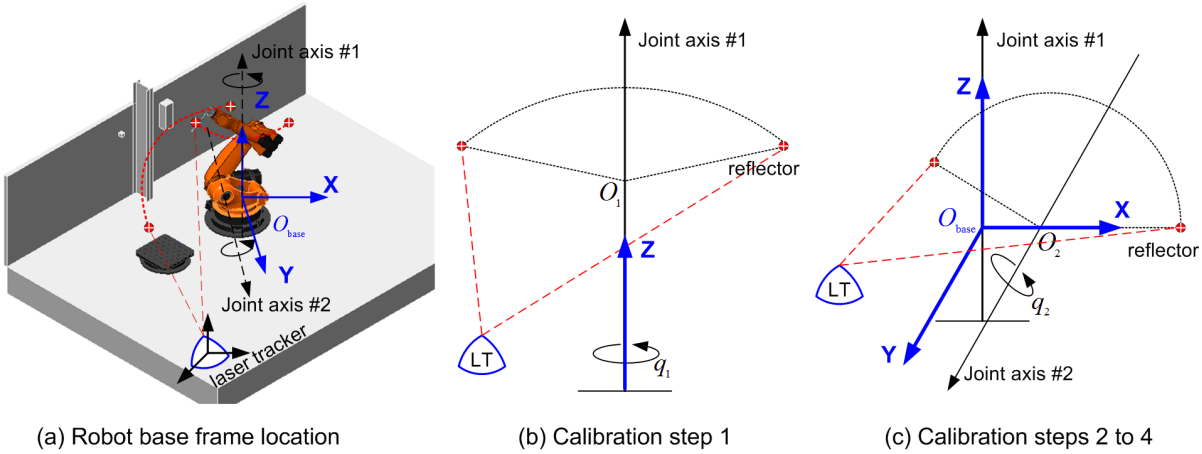

(a) Robot base frame location (b) Calibration step 1 (c) Calibration steps 2 to 4

Figure 4.11 Manipulator base frame calibration using robot movements

Stage (i) deals with the measurement of several sets of points on the circle arcs, whose centers allow us to define the gravity compensator geometry (see subsection 3.6.1). Corresponding experimental procedure includes the following steps:

Step 1 Place the laser tracker to the pre-defined position and calibrate its base frame location by applying the above presented procedure based on sequential movements of the manipulator axis #1 and axis #2.

Step 2 Move the manipulator to the first configuration, at which the joint angle $q_2 = 0°$ and the other joints can be adjusted to ensure that the gravity compensator is visible for the laser tracker;

Step 3 Measure the marker point positions defined on the rigid part of the gravity compensator;

Step 4 Move the manipulator to the next configuration with a different value of angle q_2 and repeat the measurements (similar to Step 3).

It is worth mentioning that, here the calibration technique of the laser tracker base frame allows us to ignore the Z-coordinates in relevant identification algorithm since only projections to the XY-plane are important for the considered problem. Besides, the marker locations should be selected in accordance with the optimal design of experiment technique proposed in Section 3.6. More details concerning these issues will be discussed in the following Subsection.

Stage (ii) deals with the measurement of the end-effector position coordinates before and after applying external loadings, these data allow us to identify the manipulator elastostatic parameters $k_2,...,k_6$. Using the above described experimental setup, the measurement procedure for manipulator elastostatic calibration is the following:

Step 1 Attach the measurement tool and the force application tool to the manipulator mounting flange and place the laser tracker at the pre-defined location;

Step 2 Calibrate the laser tracker base frame location by finding the directions of the joint axis #1 and axis #2 using robot movements;

Step 3 Move the manipulator to the first configuration Conf.#1.1 and measure the Cartesian coordinates of the end-effector reference points (corresponding visibility of the laser tracker can be ensured by adjust the joint angle q_1);

Step 4 Apply external loading by attaching fixed weight (corresponding gravity force magnitude is about 2500N);

Step 5 Measure the Cartesian coordinates of the end-effector reference points with the external loading;

Step 6 Unload the manipulator, then move it to the next configuration and repeat Steps 3, 4, 5.

As a result of this procedure, the measurement data of each manipulator configuration contain 30 position coordinates. An example of the measurement data structure for a single configuration is presented in Table 4.12. To reduce the influence of the robot repeatability, the measurements were performed several times for each configuration (with additional movements of the end-effector from a current location to its neighbourhood and back).

Table 4.12 Example of the measurement data structure (for a single manipulator configuration)

Manipulator configuration, [deg]	Reference point		Cartesian coordinates, [mm]		
			p_x	p_y	p_z
(85.9, –10.0, –110.0, 110.6, –43.9, –177.6) 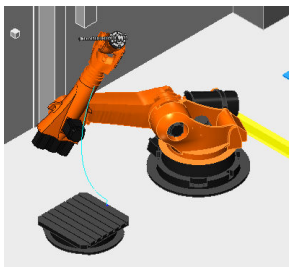	P1	Before loading	306,20	-1110,12	1383,01
		After loading	304,09	-1109,43	1384,74
	P2	Before loading	173,90	-1008,25	1469,24
		After loading	171,56	-1007,32	1470,31
	P3	Before loading	290,85	-937,32	1352,33
		After loading	289,01	-936,77	1353,80
	P4	After loading	173,90	-1008,25	1469,24

P1, P2, P3: reference points for measurement of the end-effector deflections
P4: reference point for measurement of the force direction

Stage (iii) deals with the calibration of joint compliance k_1 using the work-cell constraints, corresponding measurement procedure includes the following steps:

Step 1 Attach the multi-directional force sensor to the manipulator mounting flange;

Step 2 Move the manipulator to the first configuration Conf.#1 and apply external force by pushing the robot end-effector against the work-cell wall up to the allowable limits;

Step 3 Record the end-effector positioning coordinates provided by the robot controller and measure the 6-dimensional wrench components using the force sensor;

Step 4 Move the manipulator to the next configuration and repeat Steps 2, 3.

It should be noted that here, it is not reasonable to apply any experiments design technique because the calibration area is extremely limited by the work-cell environment. More details concerning the experiments design and identification results for the above three experimental stages will be sequentially discussed in the following subsections.

4.3.2 Identification of the gravity compensator geometry

As follows from Section 3.6, the principal geometric parameters of the gravity compensator are L, a_x and a_y (see Figure 3.15). They can be identified using relative locations of points P_0 and P_1

with respect to P_2. Since the adopted geometric model is a planar one, here the laser tracker base frame should be defined in a particular way (to ensure that the marker locations relative to the XY-plane is not significant). In the frame of this technique, the Z-axis of the laser tracker is defined to be coincident with the joint axis #2, and the Y-axis is parallel to the joint axis #1 (it intersects with Z-axis at point P_2). The X-axis is defined using the right-hand rule as usual. In more detail, relevant calibration procedure is presented in Figure 4.12.

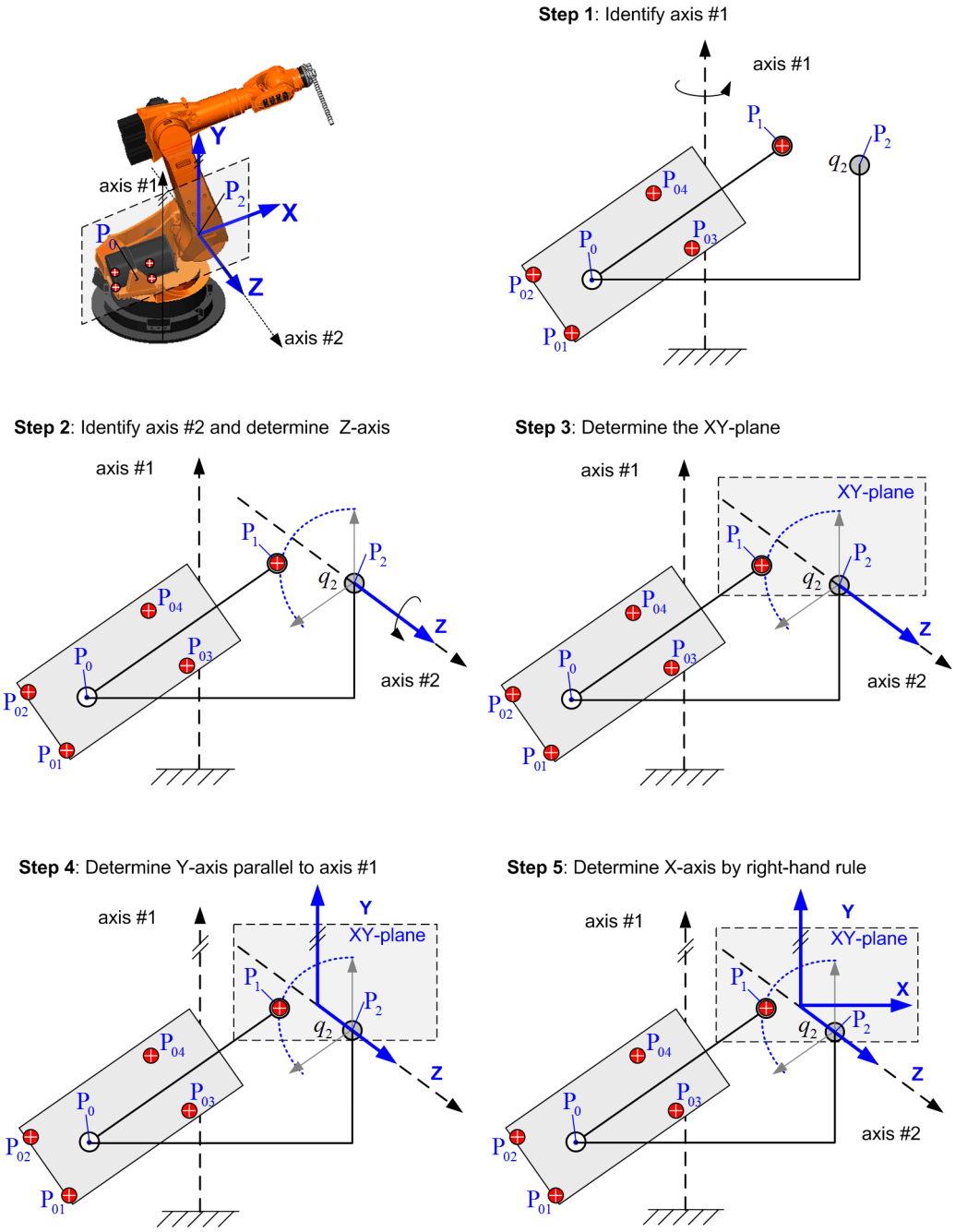

Figure 4.12 Calibration of the laser tracker base frame location for identification of gravity compensator geometry

Another important issue is related to the selection of the marker point locations on the rigid part of the gravity compensator that are used for the measurements of corresponding circle points. In accordance with the proposed technique (see Subsection 3.6.1), these markers should be located on the

opposite sides of the compensator rotational axis, such that the optimal conditions equations $\sum_{j=1}^{k} R_j \cos\beta_j = 0$ and $\sum_{j=1}^{k} R_j \sin\beta_j = 0$ are satisfied. To increase the identification accuracy, four marker points are used in the calibration experiments that are denoted as P_{01}, P_{02}, P_{03} and P_{04} respectively. Their locations are presented in Figure 4.13, where the radii $R_1 = R_3$ and $R_2 = R_4$, and the angles $\beta_3 = \pi + \beta_1$ and $\beta_4 = \pi + \beta_2$. Corresponding measurements of the circle points while rotating the joint q_2 allow us to identify the desired geometric parameters a_x and a_y with respect to the point P_2. The measurement data obtained for the set $q_2 = \{0°, -30°, -60°, -90°, -120°, -140°\}$ are provided in Table 4.13.

Table 4.13 Measurement data for the marker point coordinates for different values of q_2

q_2, [deg]		Position coordinates, [mm]				
		P_1	P_{01}	P_{02}	P_{03}	P_{04}
0	p_x	318,99	-524,51	-461,70	-192,87	-151,33
	p_y	183,71	-120,83	-264,15	17,78	-125,11
	p_z	342,58	398,80	395,78	400,83	394,39
-30	p_x	231,71	-524,77	-461,56	-193,49	-151,49
	p_y	143,65	-121,54	-264,72	17,90	-124,85
	p_z	342,54	398,75	395,68	400,99	394,43
-60	p_x	176,09	-524,54	-474,05	-182,35	-152,98
	p_y	65,30	-105,21	-253,34	4,84	-141,04
	p_z	342,55	398,67	395,60	401,15	394,59
-90	p_x	167,02	-519,62	-495,09	-163,69	-159,60
	p_y	-30,35	-73,28	-227,82	-23,10	-171,84
	p_z	342,56	398,60	395,56	401,30	394,76
-120	p_x	206,99	-509,19	-511,35	-149,92	-171,16
	p_y	-117,73	-42,59	-199,00	-53,70	-200,99
	p_z	342,58	398,54	395,55	401,37	394,86
-140	p_x	256,07	-503,35	-516,48	-145,72	
	p_y	-159,45	-30,51	-186,45	-66,89	Non visible
	p_z	342,58	398,53	395,57	401,37	

These measurement data have been processed using two identification algorithms (see subsection 3.6.2). The first algorithm is aimed at matching the set of points $\{\mathbf{p}_1^i\}$ with additional set of angles $\{q_2^i\}$, that allows us to identify the desired circle radius L. The second algorithm uses sets of point positions $\{\mathbf{p}_{01}^i\},...,\{\mathbf{p}_{04}^i\}$ to determine the relative location of point P_0 with respect to P_2 for further computations of the desired parameters a_x and a_y . The identified parameters and corresponding confidence intervals are presented in Table 4.14.

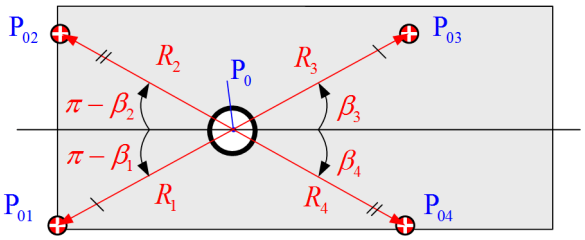

Figure 4.13 The marker point locations on the gravity compensator

Table 4.14 Identification results for the compensator geometric parameters

	L, [mm]	a_x, [mm]	a_y, [mm]
Value	184.72	685.93	123.30
CI	±0.06	±0.70	±0.69

The obtained geometric parameters $\{L,\ a_x,\ a_y\}$ of the gravity compensator allow us to integrate the impact of the compensator into the classical VJM-based stiffness model. However, this model should include also some additional parameters that are related to the elastostatic properties of the compensator.

4.3.3 Identification of manipulator elastostatic parameters using the gravity force

Using the identification results for the gravity compensator geometry, it is possible to evaluate the variation of the equivalent stiffness of the second joint caused by the gravity compensator impact. As follows from Chapter 3 (see Figure 3.16), the compensator impact is highly non-linear, differs throughout the robot workspace and highly depends on the spring preloading s_0. Nevertheless, it is possible to treat the value of k_2 as a constant in the neighbourhood of each q_2. This allows us to use the linear system of identification equations and corresponding experiment design technique. In accordance with the geometric parameters of the gravity compensator and the manipulator joint limits, the following values of joint q_2 have been selected: $\mathrm{Q}_2 = \{-0.01°, -25.2°, -56.9°, -99.8°, -140°\}$. So, the desired vector of the elastostatic parameters $\mathbf{k}$ includes four constant compliance parameters $\{k_3, k_4, k_5, k_6\}$ and a 5×1 vector $\{k_{21}, k_{22}, ..., k_{25}\}$ that describes the configuration-dependent compliance parameters for different values of joint angle q_2.

Using this idea, the optimization problem for selection of the measurement configurations can be solved for each q_2 separately. This leads to the following formulation

$$\operatorname{trace}\left(\mathbf{A}_{k0}^{(p)}\left(\sum_{i=1}^{m}\mathbf{A}_{ki}^{j(p)^T}\mathbf{A}_{ki}^{j(p)}\right)^{-1}\mathbf{A}_{k0}^{(p)^T}\right)\rightarrow\min_{\{q_3,\ldots,q_6\}}\quad\text{for}\ \ \forall\, q_2\in\mathrm{Q}_2 \tag{4.8}$$

subject to

$$\begin{aligned}&\mathbf{q}^{\min}\le\mathbf{q}_i\le\mathbf{q}^{\max}\\&\mathbf{p}^{\min}\le g^{(p)}(\mathbf{q}_i)\le\mathbf{p}^{\max},\quad i=\overline{1,6}\\&r_i\ge r^{\min}\end{aligned} \tag{4.9}$$

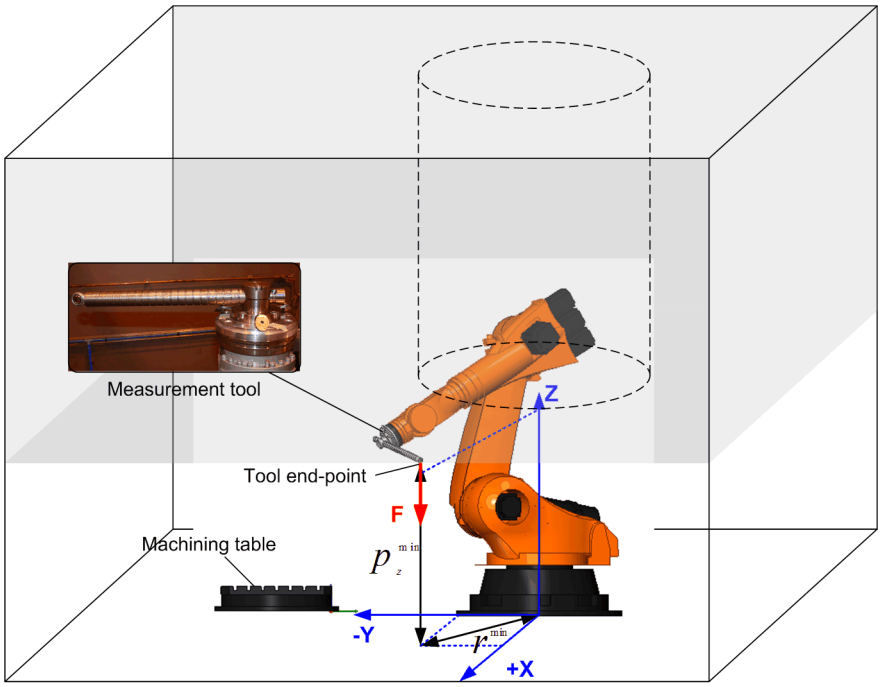

Figure 4.14 The work-cell arrangement for elastostatic calibration

where $\{\mathbf{q}^{\min}, \mathbf{q}^{\max}\}$ describe the joint limits, $\{\mathbf{p}^{\min}, \mathbf{p}^{\max}\}$ define the work-cell boundaries (taking into account the minimum height between the end-point position of the calibration tool and the work-cell floor), $r^{\min}$ is the minimum radius to avoid collisions between the applied loading and the robot body. These constraints are illustrated in Figure 4.14. Here, the matrix $\mathbf{A}_{k0}^{(p)}$ is defined by the test-pose $\mathbf{q}_0 = (0°, -56.9°, 89.3°, 45.1°, 76°, 57.2°)$ and the test-loading $\mathbf{w}_0 = (0, 280\text{N}, -180\text{N}, 0, 0, 0)$, the matrices $\mathbf{A}_{ki}^{j(p)^T}$ depend on the manipulator configurations and on the constant measurement loading $\mathbf{w} = (0, 0, -2500\text{N}, 0, 0, 0)$.

Table 4.15 The work-cell space boundaries for elastostatic calibration

	p_x	p_y	p_z	r
$\mathbf{p}^{\min}$ [mm]	-1400	-3000	800	600
$\mathbf{p}^{\max}$ [mm]	1800	2200	3500	2930

For this setting, the optimization problem (4.8) was solved for each value of joint q_2 and provided the set of optimal measurement configurations $\{q_{3i}, ..., q_{6i}, i = \overline{1,m}\}$, where $m = 3$. The joint angles q_{1i} have been chosen for better visibility of the end-effector reference points for the laser tracker. Corresponding solutions are presented in Table 4.16. In total, 15 configurations have been used for calibration experiments (with 5 different values of q_2). For each configuration, the position coordinates of the reference points (P1, P2 and P3) have been measured three times, before and after the loading.

Table 4.16 Optimal measurement configurations for elastostatic calibration

Configuration number	Joint angle coordinates, [deg]					
	q_1	q_2	q_3	q_4	q_5	q_6
Conf.# 1.1	79.2		-5.57	51.00	-97.52	-91.67
Conf.# 1.2	63	-0.01	-12.22	-56.49	41.42	150.55
Conf.# 1.3	63		-47.98	-70.04	-61.55	177.16
Conf.# 2.1	95		33.00	129.69	-98.1	90.57
Conf.# 2.2	95	-25.2	-107.01	109.95	-61.19	174.21
Conf.# 2.3	105		14.3	55.21	41.26	-152.97
Conf.# 3.1	56.6		44.54	-55.11	41.90	152.06
Conf.# 3.2	56.6	-56.9	64.73	-129.65	-98.26	-90.55
Conf.# 3.3	144.8		104.49	-69.41	61.67	-6.33
Conf.# 4.1	-41		-91.68	55.12	41.53	-152.48
Conf.# 4.2	-143	-99.8	-32.64	110.31	-61.47	-6.29
Conf.# 4.3	-143		-72.01	129.65	-98.09	90.82
Conf.# 5.1	133		147.68	129.64	-97.9	90.99
Conf.# 5.2	-60	-140	7.59	-110.09	-61.36	-174.09
Conf.# 5.3	-60		-52.00	-124.89	-41.62	27.78

Before applying the identification routines, the statistical properties of the measurement noise were evaluated. In usual engineering practice it is assumed that all measurements are corrupted by the same measurement noise, which induces errors $\boldsymbol{\varepsilon}_i$ with zero expectation and diagonal covariance matrix $E(\boldsymbol{\varepsilon}_i\boldsymbol{\varepsilon}_i^T)=\sigma^2\mathbf{I}$. However, for the laser tracker used in our experiments, the precision highly depends on the measurement direction and varies throughout the robot workspace. In this case, the covariance matrix can be still assumed to be diagonal, but with non-equal diagonal terms, i.e. $E(\boldsymbol{\varepsilon}_i\boldsymbol{\varepsilon}_i^T)=diag(\sigma_{xi}^2,\sigma_{yi}^2,\sigma_{zi}^2)$, where σ_{xi}, σ_{yi}, σ_{zi} are different and vary from one configuration to another. This phenomenon is illustrated by the experimental data presented in Table 4.17, which includes dispersions for measurements along X-, Y- and Z-directions for 15 configurations. As follows from the presented results, the measurement noise dispersion varies from 17 μm to 153 μm and highly depends both on the direction (X, Y or Z) and the end-effector location in the manipulator workspace. In particular, for the same configuration σ_{xi}, σ_{yi}, σ_{zi} can differ by a factor of 5. Besides, from one configuration to another, corresponding dispersions may differ by 7 times. For this reason, the weighted least square technique has been applied to minimize the impact of the measurement noise.

The desired elastostatic parameters have been computed using the two-step identification procedure presented in Section 3.4. On the first step, the base and tool transformations have been computed. The identification results for the manipulator base and tool parameters are presented in Table 4.18. On the second step, all measurement data as well as the obtained base and tool transformations have been used for the identification of the manipulator elastostatic parameters, which include 9 compliance coefficients $\{k_{21},...,k_{25},k_3,...,k_6\}$. Corresponding numerical results are presented in Table 4.19.

Table 4.17 Dispersions of the deflection measurements for different configurations and directions

Configuration	σ_{xi}, [μm]		σ_{yi}, [μm]		σ_{zi}, [μm]	
	mean	std	mean	std	mean	std
Conf.# 1.1	149.7	0.8	63.7	1.1	32.9	0.4
Conf.# 1.2	56.8	4.1	85.7	7.7	118.2	14.5
Conf.# 1.3	97.1	8.6	70.0	5.1	43.7	7.8
Conf.# 2.1	28.5	0.3	19.4	0.4	35.2	0.7
Conf.# 2.2	72.4	2.8	48.1	3.5	16.9	0.5
Conf.# 2.3	153.0	8.2	46.2	2.7	22.0	1.1
Conf.# 3.1	111.8	6.2	65.9	3.3	53.1	4.2
Conf.# 3.2	74.1	5.2	55.5	3.0	58.9	1.5
Conf.# 3.3	79.8	8.7	63.2	7.3	101.6	14.9
Conf.# 4.1	68.6	1.6	72.6	1.1	79.4	1.3
Conf.# 4.2	80.2	3.3	36.2	1.0	25.6	2.6
Conf.# 4.3	52.6	3.6	38.6	0.5	29.3	1.3
Conf.# 5.1	26.2	1.1	28.9	1.3	29.4	0.4
Conf.# 5.2	87.6	3.6	120.7	1.4	42.4	1.2
Conf.# 5.3	89.8	5.7	52.4	3.1	50.3	1.1

Table 4.18 Identification results for manipulator base and tool transformations

Base parameters

	Value, [mm]	CI		Value, [deg]	CI
p_x	0.27	±0.02	φ_x	0.31	±0.01
p_y	-4.83	±0.01	φ_y	0.03	±0.01
p_z	-3.73	±0.01	φ_z	-0.08	±0.01

Tool parameters

	Reference point #1 (P1)		**Reference point #2 (P2)**		**Reference point #3 (P3)**	
	Value, [mm]	CI	Value, [mm]	CI	Value, [mm]	CI
p_x	279.49	±0.01	279.45	±0.01	280.37	±0.01
p_y	-46.01	±0.01	-44.75	±0.01	105.68	±0.01
p_z	-94.25	±0.01	93.64	±0.01	-4.90	±0.01

For comparison purposes, the identification has been performed using both Ordinary Least-Square (OLS) and Weighted Least Square (WLS) techniques. For the second approach the weights have been computed using Eq.(3.50), where σ_i have been estimated using the residual analysis and σ_0 has been assigned to 10 μm corresponding to the laser tracker precision specified by the manufacturer. To tune the parameter λ, computations have been repeated three times for

$\lambda \in \{0.5,\ 1.0,\ 2.0\}$. Corresponding values of the elastostatic parameters are presented in Table 4.19. It also includes the confidence intervals computed as $\pm 3\sigma$, where the standard deviation σ has been evaluated using the Gibbs sampling technique. The results show that the confidence intervals for OLS and WLS have intersections for all parameters of interest. Moreover, the confidence intervals for WLS are always inside confidence intervals for OLS and are considerably smaller (see Table 4.20, where the mutual locations of the results for OLS and WLS are shown).

Table 4.19 Identification results for ordinary and weighted least square techniques

Parameter [rad × μm/N]	Ordinary least square		Weighted least square					
			λ=0.5		λ=1.0		λ=2.0	
k_{21}	0.297	±0.010	0.287	±0.0003	0.287	±0.0003	0.287	±0.0003
k_{22}	0.287	±0.012	0.277	±0.0004	0.277	±0.0004	0.277	±0.0004
k_{23}	0.315	±0.018	0.302	±0.0005	0.302	±0.0005	0.302	±0.0005
k_{24}	0.302	±0.032	0.293	±0.0010	0.293	±0.0010	0.293	±0.0010
k_{25}	0.251	±0.020	0.246	±0.0007	0.246	±0.0007	0.246	±0.0007
k_3	0.396	±0.031	0.416	±0.0011	0.416	±0.0011	0.416	±0.0011
k_4	3.017	±0.248	2.786	±0.0071	2.786	±0.0071	2.786	±0.0071
k_5	3.294	±0.506	3.483	±0.0120	3.483	±0.0120	3.483	±0.0120
k_6	2.248	±0.725	2.074	±0.0267	2.074	±0.0267	2.074	±0.0267

Table 4.20 Comparison of the ordinary and weighted least square techniques

k_i	Mutual location of Confidence Intervals	CI_{OLS}	CI_{WLS}	$\sigma_{OLS}/\sigma_{WLS}$
k_{21}		3.4%	0.09%	40.5
k_{22}		4.2%	0.13%	33.2
k_{23}		5.9%	0.18%	33.9
k_{24}		10.7%	0.33%	33.1
k_{25}		7.8%	0.27%	30.1
k_3		7.8%	0.26%	28.8
k_4		8.2%	0.25%	35.1
k_5		15.3%	0.34%	42.0
k_6		32.2%	1.28%	27.2

Using the obtained values of $\{k_{21},...,k_{25}\}$, it has been identified an equivalent parameter k_2, which is used in stiffness modeling of the manipulator with the gravity compensator. Figure 4.15 shows its variation with respect to q_2. The identified compensator elastostatic parameters are presented in Table 4.21, which also includes the compensator compliance and preloading.

Table 4.21 Identification results for the compensator elastostatic parameters

Elastostatic parameters	Unit	Value	Confidence interval
k_c	[rad × μm/N]	0.144	±0.031
s_0	[mm]	458	±27
k_2^0	[rad × μm/N]	0.302	±0.004

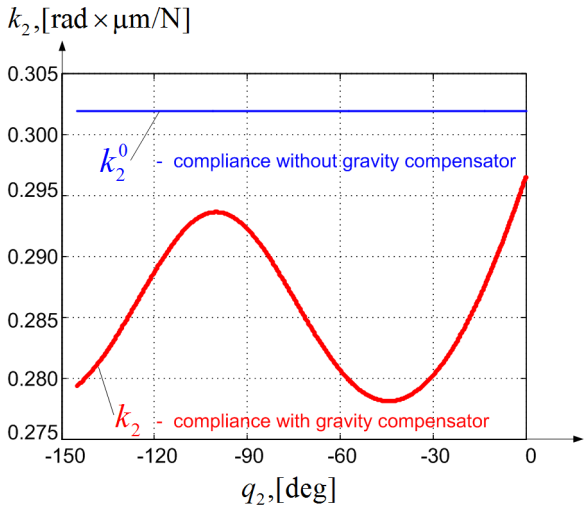

Figure 4.15 Compliance of equivalent non-linear spring in the second joint

The obtained manipulator elastostatic parameters can be used to improve the robot accuracy by compensation of the robot deformations under the external loading. For comparison purposes, the accuracy improvement due to calibration has been studied based on the residual analysis. Similar to the geometric case, two types of residuals have been examined, the coordinate-based and distance-based ones. Corresponding results are presented in Table 4.22, which includes the maximum and root mean square (RMS) values of the relevant residuals. As follows from the results, both types of the residuals have been essentially reduced after calibration. In particular, the maximum and RMS values of these two criteria have been decreased by a factor of 6.0 and 6.5 respectively.

Table 4.22 Evaluation of the manipulator accuracy improvement based on residual analysis

Criterion		Before calibration	After calibration	Improvement factor
Coordinate-based residual, [mm]	max	9.17	1.53	6.0
	RMS	2.99	0.46	6.5
Distance-based residual, [mm]	max	9.26	1.54	6.0
	RMS	5.18	0.80	6.5

4.3.4 Identification of manipulator elastostatic parameter using work-cell constraints

The above presented calibration technique (using the gravity force) is able to provide measurements for the identification of elastostatic parameters $\{k_2,...k_6\}$, but not for the parameter k_1, describing elasticity of the joint #1 whose axis is parallel to the force direction. For this reason, it is required to use an alternative experimental setup where the force is applied in a different direction.

Here, it is proposed to use the work-cell constraints (the rigid wall) in order to generate non-vertical force. More details of this setup are shown in Figure 4.16.

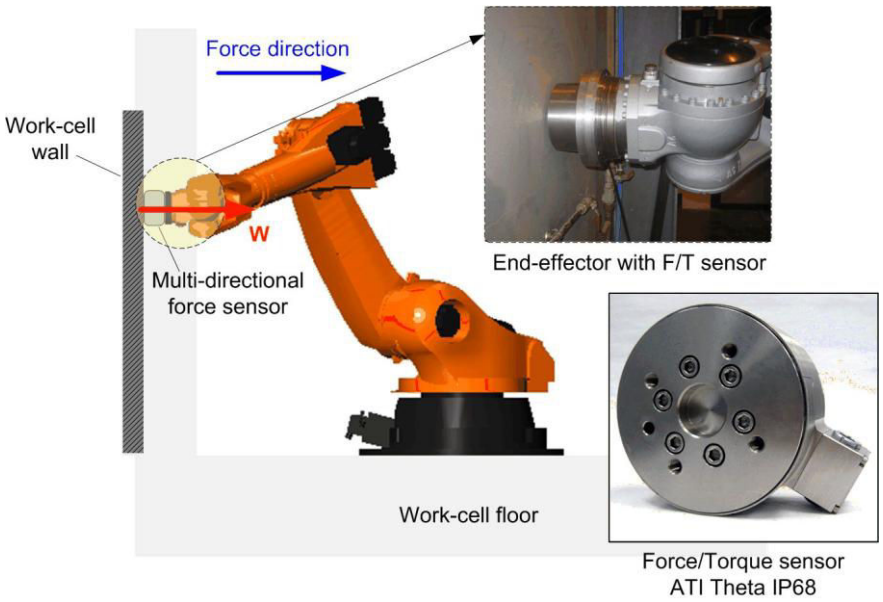

Figure 4.16 Experimental setup for calibration of elastostatic parameter k_1

As it is shown in the figure, to measure the wrench $\mathbf{w}$, the robot end-effector is equipped with a 6-dimensional force/torque sensor, ATI Theta IP68 (Ati-ia.com), whose principal parameters are presented in Table 4.24. Using this experimental setup, the manipulator end-effector deflections and corresponding force/torque have been generated by robot contact with the work-cell constraints. In this case, corresponding measurement data were obtained from the robot controller, while the target point was defined beyond the work-cell wall but the physical position of the end-effector remained the same. During this process, the measurement data were logging by the robot control unit. The data include the end-effector positions $\{p_{xi}, p_{yi}, p_{zi}\}$, corresponding changes in the actuator coordinates and six wrench components $\{F_{xi}, F_{yi}, F_{zi}, M_{xi}, M_{yi}, M_{zi}\}$. It should be noted that for 5 mm displacement of the end-effector, the deviations in robot configurations are very small (not overcome 0.3°) and can be neglected. The measurements have been taken progressively with small increments of the end-effector deflections until the maximum allowable torques in joints has been reached and the robot stopped in the break mode. This procedure provided us a set of measurements for the same configuration with different values of wrench/deflection. The calibration experiments have been carried out for three manipulator configurations, which are presented in Table 4.23.

Table 4.23 Measurement configurations for calibration of elastostatic parameter k_1

Measurement configuration	Angle coordinates, [deg]					
	q_1	q_2	q_3	q_4	q_5	q_6
Conf.#1	136.43	-55.54	72.21	-72.11	-46.06	-25.33
Conf.#2	125.20	-17.61	23.32	-85.15	-55.45	-8.52
Conf.#3	-129.31	-38.83	21.81	103.06	-52.63	157.59

Table 4.24 Specifications of the ATI Theta IP68 force/torque sensor

Physical parameters			
Weight	Diameter		Height
9 kg	160 mm		75 mm
Stiffness parameters			
K_{Fx}, K_{Fy}	K_{Fz}	K_{Mx}, K_{My}	K_{Mz}
7.1×10^{7} N/m	1.2×10^{8} N/m	3.4×10^{5} Nm/rad	5.3×10^{5} Nm/rad
Sensing ranges			
F_x, F_y	F_z	M_x, M_y	M_z
2500 N	6250 N	400 Nm	400 Nm
Resolution			
F_x, F_y	F_z	M_x, M_y	M_z
1/2 N	1 N	1/20 Nm	1/20 Nm

To identify the desired parameter k_1, the same identification algorithm has been applied (see Section 3.4), assuming that the compliances of the remaining joints are known. Using the identification results for both geometric and elastostatic parameters, it is possible to estimate the end-effector deflections that are caused by the compliances from joints #2,...,#6 and eliminate them from relevant residuals. Besides, it is also required to take into account the compliances of the force/torque sensor, which can be easily computed using the provided stiffness values. These assumptions allow us to rewrite the original identification equation (3.98) as

$$\Delta\mathbf{p}_i = \mathbf{B}_{1i}^{(p)} k_1 + \mathbf{B}_i^{*(p)} \mathbf{k}^* \tag{4.10}$$

where $\Delta\mathbf{p}_i$ is the vector of end-effector deflections obtained from the measurements, $\mathbf{B}_i^{*(p)}$ is the observation matrix corresponding to the known parameters, $\mathbf{B}_{1i}^{(p)}$ is the observation vector corresponding to the unknown parameter k_1, and the vector $\mathbf{k}^*$ aggregates the known compliance parameters, which include

- 3 parameters $\{k_{21},...,k_{23}\}$ corresponding to different values of q_2 (for different measurement configurations);
- 4 parameters $\{k_3,...,k_6\}$ corresponding to joints #3,...,#6;
- 6 parameters $\{k_{Fx},...,k_{Mz}\}$ corresponding to the force/torque sensor.

For the above listed elastostatic parameters, their impacts on relevant end-effector deflections have been computed. This allows us to simplify the identification equations (4.10) to the following form

$$\delta\mathbf{p}_i = \mathbf{B}_{1i}^{(p)} k_1 \tag{4.11}$$

where $\delta\mathbf{p}_i = \Delta\mathbf{p}_i - \mathbf{B}_i^{*(p)}\mathbf{k}^*$ is the end-effector deflection caused by joint compliance k_1 only. Applying the above described identification procedure, the elastostatic parameter k_1 and its confidence interval have been computed, corresponding results are presented in Table 4.25. Based on relevant residual analysis, the developed calibration technique allows us to compensate 91.5% the manipulator end-effector deflections and reduce the residual after calibration from 7.0 mm to 0.5 mm.

Table 4.25 Identification result of elastostatic parameter k_1

Elastostatic parameters	Unit	Value	Confidence interval
k_1	[rad×μm/N]	0.623	±0.022

Hence, combination of two methods based on utilization of the gravity force and the work-cell constraints allowed us to identify all desired elastostatic parameters of the robotic manipulator used in our experimental study. Next section will focus on the analysis of these results from point of view of robot accuracy improvement.

4.3.5 Analysis of the identification results for elastostatic calibration

To evaluate the calibration results, let us analyze the residuals computed from the identification equations for each coordinate separately. Their distributions for each configuration are presented in Figure 4.17, corresponding histograms are shown in Figure 4.18. As follows from detailed analysis, the residuals tend to follow the normal probability distributions with zero mean but different parameter σ values, which are equal to 0.53 mm, 0.38 mm, and 0.20 mm for X, Y, Z direction respectively. The latter justifies the utilization of the weighted least square technique for the parameter identification.

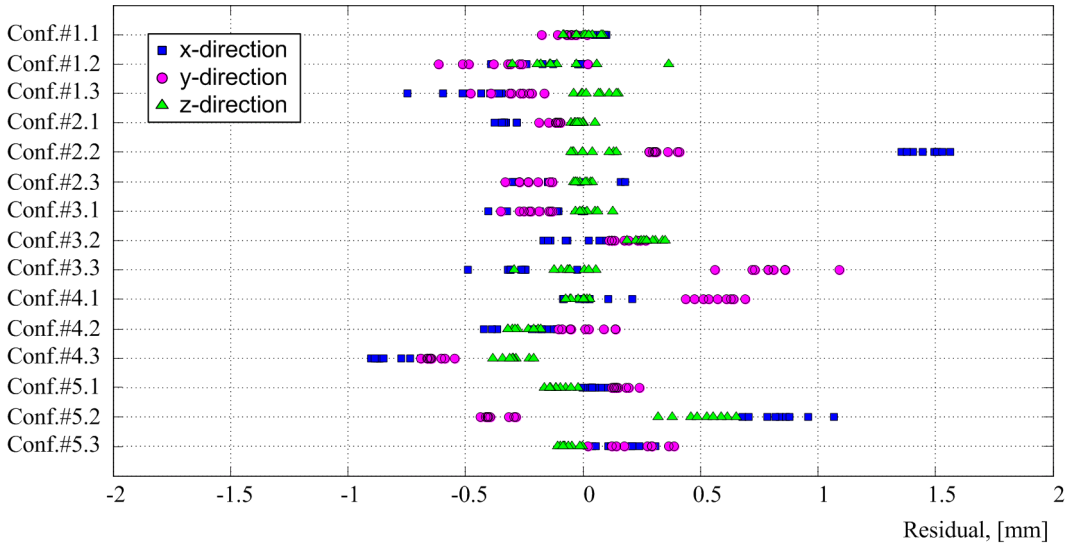

Figure 4.17 Residual distribution after elastostatic calibration for different measurement configurations

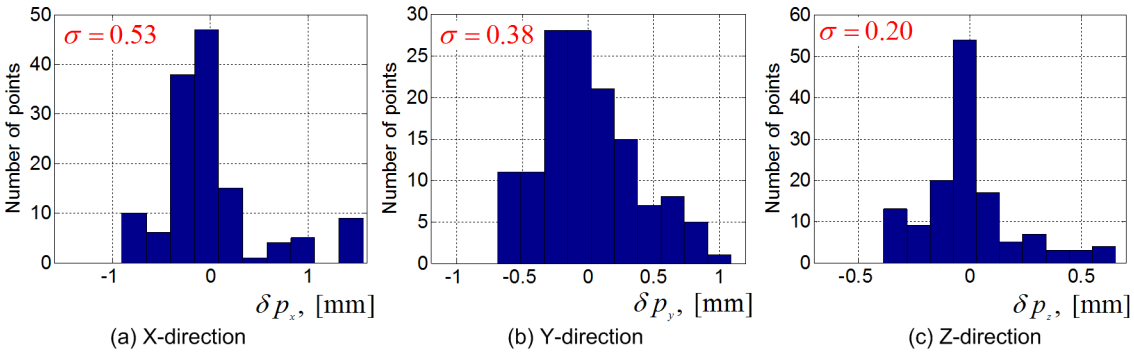

Figure 4.18 Histograms of residual distribution along X-, Y-, and Z-directions after elastostatic calibration

It is worth mentioning that the residuals after calibration along Z-direction (with the noise parameter $\sigma = 0.2$ mm) are in a good agreement with those obtained in the geometric case. Here the σ value is doubled since the measurement is performed twice for each reference point before and after the loading. In contrast, in X and Y-direction the error deviations are higher than expected. This is mainly caused by the model limitation, which is not able to describe the deflections in these two directions without taking into account the elastostatic property of joint #1. Nevertheless, as it is shown below, the elastostatic calibration ensures essential improvement of the robot accuracy.

To evaluate the robot accuracy after elastostatic calibration, expression (3.53) has been applied separately for each measurement configuration and each end-effector reference point. It allows us to compute a number of performance measures

$$\hat{\rho}_i^j = \sqrt{\text{trace}\left(\mathbf{B}_i^{j(p)}\,\text{cov}(\mathbf{k})\,\mathbf{B}_i^{j(p)T}\right)} \qquad i = \overline{1,15},\; j = \overline{1,3} \tag{4.12}$$

where i denotes the manipulator configuration number, j is the reference point number, the vector $\mathbf{k}$ collects all 9 identified stiffness parameters (5 configuration dependent compliance parameters $k_{21,\ldots,}k_{25}$ for different values of q_2, 4 constant compliance parameters $k_{3,\ldots,}k_6$), the matrix $\mathbf{B}_i^{j(p)}$ denotes the corresponding observation matrix. The covariance matrix cov($\mathbf{k}$) of size 9×9 is computed as

$$\text{cov}(\mathbf{k}) = \left(\sum_{i=1}^{15}\sum_{j=1}^{3}\mathbf{B}_i^{j(p)T}\mathbf{W}_i^{j2}\mathbf{B}_i^{j(p)}\right)^{-1}\sum_{i=1}^{15}\sum_{j=1}^{3}\mathbf{B}_i^{j(p)T}\mathbf{W}_i^{j2}\boldsymbol{\Sigma}_i^{j2}\mathbf{W}_i^{j2}\mathbf{B}_i^{j(p)}\left(\sum_{i=1}^{15}\sum_{j=1}^{3}\mathbf{B}_i^{j(p)T}\mathbf{W}_i^{j2}\mathbf{B}_i^{j(p)}\right)^{-1} \tag{4.13}$$

where the matrix $\boldsymbol{\Sigma}_i^{j2} = diag\left(\sigma_{xi}^{j2}, \sigma_{yi}^{j2}, \sigma_{zi}^{j2}\right)$ denotes the measurement errors covariance, the matrix $\mathbf{W}_i^{j2}$ collects the weighting coefficients, which are computed using expression (3.50). Table 4.26 summarizes the manipulator positioning errors evaluated using the elastostatic model and residuals after calibration for each measurement configuration separately. It also provides the residual minimum and maximum values of all the measurement points for each configuration. It should be noted that the number of measurements is equal to 9 (3 measurements for 3 end-effector reference points) for each manipulator configuration.

As follows from the results presented in Table 4.26, the positioning errors evaluated using the model are in a good agreement with the ones obtained via residual analysis (based on experimental data). It is shown that the residuals after calibration along Z-direction are essentially lower than in the other directions. For further comparison, the maximum and RMS values of the coordinate-based residuals are studied separately, corresponding results are presented in Table 4.27. In particular, the RMS values of the residuals along Z-direction has been decreased by a factor of 10.8, while along X- and Y-directions they has been reduced by a factor of 2.0 and 2.7 only. So, the developed calibration technique is able to compensate essentially the deflections in Z-direction (95% in average, see Figure 4.19).

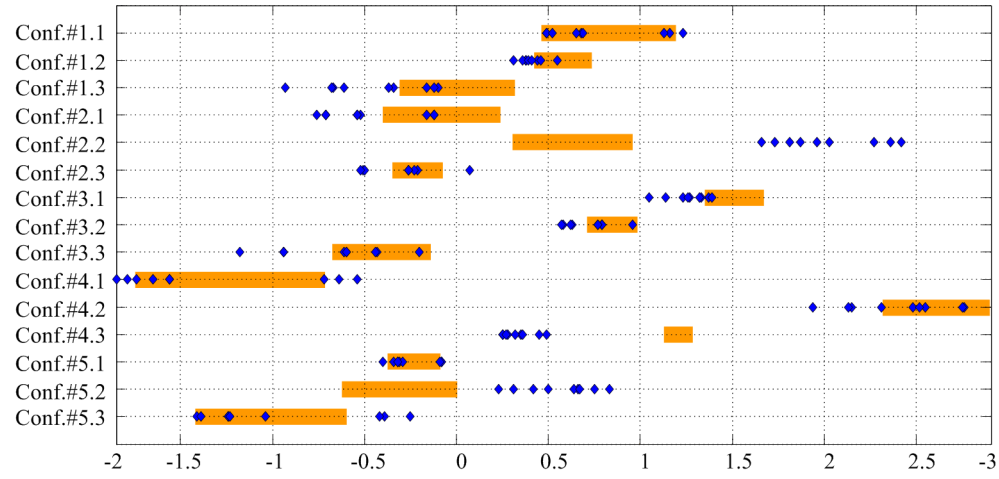

(a) Deflection distributions along X-direction

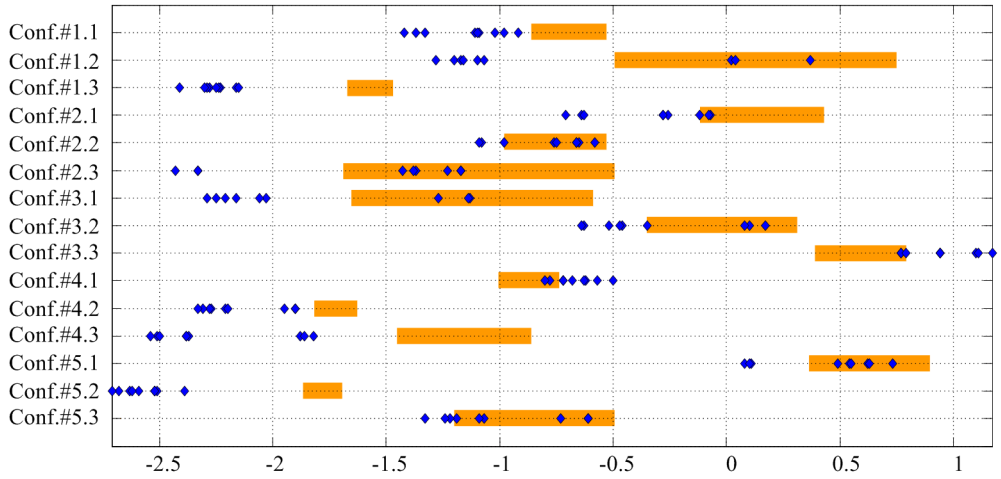

(b) Deflection distributions along Y-direction

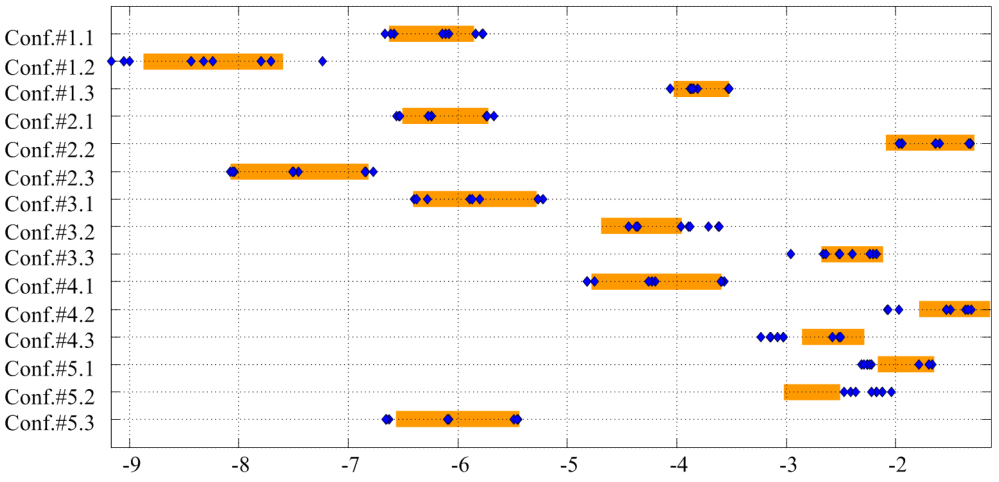

(c) Deflection distributions along Z-direction

Figure 4.19 Distributions of the manipulator end-effector deflections along X, Y, and Z directions: ♦ - experimental data; ▬ - computations based on the identified parameters

Table 4.26 Positioning errors after elastostatic calibration for each measurement configuration

Measurement configuration	Coordinate-based residuals, [mm]			Positioning error, [mm]	
	X	Y	Z	Residual-based	Model-based
Conf.# 1.1	{-0.02,...,0.10}	{-0.18,...,0.02}	{-0.08,...,0.09}	0.33	0.37
Conf.# 1.2	{-0.39,...,0.01}	{-0.61,...,0.02}	{-0.30,...,0.36}	1.05	0.71
Conf.# 1.3	{-0.74,...,-0.35}	{-0.48,...,-0.17}	{-0.04...,0.15}	0.16	0.36
Conf.# 2.1	{-0.37,...,-0.28}	{-0.19,...,-0.09}	{-0.05,...,-0.05}	0.60	0.19
Conf.# 2.2	{1.35,...,1.56}	{0.28,...,0.41}	{-0.05.,...,0.14}	0.64	0.32
Conf.# 2.3	{-0.30,...,0.18}	{-0.33,...,-0.13}	{-0.04,...,0.04}	0.25	0.31
Conf.# 3.1	{-0.40,...,0.01}	{-0.35,...,-0.13}	{-0.03,...,0.13}	0.17	0.39
Conf.# 3.2	{-0.17,...,0.10}	{0.11,...,0.27}	{0.19,...,0.35}	0.53	0.23
Conf.# 3.3	{-0.49,...,-0.03}	{0.56,...,1.09}	{-0.30,...,0.05}	0.45	0.25
Conf.# 4.1	{-0.08,...,0.21}	{0.44,...,0.69}	{-0.07,....,0.03}	0.18	0.30
Conf.# 4.2	{-0.42,...,0.11}	{-0.11,...,0.14}	{-0.32,...,-0.18}	0.13	0.17
Conf.# 4.3	{-0.90,...,0.69}	{-0.69,...,-0.55}	{-0.38,...,-0.21}	0.04	0.23
Conf.# 5.1	{-0.01,...,0.11}	{0.12,...,024}	{-0.16,...,-0.02}	0.20	0.26
Conf.# 5.2	{0.68,...,1.07}	{-0.44,...,-0.28}	{0.32,...,0.65}	0.22	0.38
Conf.# 5.3	{0.04,...,0.38}	{0.02...,0.38}	{-0.11...,-0.003}	0.37	0.38

Table 4.27 Evaluation of the elastostatic parameters identification accuracy impact on the end-effector positioning accuracy

Criterion		Coordinate-based residual, [mm]		
		Before calibration	After calibration	Improvement factor
X	max	2.50	1.56	1.6
	RMS	1.06	0.53	2.1
Y	max	2.26	1.09	2.7
	RMS	1.04	0.38	2.0
Z	max	9.02	0.65	13.8
	RMS	2.16	0.20	10.8

Hence, the elastostatic calibration experiment gives good results and justifies the theoretical contributions presented in Chapter 3. In general, the accuracy was improved by a factor of 6.5 compared to non-compensated robot, but the statistical limits have not been achieved because of the model limitations. The developed elastostatic model is able to provide quite reasonable estimates of the end-effector positioning errors for all manipulator configurations under the loading.

4.4 VALIDATION OF THE DEVELOPED POSE SELECTION TECHNIQUE

4.4.1 Validation methodology

In previous Sections, the calibration results have been evaluated for the configurations used in the identification of the model parameters. To justify further these results, it is reasonable to evaluate

them for some additional configurations (different from those employed in the calibration). In the frame of this idea, all available experimental data are divided into two non-overlapping subsets:

(i) Calibration subset, which has been used for identification of the model parameters (15 configurations, measurements for 3 reference points, repeating 3 times);

(ii) Validation subset, which has been used for evaluation of the model accuracy after calibration (5 configurations, measurements for 3 reference points, repeating 3 times).

Then, for each measurement from the validation subset, the difference between the measured end-effector position and the computed position (using the calibrated model) has been evaluated. This approach allows us to validate the model for wider set of the manipulator configurations and to avoid situation when the model is perfectly tuned for the measurement configurations only. Corresponding validation scheme is presented in Figure 4.20.

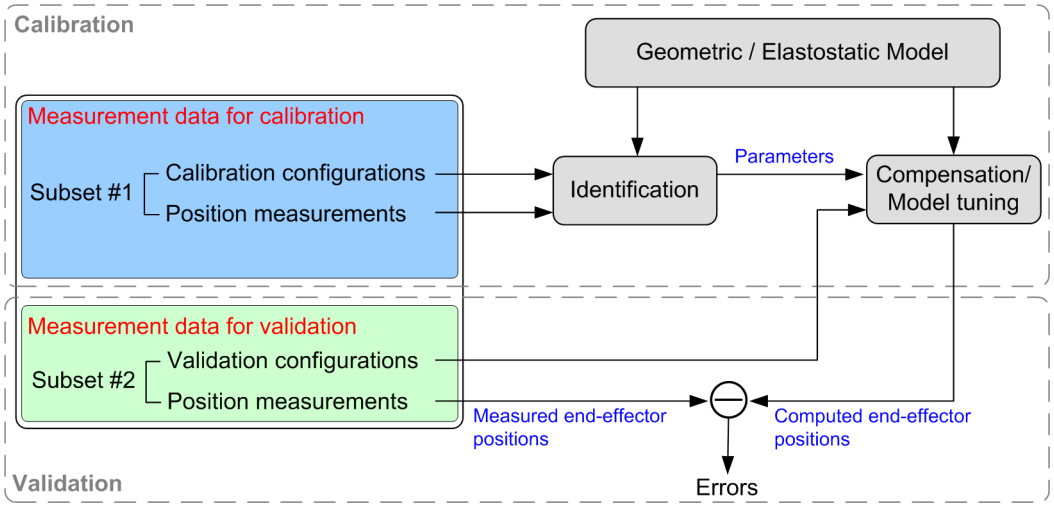

Figure 4.20 Validation scheme for the calibration results

Table 4.28 Manipulator configurations for validation of the calibration results

Validation configuration	Angle coordinates, [deg]					
	q_1	q_2	q_3	q_4	q_5	q_6
Conf.#v1	74.7	-40.0	41.9	36.1	92.8	88.8
Conf.#v2	57.1	-40.0	27.9	-64.4	58.4	155.3
Conf.#v3	72.5	-70.0	57.9	-64.4	58.4	155.3
Conf.#v4	143.3	-70.0	77.4	-33.1	107.8	-92.4
Conf.#v5	64.5	-120.0	107.9	-64.4	58.4	155.3

It should be mentioned that the validation data and the calibration data have exactly the same structure. In particular, for all validation configurations (see Table 4.28), the end-effector position coordinates before and after the loading have been measured for three reference points and repeated three times.

Further, to demonstrate advantages of the developed optimal pose selection technique, the manipulator accuracy after calibration has been compared for two distinct plans of the calibration experiments. The first one has been obtained using the industry-oriented performance measure and numerical algorithms developed in this work. In this case, the manipulator was presented as a quasi-

serial chain (in order to take into account the gravity compensator impact), and the calibration data were obtained using the enhanced partial pose measurements. The second plan used measurement configurations that were selected semi-intuitively, in accordance with some kinematic performance measures (Dumas et al., 2012). Relevant manipulator model corresponds to the strict serial architecture, and the calibration data were obtained using conventional full-pose measurements (where orientation components were computed from position measurements).

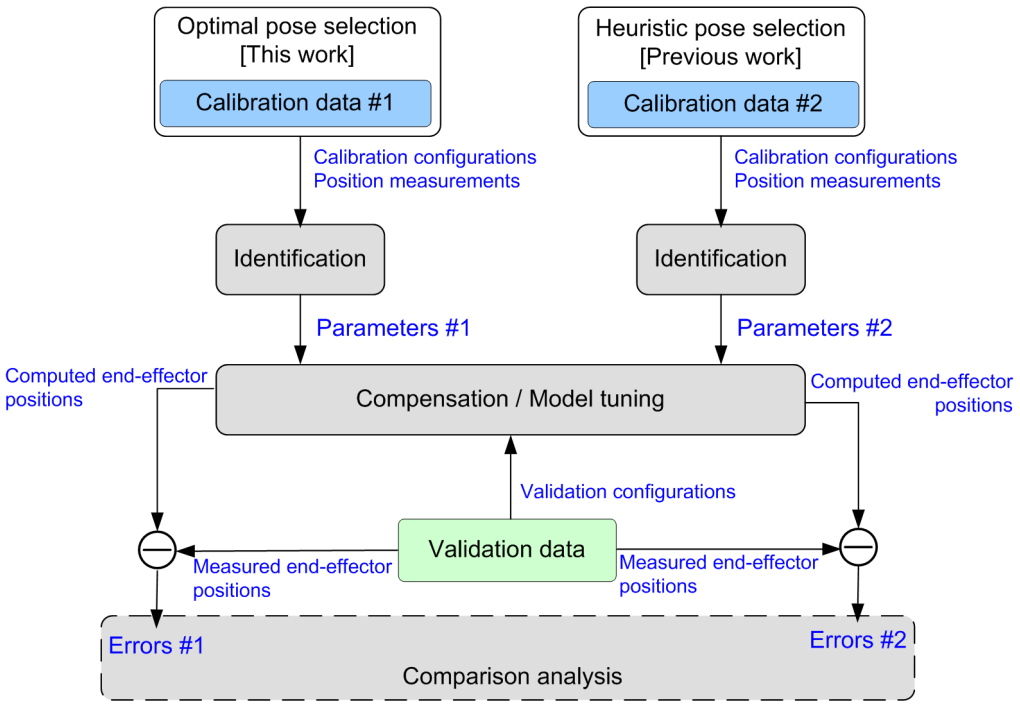

Figure 4.21 Validation scheme for the developed optimal pose selection technique

Using these two sets of calibration data, the identification yielded two slightly different sets of manipulator parameters (Table 4.29). Then, the obtained parameters (both sets) may be used to compute the end-effector positions for the validation configurations. Comparing these results with the corresponding position measurements, it is possible to evaluate the "calibration quality" and relevant plans of the experiments. In more details, the validation scheme for the developed optimal pose selection technique is shown in Figure 4.21. In the following subsections, these methodologies will be applied to validate the main contributions of this work.

Table 4.29 Manipulator elastostatic parameters obtained using known and developed approaches

	k_1	k_2	k_3	k_4	k_5	k_6
Parameters, μrad/Nm [This work]	0.623	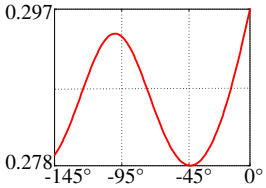	0.416	2.786	3.483	2.074
Parameters, μrad/Nm [Previous work]	3.798	0.248	0.276	1.975	2.286	3.457

4.4.2 Validation of the developed technique for geometric calibration

Similar to subsection 4.2.4, in order to validate the identification results for geometric parameters, the manipulator positioning accuracy after error compensation has been analyzed for each validation configuration separately. The geometric error distributions for these configurations are presented in Figure 4.22, corresponding histograms of errors in x, y and z direction are shown in Figure 4.23. As follows from detailed analysis, the errors have zero mean values and almost the same standard deviation σ, which is equal to 0.17 mm, 0.22 mm and 0.20 mm along X, Y, and Z directions, respectively. It should be noted that here the results tend to follow a normal distribution, however non-perfectly due to the insufficient statistical data (60 coordinates in each direction).

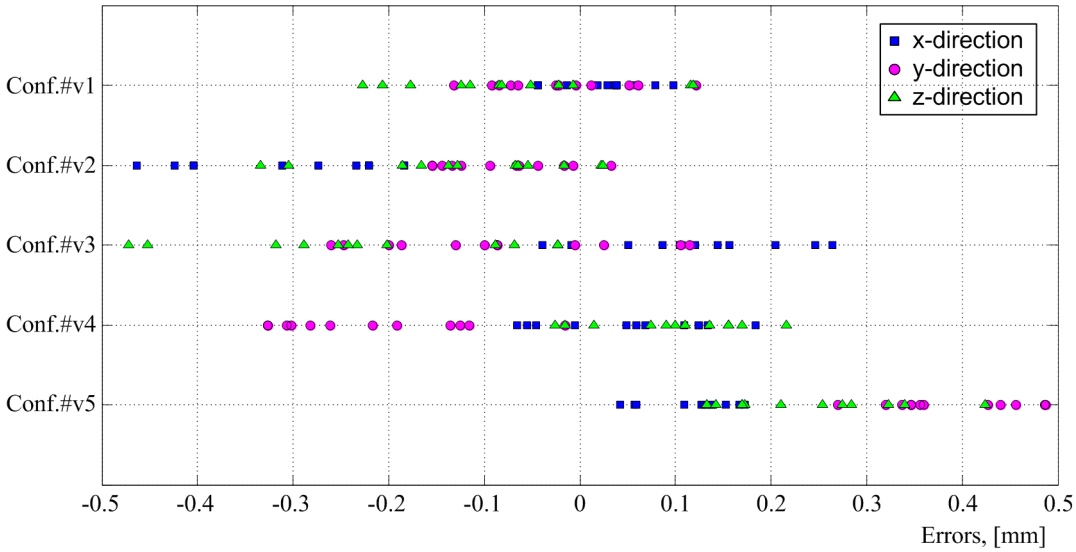

Figure 4.22 Geometric error distribution for validation configurations (from subset #2)

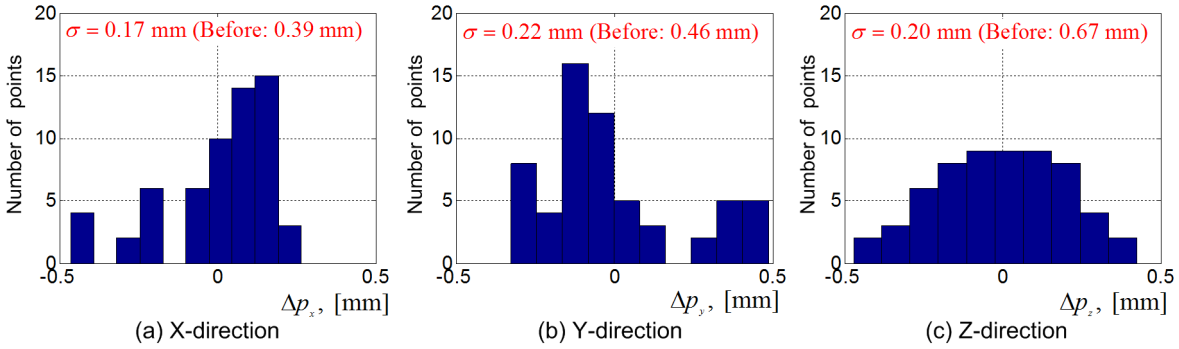

Figure 4.23 Histograms of error distribution along X, Y, and Z directions after geometric calibration (for validation configurations, data subset #2)

It is worth mentioning that the parameter σ estimated from the error analysis of the validation data (subset #2) is higher than the one computed on the identification step (using subset #1). This difference is caused by the limitation of the manipulator model used for calibration that does not take into account elastostatic properties. More detailed information is presented in Table 4.30, which contains the positioning errors for each configuration and each end-effector reference point. It also provides the average positioning errors computed from the experimental data and using the covariance matrix. The results show that the model-based predicted errors are higher compared to the previous

case (evaluated for calibration configurations) but they are in a good agreement with the ones obtained from experiments.

Table 4.30 Positioning errors after geometric compensation for each validation configuration (subset #2, without loading)

Measurement configuration	Positioning errors (experiments), [mm]			Average positioning error, [mm]	
	X	Y	Z	RMS, experiments	covariance matrix
Conf.#v1	{-0.04,...,0.10}	{-0.13,...,0.12}	{-0.23,...,0.12}	0.09	0.11
Conf.#v2	{-0.46,...,-0.18}	{-0.15,...,0.03}	{-0.33,...,0.02}	0.21	0.23
Conf.#v3	{-0.04,...,0.26}	{-0.26,...,0.12}	{-0.47...,-0.02}	0.20	0.18
Conf.#v4	{-0.07,...,0.18}	{-0.33,...,-0.02}	{-0.03,...,0.22}	0.16	0.18
Conf.#v5	{0.04,...,0.17}	{0.27...,0.49}	{0.13...,0.42}	0.28	0.12

For comparison purposes, the manipulator accuracy improvement due to geometric errors compensation has been also studied based on the residual analysis before and after compensation (for data subset #2). In particular, two types of residuals have been examined, the coordinate-based and distance-based ones. Relevant results are presented in Table 4.31, where the maximum and RMS values of corresponding criteria are provided. As follows from the obtained results, the geometric error compensation can ensure essential improvement of the robot accuracy. Here, the maximum errors have been reduced by a factor of 2.3 and 1.9 for these two criteria respectively, while the RMS errors have been decreased by a factor of 2.6. It should be mentioned that the above presented accuracy analysis has been done for the unloaded robot, the next subsection will focus on the manipulator accuracy under the loading.

Table 4.31 The manipulator accuracy improvement after geometric error compensation

Criterion		Before compensation	After compensation	Improvement factor
Coordinate-based residuals, [mm]	max	1.11	0.49	2.3
	RMS	0.52	0.20	2.6
Distance-based residuals, [mm]	max	1.28	0.66	1.9
	RMS	0.90	0.34	2.6

4.4.3 Validation of the developed technique for elastostatic calibration

Similar to Subsection 4.3.5, in order to evaluate the identification results for the elastostatic parameters, the manipulator positioning accuracy under loading has been analyzed separately for each validation configuration (data subset #2). For these configurations, the elastostatic error distributions after compensation are presented in Figure 4.24, corresponding histograms are shown in Figure 4.25. As follows from their analysis, the RMS values of these errors are equal to 0.21 mm, 0.44 mm and 0.21 mm along X, Y, and Z directions, respectively. It should be noted that here the results of positioning errors tend to follow the Maxwell-Boltzmann distribution with the overall standard deviation of 0.14 mm, however due to the insufficient statistical data, their shapes are slightly different from the theoretical one.

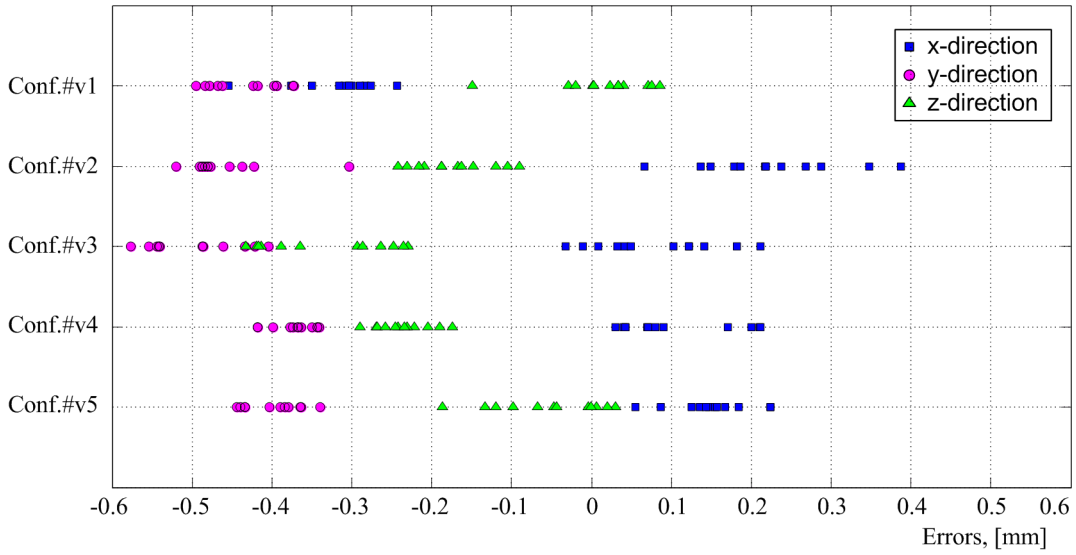

Figure 4.24 Elastostatic error distributions for validation configurations (from subset #2)

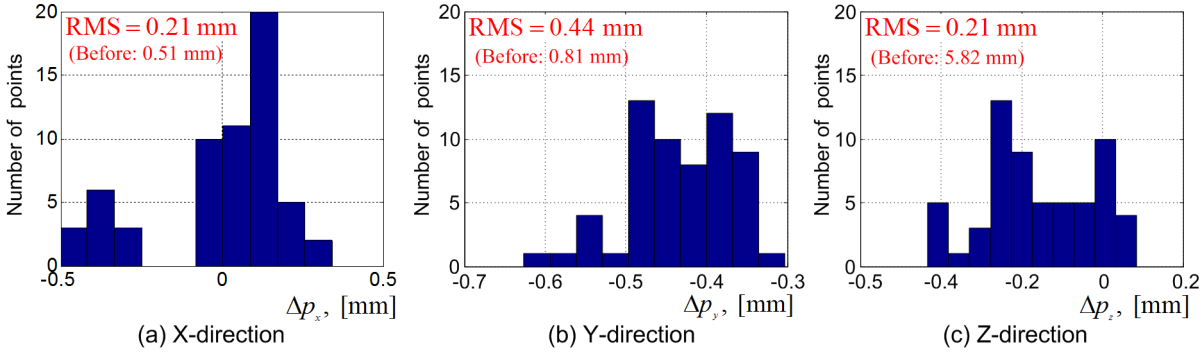

Figure 4.25 Histograms of error distribution along X-, Y-, and Z-directions after elastostatic calibration (for validation configurations, data subset #2)

It is worth mentioning that the manipulator positioning accuracy after elastostatic errors compensation along X- and Z-directions (with the RMS value equal to 0.21 mm) justifies the effectiveness of the proposed calibration technique (provided accurate manipulator parameter estimations). While the accuracy along Y-direction is not perfectly improved because of the model limitation, which is not able to describe these deflections completely. Nevertheless, as it will be shown below, the elastostatic calibration ensures essential improvement of the robot accuracy. In more details, the positioning errors concerning each configuration and each reference point are provided in Table 4.32. Similar to the geometric case, the average positioning errors are computed from the experimental data and using the covariance matrix, corresponding results indicate good agreement between these two approaches.

For comparison purposes, the manipulator accuracy improvement due to elastostatic errors compensation has been studied based on the error analysis before and after compensation. Relevant results are presented in Table 4.33, where the maximum and RMS values of the coordinate-based and distance-based residuals are provided. As follows from the obtained results, using the identified elastostatic parameters, it is possible to compensate essentially the deflections along Z-direction (96.4% in average). In general, the manipulator positioning accuracy has been improved by a factor of 11.1 compared to a non-compensated robot.

Table 4.32 Positioning errors after elastostatic calibration for each validation configuration (subset #2, under loading)

Validation configuration	Coordinate-based residuals, [mm]			Average positioning error, [mm]	
	X	Y	Z	RMS	Model-based
Conf.#v1	{-0.46,...,-0.24}	{-0.49,...,-0.37}	{-0.15,...,0.09}	0.31	0.54
Conf.#v2	{0.07,...,0.39}	{-0.52,...,-0.30}	{-0.24,...,-0.09}	0.32	0.52
Conf.#v3	{-0.03,...,0.21}	{-0.63,...,-0.40}	{-0.43...,-0.23}	0.36	0.26
Conf.#v4	{0.03,...,0.21}	{-0.42,...,-0.34}	{-0.29,...,-0.17}	0.26	0.27
Conf.#v5	{0.05,...,0.22}	{-0.44,...,-0.34}	{-0.19...,0.03}	0.25	0.22

Table 4.33 The manipulator accuracy improvement after elastostatic error compensation

Criterion		Coordinate-based residual, [mm]				
		Before compensation	After compensation		Improvement factor	
			[Previous work]*	[This work]**	[Previous work]*	[This work]**
X	max	0.79	0.51	0.46	1.5	1.7
	RMS	0.51	0.23	0.21	2.1	2.4
Y	max	1.35	0.68	0.63	1.9	2.2
	RMS	0.81	0.44	0.44	1.8	1.8
Z	max	8.06	1.63	0.43	4.9	18.7
	RMS	5.82	1.17	0.21	5.0	28.0
		Distance-based residual, [mm]				
	max	8.28	1.77	0.78	4.6	10.4
	RMS	5.90	1.27	0.53	4.6	11.1

*Using full-pose measurement method, semi-intuitively selected measurement configurations, corresponding model does not take into account the gravity compensator impact.

**Using enhanced partial pose measurement method, optimal pose selection technique and manipulator stiffness model that takes into account the gravity compensator impact.

In accordance with the proposed validation methodology (see Figure 4.21), the robot accuracy has been also evaluated using error compensation strategy that implements the parameters identified in previous work (Dumas, 2011). Comparing to the previous results, the compensation efficiency has been increased by a factor of 2.4 using almost the same number of configurations. Hence, the above presented analyses confirmed the theoretical contributions presented in Chapters 2 and 3. The developed calibration technique allows us to increase essentially the manipulator positioning accuracy under external loading using reasonable number of measurement configurations.

4.5 SUMMARY

The chapter is devoted to the experimental validation of the developed optimal pose selection technique employed in the calibration experiments. Particular attention has been paid to the positioning accuracy improvement of KUKA KR-270 industrial robot that includes the gravity compensator, and for which the influence of the compliance errors cannot be neglected. In contrast to other works, the manipulator accuracy has been evaluated not only for the measurement configurations, but also for a wider set of configurations (different from those used for calibration).

In more details, the results of Chapter 4 can be summarized as the following

(i) Using the optimal measurement configurations, the manipulator geometric parameters have been identified with the accuracy 0.15 mm and 0.01 deg for linear and angular ones respectively (in average). These results allowed us to achieve the manipulator positioning accuracy of 0.17 mm (without loading), which is 5.5 times better compared to the non-calibrated robot.

(ii) Using the developed technique, the gravity compensator parameters (both geometric and elastostatic ones) have been identified with the accuracy of 0.48 mm and 0.02 μrad/Nm respectively. These results allowed us to estimate the equivalent stiffness of joint #2 (which is configuration dependent) and to introduce a non-linear term in the conventional stiffness model of the robotic manipulator.

(iii) Using the optimal measurement configurations, the manipulator elastostatic parameters have been identified with the relative accuracy about 0.7%. These results allowed us to compensate about 95% of the compliance errors in the gravity force direction. Corresponding positioning accuracy under a loading of 2.7KN is equal to 0.21 mm, which is 11.1 times better than the one of non-compensated robot (for an arbitrary direction).

(iv) Advantages of the developed technique for optimal measurement pose selection have been confirmed by relevant comparison study, which is based on the positioning accuracy estimation of the calibrated robot for two sets of the identified elastostatic parameters and for dedicated set of manipulator configurations, which are different from ones used for calibration. Comparison results show that, due to proper selection of the measurement poses, the robot accuracy under the loading has been increased by a factor of 2.4 (with 15 measurement configurations).

In spite of promising results obtained in this chapter, there are still some problems that give directions for future work. They are caused by the limitation of the manipulator elastostatic model, which assumes that the compliances are localized in the actuated joints. This assumption imposes an obvious limit on the manipulator positioning accuracy improvement, which is not critical for this particular case study but should be taken into account in the general case.

The main results of Chapter 4 have been presented/accpeted in/by international conferences (Klimchik et al., 2013f; Klimchik et al., 2014b; Wu et al., 2014) and have been submitted to international journal (Klimchik et al., 2013g).

CONCLUSIONS AND PERSPECTIVES

CONTRIBUTIONS OF THE THESIS

This thesis was devoted to enhancement of geometric and elastostatic model calibration techniques for industrial robots employed in machining of large dimensional parts. Particular attention was paid to the robot positioning accuracy improvement by means of compensation of the geometric and elastostatic errors. The main contributions are in the area of the calibration experiment design (i.e. optimal measurement pose selection), allowing to reduce the measurement noise impact and to achieve desired accuracy using small number of calibration experiments. In more details, the main theoretical contributions are summarized as follows:

(i) A *new approach for calibration experiments design* for serial and quasi-serial industrial robots. This approach employs a new industry-oriented performance measure, which evaluates the quality of calibration plan via the manipulator positioning accuracy after geometric and compliance error compensation, and takes into account the industrial requirements of the prescribed manufacturing task (using one or several test-poses). It is proved that the proposed performance measure can be presented as the weighted trace of the relevant covariance matrix, where the weighting coefficients are defined by the corresponding test-pose. Such approach allows us to find the optimal measurement configurations for calibration experiments and to improve essentially the robot positioning accuracy for a desired manipulator test-pose.

(ii) *Enhanced partial pose measurement method*, which uses only direct position measurements from the external device for several end-effector reference points. It allows us to avoid additional computations of the end-effector orientation components, which cause non-homogeneity in relevant identification equations and do not require any normalization (which arises in the case when full pose coordinates are used, both position and orientation). It has been shown that such a method increases the parameter identification accuracy.

(iii) Stiffness modeling approach for quasi-serial *manipulators with gravity compensators* that create closed-loop chains. The proposed approach is based on an extension of the conventional stiffness model of serial manipulator by including in it some configuration dependent parameters (that are usually treated as constants). Corresponding methodology for calibration of the gravity compensator models is proposed, which is able to identify the geometric and elastostatic parameters. In contrast to other works, it is based on the singular value decomposition and uses measurement information obtained from both position and joint sensors.

The obtained theoretical results have been validated via experimental study that dealt with geometric and elastostatic calibration of a KUKA KR-270 industrial robot employed in milling of large dimensional parts for aerospace industry. The identified set of parameters allowed us to describe both geometric and elastostatic properties of the manipulator with gravity compensator. The obtained models were used for positioning error compensation during the milling process. For the unloaded mode, the calibration results allowed us to improve the manipulator positioning accuracy by a factor of 5.5 compared to the non-calibrated robot. For the loaded mode, corresponding positioning accuracy under the force a force equals to 2.7kN is 11.1 times better than the one of non-compensated robot.

Compared to the previous work (Dumas, 2011) devoted to similar problem, the robot accuracy under the loading is 2.4 time higher due to proper selection of the measurement poses (with similar number of configurations used for calibration experiments).

LIMITATIONS OF OBTAINED RESULTS

In spite of the essential advantages, the developed approach has some limitations that are mainly related to the manipulator modeling assumptions and the calibration technique employed in this work. They are summarized as follows:

Limitations of the manipulator modeling assumptions:

(i) It was assumed that the manipulator compliance is mainly caused by the elasticity of the actuated joints and relevant stiffness model includes a set of one-dimensional virtual springs only. However, in general case, the link stiffness should be also taken into account. This leads to more sophisticated stiffness model, where the link/joint compliances are described by 6×6 matrices that can be hardly identified using the calibration procedure considered in this work.

(ii) It was assumed that the external force is applied to the robot end-effector only. However in some cases, the influence of the link weights should be also taken into account if they create non-negligible deformations in the manipulator elastic components. This requires revision of the elastostatic model used in this work.

(iii) It was assumed that some other sources of the positioning errors (different from the geometric and elastostatic ones) are negligible. They include friction/backlash in joints, thermal effects, environmental factors, etc. In some cases, they may also affect the manipulator positioning accuracy and should be taken into account.

Limitations of the calibration technique:

(iv) The developed approach for optimal measurement pose selection is based on the notion of the manipulator test-pose(s), for which the robot accuracy is evaluated (after error compensation). However, it is not obvious that the same manipulator accuracy can be achieved for other workspace points.

(v) The employed measurement technique relies on the laser tracker, providing the Cartesian coordinates for the relevant reference points. This type of measurement device is usually quite expensive and induces some limitation for calibration experiments due to visibility issue. As an alternative, another measurement technique can be used (the closed-loop method, for instance) but relevant expressions should be revised, and the origin of measurement noise should be redefined. Moreover, in the frame of this work, it was assumed that the measurement noise comes from the laser tracker only, while other sources such as the actuator encoders and force measurement devices were neglected.

Nevertheless, in the frame of the considered application area, the limitations concerning the model assumptions are not critical because the desired accuracy has been achieved in the experimental study. Moreover, it is possible to extend/modify the developed approach in order to adapt other measurement techniques. However, some of the above mentioned limitations provide us the research directions for future work.

PERSPECTIVES AND FUTURE WORK

To generalize the obtained results and enlarge the application area, it is reasonable to continue research in several directions and to focus on the following issues:

(i) Enhancement of the developed optimal pose selection technique for the case where the manipulator stiffness properties are described by a set of 6×6 matrices describing the elasticity of both links and joints. Some related problems arising here include synthesis of the complete, irreducible elastostatic model for robotic manipulator and parameter identifiability issues.

(ii) Extending the gravity compensator family included in the manipulator stiffness model. Relevant problems include developing mathematical models that describe the compensator elasticity (taking into account the influence of pneumatic cylinder, for instance), methodologies and algorithms for identification of the model parameters, and corresponding design of calibration experiments. It is also interesting to extend/generalize the developed technique for calibration of quasi-serial robots, which include closed-loop kinematic chains in the general case.

(iii) Developing a regular technique allowing the users to generate automatically a set of test-poses (employed in the proposed approach) from CAD-based description of the machining process. This technique should be integrated in the simulation software providing optimal layout design and workpiece placement with respect to the robotic manipulator.

PUBLICATIONS OF THESIS CONTRIBUTIONS

Journal Papers:

Klimchik, A., **Wu, Y.**, Pashkevich, A., Caro, S., Furet, B., 2012c. Optimal Selection of Measurement Configurations for Stiffness Model Calibration of Anthropomorphic Manipulators. Applied Mechanics and Materials 162, 161-170.

Klimchik, A., Pashkevich, A., **Wu, Y.**, Caro, S., Furet, B., 2012a. Design of calibration experiments for identification of manipulator elastostatic parameters. Mechanics Engineering and Automation 2, 531-542.

Klimchik, A., Pashkevich, A., **Wu, Y.**, Caro, S., Furet, B., 2013b. Calibration experiments planning for identification of manipulator elastostatic parameters. Pomiary Automatyka Robotyka 1/2013, 128-139.

Klimchik, A., **Wu, Y.**, Caro, S., Furet, B., Pashkevich, A., 2013g. Geometric and elastostatic calibration of robotic manipulator using partial pose measurements. Advanced Robotics, Submitted in 2013.

Book Chapters:

Wu, Y., Klimchik, A., Pashkevich, A., Caro, S., Furet, B., 2013b. Industry-oriented Performance Measures for Design of Robot Calibration Experiment, New Trends in Mechanism and Machine Science. Springer, pp. 519-527.

Klimchik, A., Pashkevich, A., **Wu, Y.**, Furet, B., Caro, S., 2012b. Optimization of measurement configurations for geometrical calibration of industrial robot, Intelligent Robotics and Applications. Springer, pp. 132-143.

Klimchik, A., Caro, S., **Wu, Y.**, Chablat, D., Furet, B., Pashkevich, A., 2014a. Stiffness Modeling of Robotic Manipulator with Gravity Compensator, Computational Kinematics. Springer, pp. 185-192.

International Conference Proceedings:

Klimchik, A., **Wu, Y.**, Dumas, C., Caro, S., Furet, B., Pashkevich, A., 2013f. Identification of geometrical and elastostatic parameters of heavy industrial robots. IEEE International Conference on Robotics and Automation (ICRA 2013). IEEE, pp. 3707-3714.

Klimchik, A., **Wu, Y.**, Caro, S., Pashkevich, A., 2011. Design of experiments for calibration of planar anthropomorphic manipulators. IEEE/ASME International Conference on Advanced Intelligent Mechatronics (AIM), pp. 576-581.

Wu, Y., Klimchik, A., Pashkevich, A., Caro, S., Furet, B., 2012. Optimality criteria for measurement poses selection in calibration of robot stiffness parameters, Proceedings of the ASME 2012 11th Biennial Conference on Engineering Systems Design and Analysis, (10 pages).

Wu, Y., Klimchik, A., Pashkevich, A., Caro, S., Furet, B., 2013a. Efficiency Improvement of measurement Pose Selection Techniques in Robot Calibration, IFAC Conference on Manufacturing Modeling, Management and Control, Saint Petersburg, Russia, pp. 832-837.

Klimchik, A., **Wu, Y.**, Abba, G., Ganrnier, S., Furet, B., Pashkevich, A., 2013c. Robust algorithm for calibration of robotic manipulator model, IFAC Conference on Manufacturing Modeling, Management and Control, Saint Petersburg, Russia, pp. 838-842.

Klimchik, A., **Wu, Y.**, Caro, S., Dumas, C., Furet, B., Pashkevich, A., 2013d. Modelling of the gravity compensators in robotic manufacturing cells, IFAC Conference on Manufacturing Modeling, Management and Control, Saint Petersburg, Russia, pp. 820-825.

Klimchik, A., **Wu, Y.**, Caro, S., Furet, B., Pashkevich, A., 2013e. Advanced robot calibration using partial pose measurements, 18th International Conference on Methods and Models in Automation and Robotics (MMAR), Międzyzdroje, Poland, pp. 264-269.

Wu, Y., Klimchik, A., Caro, S., Furet, B., Pashkevich, A., 2014, Test-pose technique in geometric calibration of heavy industrial robots, The Canadian Society for Mechanical Engineering International Congress, Toronto, Ontario, Canada, June 1-4, 2014, Accepted.

Klimchik, A., **Wu, Y.**, Caro, S., Dumas, C., Furet, B., Pashkevich, A., 2014b, Accuracy improvement of robot-based milling using an enhanced manipulator model, ROMANSY-2014 CISM-IFToMM SYMPOSIUM on Theory and Practice of Robots and Manipulators, Moscow, Russia, June 23-26, 2014, Accepted.

National Conference Proceedings:

Wu, Y., Klimchik, A., Pashkevich, A., Caro, S., Furet B., 2010 Calibration of kinetostatic parameters of robots, 12e Congres Annuel de la ROADEF, 2, pp; 757-758

Klimchik, A., Pashkevich, A., **Wu**, **Y.,** Bondarenko, D., 2010 S. Caro, Experiment planning for geometric calibration of robots, 12e congres annuel de la ROADEF, 2, pp; 763-764

REFERENCES

Abele, E., Weigold, M., Rothenbücher, S., 2007. Modeling and identification of an industrial robot for machining applications. CIRP Annals-Manufacturing Technology 56, pp. 387-390.

Akin, J.E., 2005. Finite element analysis with error estimators: An introduction to the FEM and adaptive error analysis for engineering students. Butterworth-Heinemann.

Alici, G., Shirinzadeh, B., 2005. Enhanced stiffness modeling, identification and characterization for robot manipulators. IEEE Transactions on Robotics, 21, pp. 554-564.

Angeles, J., 2007. Fundamentals of robotic mechanical systems: theory, methods, and algorithms. Springer.

Arumugam, H.K., Voyles, R.M., Bapat, S., 2004. Stiffness analysis of a class of parallel mechanisms for micro-positioning applications. Proceedings. of IEEE/RSJ International Conference on Intelligent Robots and Systems (IROS), pp. 1826-1831.

Aspragathos, N.A., Dimitros, J.K., 1998. A comparative study of three methods for robot kinematics. IEEE Transactions on Systems, Man, and Cybernetics, Part B: Cybernetics, 28, pp. 135-145.

Ati-ia.com, ATI Industrial Automation, http://www.ati-ia.com/.

Atkinson, A.C., Donev, A.N., Tobias, R.D., 2007. Optimum experimental designs, with SAS. Oxford University Press Oxford.

Bai, Y., Zhuang, H., Roth, Z.S., 2003. Experiment study of PUMA robot calibration using a laser tracking system. Proceedings of IEEE International Workshop on Soft Computing in Industrial Applications (SMCia'03), pp. 139-144.

Becquet, M., 1987. Analysis of flexibility sources in robot structure, IMACS/IFAC International Symp. Modeling and Simulation of Distributed Parameters Hiroshima, Japan, pp. 419-424.

Bennett, D.J., Geiger, D., Hollerbach, J.M., 1991. Autonomous robot calibration for hand-eye coordination. The International journal of robotics research, 10, pp. 550-559.

Bernhardt, R., Bernhardt, R., Albright, S., 1993. Robot calibration. Springer.

Besnard, S., Khalil, W., 1999. Calibration of parallel robots using two inclinometers. Proceedings. of IEEE International Conference on Robotics and Automation, pp. 1758-1763.

Besnard, S., Khalil, W., 2001. Identifiable parameters for parallel robots kinematic calibration. Proceedings of. IEEE International Conference on Robotics and Automation (ICRA), pp. 2859-2866.

Bogdan, I.-C., Abba, G., 2009. Identification of the servomechanism used for micro-displacement. IEEE/RSJ International Conference on Intelligent Robots and Systems (IROS), pp. 1986-1991.

Borm, J.-H., Meng, C.-H., 1991. Determination of optimal measurement configurations for robot calibration based on observability measure. The International Journal of Robotics Research, 10, pp. 51-63.

Bouzgarrou, B., Fauroux, J., Gogu, G., Heerah, Y., 2004. Rigidity analysis of T3R1 parallel robot with uncoupled kinematics, Proc. of the 35th International Symposium on Robotics (ISR), Paris, France.

Carbone, G., Ceccarelli, M., 2010. Comparison of indices for stiffness performance evaluation. Frontiers of Mechanical Engineering in China, 5, pp. 270-278.

Caro, S., Dumas, C., Garnier, S., Furet, B., 2013. Workpiece placement optimization for machining operations with a KUKA KR270-2 robot. IEEE International Conference on Robotics and Automation (ICRA), pp. 2921-2926.

Castelino, K., D'Souza, R., Wright, P.K., 2003. Toolpath optimization for minimizing airtime during machining. Journal of Manufacturing Systems 22, pp. 173-180.

Chen, S.-F., Kao, I., 2000. Conservative congruence transformation for joint and Cartesian stiffness matrices of robotic hands and fingers. The International Journal of Robotics Research 19, pp.835-847.

Chen, S.-F., Kao, I., 2002. Geometrical approach to the conservative congruence transformation (CCT) for robotic stiffness control. Proceedings of IEEE International Conference on Robotics and Automation, pp. 544-549.

Chen, Y., Gao, J., Deng, H., Zheng, D., Chen, X., Kelly, R., 2013. Spatial statistical analysis and compensation of machining errors for complex surfaces, Precision Engineering 37, 203-212.

Chou, J.C., Kamel, M., 1991. Finding the position and orientation of a sensor on a robot manipulator using quaternions. The international journal of robotics research 10, 240-254.

Ciblak, N., Lipkin, H., 1999. Synthesis of Cartesian stiffness for robotic applications. Proceedings. of IEEE International Conference on Robotics and Automation, pp. 2147-2152.

Cherif, M., K'nevez, J.-Y., Ballu, A., 2010. Quantification des effets thermiques sur la précision d'un robot d'usinage, Intercut 2010 - 6ème Assises MUGV, Arts et Métiers ParisTech, Cluny.

Coleman, T.F., Verma, A., 1996. Structure and efficient Jacobian calculation. Cornell Theory Center Technical Report CTC96TR238, Cornell University.

Conrad, K.L., Shiakolas, P.S., Yih, T., 2000. Robotic calibration issues: Accuracy, repeatability and calibration, Proceedings of the 8th Mediterranean Conference on Control and Automation (MED2000), Rio, Patras, Greece.

Corradini, C., Fauroux, J.-C., Krut, S., 2003. Evaluation of a 4-degree of freedom parallel manipulator stiffness, Proceedings of the 11th World Congress in Mechanisms and Machine Science, Tianjin (China).

Cui, H., Zhu, Z., 2006. Error Modeling and Accuracy of Parallel Industrial Robots, Source: Industrial-Robotics-Theory-Modelling-Control. ISBN 3-86611-285-8.

Daney, D., 2002. Optimal measurement configurations for Gough platform calibration. Proceedings of IEEE International Conference on Robotics and Automation, pp. 147-152.

Daney, D., Andreff, N., Chabert, G., Papegay, Y., 2006. Interval method for calibration of parallel robots: Vision-based experiments. Mechanism and Machine Theory 41, 929-944.

Daney, D., Emiris, I.Z., 2001. Robust parallel robot calibration with partial information. Proceedings of IEEE International Conference on Robotics and Automation, pp. 3262-3267.

Daney, D., Papegay, Y., Madeline, B., 2005. Choosing measurement poses for robot calibration with the local convergence method and Tabu search. The International Journal of Robotics Research 24, 501-518.

De Luca, A., Flacco, F., 2011. A PD-type regulator with exact gravity cancellation for robots with flexible joints. IEEE International Conference on Robotics and Automation, pp. 317-323.

De Pauw, D., 2005. Optimal experimental design for calibration of bioprocess models: a validated software toolbox, PhD thesis, Ghent University.

Deblaise, D., Hernot, X., Maurine, P., 2006. A systematic analytical method for PKM stiffness matrix calculation. Proceedings of IEEE International Conference on Robotics and Automation, pp. 4213-4219.

Delcam, 2013. Delcam launches PowerMILL Robot Interface, http://www.delcam.com/languages/es/news/press_article.asp?releaseId=1565.

Denavit, J., Hartenberg, R., 1955. A kinematic notation for lower-pair mechanisms based on matrices. Trans. of the ASME, Journal of Applied Mechanics 23, 215–221.

Dépincé, P., Hascoët, J.-Y., 2006. Active integration of tool deflection effects in end milling. Part 2. Compensation of tool deflection. International Journal of Machine Tools and Manufacture 46, 945-956.

DML, Typical Tolerances of Manufacturing Processes. MAE Design and Manufacturing Laboratory.

Driels, M.R., 1993. Full-pose calibration of a robot manipulator using a coordinate-measuring machine. The International Journal of Advanced Manufacturing Technology 8, 34-41.

Driels, M.R., Pathre, U.S., 1990. Significance of observation strategy on the design of robot calibration experiments. Journal of Robotic Systems 7, 197-223.

Driels, M.R., Swayze, W., 1994. Automated partial pose measurement system for manipulator calibration experiments. IEEE Transactions on Robotics and Automation 10, 430-440.

Duelen, G., Schröer, K., 1991. Robot calibration—method and results. Robotics and computer-integrated manufacturing 8, 223-231.

Dumas, C., 2011. Développement de méthodes robotisées pour le parachèvement de pièces métalliques et composites, thèse de doctorat, IRCCyN, Université de Nantes.

Dumas, C., Caro, S., Cherif, M., Garnier, S., Furet, B., Zha, X., Kim, T., Sarma, S., Matsuoka, S., Shimizu, K., 2012. Joint stiffness identification of industrial serial robots. Robotica 30, 649-659.

Elatta, A., Gen, L.P., Zhi, F.L., Daoyuan, Y., Fei, L., 2004. An overview of robot calibration. Information Technology Journal 3, 74-78.

Everett, L., Driels, M., Mooring, B., 1987. Kinematic modelling for robot calibration,. Proceedings of IEEE International Conference on Robotics and Automation, pp. 183-189.

Fanuc.co, http://www.fanuc.co.jp/eindex.htm.

Fletcher, R., 2013. Practical methods of optimization. John Wiley & Sons.

Franceschini, G., Macchietto, S., 2008. Model-based design of experiments for parameter precision: State of the art. Chemical Engineering Science 63, 4846-4872.

Funda, J., Paul, R.P., 1990. A computational analysis of screw transformations in robotics. IEEE Transactions on Robotics and Automation 6, 348-356.

Funda, J., Taylor, R.H., Paul, R.P., 1990. On homogeneous transforms, quaternions, and computational efficiency. IEEE Transactions on Robotics and Automation 6, 382-388.

Garant, 2010. garant machining handbook, http://www.hoffmann-group.com/fileadmin/catalog/de/ZHB/BK/index.html.

Gautier, M., Briot, S., 2013. Dynamic parameter identification of a 6 DOF industrial robot using power model, IEEE International Conference on Robotics and Automation, pp. 2914-2920.

Gautier, M., Janot, A., Jubien, A., Vandanjon, P.O., 2011. Joint stiffness identification from only motor force/torque data. The 50th IEEE Conference on Decision and Control and European Control Conference (CDC-ECC), pp. 5088-5093.

Gong, C., Yuan, J., Ni, J., 2000. Nongeometric error identification and compensation for robotic system by inverse calibration. International Journal of Machine Tools and Manufacture 40, 2119-2137.

Goodwin, G.C., Payne, R.L., 1977. Dynamic system identification: experiment design and data analysis, Mathematics in science and engineering, pp.136.

Gosselin, C., 1990. Stiffness mapping for parallel manipulators. IEEE Transactions on Robotics and Automation 6, 377-382.

Gosselin, C., Zhang, D., 2002. Stiffness analysis of parallel mechanisms using a lumped model. International Journal of Robotics and Automation 17, 17-27.

Goswami, A., Quaid, A., Peshkin, M., 1993. Complete parameter identification of a robot from partial pose information. Proceedings of IEEE International Conference on Robotics and Automation, pp. 168-173.

Groover, M.P., 2010. Fundamentals of Modern Manufacturing: Materials, Processes, and Systems. John Wiley & Sons.

Gu, Y., 1988. Analysis of orientation representations by Lie algebra in robotics. Proceedings of IEEE International Conference on Robotics and Automation, pp. 874-879.

Gu, Y.L., 1990. An exploration of orientation representation by Lie algebra for robotic applications. IEEE Transactions on Systems, Man and Cybernetics 20, 243-248.

Guizzo, E., 2008. The Rise of the Machines. IEEE Spectrum 45, 88-88.

Hayati, S.A., 1983. Robot arm geometric link parameter estimation. The 22nd IEEE Conference on Decision and Control, pp. 1477-1483.

HHI.co, Hyundai Heavy Develops Mini Welding Robot for Shipbuilding, http://english.hhi.co.kr/news/view?idx=483.

Hollerbach, J.M., 1989. A Survey of Kinematic Calibration, The Robotics Review 1. MIT Press, Cambridge, pp. 207-242.

Hollerbach, J.M., Khalil. W., Lemoine, P., 2008. Model identification, Handbook of Robotics. Springer, pp. 321-344.

Huang, C., Xie, C., Zhang, T., 2008. Determination of optimal measurement configurations for robot calibration based on a hybrid optimal method. IEEE International Conference on Information and Automation(ICIA), pp. 789-793.

Huang, H., Lin, G.C., 2003. Rapid and flexible prototyping through a dual-robot workcell. Robotics and Computer-Integrated Manufacturing 19, 263-272.

Huang, S., Tan, K.K., Lee, T.H., 2000. Adaptive friction compensation using neural network approximations. IEEE Transactions on Systems, Man, and Cybernetics, Part C: Applications and Reviews 30, 551-557.

Huang, Z., Li, Q., Ding, H., 2013. Basics of Screw Theory, Theory of Parallel Mechanisms. Springer, pp. 1-16.

ICC.com, Innovative Conveyor Concepts: robotics palletizing, http://www.iccrobotics.com/palletizing.html.

Ikits, M., Hollerbach, J.M., 1997. Kinematic calibration using a plane constraint. Proceedings of IEEE International Conference on Robotics and Automation, pp. 3191-3196.

Imoto, J., Takeda, Y., Saito, H., Ichiryu, K., 2009. Optimal kinematic calibration of robots based on maximum positioning-error estimation (Theory and application to a parallel-mechanism pipe bender), Computational Kinematics. Springer, pp. 133-140.

Ishiguro, A., Furuhashi, T., Okuma, S., Uchikawa, Y., 1992. A neural network compensator for uncertainties of robotics manipulators. IEEE Transactions on Industrial Electronics 39, 565-570.

Jang, J.H., Kim, S.H., Kwak, Y.K., 2001. Calibration of geometric and non-geometric errors of an industrial robot. Robotica 19, 311-321.

Judd, R.P., Knasinski, A.B., 1990. A technique to calibrate industrial robots with experimental verification. IEEE Transactions on Robotics and Automation 6, 20-30.

Kao, I., Ngo, C., 1999. Properties of the grasp stiffness matrix and conservative control strategies. The International Journal of Robotics Research 18, 159-167.

Khalil, W., Besnard, S., 2002. Geometric calibration of robots with flexible joints and links. Journal of Intelligent and Robotic systems 34, 357-379.

Khalil, W., Besnard, S., Lemoine, P., 2000. Comparison study of the geometric parameters calibration methods. International Journal of Robotics and Automation 15, pp.56-67.

Khalil, W., Creusot, D., 1997. SYMORO+: A system for the symbolic modelling of robots. Robotica 15, 153-161.

Khalil, W., Dombre, E., 2004. Modeling, identification and control of robots. Butterworth-Heinemann.

Khalil, W., Gautier, M., Enguehard, C., 1991. Identifiable parameters and optimum configurations for robots calibration. Robotica 9, 63-70.

Khalil, W., Lemoine, P., 1999. GECARO: A system for the GEometric CAlibration of RObots. European Journal of Automation 33, 717-739.

Klimchik, A., 2011. Enhanced stiffness modeling of serial and parallel manipulators for robotic-based processing of high performance materials, PhD thesis, Ecole centrale de nantes-ECN.

Klimchik, A., Caro, S., Pashkevich, A., 2013a. Practical identifiability of the manipulator link stiffness parameters, ASME 2013 International Mechanical Engineering Congress & Exposition, San Diego, CA, USA.

Klimchik, A., Pashkevich, A., Chablat, D., 2013b. CAD-based approach for identification of elasto-static parameters of robotic manipulators. Finite Elements in Analysis and Design 75, 19-30.

Korn, D., 2005. Optimize cutting efficiency, optimize throughput. Modern Machine Shop 77, 86-89.

Kranendonk.com, http://www.kranendonk.com/en.

Kuipers, J.B., 1999. Quaternions and rotation sequences. Princeton university press, Princeton.

Kuka, http://www.kuka-robotics.com.

Leica-geosystems, http://metrology.leica-geosystems.com/en/index.htm.

Li, Y.-W., Wang, J.-S., Wang, L.-P., 2002. Stiffness analysis of a Stewart platform-based parallel kinematic machine. Proceedings of IEEE International Conference on Robotics and Automation, pp. 3672-3677.

Lightcap, C., Hamner, S., Schmitz, T., Banks, S., 2008. Improved positioning accuracy of the PA10-6CE robot with geometric and flexibility calibration. IEEE Transactions on Robotics 24, 452-456.

Lintott, A., Dunlop, G., 1997. Parallel topology robot calibration. Robotica 15, 395-398.

Long, C.S., Snyman, J., Groenwold, A., 2003. Optimal structural design of a planar parallel platform for machining. Applied Mathematical Modelling 27, 581-609.

Lu, T.-F., Lin, G.C., He, J.R., 1997. Neural-network-based 3D force/torque sensor calibration for robot applications. Engineering Applications of Artificial Intelligence 10, 87-97.

Majou, F., Gosselin, C., Wenger, P., Chablat, D., 2007. Parametric stiffness analysis of the Orthoglide. Mechanism and Machine Theory 42, 296-311.

Marie, S., Maurine, P., 2008. Elasto-geometrical modelling of closed-loop industrial robots used for machining application. IEEE International Conference on Robotics and Automation, pp. 1294-1300.

Martin, H.C., 1966. Introduction to matrix methods of structural analysis. McGraw-Hill.

MathWorks.com, MATLAB and Simulink for Technical Computing, www.mathworks.com.

Maxwell, E.A., 1951. General Homogeneous Coordinates in Space of Three Dimensions. CUP Archive.

Meggiolaro, M.A., Dubowsky, S., 2000. An analytical method to eliminate the redundant parameters in robot calibration. Proceedings of ICRA'00, IEEE International Conference on Robotics and Automation, pp. 3609-3615.

Meggiolaro, M.A., Dubowsky, S., Mavroidis, C., 2005. Geometric and elastic error calibration of a high accuracy patient positioning system. Mechanism and Machine Theory 40, 415-427.

Meggiolaro, M.A., Scriffignano, G., Dubowsky, S., 2000. Manipulator calibration using a single endpoint contact constraint, Proceedings of ASME Design Engineering Technical Conference, Baltimore, USA.

Moore , E., H., , 1920. On the reciprocal of the general algebraic matrix. Bulletin of the American Mathematical Society 26, 394-395.

Mooring, B., 1983. The effect of joint axis misalignment on robot positioning accuracy, Proceedings of the ASME international computers in engineering conference, pp. 151-156.

Mooring, B.W., Roth, Z.S., Driels, M.R., 1991. Fundamentals of manipulator calibration. Wiley New York.

Murray, P., 2012. Better, Faster, and Cheaper – These Robots Are Invading Car Manufacturing Plants.

Nagai, K., Liu, Z., 2008. A systematic approach to stiffness analysis of parallel mechanisms. IEEE International Conference on Robotics and Automation, pp. 1543-1548.

Nahvi, A., Hollerbach, J.M., 1996. The noise amplification index for optimal pose selection in robot calibration. Proceedings of IEEE International Conference on Robotics and Automation, pp. 647-654.

Nahvi, A., Hollerbach, J.M., Hayward, V., 1994. Calibration of a parallel robot using multiple kinematic closed loops. Proceedings of IEEE International Conference on Robotics and Automation, pp. 407-412.

Nektarios, A., Aspragathos, N.A., 2010. Optimal location of a general position and orientation end-effector's path relative to manipulator's base, considering velocity performance. Robotics and Computer-Integrated Manufacturing 26, 162-173.

Nubiola, A., Bonev, I.A., 2012. Absolute calibration of an ABB IRB 1600 robot using a laser tracker. Robotics and Computer-Integrated Manufacturing, 236–245.

Ortmeier, H., Engelhardt, D., 2002. Device and method for balancing the weight on a robot arm. Google Patents.

Oysu, C., Bingul, Z., 2009. Application of heuristic and hybrid-GASA algorithms to tool-path optimization problem for minimizing airtime during machining. Engineering Applications of Artificial Intelligence 22, 389-396.

Ozaki, T., Suzuki, T., Furuhashi, T., Okuma, S., Uchikawa, Y., 1991. Trajectory control of robotic manipulators using neural networks. IEEE Transactions on Industrial Electronics 38, 195-202.

Pashkevich, A., 2001. Computer-aided generation of complete irreducible models for robotic manipulators, The 3rd Int. Conference of Modellimg and Simulation. University of Technology of Troyes, France, pp. 293-298.

Pashkevich, A., Chablat, D., Wenger, P., 2008. Stiffness analysis of 3-dof overconstrained translational parallel manipulators. IEEE International Conference on Robotics and Automation (ICRA'08), pp. 1562-1567.

Pashkevich, A., Chablat, D., Wenger, P., 2009a. Stiffness analysis of overconstrained parallel manipulators. Mechanism and Machine Theory 44, 966-982.

Pashkevich, A., Klimchik, A., Chablat, D., 2009b. Nonlinear Effects in Stiffness Modeling of Robotic Manipulators. World Academy of Science, Engineering and Technology 58, 168-173.

Paul, R.P., 1981. Robot manipulators: mathematics, programming, and control: the computer control of robot manipulators. Richard Paul.

Paul, R.P., Zhang, H., 1986. Computationally efficient kinematics for manipulators with spherical wrists based on the homogeneous transformation representation. The International Journal of Robotics Research 5, 32-44.

Paziani, F.T., Di Giacomo, B., Tsunaki, R.H., 2009. Robot measuring form errors. Robotics and Computer-Integrated Manufacturing 25, 168-177.

Penrose, R., 1955. A generalized inverse for matrices, Proc. Cambridge Philos. Soc. Cambridge Univ Press, pp. 406-413.

Pigoski, T., Griffis, M., Duffy, J., 1998. Stiffness mappings employing different frames of reference. Mechanism and machine theory 33, 825-838.

Pinto, J., Lobão, M., Monteiro, J., 1990. Sequential experimental design for parameter estimation: a different approach. Chemical engineering science 45, 883-892.

Pritschow, G., Eppler, C., Garber, T., 2002. Influence of the dynamic stiffness on the accuracy of PKM. the 3rd Chemnitz Parallel Kinematic Seminar, Chemnitz, pp. 313‑333.

Quennouelle, C., 2009. Modélisation géométrique-statique des mécanismes parallèles compliance, thèse de doctorat, Universite Laval, Quebec.

Rahman, T., Ramanathan, R., Seliktar, R., Harwin, W., 1995. A simple technique to passively gravity-balance articulated mechanisms. Transactions-American Society Of Mechanical Engineers Journal Of Mechanical Design 117, 655-657.

Rao, C.R., Toutenburg, H., 1999. Linear models and generalizations: least squares and alternatives. Springer.

Rauf, A., Pervez, A., Ryu, J., 2006. Experimental results on kinematic calibration of parallel manipulators using a partial pose measurement device. IEEE Transactions on Robotics 22, 379-384.

Rauf, A., Ryu, J., 2001. Fully autonomous calibration of parallel manipulators by imposing position constraint. Proceedings of IEEE International Conference on Robotics and Automation, pp. 2389-2394.

Renders, J.-M., Rossignol, E., Becquet, M., Hanus, R., 1991. Kinematic calibration and geometrical parameter identification for robots. Robotics and Automation, IEEE Transactions on 7, 721-732.

Rizk, R., Fauroux, J.C., Mumteanu, M., Gogu, G., 2006. A comparative stiffness analysis of a reconfigurable parallel machine with three or four degrees of mobility. Journal of machine engineering 6, 45-55.

Rolland, L., 2003. Outils algébriques pour la résolution de problèmes géométriques et l'analyse de trajectoire de robots parallèles prévus pour des applications à haute cadence et grande précision, thèse de doctorat, Université Henri Poincaré

Roth, Z., Mooring, B., Ravani, B., 1987. An overview of robot calibration. IEEE Journal of Robotics and Automation 3, 377-385.

Salisbury, J.K., 1980. Active stiffness control of a manipulator in Cartesian coordinates. The 19th IEEE Conference on Decision and Control including the Symposium on Adaptive Processes, pp. 95-100.

Sariyildiz, E., Temeltas, H., 2011. A comparison study of three screw theory based kinematic solution methods for the industrial robot manipulators. IEEE International Conference on Mechatronics and Automation (ICMA), pp. 52-57.

Schröer, K., Albright, S.L., Grethlein, M., 1997. Complete, minimal and model-continuous kinematic models for robot calibration. Robotics and Computer-Integrated Manufacturing 13, 73-85.

Seo, T.I., 1998. Intégration des effets de déformation d'outil en génération de trajectoire d'usinage, thèse de doctorat, IRCCyN, Ecole Centrale de Nantes.

Sheather, S.J., 2009. Weighted Least Squares, A Modern Approach to Regression with R. Springer, pp. 115-123.

Sidoli, F., Mantalaris, A., Asprey, S., 2004. Modelling of mammalian cells and cell culture processes. Cytotechnology 44, 27-46.

Slabaugh, G.G., 1999. Computing Euler angles from a rotation matrix. Retrieved on August 6, 2000.

Stone, H., Sanderson, A., Neuman, C., 1986. Arm signature identification. Proceedings of IEEE International Conference on Robotics and Automation, pp. 41-48.

Stone, H.W., 1987. Kinematic modeling, identification, and control of robotic manipulators. Springer.

Sun, Y., Hollerbach, J.M., 2008a. Active robot calibration algorithm. IEEE International Conference on Robotics and Automation (ICRA'08), pp. 1276-1281.

Sun, Y., Hollerbach, J.M., 2008b. Observability index selection for robot calibration. IEEE International Conference on Robotics and Automation (ICRA'08), pp. 831-836.

Takesue, N., Ikematsu, T., Murayama, H., Fujimoto, H., 2011. Design and Prototype of Variable Gravity Compensation Mechanism (VGCM). Journal of Robotics and Mechatronics 23, 249.

Tyapin, I., Hovland, G., 2009. Kinematic and Elastostatic Design Optimisation of the 3-DOF Gantry-Tau Parallel Kinematic Manipulator. Modeling, Identification and Control 30, 39-56.

Ulrich, N., Kumar, V., 1991. Passive mechanical gravity compensation for robot manipulators. Proceedings of IEEE International Conference on Robotics and Automation, pp. 1536-1541.

Vanrolleghem, P.A., Daele, M.V., Dochain, D., 1995. Practical identifiability of a biokinetic model of activated sludge respiration. Water Research 29, 2561-2570.

Veeramani, D., Gau, Y.-S., 1998. Models for tool-path plan optimization in patch-by-patch machining. International journal of production research 36, 1633-1651.

Veitschegger, W., Wu, C.-h., 1987. A method for calibrating and compensating robot kinematic errors. Proceedings of IEEE International Conference on Robotics and Automation, pp. 39-44.

Vertechy, R., Parenti-Castelli, V., 2007. Static and stiffness analyses of a class of over-constrained parallel manipulators with legs of type US and UPS. IEEE International Conference on Robotics and Automation, pp. 561-567.

Waldron, K., Schmiedeler, J., 2008. Kinematics, Springer handbook of robotics. Springer, pp. 26-28.

Wang, J., Zhang, H., Fuhlbrigge, T., 2009. Improving machining accuracy with robot deformation compensation. IEEE/RSJ International Conference on Intelligent Robots and Systems (IROS'09.), pp. 3826-3831.

Waurzyniak, P., 2013. Aerospace Automation Picks Up the Pace. Manufacturing Engineering 150, 55-+.

Whitney, D.E., Lozinski, C.A., Rourke, J.M., 1985. Industrial robot calibration method and results. Department of Mechanical Engineering, MIT.

Xi, F., Zhang, D., Mechefske, C.M., Lang, S.Y., 2004. Global kinetostatic modelling of tripod-based parallel kinematic machine. Mechanism and Machine Theory 39, 357-377.

Yi, B.J., Freeman, R.A., 1993. Geometric analysis of antagonistic stiffness in redundantly actuated parallel mechanisms. Journal of Robotic Systems 10, 581-603.

Yoo, B.K., Ham, W.C., 2000. Adaptive control of robot manipulator using fuzzy compensator. IEEE Transactions on Fuzzy Systems 8, 186-199.

Zhang, D., 2000. Kinetostatic analysis and optimization of parallel and hybrid architectures for machine tools, thèse de doctorat, Universitre Laval, Quebec.

Zhong, X.-L., Lewis, J.M., 1995. A new method for autonomous robot calibration. Proceedings of IEEE International Conference on Robotics and Automation, pp. 1790-1795.

Zhou, J., Kang, H.-J., Ro, Y.-S., 2010. Comparison of the Observability Indices for Robot Calibration considering Joint Stiffness Parameters, Advanced Intelligent Computing Theories and Applications. Springer, pp. 372-380.

Zhuang, H., Adviser-Hamano, F., Adviser-Roth, Z.S., 1989. Kinematic modeling, identification and compensation of robot manipulators, PhD thesis, Florida Atlantic University.

Zhuang, H., Roth, Z.S., Hamano, F., 1992. A complete and parametrically continuous kinematic model for robot manipulators. IEEE Transactions on Robotics and Automation 8, 451-463.

Zhuang, H., Wang, K., Roth, Z.S., 1994. Optimal selection of measurement configurations for robot calibration using simulated annealing. Proceedings of IEEE International Conference on Robotics and Automation, pp. 393-398.

Zhuang, H., Wu, J., Huang, W., 1996. Optimal planning of robot calibration experiments by genetic algorithms, Proceedings of IEEE International Conference on Robotics and Automation, pp. 981-986.

Zhuang, H., Yan, J., Masory, O., 1998. Calibration of Stewart platforms and other parallel manipulators by minimizing inverse kinematic residuals. Journal of Robotic Systems 15, 395-405.

Zullo, L.C., 1991. Computer aided design of experiments: an engineering approach. Imperial College London (University of London).

Thèse de Doctorat

Yier WU

Sélection de Poses Optimales pour l'identification des Paramètres Géométriques et Elasto-statiques de Robots d'Usinage

Optimal Pose Selection for the Identification of Geometric and Elastostatic Parameters of Machining Robots

Résumé

La thèse porte sur la sélection de poses optimales pour la calibration géométrique et élasto-statique de robots industriels utilisés pour l'usinage de pièces des grandes dimensions. Une attention particulière est accordée à l'amélioration de la précision de positionnement du robot après compensation des erreurs géométriques et élasto-statiques. Pour répondre aux exigences industrielles des opérations d'usinage, une nouvelle approche pour la définition d'essais pour la calibration de robots sériels et quasi-sériels est proposée. Cette approche est basée sur un nouveau critère de performance, orienté applications industrielles, qui évalue la qualité du plan d'essais pour la calibration via la précision de positionnement du manipulateur après compensation d'erreurs, et tient compte des spécificités de la tâche manufacturière à réaliser au moyen de configurations tests. Contrairement aux travaux précédents, l'approche développée requiert seulement une mesure des positions de points et non d'orientation de corps rigides à l'aide d'un système de mesure externe tel qu'un laser tracker. Cette méthode permet ainsi d'éviter les problèmes de non-homogénéité dans les équations d'identification. Par ailleurs, afin de prendre en compte l'impact du compensateur de gravité, qui induit une chaîne cinématique fermée, le modèle de raideur est étendu en y incluant certains paramètres élasto-statiques dont les valeurs dépendent de la configurations du robot. Une méthodologie pour la calibration des modèles de compensateurs de gravité est ainsi proposée. Les avantages des techniques développées pour la calibration de robots industriels dédiés à des opérations d'usinage sont validés et mis en évidence expérimentalement, à travers la calibration géométrique et élasto-statique du robot industriel KUKA KR-270.

Mots clés
calibration géométrique et élasto-statique, définition d'essais de calibration, mesure de poses partielles, robots sériels et quasi-sériels, compensateur de gravité, robotique d'usinage

Abstract

The thesis deals with the optimal pose selection for geometric and elastostatic calibration for industrial robots employed in machining of large parts. Particular attention is paid to the improvement of robot positioning accuracy after compensation of the geometric and elastostatic errors. To meet the industrial requirements of machining operations, a new approach for calibration experiments design for serial and quasi-serial industrial robots is proposed. This approach is based on a new industry-oriented performance measure that evaluates the quality of calibration experiment plan via the manipulator positioning accuracy after error compensation, and takes into account the particularities of prescribed manufacturing task by introducing manipulator test-poses. Contrary to previous works, the developed approach employs an enhanced partial pose measurement method, which uses only direct position measurements from an external device and allows us to avoid the non-homogeneity of relevant identification equations. In order to consider the impact of gravity compensator that creates closed-loop chains, the conventional stiffness model is extended by including in it some configuration dependent elastostatic parameters, which are assumed to be constant for strictly serial robots. Corresponding methodology for calibration of the gravity compensator models is also proposed. The advantages of the developed calibration techniques are validated via experimental study, which deals with geometric and elastostatic calibration of a KUKA KR-270 industrial robot.

Key Words
geometric and elastostatic calibration, design of calibration experiments, partial pose measurements, serial/quasi-serial industrial robots, gravity compensator, robotic-based machining